THE UNIVERSITY OF QUEENSLAND

SCHOOL OF CIVIL ENGINEERING

REPORT CH87/12

AIR-WATER FLOW PROPERTIES AND ENERGY DISSIPATION ON STEPPED SPILLWAYS: A PHYSICAL STUDY OF SEVERAL POOLED STEPPED CONFIGURATIONS

AUTHORS: Stefan FELDER, Philipp GUENTHER and Hubert CHANSON

HYDRAULIC MODEL REPORTS

This report is published by the School of Civil Engineering at the University of Queensland. Lists of recently-published titles of this series and of other publications are provided at the end of this report. Requests for copies of any of these documents should be addressed to the Civil Engineering Secretary.

School of Civil Engineering
The University of Queensland
Brisbane QLD 4072
AUSTRALIA

Telephone: (61 7) 3365 4163
Fax: (61 7) 3365 4599

URL: http://www.eng.uq.edu.au/civil/

First published in 2012 by
School of Civil Engineering
The University of Queensland, Brisbane QLD 4072, Australia

ISBN No. 9781742720555

The University of Queensland, St Lucia QLD

Air-Water Flow Properties and Energy Dissipation on Stepped Spillways: a Physical Study of Several Pooled Stepped Configurations

by

Stefan FELDER

PhD student, The University of Queensland, School of Civil Engineering, Brisbane QLD 4072, Australia

Philipp GUENTHER

Visiting research fellow, The University of Queensland, School of Civil Engineering, Brisbane QLD 4072, Australia

Diploma thesis student, RWTH Aachen University, Institute of Hydraulic Engineering and Water Resources Management, Aachen 52056, Germany

and

Hubert CHANSON

Professor, The University of Queensland, School of Civil Engineering, Brisbane QLD 4072, Australia, Email: h.chanson@uq.edu.au

REPORT No. CH87/12

ISBN 9781742720555

School of Civil Engineering, The University of Queensland, July 2012

Sorpe dam pooled stepped spillway in September 2003 (Courtesy of Dr Carlos GONZALEZ)

ABSTRACT

In the last few decades, a number of experimental investigations of stepped spillways took place with a focus on the energy dissipation and air-entrainment processes on stepped spillways with flat horizontal steps. Recently some studies investigated the pooled stepped spillway configurations. Herein a physical study was performed on a relatively large size stepped spillway channel with a 26.6° slope and 0.10 m high steps. Four stepped chute configurations were tested including a stepped spillway with flat horizontal steps, a pooled stepped spillway, and two stepped spillway configurations with in-line and staggered arrangements of flat and pooled steps. The flat stepped spillway showed some typical flow patterns with nappe, transition and skimming flow regimes depending upon the flow rate. Some similar flow regimes were observed on the pooled stepped spillway, although some pulsating flow was seen for some nappe flow rates associated with the downstream propagation of small instabilities. On the in-line and staggered configurations of flat and pooled steps, the flow was highly three-dimensional. Some strong instabilities and three dimensional flow motion were observed. For all stepped spillway configurations some detailed air-water flow measurements were conducted downstream of the inception point of free-surface aeration. The experimental data showed similar void fraction distributions and mean air concentrations on both flat and pooled stepped spillways. The turbulence levels and the air bubble and water droplet chord sizes were also comparable between the two configurations. On the other hand, some larger bubble frequencies and integral turbulent length scales were observed on the flat stepped spillway, while larger velocities were recorded on the pooled stepped chute for identical flow rates. The measurements on the stepped spillways of in-line and staggered configurations of flat and pooled steps presented some significant transverse differences in terms of air-water flow properties between the flat and pooled stepped sides. Further data analyses showed that the rate of energy dissipation was smaller on the pooled stepped spillway compared to that on the flat stepped chute. Conversely the residual energy was larger at the downstream end of the pooled stepped chute. The data for the stepped spillway configuration with in-line and staggered configurations of flat and pooled steps showed large differences in the transverse direction, although the transverse averaged rates of energy dissipation and residual energy were comparable to the pooled stepped spillway results. Altogether the present study demonstrated that, on a 26.6° stepped chute, the designs with pooled steps and in-line and staggered configurations of flat and pooled steps did not provide any advantageous performances in terms of energy dissipation and flow aeration, while they were affected by flow instabilities and three-dimensional patterns leading to some flow concentration.

Keywords: Air-water flow, Stepped spillway, Pooled stepped spillway, In-line stepped spillway, Staggered stepped spillway, Air entrainment, Energy dissipation, Residual head, Flow resistance, Turbulence, Cavity ejections, Pulsating flow, Instabilities.

TABLE OF CONTENTS

LIST OF SYMBOLS

The following symbols are used in this report:

a	dimensionless factor;
b	dimensionless factor;
C	void fraction defined as the volume of air per unit volume of air and water; it is also called air concentration or local air content;
C_{mean}	depth-average void fraction defined in terms of Y_{90}: $C_{mean} = 1 - d/Y_{90}$;
D_o	dimensionless constant;
D_H	hydraulic diameter (m);
d	equivalent clear water flow depth (m);
d_{ab}	characteristic bubble size (m);
d_c	critical flow depth (m);
d_{local}	local flow depth (m);
d_{SS}	height of the standing sidewall waves (m);
F	air bubble count rate or bubble frequency (Hz) defined as the number of detected air bubbles per unit time;
F_{ej}	cavity ejection frequency (Hz);
F_{max}	maximum bubble count rate in a cross-section (Hz);
F^*	Froude number defined in terms of the step height;
f_e	equivalent Darcy-Weisbach friction factor in air-water flows;
g	gravity constant: $g = 9.80$ m/s^2 in Brisbane, Australia;
H	total head (m);
H_{dam}	dam height (m);
H_{max}	maximum upstream head (m) above chute toe: $H_{max} = H_{dam} + 3/2 \times d_c$;
H_{res}	residual head (m);
H_1	upstream head (m) above crest;
h	vertical step height (m);
K'	dimensionless integration constant;
k_s	step cavity roughness height (m): $k_s = (h+w) \times \cos\theta$;
k_s'	equivalent sand roughness height of the step face surface (m);
L_{cavity}	length of the step cavity (m);
L_{crest}	length of the broad-crested weir (m);
L_I	longitudinal distance (m) measured from the weir crest to the inception point of free-surface aeration;
L_{xz}	transverse integral turbulent length scale (m);
$(L_{xz})_{max}$	maximum transverse integral turbulent length scale (m) in a cross-section;
l	horizontal step length (m);
l_{SS}	length of the standing sidewall waves (m);
l_w	pool weir length (m);

N	power law exponent;
n	number of detected air packets per position;
Q	water discharge (m^3/s);
q_{local}	local water discharge per unit width (m^2/s);
q	water discharge per unit width (m^2/s);
Re	Reynolds number defined in terms of the hydraulic diameter: $Re = \rho_w \times U_w \times D_H / \mu_w$;
R_{xx}	normalised auto-correlation function (reference) probe;
R_{xy}	normalised cross-correlation function between two probe output signals in flow direction;
R_{xz}	normalised cross-correlation function between two probe output signals in transverse direction;
$(R_{xy})_{max}$	maximum cross-correlation between two probe output signals in flow direction;
$(R_{xz})_{max}$	maximum cross-correlation between two probe output signals in transverse direction;
S_f	friction slope: $S_f = - \partial H / \partial x$;
r	radius of the upstream rounded corner of the broad-crested weir (m);
T	time lag (s) for which $R_{xy} = (R_{xy})_{max}$;
Tu	turbulence intensity;
Tu_{max}	maximum turbulence intensity in a cross-section;
T_{xx}	auto-correlation integral time scale (s);
T_{xy}	cross-correlation integral time scale in flow direction (s);
T_{xz}	cross-correlation integral time scale in transverse direction (s);
T_{int}	integral turbulent time scale (s);
$(T_{int})_{max}$	maximum integral turbulent time scale (s) in a cross-section;
$T_{0.5}$	characteristic time lag (s) for which $R_{xx} = 0.5$;
t	time (s) or video duration;
U_{local}	local mean flow velocity (m/s)
U_w	mean flow velocity (m/s): $U_w = q/d$;
u'	turbulent velocity fluctuations (m/s);
V	interfacial velocity (m/s);
V_c	critical flow velocity (m/s);
V_{90}	characteristic interfacial velocity (m/s) where the void fraction is 90%;
W	channel width (m);
W_w	widths of the pooled and flat part in the staggered and in-line configurations of flat and pooled steps (m);
w	weir height in pooled stepped spillway configuration (m), also called pool height;
x	distance along the channel bottom (m);
Y_{90}	characteristic depth (m) where the void fraction is 90%;
y	distance (m) measured normal to the invert (or channel bed);
z	transverse distance (m) in the channel;
ΔH	total loss (m): $\Delta H = H_{max} - H_{res}$;

Δx	streamwise separation distance (m) between probe sensors;
Δz	transverse separation distance (m) between probe sensors;
Δz_o	height from the weir crest to the calculated step edge (m);
δ	shockwave angle;
η	ratio of average cavity ejection period to burst duration;
λ	ratio of average fluid ejection volume to total cavity volume;
μ	dynamic viscosity (Pa.s);
θ	angle between pseudo-bottom formed by the step edges and the horizontal;
ρ	density (kg/m^3);
σ	surface tension between air and water (N/m);
τ	time lag (s);
$\tau_{0.5}$	characteristic time lag (s) for which $R_{xy} = 0.5 \times (R_{xy})_{max}$;
Ø	probe sensor diameter (m);

Subscript

c	critical flow conditions;
max	maximum value;
mean	mean signal component;
xx	auto-correlation of reference probe signal;
xy	cross-correlation in flow direction;
xz	cross-correlation in transverse direction;
w	water properties;

Abbreviations

NA	nappe flow regime;
PDF	probability density function;
SK	skimming flow regime;
TRA	transition flow regime;
TRA1	transition flow sub-regime 1.

1. INTRODUCTION

1.1 PRESENTATION

For the last decades, some experimental investigations of stepped spillway flows took place in several laboratory facilities around the world (e.g. HORNER 1969; SORENSEN 1985; CHANSON 1995,2001; OHTSU & YASUDA 1997; BOES 2000; TOOMBES 2002; AMADOR et al. 2006; CHANSON & CAROSI 2007; MEIRELES & MATOS 2009; FELDER & CHANSON 2009a,2011a; BUNG 2011). The studies provided insights into the energy dissipation and air-entrainment processes on flat stepped spillways for a wide range of channel slopes. The understanding of the air-water flows advanced in the last decade and this included some detailed information about the microscopic air-water flow properties and the turbulence levels (e.g. CHANSON & TOOMBES 2002; GONZALEZ & CHANSON 2004; CHANSON & CAROSI 2006; FELDER & CHANSON 2009b). However the design for stepped spillways is still relatively crude, often restricted to stepped chutes with flat horizontal steps in rectangular prismatic channels. Experimental studies with alternative designs might lead to some further optimisation (e.g. PEYRAS et al. 1992; GONZALEZ & CHANSON 2008; RELVAS & PINHEIRO 2008,2011; FELDER & CHANSON 2011b).

In recent years, the air-water flows on pooled stepped spillways were researched in a few studies (Table 1-1). Table 1-1 lists the most important air-water flow studies on pooled stepped spillways and Figure 1-1 shows a number of prototype pooled stepped spillways. ANDRÉ (2004) and KÖKPINAR (2004) investigated the air entrainment processes on flat, pooled and a combination of flat and pooled steps on channel slopes of 18.6° and 30°. THORWARTH & KOENGETER (2006) and THORWARTH (2008) researched the self-induced instabilities on pooled stepped spillways with slopes of 8.9° and 14.6°. Recently FELDER & CHANSON (2012a) and FELDER et al. (2012) conducted a detailed study of the air-water flow properties, the turbulent properties and the instationarities on a stepped spillway with flat, pooled and combination of flat and pooled steps with a slope of 8.9°.

A related form of pooled stepped chutes is some stepped fishway design. Figure 1-2 shows some fishways designed with a staggered combination of flat and pooled steps. These particular structures cannot be considered successful however. In one case, some flow concentration yielded some very high velocities at the downstream end of the fish passage which were detrimental to the upstream fish migration (Fig. 1-2A). The other example became fully-silted rapidly, while its downstream steps were heavily eroded by the river sediment bed load materials (Fig. 1-2B).

Table 1-1 - Summary of experimental studies of air-water flow properties on pooled stepped spillway configurations

Reference (1)	θ [°] (2)	Step geometry (3)	Flow conditions (4)	Instrumen-tation (5)	Comment (6)
KÖKPINAR (2004)	30	Flat steps: h = 6 cm, l = 10.4 cm Pooled steps: h = 6 cm, l = 10.4 cm, w = 3 cm Combination of flat/pooled steps: h = 6 cm, l = 10.4 cm, w = 3 cm	Q = 0.03 – 0.100 m^3/s, Re = 2.4×10^5 – 8.0×10^5	Double-tip fiber-optical probe (Ø = 0.08 mm)	W = 0.5 m, 64 steps, l_w = 2.6 cm
ANDRÉ (2004)	18.6	Flat steps: h = 6 cm, l = 17.8 cm Pooled steps: h = 6 cm, l = 17.8 cm, w = 3 cm Combination of flat/pooled steps: h = 6 cm, l = 17.8 cm, w = 3 cm	Q = 0.02 – 0.130 m^3/s, Re = 1.6×10^5 – 1.0×10^6	Double-tip fiber-optical probe (Ø = 0.08 mm)	W = 0.5 m, 42/64 steps, l_w = 2.6 cm
	30	Flat steps: h = 6 cm, l = 10.4 cm Pooled steps: h = 6 cm, l = 10.4 cm, w = 3 cm Combination of flat/pooled steps: h = 6 cm, l = 10.4 cm, w = 3 cm			
THORWARTH (2008); THORWARTH & KOENGETER (2006)	8.9	Pooled steps: h = 5 cm, l = 31.9 cm, w = 0 – 5 cm	Q = 0.025 – 0.117 m^3/s, Re = 2.0×10^5 - 9.3×10^5	Double-tip conductivity probe (Ø = 0.13 mm)	W = 0.5 m, 22/26 steps, l_w = 1.5 cm
	14.6	Pooled steps: h = 5 cm, l = 19.2 cm, w = 0 – 5 cm			
FELDER & CHANSON (2012a) FELDER et al. (2012)	8.9	Flat steps: h = 5 cm, l = 31.9 cm	Q = 0.018 – 0.117 m^3/s, Re = 1.4×10^5 - 9.3×10^5	Double-tip conductivity probe (Ø = 0.13 mm)	W = 0.5 m, 21 steps, l_w = 1.5 cm
		Pooled steps: h = w = 5 cm, l = 31.9 cm	Q = 0.027 – 0.117 m^3/s, Re = 2.2×10^5 - 9.3×10^5		
		Combination of flat/pooled steps: h = w = 5 cm, l = 31.9 cm	Q = 0.027 – 0.117 m^3/s, Re = 2.2×10^5 - 9.3×10^5		
Present study	26.6	Flat steps: h = 10 cm, l = 20 cm	Q = 0.030 – 0.113 m^3/s, Re = 2.3×10^5 – 8.7×10^5	Double-tip conductivity probe (Ø = 0.25 mm); Array of 2 single tip conductivity probes (Ø = 0.35 mm)	W = 0.52 m, 10 steps, l_w = 1.5 cm
		Pooled steps: h = 10 cm, l = 20 cm, w = 3.1 cm	Q = 0.013 – 0.130 m^3/s, Re = 1.0×10^5 – 9.9×10^5		
		In-line configuration (Pooled and flat steps in-line): h = 10 cm, l = 20 cm, w = 3.1 cm	Q = 0.016 – 0.113 m^3/s, Re = 1.4×10^5 – 8.7×10^5		
		Staggered configuration (Pooled and flat staggered): h = 10 cm, l = 20 cm, w = 3.1 cm	Q = 0.030 – 0.113 m^3/s, Re = 2.3×10^5 – 8.7×10^5		

Notes: θ: channel slope; h: step height; l: step length; w: weir height; l_w: pool weir length; W: channel width; Q: water discharge; Re: Reynolds number defined in terms of hydraulic diameter.

Fig. 1-1 - Photographs of pooled stepped spillways and pooled configurations

(A) Sorpe dam pooled stepped spillway (Germany) in September 2003 (Courtesy of Dr Carlos GONZALEZ) - Left: View from the downstream end; Right: step details looking downstream; note the small drain

(B) Pooled stepped spillway of Le Pont dam (France) in June 1998 - Left: looking downstream, Right: looking upstream

(C) Neil Turner weir in the Maranoa River (Qld, Australia) in July 2001 (Courtesy of Chris PROCTOR) - Weir height: 5.8 m, Storage capacity: 2 Mm^3, overflow stepped weir with 5 steps equipped with small concrete blocks at downstream step edges

Fig. 1-1 - Fishway structures on the Okura River (Japan) on 9 October 2012 - The stepped channel consists of a staggered combination of flat and pooled steps

(A) Looking upstream of a structure

(B) Looking at the downstream end of a fully-silted fishway - Note the eroded step edges

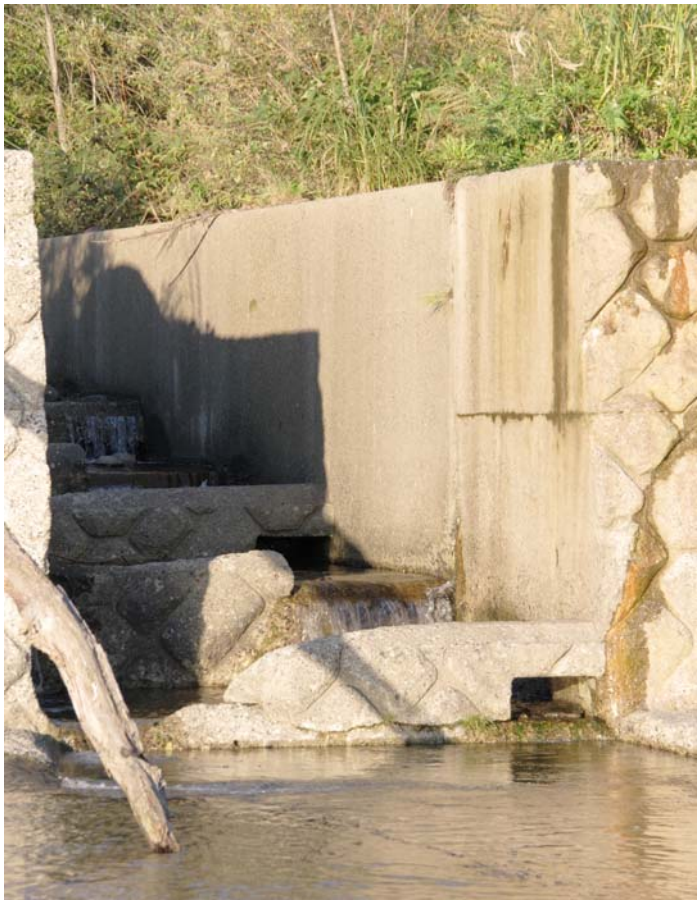

1.2 OUTLINE OF THE REPORT

In the present study, some detailed air-water flow measurements were conducted on a stepped spillway with flat horizontal and pooled steps, as well as two configurations of in-line and staggered flat and pooled steps (Table 1-1). The experimental study focused upon the air-water flow patterns, the air-water flow properties and the energy dissipation processes for the investigated configurations. The experiments provided some new insights in alternative stepped spillway designs including staggered stepped spillways used in some fishways (Fig. 1-2). In section 2, the experimental facility, the instrumentation and the experimental flow conditions are described. Some detailed visual observations of the flow patterns were conducted and some characteristic results are illustrated in section 3 including the air-water flow regimes, the inception point of air-entrainment, some cavity ejection processes and free-surface waves. In section 4, the air-water flow properties for flat and pooled stepped spillways are compared. Section 5 shows a comparative analysis of the air-water flow properties on the two staggered and in-line stepped spillway configurations of flat and pooled steps. In section 6, the energy dissipation and the flow resistance for all configurations are shown and compared with other studies on pooled stepped spillways. Section 7 concludes the report. Some further results are presented in the Appendices A to F.

2. DIMENSIONAL ANALYSIS, EXPERIMENTAL FACILITY AND INSTRUMENTATION

2.1 DIMENSIONAL ANALYSIS

In free-surface flows, a Froude similitude is typically used to scale the flow motion. For the rectangular stepped chute, a simplified dimensional analysis leads to a number of relationships between the air-water flow properties, fluid properties, boundary conditions and channel geometries, as shown in Equation (2-1):

$$C, \frac{V}{\sqrt{g \times d_c}}, \frac{u'}{V}, T_{int} \times \sqrt{\frac{g}{d_c}}, \frac{L_{xz}}{d_c}, \frac{d_{ab}}{d_c}, \frac{F \times d_c}{V_c} = F\left(\frac{x}{d_c}, \frac{y}{d_c}, \frac{z}{d_c}, \frac{w}{h}, \frac{w}{l}, \frac{l_w}{d_c}, \frac{W_w}{W}, \frac{d_c}{h}, \frac{q}{\sqrt{g \times {d_c}^3}}, \rho_w \times \frac{V \times D_H}{\mu_w}, \frac{g \times {\mu_w}^4}{\rho_w \times \sigma^3}, \frac{W}{d_c}, \theta, \frac{k_s'}{d_c} \right) \quad (2\text{-}1)$$

where C is the void fraction, V is the interfacial velocity, d_c is the critical flow depth, D_H is the hydraulic diameter, q is the water discharge per unit width, W is the channel width, h is the vertical step height, l is the step length, w is the pool weir height for a pooled stepped spillway, l_w is the horizontal pool weir length, W_w is the width of the pooled and flat part in the staggered and in-line configurations of flat and pooled steps, g is the gravity acceleration, θ is the chute slope, u' is the characteristic turbulent velocity, T_{int} is the integral turbulent time scale, L_{xz} is the integral turbulent length scale, x, y, z are respectively the longitudinal, normal and transverse coordinates, μ_w is the dynamic viscosity of water, ρ_w is the water density, σ is the surface tension between air and water, F is the bubble count rate, d_{ab} is the characteristic bubble size and k_s' is the equivalent sand roughness height of the step surface.

Equation (2-1) expresses the dimensionless air-water flow properties at a location (x,y,z) as functions of the relevant dimensionless parameters, including Froude ([1]) and Reynolds numbers Re. Herein the same fluids were used in model and prototype: that is, the Morton number was an invariant (WOOD 1991; CHANSON 2009). Similarly, the chute slope h/l, the channel width W, the horizontal pool weir length l_w and the step surface skin roughness k_s' were kept constant during the experiments. Some experiments were conducted in the centreline, and others different transverse locations z/d_c. Hence Equation (2-1) could be simplified into:

$$C, \frac{V}{\sqrt{g \times d_c}}, \frac{u'}{V}, T_{int} \times \sqrt{\frac{g}{d_c}}, \frac{L_{xz}}{d_c}, \frac{d_{ab}}{d_c}, \frac{F \times d_c}{V_c} = F\left(\frac{x}{d_c}, \frac{y}{d_c}, \frac{z}{d_c}, \frac{w}{h}, \frac{w}{l}, \frac{W_w}{W}, \frac{d_c}{h}, Re \right) \quad (2\text{-}2)$$

In the present study, the flow was gradually-varied for all configurations and a comparison of the

[1] In Equation (2-1), the dimensionless discharge d_c/h is proportional to a Froude number defined in terms of the step height: $d_c / h = (q / \sqrt{g \times h^3})^{2/3}$.

air-water flow properties must rely on the Froude similitude. The experiments were conducted in a large size facility operating at large Reynolds numbers (section 2.4, Table 2-1). These conditions may be representative of a full-scale storm waterway and ensure that the extrapolation of the data to prototype conditions is unlikely to be affected by scale effects.

2.2 EXPERIMENTAL FACILITY

New experiments were performed at the University of Queensland on a large size stepped spillway model with a slope of 26.6°. The experimental facility was newly designed and the present study comprised the first air-water flow experiments in the stepped spillway test section (Fig. 2-1). The stepped spillway consisted of 10 steps with step height h = 10 cm, and step length of l = 20 cm. The chute had a width W = 0.52 m. The steps were made out of plywood and the channel walls out of perspex. Constant flow rates were supplied by a large upstream intake basin with a size of 2.9 m × 2.2 m and a depth of 1.5 m. A smooth inflow was supplied by a 1.01 m long smooth sidewall convergent with a 4.23:1 contraction ratio. At the upstream end of a test section, the flow was controlled by a broad-crested weir with height of 1 m, width W = 0.52 m, length L_{crest} = 1.01 m and an upstream rounded corner (r = 0.08 m). The broad-crested weir was previously tested and some detailed velocity and pressure measurements (FELDER & CHANSON 2012b) provided the discharge calibration curve used in the present study:

$$\frac{Q}{W} = \left(0.92 + 0.153 \times \frac{H_1}{L_{crest}}\right) \times \sqrt{g \times \left(\frac{2}{3} \times H_1\right)^3} \qquad 0.02 \leq H_1/L_{crest} \leq 0.3 \quad (2\text{-}3)$$

where Q is the water discharge and H_1 is the upstream total head measured using a point gauge.

At the downstream end, the stepped chute was followed by a smooth horizontal raceway ending with an overfall into the recirculation sump pit. The flow was supercritical in the horizontal raceway and did not interfere with the stepped chute flow.

Fig. 2-1 – Experimental test section in the present study: pooled stepped spillway configuration - Flow conditions: $d_c/h = 0.53$, $Q = 0.020$ m^3/s, $Re = 1.54 \times 10^5$ (Note the broad-crested weir upstream of the first step edge) - Flow direction from left to right

2.3 INSTRUMENTATION AND SIGNAL PROCESSING

The air-water flow measurements were conducted with phase detection intrusive probes. Two types of conductivity probe systems were used. Measurements were conducted at all step edges downstream of the inception point of free-surface aeration with a double-tip conductivity probe with an inner tip diameter Ø = 0.25 mm and a separation of probe tips $\Delta x = 7.2$ mm in the longitudinal direction and $\Delta z = 1.5$ mm in the transverse direction (Fig. 2-2A). The probe was manufactured with two identical tips based upon a needle tip design. In Figure 2-2A, the double-tip conductivity probe is illustrated. Similar double-tip conductivity probes were used successfully in a number of air-water flow studies at the University of Queensland (e.g. CHANSON & TOOMBES 2002; GONZALEZ 2005; CAROSI & CHANSON 2008; FELDER & CHANSON 2009a,2011b).

Some additional measurements were conducted with an array of two single-tip conductivity probes (Ø = 0.35 mm) separated by a range of well-defined transverse distances $3.5 \leq \Delta z \leq 80.5$ mm (Fig. 2-2B). Both single-tip probes were positioned at the same vertical and horizontal positions. Some experiments with the two single-tip probes were performed successfully in some previous air-water flow studies (CHANSON & CAROSI 2007; FELDER & CHANSON 2009b,2011a).

All measurements were conducted for a sampling duration of 45 s with a sampling frequency of 20 kHz per probe sensor. Note that, for one discharge with a pulsating flow motion, a sampling duration of 180 s was used and the results are discussed in Appendix E. All conductivity probe tips

were mounted on a trolley and their elevation in the direction perpendicular to the pseudo bottom formed by the step edges (i.e. y-direction) was controlled by a fine adjustment screw-drive mechanism equipped with a Mitutoyo^{TM} digital ruler (accuracy < 0.1 mm). Each probe tip was excited with an electronic system, called an "air-bubble detector" (Ref. UQ82.518). The electronics translated the changes of the air/water phase resistance into a voltage signal which was sampled by a high-speed data acquisition system (National Instruments, USB-6251) and recorded to a laboratory computer. A data acquisition program was developed in LabVIEW^{TM} which embedded a Fortran subroutine for online data analysis.

Fig. 2-2 – Phase detection intrusive probes used in the present study

(A) Double-tip conductivity probe (Ø = 0.25 mm); Δx = 7.2 mm, Δz = 1.5 mm (Flow from right to left)

(B) Two single-tip conductivity probes (Ø = 0.35 mm); Δx = 0 mm, Δz = 50.1 mm (Flow from front to back)

All air-water flow properties were post-processed with a Fortran code used in previous studies (FELDER & CHANSON 2011a,b,2012a; FELDER et al. 2012). Herewith the raw data recorded with the double-tip conductivity probe yielded the void fraction C, the bubble count rate F, the interfacial velocity V, the turbulence intensity Tu and the air bubble and water droplet chord sizes. The data for the array of the two single-tip probes provided further the transverse integral turbulent time and length scales T_{int} and L_{xz} (section 4.1). For all experiments, the void fraction C, bubble frequency and particle chord sizes were calculated based upon a single-threshold technique with a threshold set at 50% of the air-water range (TOOMBES 2002; CHANSON & FELDER 2010). The velocity turbulence and integral turbulent scales were calculated using some correlation technique (CHANSON 2002; CHANSON & CAROSI 2007).

Further observations were conducted with a HD video camera Sony^{TM} HDR-XR160E (Standard HQ HD quality 25 fps), two dSLR camera Pentax^{TM} K-7 and Canon^{TM} 450D, and further smaller digital

cameras.

2.4 EXPERIMENTAL FLOW CONDITIONS

The experimental study was conducted for four stepped spillway configurations (Fig. 2-3). In Figure 2-3, all four configurations are shown including a flat stepped spillway (Fig. 2-3A), a pooled stepped spillway with weir height w = 3.1 cm (Fig. 2-3B) and two stepped spillways with in-line and staggered configurations of flat and pooled steps (Fig. 2-3C and 2-D respectively). The in-line stepped spillway configuration consisted of pooled steps and flat steps in-line for exactly half the channel width (Fig. 2-3C). The staggered pooled stepped spillway configuration was characterised by alternating flat and pooled steps with width W_w = 0.26 m (Fig. 2-3D). The four stepped spillway configurations are sketched in Figure 2-4 where the measurement positions of the double-tip conductivity probe are shown. The distance y normal to the pseudo-bottom formed by the step edges was defined with y = 0 at the step edges. For the pooled steps, y = 0 was set at the pool weir edges. For the flat and pooled stepped spillways, the conductivity probe measurements were conducted on the channel centreline (Fig. 2-4). On the inline and staggered stepped spillway configurations, three transverse measurement locations were used: on the channel centreline (z/W = 0.5) and at two further transverse positions in the middle of the flat and pooled halves (z/W = 0.25 and z/W = 0.75) (Fig. 2-4).

For the experiments with the array of two single-tip probes conducted on the flat and pooled stepped spillways, the reference probe was positioned on channel centreline and the second probe was separated by a transverse distance Δz.

For all configurations, the flow patterns were observed for a wide range of discharges 0.002 $m^3/s \leq Q \leq 0.155$ m^3/s (see section 3). The air-water flow measurements were performed for a range of discharges between $0.4 \leq d_c/h \leq 1.85$ corresponding to Reynolds numbers within one order of magnitude (Table 2-1). Table 2-1 lists the experimental flow conditions for the air-water flow experiments with the double- and single-tip conductivity probes. Most experiments were conducted in the transition and skimming flow regimes.

Fig. 2-3 – Photos of stepped spillway configurations in the present study (θ = 26.6°)

(A) Flat stepped spillway

(B) Pooled stepped spillway

(C) Stepped spillway with in-line configuration of flat and pooled steps

(D) Stepped spillway with staggered configuration of flat and pooled steps

Table 2-1 - Experimental flow conditions for the air-water flow measurements with the conductivity probes for the stepped spillway configurations (θ = 26.6°)

Configuration (1)	Q [m^3/s] (2)	d_c/h [-] (3)	Re [-] (4)	Instrumentation (5)	Measurement locations (6)
Flat stepped spillway (h = 0.1 m)	0.030 – 0.113	0.7 – 1.7	2.3×10^5 – 8.7×10^5	Double-tip conductivity probe (Ø = 0.25 mm)	Step edges downstream of inception point
	0.063 0.090	1.15 1.45	4.9×10^5 6.9×10^5	Two single-tip conductivity probes (Ø = 0.35 mm)	Step edge 10
Pooled stepped spillway (h = 0.1 m, w = 0.031 m)	0.013 – 0.130	0.4 – 1.85	1.0×10^5 – 9.9×10^5	Double-tip conductivity probe (Ø = 0.25 mm)	Step edges downstream of inception point
	0.063 0.090	1.15 1.45	4.9×10^5 6.9×10^5	Two single-tip conductivity probes (Ø = 0.35 mm)	Step edge 10
Stepped spillway with in-line configuration of flat and pooled steps (h = 0.1 m, w = 0.031 m, W_w = 0.26 m)	0.016 – 0.113	0.5 – 1.7	1.4×10^5 – 8.7×10^5	Double-tip conductivity probe (Ø = 0.25 mm)	Step edges downstream of inception point; three transverse positions
Stepped spillway with staggered configuration of flat and pooled steps (h = 0.1 m, w = 0.031 m, W_w = 0.26 m)	0.030 – 0.113	0.7 – 1.7	2.3×10^5 – 8.7×10^5	Double-tip conductivity probe (Ø = 0.25 mm)	Step edges downstream of inception point; three transverse positions

Notes: d_c: critical flow depth: $d_c = \sqrt[3]{Q^2/(g\times W^2)}$; Q: total discharge; Re: Reynolds number defined in terms of the equivalent pipe diameter.

Fig. 2-4 - Sketch of stepped spillway configurations and measurement positions (θ = 26.6°)

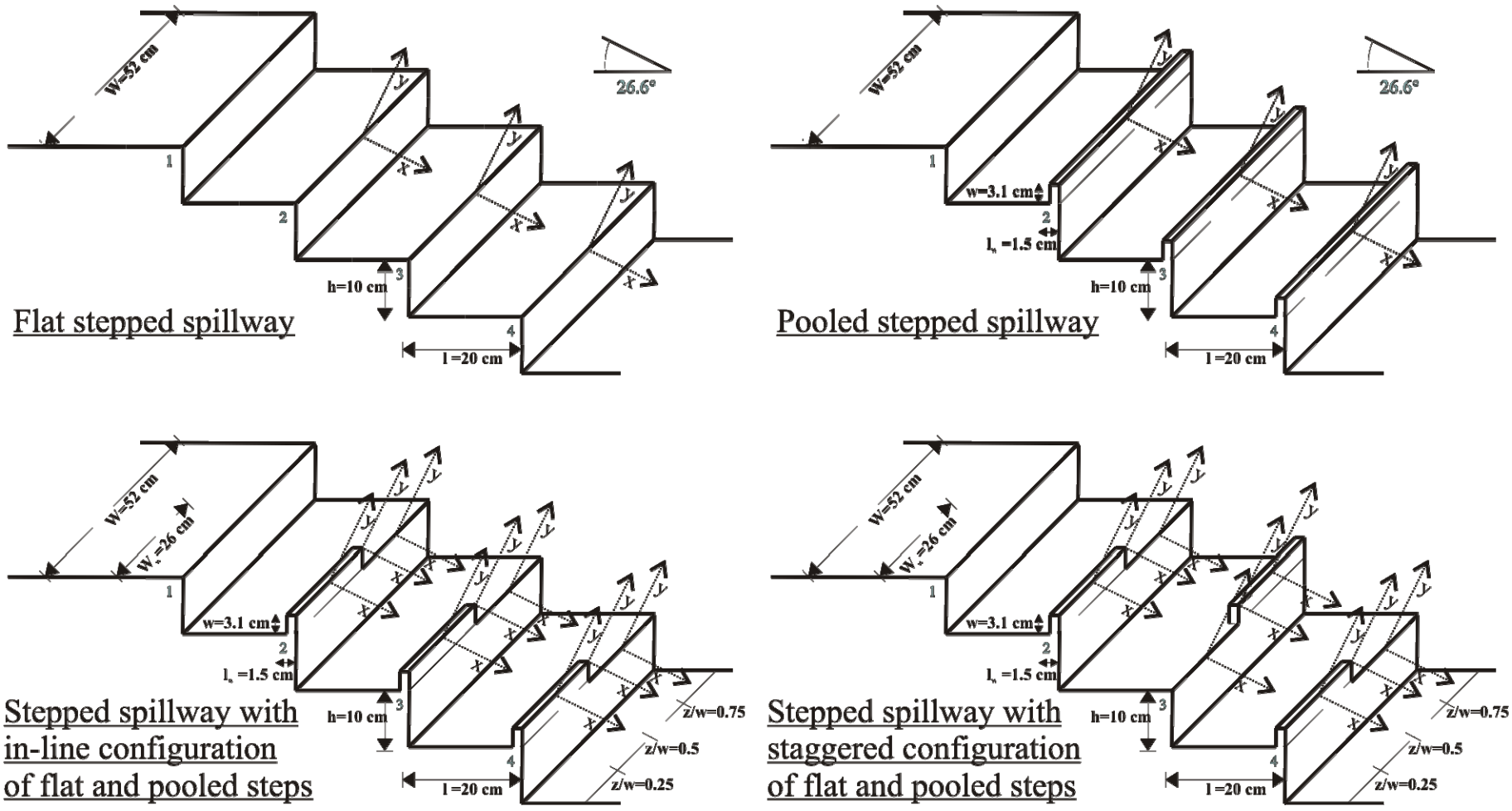

3. FLOW PATTERNS ON THE STEPPED SPILLWAYS

3.1 PRESENTATION

In this section, the flow patterns are presented for the flat and pooled stepped spillways and for the stepped spillways with in-line and staggered configurations of flat and pooled steps. The visual investigations of the flow patterns included the observations of the air-water flow patterns for all stepped spillway configurations for a broad range of discharges 0.002 $m^3/s \leq Q \leq 0.155$ m^3/s. The observation comprised the mono- and two-phase flow regions, the air entrainment processes and the key characteristics for each stepped spillway configuration. For some flow rates, the air-water flows on the pooled stepped spillway included some small instabilities linked with some pulsations for small discharges. The flow processes on the stepped spillways with in-line and staggered configurations of flat and pooled steps showed some complex air-water flow features including standing sidewall waves and supercritical shock waves. Furthermore the location of the inception points of free-surface aeration was recorded for all stepped spillway configurations and presented below. Some detailed investigations of the cavity ejection processes were also conducted for the flat and pooled stepped spillways.

Table 3-1 lists the experimental flow conditions for the visual observations of the flow patterns and the key characteristics for each stepped spillway configuration. Some further visual observations for all stepped spillway configurations are presented in Appendix A and some details about the ejection processes in Appendix B.

Table 3-1 – Experimental flow conditions for the visual observations of the flow patterns for the stepped spillway configuration ($\theta = 26.6°$)

Configuration (1)	Q [m^3/s] (2)	d_c/h [-] (3)	Re [-] (4)	Observations (5)
Flat stepped spillway	0.002 - 0.148	0.12 – 2.02	1.6×10^4 – 1.1×10^6	Flow regimes, Inception point of air-entrainment, Cavity ejection process
Pooled stepped spillway	0.002 - 0.139	0.11 – 1.94	1.5×10^4 – 1.1×10^6	Flow regimes, Inception point of air-entrainment, Cavity ejection process, Instabilities linked with pulsating flow
Stepped spillway with in-line configuration of flat and pooled steps	0.002 - 0.146	0.11 – 2.01	1.4×10^4 – 1.1×10^6	Flow regimes, Inception point of air-entrainment, Standing sidewall waves, Supercritical shock waves
Stepped spillway with staggered configuration of flat and pooled steps	0.003 - 0.155	0.15 – 2.09	2.3×10^4 – 1.2×10^6	Flow regimes, Inception point of air-entrainment, Standing sidewall waves, Supercritical shock waves

3.2 AIR-WATER FLOW PATTERNS ON THE FLAT STEPPED SPILLWAY

The flat stepped spillway exhibited some typical flow patterns previously observed on other stepped spillway investigations with similar channel slopes (e.g. CHANSON & TOOMBES 2002; GONZALEZ 2005; CAROSI & CHANSON 2008; FELDER & CHANSON 2009a). For the smallest flow rates $d_c/h < 0.5$, the water flowed down the steps as a succession of free-falling jets: i.e., a nappe flow regime (Fig. 3-1A) as described previously by CHANSON (1994) and TOOMBES & CHANSON (2008). With increasing discharges, the flow became more instable and some strong splashing was observed: i.e., the transition flow regime (Fig. 3-1B). The transition flow was observed for dimensionless flow rates $0.5 < d_c/h < 0.9$. The air-entrainment appeared at and downstream of the inception point of air entrainment. For $d_c/h > 0.9$, a skimming flow regime was seen with some stable recirculation in the step cavities downstream of the inception point of free-surface aeration (Fig. 3-1C).

Fig. 3-1 – Air-water flow pattern on flat stepped spillway ($\theta = 26.6°$)

(A) Nappe flow regime: $d_c/h = 0.18$, $Q = 0.004$ m^3/s, $Re = 3.1\times10^4$

(B) Transition flow regime: $d_c/h = 0.66$, $Q = 0.027$ m^3/s, $Re = 2.1\times10^5$

(C) Skimming flow regime: $d_c/h = 1.51$, $Q = 0.095$ m^3/s, $Re = 7.3\times10^5$

3.3 AIR-WATER FLOW PATTERNS ON THE POOLED STEPPED SPILLWAY

On the pooled stepped spillway, the flow patterns exhibited some features comparable to the observations on the flat stepped spillway (section 3.2). The different flow regimes were clearly distinguishable: i.e., nappe, transition and skimming flow regimes.

For the smallest flow rates $d_c/h < 0.45$, a nappe flow regime was observed and the water discharged in a succession of free-falling nappes from one step pool to the following (Fig. 3-2). Figure 3-2 shows the stability of the flow and suggests that most kinetic energy of the flow was dissipated above the steps. However, for a range of flow rates $0.30 \leq d_c/h \leq 0.45$, a pulsating flow was observed in the first step cavity leading to some small instabilities of the free-falling nappes (Fig. 3-3). The pulsations in the first step cavity were periodic and had a frequency of about 1 Hz (1 s period) for $d_c/h = 0.3$. The pulsation frequency was about 0.2 Hz for $d_c/h = 0.45$. During the pulsations, some small waves were ejected from the first step cavity and caused some deviations to the lengths of the free jet nappes. With every pulsation, the nappe impact cavity shifted from the next step cavity to one step cavity further downstream (Fig. 3-3). The pulsating mechanism was comparable to the self-induced instabilities on pooled stepped spillways with 8.9° and 30º slopes observed by THORWARTH (2008) and FELDER & CHANSON (2012a) ($\theta = 8.9°$), and TAKAHASHI et al. (2008) ($\theta = 30°$). On the 8.9° pooled stepped spillways, the instabilities occurred in the transition flow regime for $1.08 \leq d_c/h \leq 1.76$, causing some significantly large flow disturbances including jump waves and instable cavity ejections. The instabilities were observed for $0.3 < d_c/h < 0.4$ on the 30º slope chute. The instabilities on the pooled stepped spillway herein ($\theta = 26.6º$) were smaller and did not cause as such significant disturbances. The flow pattern and the air-water flow properties for a typical pulsating flow rate $d_c/h = 0.4$ were investigated in details and the findings are reported in Appendix E.

Fig. 3-2 –Nappe flow regime on pooled stepped spillway: $d_c/h = 0.26$, $Q = 0.007$ m^3/s, $Re = 5.1\times10^4$

Fig. 3-3 – Instabilities caused by some pulsating flows in first step cavity in nappe flow regime on pooled stepped spillway: $d_c/h = 0.40$, $Q = 0.013$ m^3/s, $Re = 1.0\times10^5$ – Chronological order from top left to bottom right corner

Fig. 3-4 – Transition flow regime on pooled stepped spillway: $d_c/h = 0.71$, $Q = 0.031$ m^3/s, $Re = 2.4\times10^5$

Fig. 3-5 – Skimming flow regime on pooled stepped spillway: $d_c/h = 1.27$, $Q = 0.074$ m^3/s, $Re = 5.6\times10^5$

For intermediate flow rates $0.45 \leq d_c/h \leq 0.97$, a transition flow regime was observed with some strong splashing in the air-water flow region downstream of the inception point of air-entrainment (Fig. 3-4). No pulsation in the first step cavity was observed. The transition flow regime was comparable to typical observations on the flat stepped spillway with some small instabilities in the air-water flows.

For larger discharges $d_c/h > 0.97$, a skimming flow regime occurred with some stable recirculation motions in the step cavities. At the upstream end of the chute, the flow was transparent (clear-waters) and the water surface was parallel to the pseudo-bottom formed by the pool step weirs equivalent to skimming flows on flat stepped spillways. The flow depth above the steps however was larger than on flat stepped chutes because of the pool weirs. Downstream of the inception point of free-surface aeration, the flow was highly aerated (Fig. 3-5).

3.4 AIR-WATER FLOW PATTERNS ON THE STEPPED SPILLWAY WITH IN-LINE CONFIGURATION OF FLAT AND POOLED STEPS

3.4.1 Presentation

The flow over the stepped spillway with in-line configuration of flat and pooled steps was visually investigated for a wide range of dimensionless discharges $0.05 \leq d_c/h \leq 2.0$. The observations were conducted on both the flat and pooled sides of the channel with some distinct differences. A key feature for the air-water flow was the three-dimensional flow motion in the transverse channel direction and the flow disturbances caused by the different step shape. These were seen for all the flow rates.

Some typical stepped spillway flow features such as the nappe, transition and skimming flow regimes were observed, but their appearance varied significantly between the flat and pooled side of the channel (see section 3.4.2). Hence some intermediate flow regions existed where a clear definition was not definite in terms of the flow regimes and patterns.

Furthermore some distinct instabilities were documented, including standing sidewall waves, shock waves and transverse flow interactions on the channel centreline. They are documented in paragraph 3.4.3. Further photographs of the air-water flow patterns are presented in Appendix A.

3.4.2 Flow regime observations

The pool weirs contributed to larger air-water depths at the pooled side of the channel, while a faster flow motion was observed at the flat stepped side. As a result, significant instabilities were observed on the pooled side, yielding some strong droplet ejection and splashing on the channel centreline. With increasing discharges, the three-dimensional nature of the flow became less pronounced. Between step edges 1 and 4, some chaotic flow features including jet deflection and shock waves were observed for all flow regimes in the clear-water flow downstream of the broad-crested weir.

The formation of nappe, transition and skimming flows could be determined separately on both sections of the channel: i.e., flat and pooled side. The flow features within each flow regime were

somehow comparable to the observations on flat and pooled steps, despite some unsteady flow motion for some ranges of discharges.

For small flow rates $d_c/h \leq 0.46$, a nappe flow regime was observed on both sides of the spillway chute with plunging jets from step to step on the flat side and from pool to pool on the pooled side. Some distinct jets on the pooled side and high velocities on the flat steps were seen in this flow regime as illustrated in Figure 3-6B. Figure 3-6A presents a side view on the pooled side, with a series of free-falling jets taking off from each pool weir. The nappe flow regime was significantly more unstable across the channel width than on the uniform flat and pooled stepped spillways. Some transverse flow motions as well as strong droplet ejections were seen along the entire channel length. The jets were highly aerated and singular air entrainment processes at the pooled side of the channel were observed.

Fig. 3-6 – Nappe flow regime on the stepped spillway with in-line configuration of flat and pooled steps: $d_c/h = 0.39$, $Q = 0.013 m^3/s$, $Re = 9.6 \times 10^4$

(A) Pooled stepped side (B) Flat stepped side

With increasing discharges $0.46 \leq d_c/h \leq 0.57$, the flow became more unstable and could not clearly be identified as nappe or transition flow across the entire channel width. This intermediate flow domain was characterised by plunging jets interacting in channel centreline and chaotic flow behaviour (Fig. 3-7). On the flat stepped side, the water spilled downstream as some nappe flow (Fig. 3-7 B), whereas, on the pooled side, a succession of distinctive plunging jets impacting into water filled cavities featured the flow as transition flow (Fig. 3-7A). A simple definition of this intermediate flow regime was not possible for the entire channel width. Visually, the transverse profile of the water surface appeared inclined down towards the flat stepped side, and the air-water discharge took place mostly in the flat stepped section of the channel. The pools induced large flow disturbances and some three-dimensional flow motion was observed. The flow was highly aerated

by singular aeration processes of the jets which caused also some instabilities including jet deflection and cross-waves. The distinction between the air-water flow patterns in the transverse direction was not consistent with the previous observations on the flat and pooled stepped spillways.

Fig. 3-7 – Nappe flows (flat stepped side) and transition flows (pooled stepped side) on the stepped spillway with in-line configuration of flat and pooled steps ($\theta = 26.6°$): $d_c/h = 0.50$, $Q = 0.018$ m^3/s, $Re = 1.4\times10^5$

(A) Pooled stepped side (Transition flows) (B) Flat stepped side (Nappe flows)

For discharges between $0.57 \leq d_c/h \leq 0.86$, a transition flow regime was observed on both sides of the channel with some distinct droplet ejection downstream of the inception point of aeration. In the upper section of the channel, some singular aeration processes were caused by some jets (Fig. 3-8). The air-water depths on the pooled stepped side were larger than on the flat stepped side. The transverse surface profile appeared to be inclined from the pooled stepped side down to the flat stepped side of the spillway. Some significant surface flapping was observed next to the inception point of free-surface aeration. In the clear-water region, the water surface was not parallel to the pseudo-bottom formed by the step edges. It showed some transverse flow features which led to a chaotic flow development at the inception point of free-surface aeration.

Some transverse flow interactions took place on channel centreline and yielded some three-dimensional flow motions along the entire channel downstream of the inception point (Fig. 3-8). The droplet ejections appeared moslty on the centreline and were consistently more intense than those observed on the flat stepped and pooled stepped spillways. The general appearance of the transition flow regime showed however some similar patterns as observed in other configurations, with some substantial free-surface aeration and the step cavities were consistently filled (i.e. no air cavity).

Fig. 3-8 – Transition flow regime on the stepped spillway with in-line configuration of flat and pooled steps ($\theta = 26.6°$): $d_c/h = 0.70$, $Q = 0.030$ m^3/s, $Re = 2.30 \times 10^5$

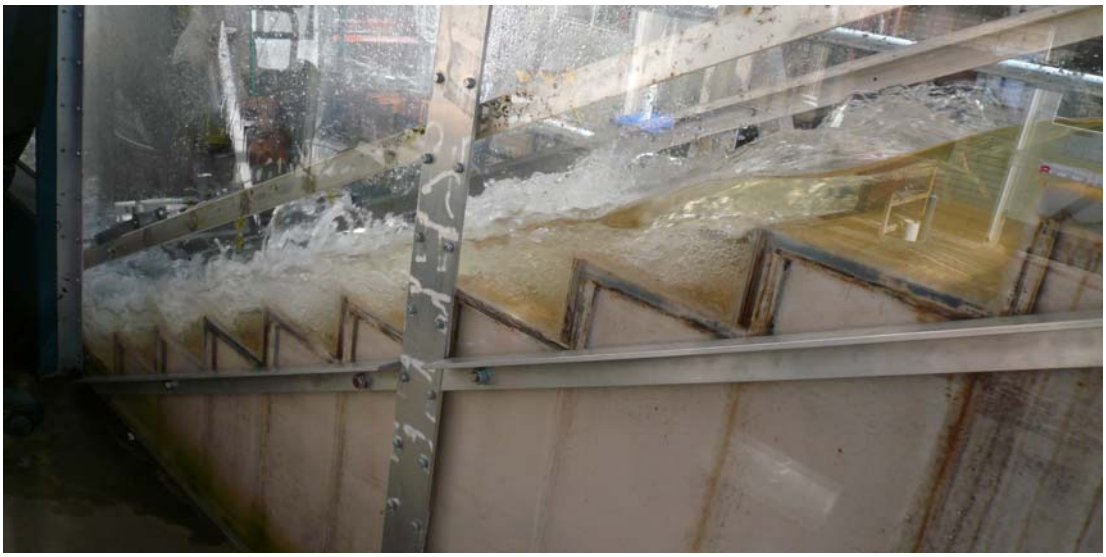

An intermediate flow regime ($0.86 \leq d_c/h \leq 1.03$) was characterised by a skimming flow regime on the pooled stepped side, and some transition flow on the flat stepped side of the spillway. On the pooled side of the stepped chute, the large air-water depth above the pool weir yielded some recirculation processes beneath the pseudo-bottom formed by the pool weir edges. At the flat side of the channel, the flow remained highly chaotic with some singular aeration processes caused by jets from the pooled side and air pockets in the cavities. These disturbances were caused by the three-dimensional flow motion. Free-surface aeration and a flapping air-water surface at the inception point of air entrainment was clearly seen for this intermediate flow regime. The transverse slope of the free-surface became smaller compared to the transition flow regime. The air-water depths at the pool side of the channel were larger than on the flat side. In the clear-water flow region upstream of the inception point, the water surface appeared three-dimensional and was not parallel to the pseudo-bottom formed by the step edges. Generally, the three-dimensional flow motion and flow disturbances caused by the pools became comparatively less significant with increasing discharges. A consistent definition of the flow across the entire channel width was not possible.

With increasing discharges $d_c/h > 1.03$, a skimming flow was observed on both sides of the channel. Some recirculation processes in the step cavities were observed with some distinct free-surface aeration (Fig. 3-9). In the skimming flows, the singular aeration processes by jets were much less intense while, the flow became more uniform across the different channel sides downstream of the inception point of free-surface aeration. The free-surface was almost horizontal in the transverse direction and there was almost no flow motion in the transverse direction (Fig. 3-9). In Figure 3-9, some flow disturbances remained visible in the clear-water flow region upstream of the inception point together with some distinct surface flapping immediately upstream of the inception point.

Fig. 3-9 – Skimming flow regime on the stepped spillway with in-line configuration of flat and pooled steps ($\theta = 26.6°$): $d_c/h = 1.15$, $Q = 0.063$ m^3/s, $Re = 4.9\times10^5$

The skimming flows showed some similarities to those observed on the flat and pooled stepped spillways. However the flow showed comparatively larger droplet ejections and the recirculation processes in the cavities appeared more irregular and disturbed compared to the uniform flat and pooled stepped spillways.

3.4.3 Specific air-water flow features and instabilities

For all flow rates, some standing sidewall waves and shock waves were observed on the stepped spillway with in-line configuration of flat and pooled steps. Examples of sidewall standing waves and shock waves on the channel centreline are shown in Figure 3-10. These instabilities were associated with discontinuities often observed in supercritical flows (TOOMBES 2002; TOOMBES & CHANSON 2008b). The sidewall standing waves and the shock waves in channel centreline led to some singular aeration processes by plunging jets. A clear separation between free-falling jets and standing sidewall waves was not always possible.

A change in flow direction at the first step resulted in the formation of the sidewall standing waves. The water was forced against the wall and narrow standing waves formed similar to the bow-waves on a ship (TOOMBES 2002). SCHWALT & HAGER (1993) observed some similar patterns on the wall opposite to channel junctions and mitre bends. Abrupt channel expansions may also cause standing sidewall waves (HAGER & MAZUMDER 1992). Herein, the maximum height of the waves tended to decrease with increasing discharges.

The different invert design between the two channel sides prevented a symmetrical behaviour. Sidewall standing waves were seen on the pooled side of the channel only. The sidewall standing

waves were not highly aerated but yielded some air entrainment in the downstream step cavity. In transition and skimming flows, some sidewall waves leaned inwards towards the centreline and caused some droplet spray and splashing. The height of the standing sidewall waves reached a maximum value of about three times the step height: that is, $d_{SS} \approx 3 \times h = 0.3$ m. The wave length varied from a minimum of one step length ($l_{SS} = 0.2$ m) to a maximum wave length of over 3 steps ($l_{SS} > 3 \times l = 0.6$ m). With increasing discharges, both the wave height and wave length decreased.

Fig. 3-10 – Definition sketch and photograph of shock waves and standing sidewall waves for the stepped spillway with in-line configuration of flat and pooled steps ($\theta = 26.6°$)

(A) Sketch of dimensions of the sidewall standing waves and shock waves

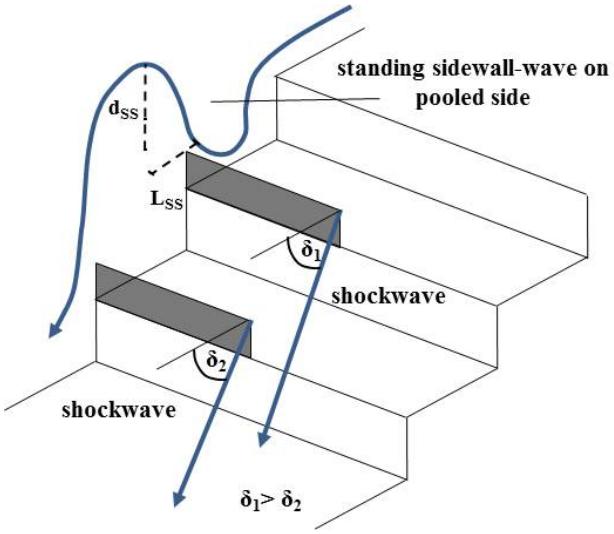

(B) Standing sidewall waves, $d_c/h = 0.50$, $Q = 0.018$ m^3/s, $Re = 1.4 \times 10^5$

(C) Shockwaves, $d_c/h = 0.50$, $Q = 0.018$ m^3/s, $Re = 1.4 \times 10^5$

(D) Standing sidewall waves, $d_c/h = 0.50$, $Q = 0.018$ m^3/s, $Re = 1.4 \times 10^5$

In addition, some shock waves, also termed cross-waves, were observed in the present study. They can be described as oblique waves that leaned inwards from the sidewalls and propagated across the

channel (TOOMBES 2002). They were flow discontinuities associated with large shear stresses. Figure 3-10 shows some example of shock waves on the spillway centreline, where δ_1 and δ_2 are the shock wave angles to the flow direction at the first and second pool weir respectively. Present observations yielded $\delta_1 > \delta_2$ while δ_1 and δ_2 varied between 5° and 30°, becoming smaller with increasing discharges. Further downstream, the values of the angles became very close to each other between subsequent step edges.

3.5 AIR-WATER FLOW PATTERNS ON THE STEPPED SPILLWAY WITH STAGGERED CONFIGURATION OF FLAT AND POOLED STEPS

3.5.1 Presentation

Detailed visual observations were conducted on the stepped spillway with a staggered arrangement of flat and pooled steps for a range of dimensionless discharges $0.02 \leq d_c/h \leq 2.0$. For all discharges, the flow was characterised by some relatively uniform flow features across the channel width. However some wavy flow patterns from side to side of the channel were seen. Typical flow regimes such as nappe, transition and skimming flows were distinguished, presenting some similarities to the observations on flat and pooled stepped spillway configurations. Details are presented in section 3.5.2.

In the transverse direction, the flow was observed to be reasonably uniformly distributed in both sections of the channel for each second adjacent step edge for regions far downstream of the inception point of free-surface aeration. At the upstream end of the chute, the clear-water flow region between broad-crested weir and inception point showed some instabilities in terms of standing sidewall waves, shock waves and transverse interactions on the channel centreline depending on the discharge (see paragraph 3.5.3). Further photographs of the flow patterns are presented in Appendix A.

3.5.2 Flow regime observations

The staggered stepped spillway configuration yielded some significant droplet ejections as well as some differences in water depth on every second adjacent flat and pooled step edges. The flow was characterised by some unsteady air pocket distributions in the cavities and singular aeration processes could be observed.

For small flow rates $d_c/h < 0.56$, a nappe flow regime existed with a succession of free-falling jets (Fig. 3-11). For the lowest discharges $d_c/h < 0.40$, the jets plunged from each step edge to the next adjacent pool, yielding some larger water depth upon the pooled step weirs (Fig. 3-11A). With increasing discharges $0.40 < d_c/h < 0.56$, the jets plunged over each second step from pool to pool

leading to distinct air pockets in the flat step cavities and the pooled step cavities were filled with air-water flows (Fig. 3-11B). The pools seemed to induce a succession of longer free-falling nappes along two step lengths. This feature was observed on both sides of the channel and yielded to some transverse interactions across the channel centreline.

Fig. 3-11 - Nappe flow regime on the stepped spillway with staggered configuration of flat and pooled steps ($\theta = 26.6°$)

(A) $d_c/h = 0.29$, $Q = 0.009$ m^3/s, $Re = 6.2\times10^4$

(B) $d_c/h = 0.56$, $Q = 0.020$ m^3/s, $Re = 1.64\times10^5$

A wavy flow appearance from side to side was observed along the entire channel length. It was associated with distinctive jet flows which were highly aerated and induced some singular aeration in the downstream cavity. Some distinct ejected droplets and splashing featured the flow as chaotic and unstable. The resulting flow motion in the transverse direction with strong waving flow feature

was not comparable to the observations on the stepped spillways with flat or pooled stepped, or even in-line stepped, configurations.

For larger discharges $0.56 \leq d_c/h \leq 0.92$, a transition flow occurred along the stepped chute. Some jets plunged over each second adjacent step edge. The step cavities of both flat and pooled steps showed no air pockets and some intense free-surface aeration was observed. However, the water depths at the pooled steps were consistently larger than those at the flat steps. The air-water mixture was highly aerated, showing some chaotic behaviour and transverse interactions on the channel centreline. The waving appearance of the flow from side to side became less significant than in the nappe flow regime. Distinct droplet ejection and spray were observed downstream of the inception point. The bulk of the flow appeared chaotic with lateral flow motion in the transverse direction across the channel width. Singular aeration processes were present mainly in the pooled step cavities. Some similarities of the transition flow regime on the staggered stepped spillway configuration were observed comparable to the flat and pooled stepped spillway flow patterns.

For larger discharges $d_c/h > 0.92$, a skimming flow regime was observed. The recirculation in the step cavities was clearly observed. The basic flow features were comparable to those on flat and pooled stepped spillways. However, the recirculation processes were unsteady and disturbed by the staggered stepped configuration. Some three-dimensional flow motion in the transverse direction was present leading to some distinct droplet ejection and spraying. The flow appeared highly aerated and the water depths above the pooled step weirs were larger than on the flat step edges. The air-water surface at the inception point of free-surface aeration showed some irregular flapping. Figure 3-13 shows a side view of the flow next to the inception point. Note the droplet ejection in the downstream section of the channel.

Fig. 3-12 – Transition flow regime on the stepped spillway with staggered configuration of flat and pooled steps ($\theta = 26.6°$): $d_c/h = 0.70$, $Q = 0.030$ m^3/s, $Re = 2.30 \times 10^5$

Fig. 3-13 – Skimming flow regime on the stepped spillway with staggered configuration of flat and pooled steps ($\theta = 26.6°$): $d_c/h = 1.45$, $Q = 0.090$ m^3/s, $Re = 6.9\times10^5$

3.5.3 Specific air-water flow features and instabilities

The stepped spillway with staggered stepped configuration of flat and pooled steps showed some irregular occurrence of standing sidewall and shock waves for all flow regimes (Fig. 3-14). Figure 3-14 illustrates some examples. An asymmetrical and three-dimensional flow motion was observed in the clear-water flow in the upstream part of the channel for all discharges. They caused some instabilities in the downstream air-water flow region. Further downstream some waves could be observed for each second adjacent step. The height of the standing sidewall waves showed a maximum value of about three times the step height: i.e., $d_{SS} \approx 3\times h = 0.3$ m. The wave length varied from a minimum wave length of one step length ($l_{SS} = 0.2$ m) and a maximum wave length over 3 step lengths ($l_{SS} \approx 3\times l = 0.6$ m). The sidewall standing wave lengths and heights were comparable to those observed on the stepped spillway with in-line configuration of flat and pooled steps. With increasing discharges, both wave height and wave length became smaller.

The shock waves occurred predominantly on the spillway centreline and the direction of the shock waves differed between adjacent steps because of the staggered configuration of flat and pooled steps (Fig. 3-14A & 3-14C). Further downstream the shock waves intersected the downstream shock waves leading to some visible air-water mixing and air entrainment. Downstream of the shock wave intersection, the flow appeared almost uniform.

The shock waves occurred mainly in the upstream part of the stepped spillway with nearly constant angles δ between adjacent pool weir edges (Fig. 3-14A). The cross-waves were seen for all flow

rates. The shock wave angle δ ranged between δ = 5° to 20°. Figure 3-14 illustrates some standing sidewall and shock waves for the staggered stepped configuration.

Fig. 3-14 – Shockwaves and standing sidewall waves for the stepped spillway with staggered configuration of flat and pooled steps

(A) Definition sketch of sidewall standing waves and shock waves

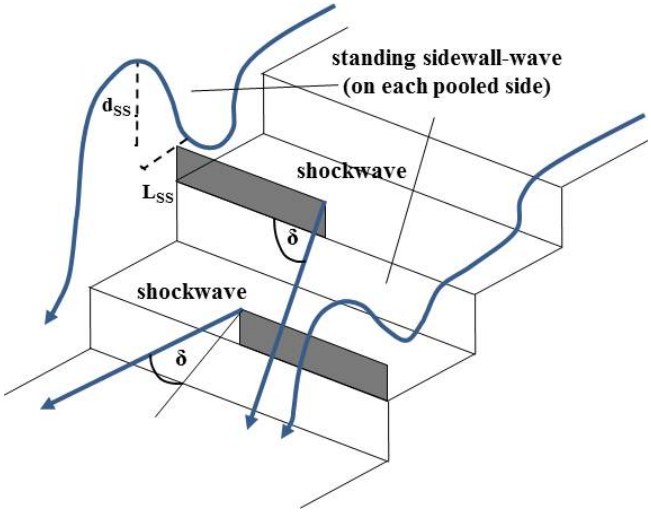

(B) Standing sidewall waves, d_c/h = 0.66, Q = 0.028 m^3/s, Re = 2.1×10^5

(C) Shockwaves, d_c/h = 0.86, Q = 0.041 m^3/s, Re = 3.1×10^5

(D) Standing sidewall waves, d_c/h = 0.59, Q = 0.023 m^3/s, Re = 1.8×10^5

3.6 INCEPTION POINT OF AIR ENTRAINMENT

For all stepped spillway configurations, the location of the inception point of free-surface aeration was documented. Table 3-2 summarises further the changes in flow regimes for all configurations. For the stepped spillway with in-line configuration of flat and pooled steps, the changes in flow regimes are shown for both halves of the stepped chute, i.e. for the pooled stepped and the flat stepped sides respectively (Table 3-2). The changes in flow regimes were reasonably close for all

stepped spillway configurations, with some small differences for the stepped spillway geometries with in-line and staggered stepped configurations. Overall the changes in flow regimes in the present study were close to previous findings on stepped spillways with similar slopes $21.8° \leq \theta \leq 30°$ (CHANSON 2001; CHANSON & TOOMBES 2002b; CAROSI & CHANSON 2008; KÖKPINAR 2004; FELDER & CHANSON 2009a,2011b).

The location of the inception points of free-surface aeration was recorded for $0.002 \leq Q \leq 0.155$ m^3/s. The results are reported in Figure 3-15 in dimensionless terms, where L_I is the distance from the first step edge (i.e. downstream end of broad-crest) to the inception point of free-surface aeration and k_s is the step cavity height normal to the main stream flow: $k_s = h \times \cos\theta$ for flat stepped spillway and $k_s = (h+w) \times \cos\theta$ for the pooled stepped spillway. For the stepped spillway configuration with in-line configurations of flat and pooled stepped steps, the step cavity height was calculated with $k_s = h \times \cos\theta$ for the inception point data on the channel half with flat steps and for the pooled stepped side $k_s = (h+w) \times \cos\theta$. It was not possible to identify a clear step cavity height for the staggered configuration of flat and pooled steps and the inception point data are presented for both cavity height definitions in Figure 3-15. The data are presented as a function of the Froude number F* defined in terms of the step cavity roughness:

$$F^* = \frac{q_w}{\sqrt{g \times \sin\theta \times k_s^3}} \quad (3\text{-}1)$$

The inception point data for all configurations were in good agreement (Fig. 3-15). Some small differences were visible for the side with flat steps in the stepped spillway configuration with in-line configuration of flat and pooled steps. For the smallest flow rates, the inception point location did not change on the flat stepped side in this configuration which was linked with a jet causing the air-entrainment at step edges 4 to 5 for a range of discharges. Furthermore some small differences in the position of inception points were observed for the staggered configuration of flat and pooled steps calculated with step cavity height $k_s = (h+w) \times \cos\theta$ and the air entrainment appeared further upstream compared to the other stepped spillway configurations.

The present inception point observations were compared with two empirical correlations for flat stepped spillways by CHANSON (1995):

$$\frac{L_I}{h \times \cos\theta} = 9.719 \times (\sin\theta)^{0.0796} \times F^{*0.713} \quad 27° \leq \theta \leq 53° \quad (3\text{-}2)$$

and by CAROSI & CHANSON (2008) for a flat stepped spillway with a slope of 21.8°:

$$\frac{L_I}{h \times \cos\theta} = 1.05 + 5.11 \times F^* \quad 0.45 \leq d_c/h \leq 1.6 \quad (3\text{-}3)$$

Table 3-2 - Flow regime changes for the stepped spillway configurations investigated in the present study (θ = 26.6°)

Configuration (1)	NA - TRA (2)	TRA - SK (3)
Flat stepped spillway	$d_c/h = 0.5$	$d_c/h = 0.9$
Pooled stepped spillway	$d_c/h = 0.45$	$d_c/h = 0.97$
Stepped spillway with in-line configuration of flat & pooled steps		
Pooled stepped side	$d_c/h = 0.46$	$d_c/h = 0.86$
Flat stepped side	$d_c/h = 0.57$	$d_c/h = 1.03$
Stepped spillway with staggered configuration of flat and pooled steps	$d_c/h = 0.56$	$d_c/h = 0.92$

Notes: d_c: critical flow depth; h: vertical step height; NA: nappe flow regime; TRA: transition flow regime; SK: skimming flow regime

Fig. 3-15 – Location of inception point of air entrainment for the stepped spillway configurations in the present study; Comparison with empirical correlations and pooled stepped spillway data

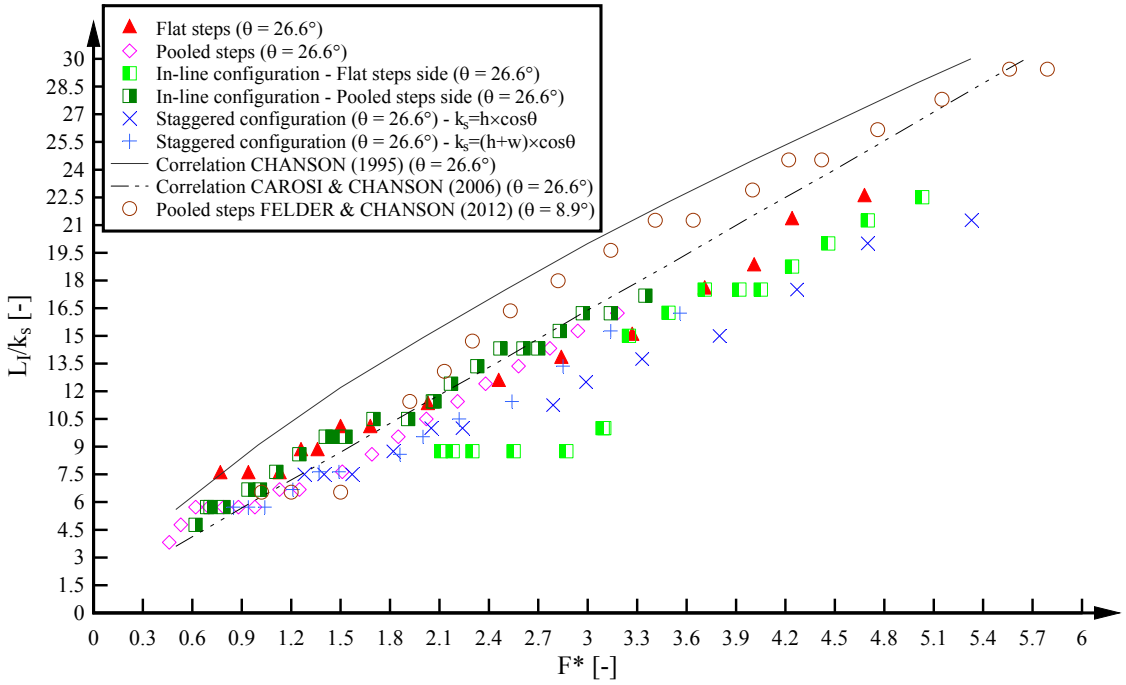

Both empirical equations are shown for the channel slope of 26.6° in Figure 3-15 and the results showed a reasonable agreement with Equation (3-2) and a close agreement for the correlation of CAROSI & CHANSON (2008). The present data are further compared with some inception point observations on a pooled stepped spillway with 8.9° slope by FELDER & CHANSON (2012a) (Fig. 3-15). Overall there was a good agreement between all data sets, independently of the step type (flat

or pooled).

3.7 CAVITY EJECTION PROCESSES ON FLAT AND POOLED STEPPED SPILLWAYS

At large flow rates, the waters skimmed over the pseudo-bottom formed by the step edges with some cavity recirculation processes in the cavities underneath. The cavity recirculation was highly energetic and it was maintained by the transmission of shear stress from the main stream and some momentum exchanges between main stream and cavity flows (DJENEDI et al. 1999; CHANSON et al. 2002). At irregular time intervals, some air-water volume was ejected out and replaced by some fresh fluid flow into the step cavity. The present observations indicated that the ejection processes were comparable on both flat and pooled stepped spillway configurations.

Herein the cavity ejection frequencies were visually observed for the flat and pooled stepped spillways and a detailed frame-by-frame video analysis was performed. Figure 3-16 illustrates the dimensionless cavity ejection frequencies $F_{ej} \times d_c/V_c$ as a function of the Reynolds number Re defined in terms of the hydraulic diameter for both flat and pooled stepped spillway data. For each discharge, the ejection frequencies were observed at several successive step cavities downstream of the inception point of air entrainment and at different positions within the step cavity. Figure 3-16 includes also the longitudinally-averaged and median ejection frequencies.

Fig. 3-16 - Average dimensionless ejection frequencies $F_{ej} \times d_c/V_c$ as function of the Reynolds number Re for flat and pooled stepped spillways ($\theta = 26.6°$) in skimming flows

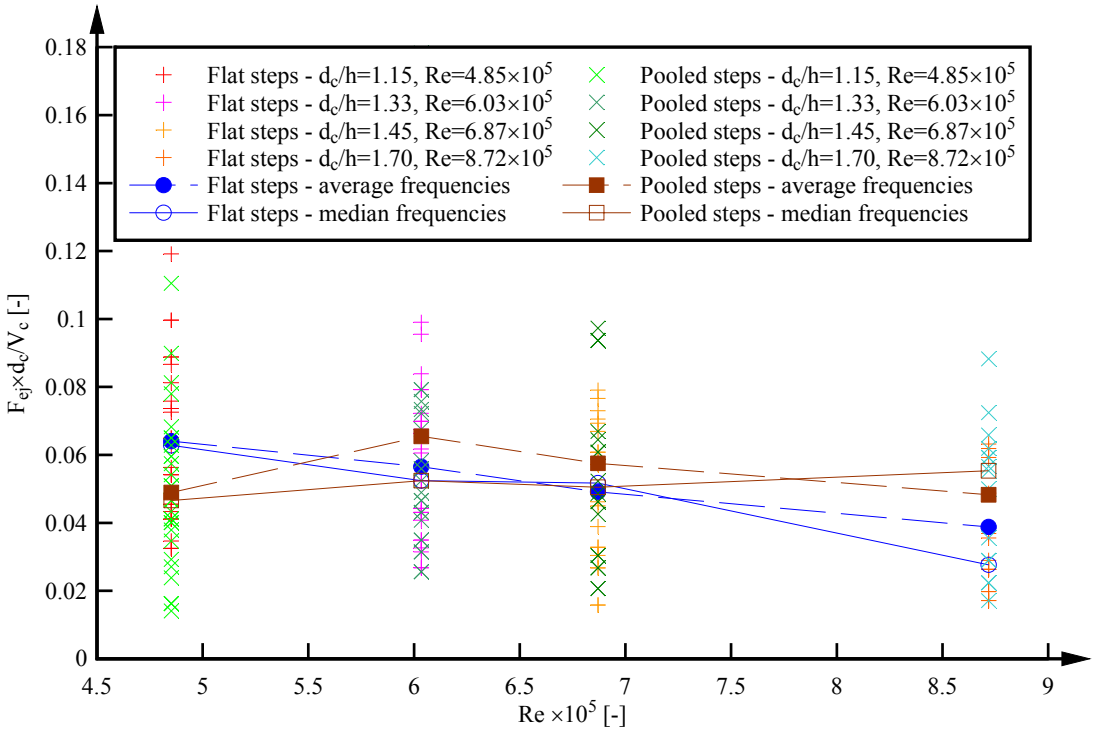

The data yielded on average a dimensionless cavity ejection frequency $F_{ej} \times d_c/V_c$ between 0.07 and 0.03, with a decreasing frequency with increasing Reynolds numbers for both spillway configurations (Fig. 3-16). Further details about the experiments and the results can be found in Appendix B.

3.8 SUMMARY AND DISCUSSION

A number of visual observations were conducted on stepped spillways equipped with several step configurations: flat steps, pooled steps, in-line and staggered configurations of flat and pooled steps. For a relatively wide range of flow rates, the basic flow patterns were documented in nappe, transition and skimming flows. All stepped spillway flows showed some intense free-surface aeration downstream of the inception point of air entrainment. Some instabilities were observed for several stepped spillway configurations.

The air-water flow patterns on the flat stepped spillway were identical to previous observations. The air-water flow patterns on the pooled stepped spillway were close to those observed on the flat stepped spillway, but with some stronger droplet ejections and instabilities. For the smallest flow rates in the nappe flow regime, some pulsating flow pattern was observed in the first pooled step cavity and the instabilities propagated downstream. Overall, however, the pooled stepped spillway with a slope of $\theta = 26.6°$ exhibited much smaller instabilities compared to those observed on a pooled stepped spillway with $\theta = 8.9°$ (THORWARTH 2008; FELDER et al. 2012, FELDER & CHANSON 2012a).

Some cavity ejection frequencies were documented in some frame-by-frame video analyses for both flat and pooled stepped spillways in skimming flows. The ejection frequencies were close for the flat and pooled stepped spillway configurations.

The stepped spillways with in-line and staggered configurations of flat and pooled steps showed much more complicated flow patterns. Some strong three-dimensional flow motion was seen for all flow rates. The flow motion in the transverse direction caused some strong instabilities along the stepped spillways as well as some shock waves on the channel centreline while some sidewall standing waves were observed along the stepped spillway walls. The instabilities led to some very strong splashing of droplets in all flow directions along the stepped spillways. Both the in-line and staggered stepped spillway configurations showed more irregular flow patterns compared to the flat and pooled stepped spillways. The findings suggest that the flat stepped spillway designs may be better suited for stepped spillway designs. For example, the sidewall standing waves would result in a larger sidewall height and an increased spillway cost.

For all stepped spillway configurations, the location of the inception point of air entrainment was documented for a range of flow rates. Overall the results were in relatively close agreement with

some differences for the in-line and staggered configured stepped spillways.

In conclusion, the flat stepped spillway appeared to be best suited in terms of the flow patterns for a practical design. The pooled stepped spillway showed some small differences, including some strong instabilities for a flow rate. The more complex in-line and staggered designs of stepped spillways showed some flow instabilities with some strong three-dimensional flow patterns including shock waves in centreline and standing sidewall waves at the channel walls.

4. AIR-WATER FLOW PROPERTIES ON THE STEPPED SPILLWAYS: FLAT VERSUS POOLED STEPS

4.1 PRESENTATION

The air-water flow measurements were performed on the flat and pooled stepped spillway configurations for $0.03 \leq Q \leq 0.13$ m^3/s. The stepped spillway flow was characterised by significant air entrainment downstream of the inception point and detailed two-phase flow measurements were conducted. Some experiments were performed with a double-tip conductivity probe at all step edges downstream of the inception point (Table 4-1). Table 4-1 lists the investigated flow conditions in transition and skimming flows for the experiments with the double-tip probe. The measurements yielded some air-water flow properties including the void fraction C, the bubble count rate F, the interfacial velocity V, the turbulence intensity Tu and the air bubble and water droplet chord sizes.

Some additional experiments were conducted with an array of two identical single-tip conductivity probes for the flat and pooled stepped spillways. The measurements were conducted at the downstream end of the spillway (step edge 10) for two flow rates in the skimming flow regime (Table 4-2). Table 4-2 presents the flow conditions and lists the transverse distances between the two single-tip probes $3.5 \leq \Delta z \leq 81.3$ mm. An integration of the maximum cross-correlation values $(R_{xz})_{max}$ between the raw data of the two single-tip probes with various spacing Δz provided the integral turbulent length scale (CHANSON & CAROSI 2007):

$$L_{xz} = \int_{z=0}^{z=z((R_{xz})_{max}=0)} (R_{xz})_{max} \times dz \quad (4\text{-}1)$$

The corresponding integral turbulent time scale was also calculated:

$$T_{int} = \frac{1}{L_{xz}} \times \int_{z=0}^{z=z((R_{xz})_{max}=0)} (R_{xz})_{max} \times T_{xz} \times dz \quad (4\text{-}2)$$

where T_{xz} is the cross-correlation integral time scale calculated in an integration from the maximum of the cross-correlation function until the first crossing of the x-axis.

A range of experiments was systematically conducted with the double-tip and the two single-tip conductivity probes. All probes were sampled for 45 s with a sampling frequency of 20 kHz. In this section, the characteristic results for the flat and pooled stepped spillways are compared and additional experimental data are shown in Appendix C. Some further flow features for the pulsating flow on the pooled stepped spillway ($d_c/h = 0.4$) are presented and discussed in Appendix E.

Table 4-1 - Air-water flow measurements with a double-tip conductivity probe (Ø = 0.25 mm) for the flat and pooled stepped spillways (θ = 26.6°)

Configuration (1)	d_c/h [-] (2)	Q [m^3/s] (3)	Re [-] (4)	Measurements at step edge (5)	Inception point step edge (6)	Flow regime (7)
Flat stepped spillway	0.7	0.030	2.30×10^5	4-10	3 to 4	TRA
	0.82	0.038	2.90×10^5	4-10	4	TRA
	0.96	0.049	3.71×10^5	5-10	5	SK
	1.15	0.063	4.85×10^5	5-10	5 to 6	SK
	1.29	0.075	5.73×10^5	6-10	6	SK
	1.45	0.090	6.87×10^5	7-10	7	SK
	1.52	0.097	7.39×10^5	8-10	8	SK
	1.7	0.113	8.72×10^5	8-10	8 to 9	SK
Pooled stepped spillway	0.4	0.013	9.95×10^4	2-10	2	NA
	0.7	0.030	2.30×10^5	4-10	4	TRA
	0.82	0.038	2.90×10^5	5-10	4 to 5	TRA
	0.96	0.049	3.71×10^5	6-10	5 to 6	TRA/SK
	1.15	0.063	4.85×10^5	5-10	5 to 6	SK
	1.29	0.075	5.73×10^5	7-10	6 to 7	SK
	1.45	0.090	6.87×10^5	7-10	7	SK
	1.52	0.097	7.39×10^5	8-10	8	SK
	1.7	0.113	8.72×10^5	8-10	8	SK
	1.85	0.130	9.89×10^5	10	9 to 10	SK

Notes: d_c: critical flow depth; h: vertical step height; Q: water discharge; Re: Reynolds number defined in terms of the hydraulic diameter; SK: skimming flow regime; TRA: transition flow regime; NA: nappe flow regime.

Table 4-2 - Air-water flow measurements with an array of two single-tip conductivity probes (Ø = 0.35 mm) for the flat and pooled stepped spillways (θ = 26.6°)

Configuration (1)	d_c/h [-] (2)	Q [m^3/s] (3)	Re [-] (4)	Measurement at step edge (5)	Transverse distances between single-tip probes Δz (mm) (6)
Flat stepped spillway	1.15	0.063	4.85×10^5	10	3.5, 6.9, 10.5, 16.2, 21.6, 28.2, 35.1, 41.4, 49.2, 61.2, 81.3
	1.45	0.090	6.87×10^5	10	3.5, 6.5, 10.1, 15.1, 20.9, 27.8, 34.4, 44.0, 50.1, 60.6, 80.5
Pooled stepped spillway	1.15	0.063	4.85×10^5	10	3.5, 6.5, 11.1, 15.7, 21.2, 26.5, 34.7, 41.3, 50.1, 61.2, 80.1
	1.45	0.090	6.87×10^5	10	3.5, 6.5, 11.1, 15.7, 21.2, 26.5, 34.7, 41.3, 50.1, 61.2, 80.1

4.2 COMPARISON OF AIR-WATER FLOW PROPERTIES

4.2.1 Void fraction

Some typical void fraction distributions in a skimming flow regime are illustrated in Figure 4-1 as a function of y/Y_{90} (Fig. 4-1A) and as a function of $(y+w)/d_c$ (Fig. 4-1B). Herein y is the distance perpendicular to the pseudo-bottom formed by the step edges, Y_{90} is the elevation y where the void fraction was 90%, d_c is the critical flow depth and w is the pool weir height for the pooled steps. For the flat steps, y = 0 was located at the step edge. For the pooled steps, y = 0 was at the edge of the pool weir.

The void fraction distributions for both stepped configurations showed some typical S-shapes which were observed in many previous studies on flat stepped spillways in transition and skimming flows (Fig. 4-1) (CHANSON & TOOMBES 2002; GONZALEZ 2005; BUNG 2011). Little difference was visible between flat and pooled stepped spillways (Fig. 4-1A). In Figure 4-1A, the distributions of void fraction are compared with the advective diffusion equation developed by CHANSON & TOOMBES (2002):

$$C = 1 - \tanh^2\left(K' - \frac{y/Y_{90}}{2 \times D_o} + \frac{(y/Y_{90} - 1/3)^3}{3 \times D_o}\right) \quad (4\text{-}3)$$

where K' is an integration constant and D_o is a function of the depth-averaged void fraction C_{mean} only:

$$K' = 0.32745015 + \frac{1}{2 \times D_o} - \frac{8}{81 \times D_o} \quad (4\text{-}4)$$

$$C_{mean} = 0.7622 \times (1.0434 - \exp(-3.614 \times D_o)) \quad (4\text{-}5)$$

Figure 4-1B illustrated a different presentation of the void fraction distributions: i.e., in terms of $(y+w)/d_c$. The results showed also little differences between the data, but an upward shift of the void fraction profile for the pooled steps by the dimensionless pool height w/d_c. For the first two step edges immediately downstream of the inception point, some slightly different void fraction profiles were observed, but these were consistent with the rapidly varying nature of the flow in the vicinity the inception point of air entrainment.

For the flat stepped spillway, the void fraction data seemed to suggest a local maximum in void fraction for y/Y_{90} = 0.1 to 0.2 at some step edge (Fig. 4-1). The cause of the local maxima was not entirely clear, but it might be linked with a longitudinal seesaw pattern earlier documented in terms of several characteristic air-water flow properties (BOES 2000; CHANSON & TOOMBES 2002; FELDER & CHANSON 2009b).

Overall the present observations tended to confirm the comparative findings of FELDER & CHANSON (2012a) on a stepped spillway with 8.9° slope and of KÖKPINAR (2004) with a slope

of 30°.

Fig. 4-1 – Comparison of void fraction distributions on the flat and pooled stepped spillways in skimming flows (θ = 26.6°)

(A) $d_c/h = 1.52$, $Q = 0.097$ m^3/s, $Re = 7.4\times10^5$ (B) $d_c/h = 1.15$, $Q = 0.063$ m^3/s, $Re = 4.9\times10^5$

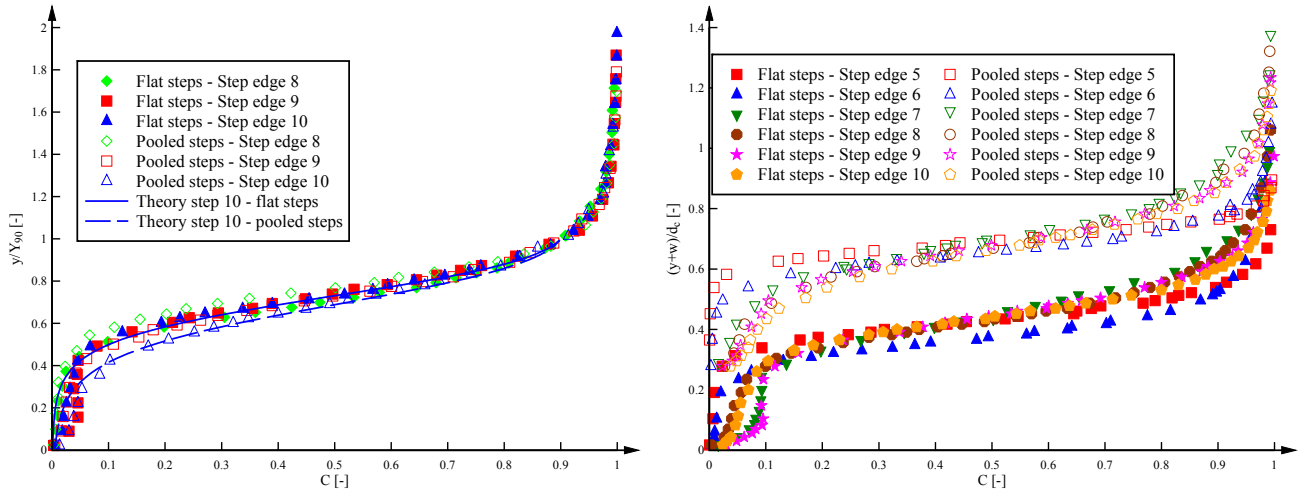

4.2.2 Bubble count rate

Figure 4-2 shows some typical dimensionless distributions of the bubble count rate $F\times d_c/V_c$ in skimming flows as functions of y/Y_{90} (Fig. 4-2A) and $(y+w)/d_c$ (Fig. 4-2B). Herein V_c is the critical flow velocity ($V_c = \sqrt{g\times d_c}$). The distribution of bubble count rates showed typical shapes with maxima in the intermediate flow region for void fractions of about C = 0.4 to 0.5 for both flat and pooled steps. For all data sets, the number of entrained air bubbles was larger on the flat stepped spillway compared to the results on the pooled stepped configuration (Fig. 4-2). The differences between the two configurations tended to decrease with increasing distance from the inception point of air entrainment. Note that, for all experiments, the equilibrium flow conditions were not achieved and the bubble count rates increased monotonically with longitudinal distance for both flat and pooled steps along the stepped spillway.

The present results were consistent with earlier experimental results on flat stepped spillways (e.g. CHANSON & TOOMBES 2002; BUNG 2011). Interestingly FELDER & CHANSON (2012a) and FELDER et al. (2012) observed also a larger numbers of entrained air bubbles on a flat stepped spillway with a slope of 8.9° compared to a pooled stepped spillway with the same ratio of w/l = 0.16 as in the present study. On the other hand, however, KÖKPINAR (2004) observed much smaller differences in terms of bubble count rates between flat and pooled steps down a 30° stepped chute. This might be linked with the different cavity size on the pooled stepped spillway with a rate w/l = 0.29.

Fig. 4-2 – Comparison of dimensionless bubble count rate distributions on the flat and pooled stepped spillways in skimming flows (θ = 26.6°)

(A) $d_c/h = 0.96$, Q = 0.049 m^3/s, Re = 3.7×10^5 (B) $d_c/h = 1.45$, Q = 0.090 m^3/s, Re = 6.9×10^5

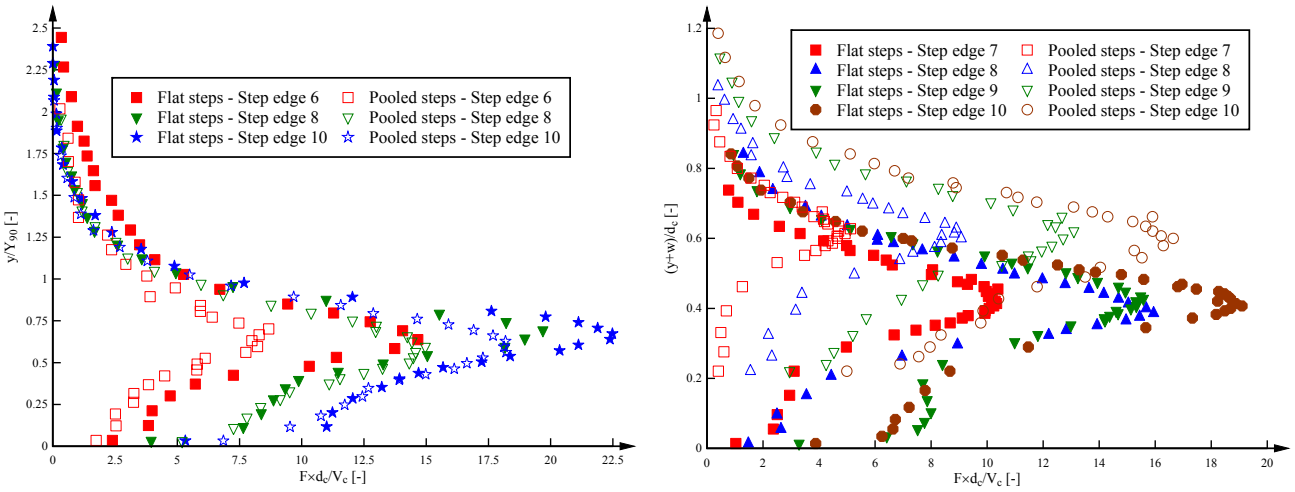

4.2.3 Interfacial velocity

The interfacial time averaged local velocity V was calculated based upon a cross-correlation analysis of the raw signals of the two tips of the double-tip conductivity probe. Some typical results for the skimming flow experiments are illustrated in Figure 4-3. In Figure 4-3A, some distributions of the dimensionless interfacial velocity V/V_{90} are illustrated as a function of y/Y_{90}, where V_{90} is the characteristic velocity at C = 90%. All data on the flat and pooled stepped spillways were in good agreement and they compared very well with a power law (Fig. 4-3A):

$$\frac{V}{V_{90}} = \left(\frac{y}{Y_{90}}\right)^{1/N} \qquad 0 \leq y/Y_{90} \leq 1 \quad (4\text{-}4)$$

The exact value of N may vary from one step edge to the next one for a given flow rate, with N = 10 on average. In Figure 4-3, the data are compared with a 1/10 power law. For $y/Y_{90} > 1$, the velocity distributions had a uniform profile and were best correlated by:

$$\frac{V}{V_{90}} = 1 \qquad 1 > y/Y_{90} \quad (4\text{-}5)$$

The observations were consistent with previous data on flat stepped spillways (GONZALEZ 2005; CHANSON & CAROSI 2007; FELDER & CHANSON 2009b). Furthermore the velocity data agreed well with the observations on flat and pooled stepped spillways with 8.9° slope by FELDER & CHANSON (2012a) and FELDER et al. (2012). KÖKPINAR (2004) observed a power law exponent of N = 6 for his data on flat and pooled steps with 30° slopes, together with a good agreement between flat and pooled step data. BUNG's (2011) approach yielded N = 8 for flat stepped spillways with a 26.6° slope.

Some differences were however visible in terms of the dimensionless interfacial velocity V/V_c in the present study (Fig. 4-3B). For all present experiments, the data implied larger interfacial velocities on the pooled stepped spillway (Fig. 4-3B). This finding was counter-intuitive and contradicted the observations on a 8.9º slope pooled stepped chute (FELDER & CHANSON 2012a; FELDER et al. 2012). The present observations nonetheless showed consistently a faster flow motion down the pooled stepped chute ($\theta = 26.6°$) for a wide range of flow conditions ($0.8 < d_c/h < 1.85$).

Fig. 4-3 – Comparison of dimensionless interfacial velocity distributions on the flat and pooled stepped spillways in skimming flows ($\theta = 26.6°$)

(A) $d_c/h = 1.29$, $Q = 0.075$ m^3/s, $Re = 5.7\times10^5$ (B) $d_c/h = 1.7$, $Q = 0.113$ m^3/s, $Re = 8.7\times10^5$

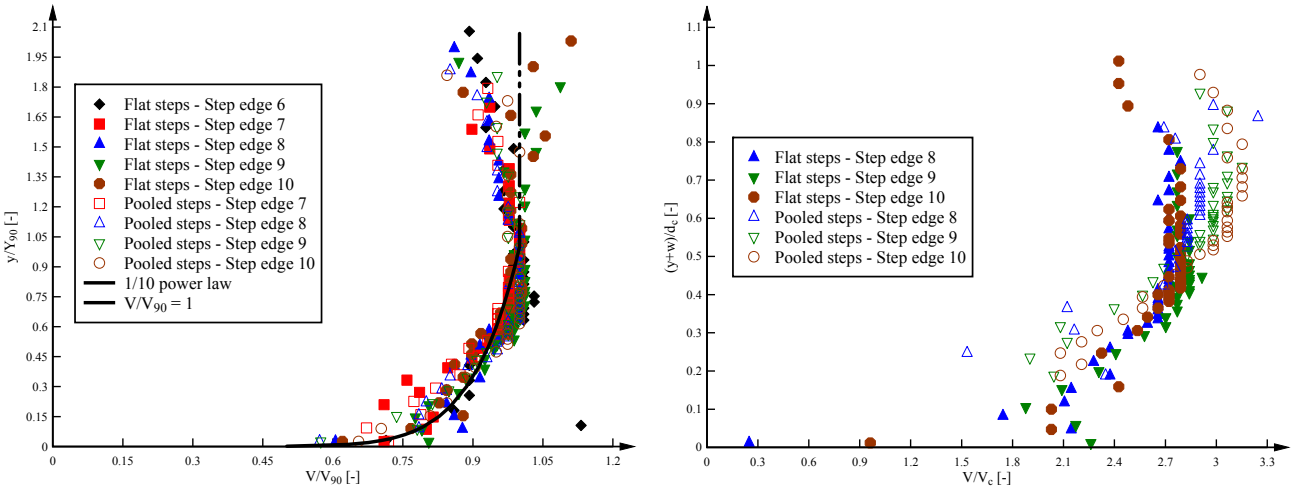

4.2.4 Turbulence intensity

The shape of the cross-correlation function of the double-tip conductivity probe provided some information about the turbulence levels in the two phase flow. Following CHANSON & TOOMBES (2002), the turbulence intensities were calculated as:

$$Tu = 0.851 \times \frac{\sqrt{\tau_{0.5}^{\ 2} - T_{0.5}^{\ 2}}}{T} \qquad (4\text{-}6)$$

where $\tau_{0.5}$ is the time scale for which the cross-correlation function is half of its maximum value such as: $R_{xy}(T+\tau_{0.5}) = 0.5\times R_{xy}(T)$, R_{xy} is the normalised cross-correlation function and $T_{0.5}$ is the characteristic time for which the normalised auto-correlation function equals: $R_{xx}(T_{0.5}) = 0.5$. The turbulence intensity Tu is a measure of the turbulence levels within the air-water flows, although it might not be truly comparable to the turbulent intensity in monophase flows (CHANSON & TOOMBES 2002).

Some typical turbulence intensity distributions are illustrated in Figure 4-4 as functions of y/Y_{90} and

$(y+w)/d_c$. For all skimming flow data, little difference was visible qualitatively and quantitatively between flat and pooled stepped spillways (Fig. 4-4). Please note, that some local maxima in turbulence intensity were found for some step edges on the flat stepped spillway in a region close to the step face. These local maxima were consistent with some local maxima in void fraction and bubble count rate data on the same step edges (see above). It is believed that these were linked with some irregular impingement of air-water flow on the step face associated with a characteristic longitudinal seesaw pattern in skimming flows (CHANSON & TOOMBES 2002; YASUDA & CHANSON 2003; FELDER & CHANSON 2009b).

The present findings indicated similar levels of turbulence on the flat and pooled stepped spillways. Such a result contradicted the observations of FELDER & CHANSON (2012a) and FELDER et al. (2012) on a stepped spillway with 8.9°. On the 8.9° chute, larger turbulence levels were observed on the pooled stepped spillway, and FELDER & CHANSON (2012a) showed that these were linked with some flow instabilities which enhanced the turbulent kinetic energy of the flow.

Fig. 4-4 – Comparison of turbulence intensity distributions on the flat and pooled stepped spillways in skimming flows (θ = 26.6°)

(A) $d_c/h = 1.52$, $Q = 0.097$ m^3/s, $Re = 7.4\times10^5$ (B) $d_c/h = 1.15$, $Q = 0.063$ m^3/s, $Re = 4.9\times10^5$

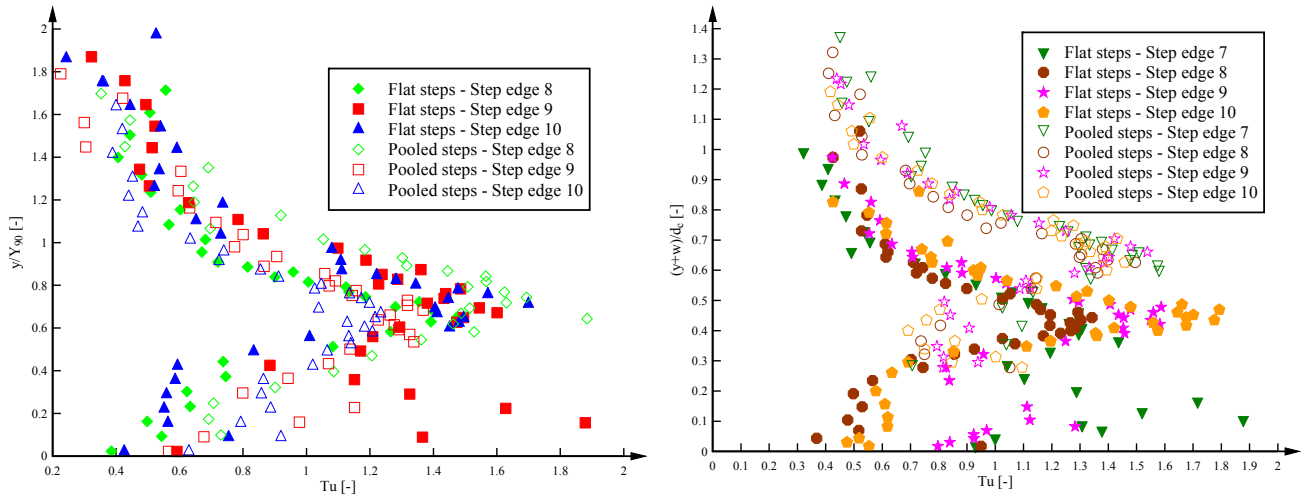

4.2.5 Integral turbulent time and length scales

Some experiments were conducted using an array of two single-tip conductivity probes separated by various transverse distances between probe tips ($3.5 \leq \Delta z \leq 81.3$ mm) (Table 4-2). The experiments were performed with flat and pooled steps for two skimming flow rates at the downstream end of the stepped spillway, at about the same distance from the inception point of air entrainment for both stepped chute configurations.

The results are presented in dimensionless terms in Figure 4-5 in terms of the integral turbulent

length scale L_{xz} and the integral turbulent time scale T_{int}. In Figures 4-5A and 4-5B, the dimensionless integral turbulent length scales are shown respectively as functions of y/Y_{90} and $(y+w)/d_c$. The comparative results highlighted the larger integral turbulent lengths scales on the flat stepped chute suggesting larger transverse air-water vortices (Fig. 4-5A and 4-5B).

The corresponding integral turbulent time scale data are presented in Figures 4-5C and 4-5D as functions of y/Y_{90} and $(y+w)/d_c$ respectively. The dimensionless time scales $T_{int} \times \sqrt{g/Y_{90}}$ (Fig. 4-5C) were larger in the flat stepped spillway flow. However, the dimensionless turbulent time scales $T_{int} \times \sqrt{g/d_c}$ were almost identical for the flat and pooled stepped spillways (Fig. 4-5D). Simply the results were closely linked with the characteristic length scale used in the dimensionless presentations.

The integral turbulent time and length scale data highlighted some maxima in the intermediate flow region ($0.3 < C < 0.7$) (Fig. 4-5). All distributions showed very small integral scale values in the bubbly flow region, while the values of L_{xz} decreased also in the upper spray region. On the other hand, some large integral turbulent time scale values were recorded in the upper spray region ($C > 0.97$) for the pooled stepped spillway, while the values of T_{int} were smaller on the flat stepped spillway. The reason for the differences in the upper spray region are unknown. The finding might indicate a different nature of ejected droplets above the pooled stepped spillway, although the visual observations did not show any obvious difference in terms of droplet ejections and air-water free-surfaces for both configurations. However some small differences in the upper spray region were also recorded in terms of some air-water flow properties including the bubble count rate and the water droplet chord sizes (see section 4.2.7).

Some characteristic values in terms of maximum integral turbulent time and length scales are reported in Table 4-3 for both flat and pooled stepped spillways. The data highlighted the larger turbulent lengths and time scales in the flat stepped spillway flow. The integral time scale data $(T_{int})_{max} \times \sqrt{g/d_c}$ were very close for both stepped spillway configurations.

The distribution of integral turbulent time and length scales for the flat stepped spillway had similar shapes to previous experimental studies on flat stepped spillways with 21.8° and 26.6° (CHANSON & CAROSI 2007; FELDER & CHANSON 2009b,2011a), although the present experiments showed some slightly larger integral turbulent time and length scales. Since the experiments were conducted on different physical facilities, further comparative analyses might provide some more insights into the cause of these differences.

Fig. 4-5 – Comparison of dimensionless integral turbulent length and time scales on the flat and pooled stepped spillways in skimming flows (θ = 26.6°) – Flow conditions: d_c/h = 1.15, Q = 0.063 m^3/s, Re = 4.9×10^5 and d_c/h = 1.45, Q = 0.090 m^3/s, Re = 6.9×10^5

(A) Integral turbulent length scales L_{xz}/Y_{90} (B) Integral turbulent length scales L_{xz}/d_c

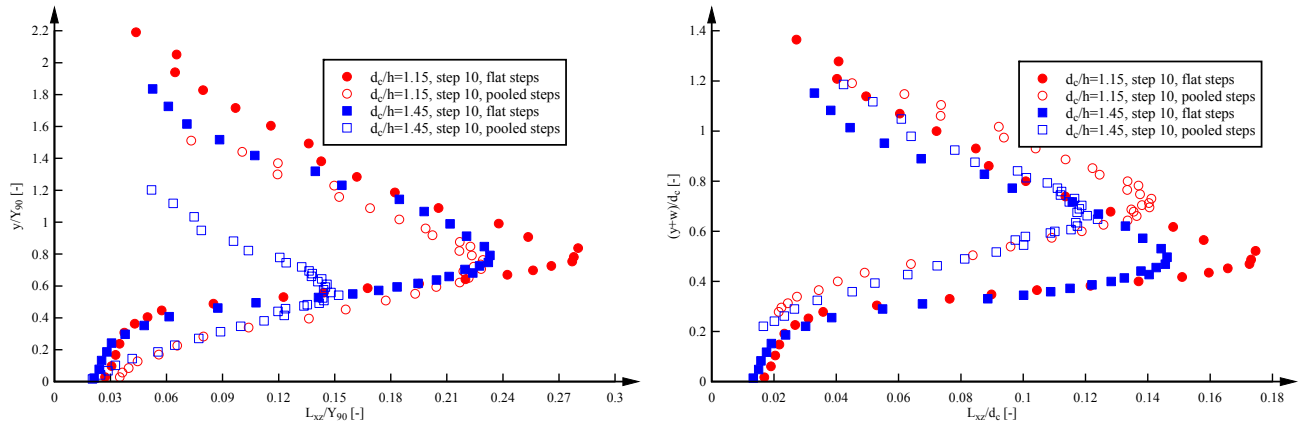

(C) Integral turbulent time scales $T_{int}\times\sqrt{g/Y_{90}}$ (D) Integral turbulent time scales $T_{int}\times\sqrt{g/d_c}$

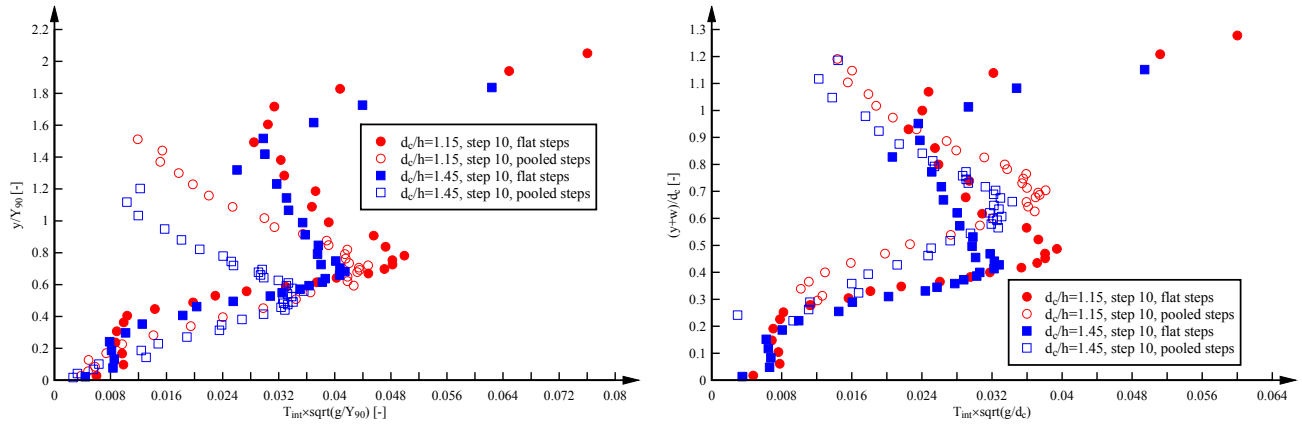

Table 4-3 – Summary of characteristic integral turbulent time and length scales for the flat and pooled stepped spillways (θ = 26.6°)

Configuration (1)	d_c/h [-] (2)	$(L_{xz})_{max}$ [mm] (3)	$(L_{xz})_{max}/d_c$ [-] (4)	$(L_{xz})_{max}/Y_{90}$ [-] (5)	$(T_{int})_{max}$ [ms] (6)	$(T_{int})_{max}\times\sqrt{g/Y_{90}}$ (7)	$(T_{int})_{max}\times\sqrt{g/d_c}$ (8)
Flat stepped spillway	1.15	20.1	0.17	0.28	4.1	0.050	0.039
	1.45	21.2	0.15	0.23	3.8	0.041	0.033
Pooled stepped spillway	1.15	16.2	0.14	0.23	3.8	0.045	0.038
	1.45	18.0	0.12	0.15	3.9	0.036	0.034

Note: maximum values calculated for 0 < C < 0.97

4.2.6 Air-water flow properties in transition flows

A small number of experiments were conducted in the transition flow regime and the data are discussed below. CHANSON & TOOMBES (2004) presented a seminal study of the transition flow regime, introducing the transition flow sub-regimes TRA1 and TRA2. Herein the observations for $d_c/h = 0.7$ showed some typical features of the transition flow sub-regime TRA1. These data ($d_c/h = 0.7$) differed substantially from the air-water flow data observed for $d_c/h > 0.7$ (see above).

The air-water flow properties in the transition flow ($d_c/h = 0.7$) are compared for the flat and pooled stepped spillways in Figure 4-6 as a function of $(y+w)/d_c$. Figure 4-6A illustrates the void fraction distributions C for the flat and pooled steps. On the flat steps, the data showed typical void fraction distributions for the transition flow sub-regimes TRA1 (CHANSON & TOOMBES 2004). That is, two different types of void fraction distributions were observed, i.e. a flat, straight profile and the S-shape distribution. The type of void fraction profile differed between adjacent step edges in the present study. For the pooled stepped configuration, the void fraction distributions exhibited a S-shape as observed in the skimming flow regime (Fig. 4-6A).

The dimensionless bubble count rate distributions are presented in Figure 4-6B. For all distributions, the maximum numbers of bubbles were observed in the intermediate flow region. The maximum bubble count rate increased with increasing distance from the inception point. The bubble count rate was about the same for the flat and pooled stepped configuration in the transition flow ($d_c/h = 0.7$) (Fig. 4-1B).

The dimensionless interfacial velocity distributions V/V_c are presented in Figure 4-6C for the flat and pooled stepped configurations. For both configurations, the interfacial velocities were about identical on flat and pooled steps. This observation contradicted the larger interfacial velocities for the pooled stepped spillway observed in skimming flows. The velocity profiles in the transition differed from the power shape seen in skimming flow. The transition flow data presented some smaller velocities in the spray region (Fig. 4-6C).

In the transition flow ($d_c/h = 0.7$), some differences were observed in terms of the turbulence intensity Tu distributions between the flat and pooled stepped spillways (Fig. 4-6D). The turbulence intensity distributions in the pooled stepped spillway flow were similar to those observed in the skimming flow regime: i.e., with a maximum of similar magnitude in the intermediate flow region. On the flat stepped spillway, the shapes of the turbulence intensity distribution were completely different, with the largest turbulence levels close to the step face for most step edges. This shape was typically observed at the step edges where a flat, straight void fraction profile was observed (Fig. 4-6A). At step edges where the void fractions exhibited a S-shape, the distributions of turbulence intensity were closer to the shapes observed in the skimming flow regime. Importantly, the turbulence levels on the flat stepped spillway were smaller than those observed on the pooled

stepped spillway.

Fig. 4-6 – Comparison of air-water flow properties on the flat and pooled stepped spillways in transition flow sub-regime TRA1 ($\theta = 26.6°$) - $d_c/h = 0.70$, $Q = 0.030$ m^3/s, $Re = 2.3\times10^5$

(A) Void fraction distributions

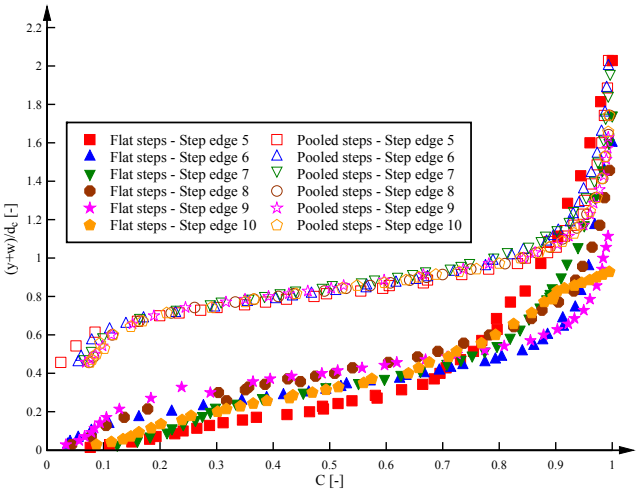

(B) Bubble count rate distributions

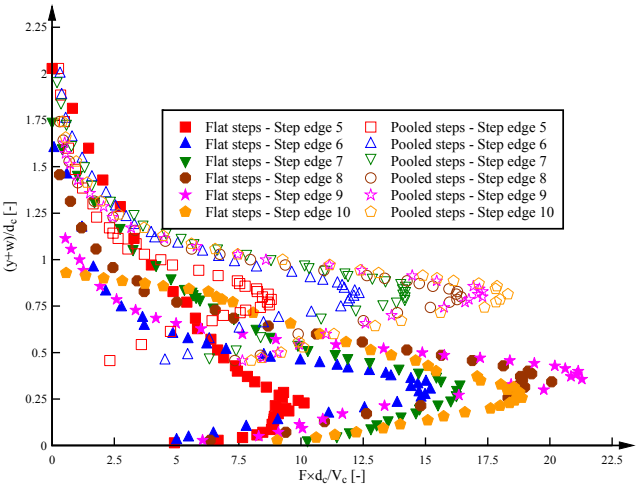

(C) Interfacial velocity distributions

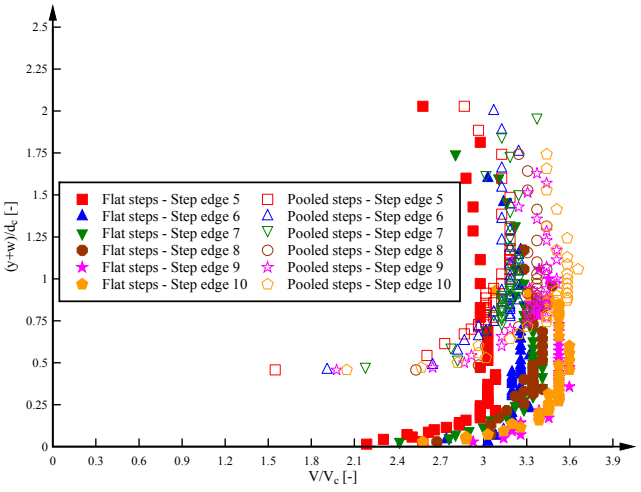

(D) Turbulence intensity distributions

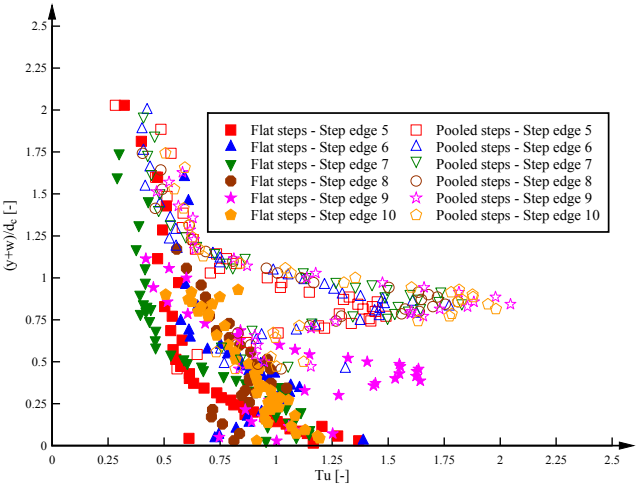

4.2.7 Microscopic air-water flow property: air bubble and water droplet chord sizes

The air bubble and water droplet chord sizes were calculated for all experiments. Some typical results are compared for the flat and pooled stepped spillway configurations in Figures 4-7 and 4-8. In Figure 4-7, some characteristic probability distribution functions (PDFs) of air bubble chord lengths are shown for two discharges. There was a close agreement between the air bubble chord sizes for the flat and pooled steps. Some typical results in terms of the water droplet chord lengths are illustrated in Figures 4-8 for two discharges. The water droplet chord sizes for both flat and pooled steps were in close agreement despite some small differences.

The present findings were consistent with some observations on a 8.9° sloped spillway, showing

little difference between flat and pooled stepped spillways in terms of the bubble and droplet chord sizes (FELDER & CHANSON 2012a; FELDER et al. 2012).

Fig. 4-7 – Comparison of probability distribution functions of air bubble chord sizes on the flat and pooled stepped spillways (θ = 26.6°):
(A) $d_c/h = 0.82$, Q = 0.038 m^3/s, Re = 2.9×10^5; Step edge 10

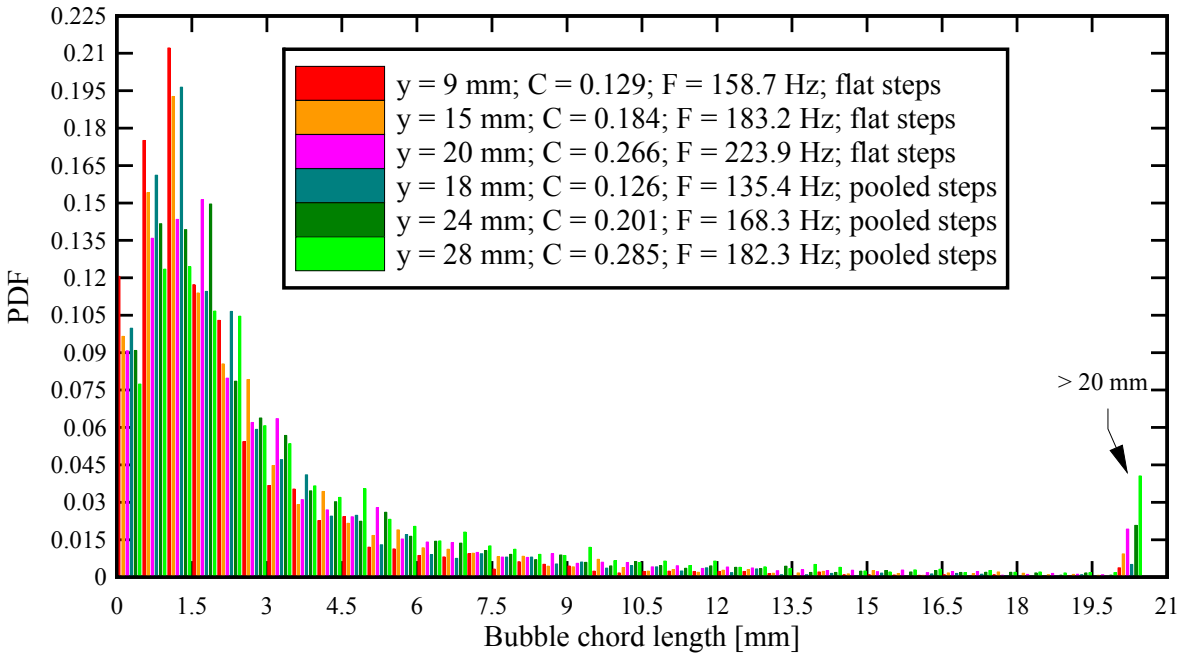

(B) $d_c/h = 1.29$, Q = 0.075 m^3/s, Re = 5.7×10^5; Step edge 10

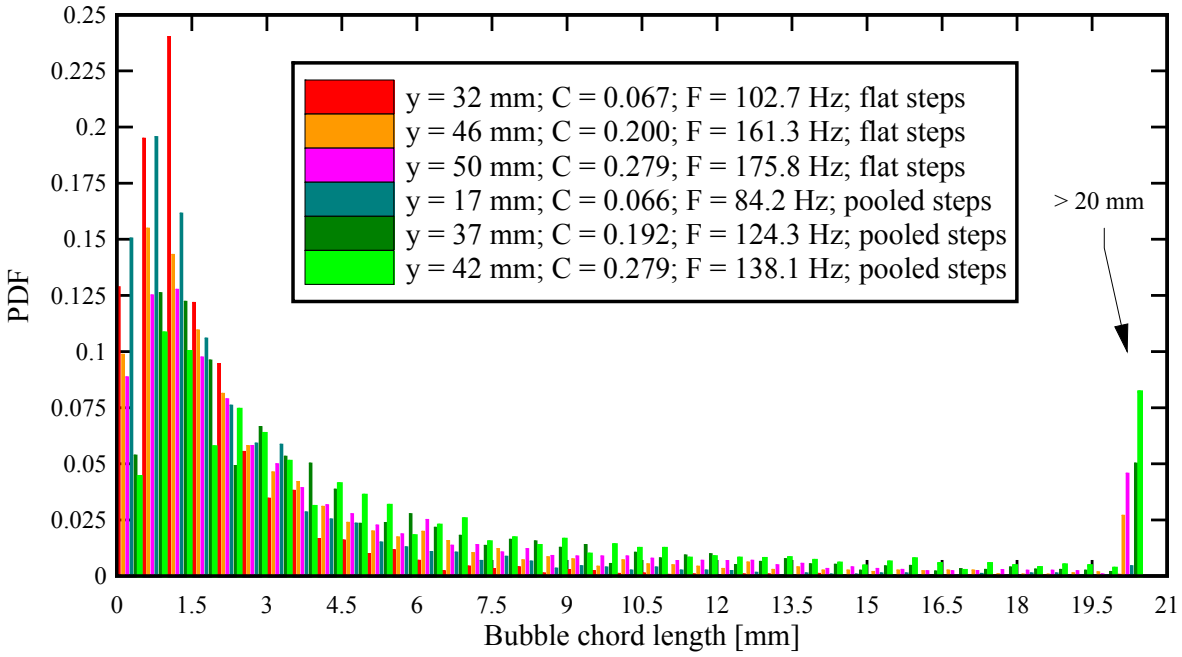

Fig. 4-8 – Comparison of probability distribution functions of water droplet chord sizes on the flat and pooled stepped spillways (θ = 26.6°)

(A) $d_c/h = 0.82$, $Q = 0.038$ m^3/s, $Re = 2.9\times10^5$; Step edge 10

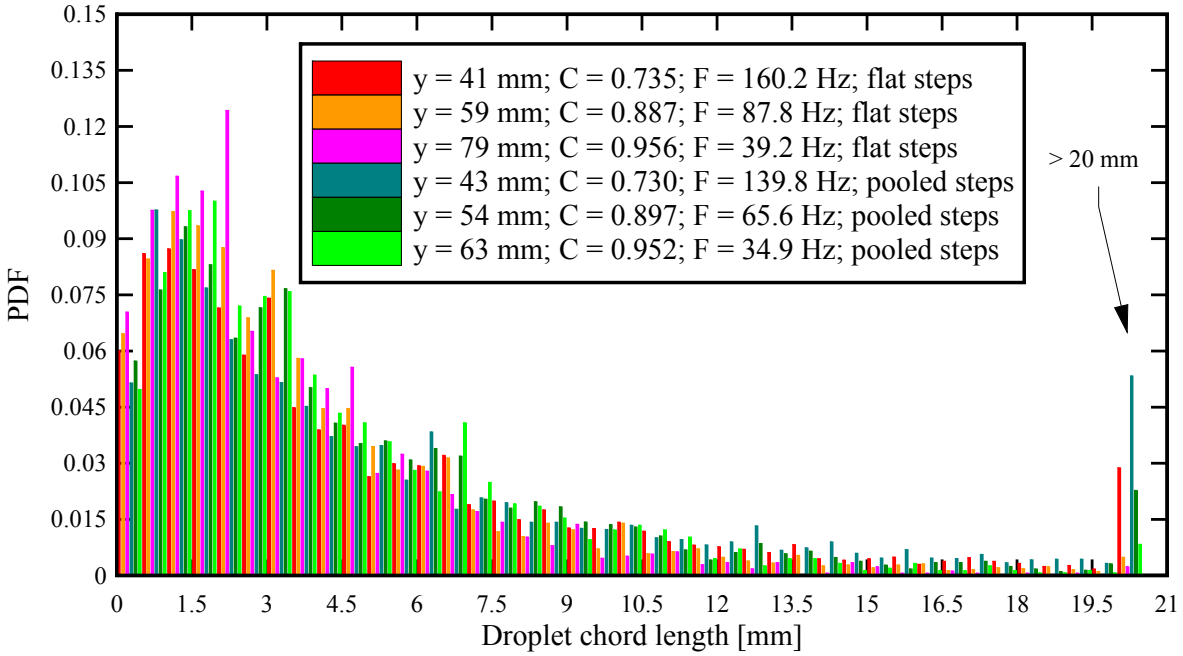

(B) $d_c/h = 1.52$, $Q = 0.097$ m^3/s, $Re = 7.4\times10^5$; Step edge 10

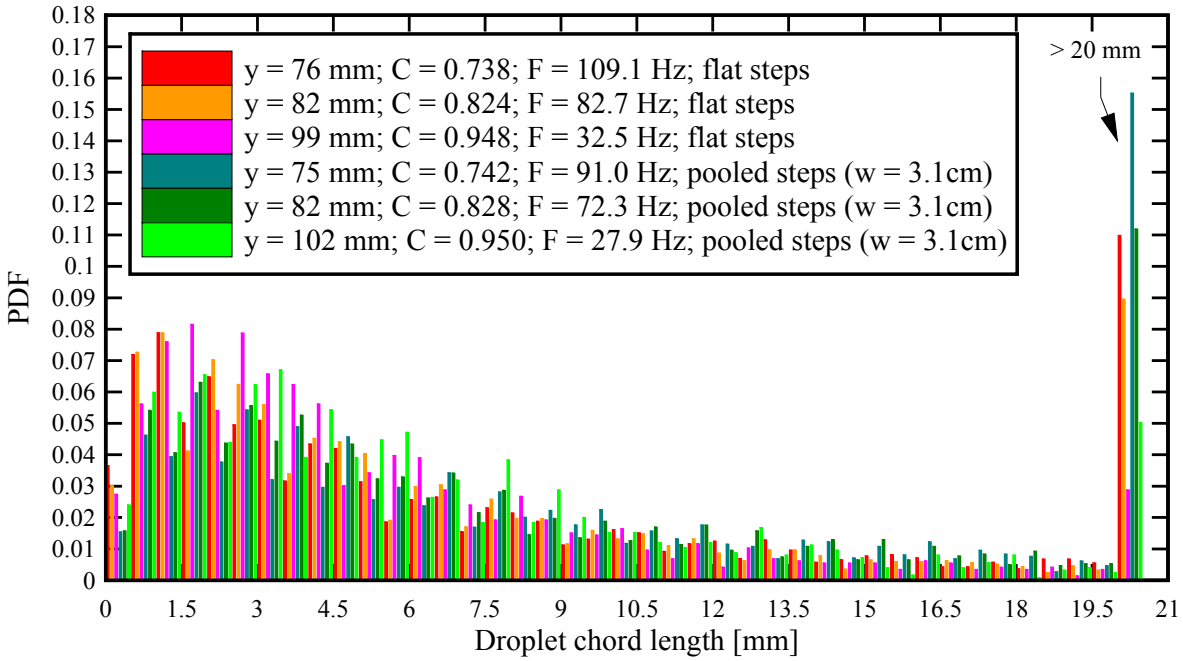

4.2.8 Longitudinal distributions of characteristic air-water flow parameters

For all experiments, the longitudinal distributions of characteristic air-water flow properties were calculated, including the mean air concentration C_{mean}, the maximum bubble count rate in a cross section F_{max}, the characteristic interfacial velocity V_{90} where C = 90%, the maximum turbulence

intensity in a cross section Tu_{max}, the mean flow velocity U_w, the equivalent clear water flow depth d and the characteristic depth Y_{90} where C = 90%. The tabular data are presented in Appendix C (Tables C-1 and C-2).

Figure 4-9 regroups some longitudinal distributions of dimensionless air-water flow parameters for several flow rates on the flat and pooled stepped spillway configurations. Figure 4-9A illustrates the mean air concentration C_{mean} as a function of the dimensionless distance from the inception point of air entrainment $(x-L_I)/d_c$, where x is the distance along the channel bottom and L_I the longitudinal distance measured from the weir crest to the inception point of air entrainment. A comparison between the two stepped spillway configurations showed some small difference in terms of C_{mean}, but no clear trend (Fig. 4-9A). At some step edges, the mean air content appeared larger for the flat steps for a given flow rate, although the opposite trend was seen at the next step edge. For all experiments, The mean air content increased with increasing distance from the inception point and no uniform equilibrium value was reached in the present study (Fig. 4-9A). Overall, the mean air concentration data were in fairly close agreement between the flat and pooled stepped spillways, as previously shown with the comparison of the void fraction distributions (Fig. 4-1).

A more distinctive difference was observed in terms of the maximum bubble count rate. Some longitudinal distributions of dimensionless bubble count rates $F_{max} \times d_c/V_c$ are illustrated as a function of $(x-L_I)/d_c$ for several flow rates in Figure 4-9B. The bubble count rates were consistently larger on the flat stepped spillway for all flow rates and at all measured positions downstream of the inception point. This trend was consistent with the bubble frequency distribution data (Fig. 4-2). The present finding was consistent with some results on a slope of 8.9° (FELDER et al. 2012). Herein no uniform equilibrium was reached and the maximum bubble count rate increased with increasing distance from the inception point.

Typical longitudinal distributions of the dimensionless interfacial velocity V_{90}/V_c are illustrated in Figure 4-9C. For the pooled stepped spillway, V_{90} was larger for all discharges. The finding was consistent with the larger interfacial velocity distributions observed on the pooled stepped spillway (Fig. 4-3B). The result was significant and implied a lesser rate of energy dissipation on the pooled stepped spillway. This was in contrast to some findings on a 8.9° pooled stepped spillway (FELDER et al. 2012).

Some longitudinal distributions of maximum turbulence intensity Tu_{max} are shown in Fig. 4-9D as a function of the dimensionless distance from the inception point. As seen in Figure 4-9D, no significant differences between the two configurations were observed. Some data scatter existed and large turbulence levels were recorded. The findings were in contrast to the much larger turbulence intensities observed on a 8.9° pooled stepped spillway (FELDER & CHANSON 2012a; FELDER at al. 2012).

Fig. 4-9 – Comparison of longitudinal distributions of characteristic parameters for the flat and pooled stepped spillways (θ = 26.6°)

(A) Mean air-concentration C_{mean}

(B) Characteristic dimensionless maximum bubble count rate $F_{max} \times d_c/V_c$

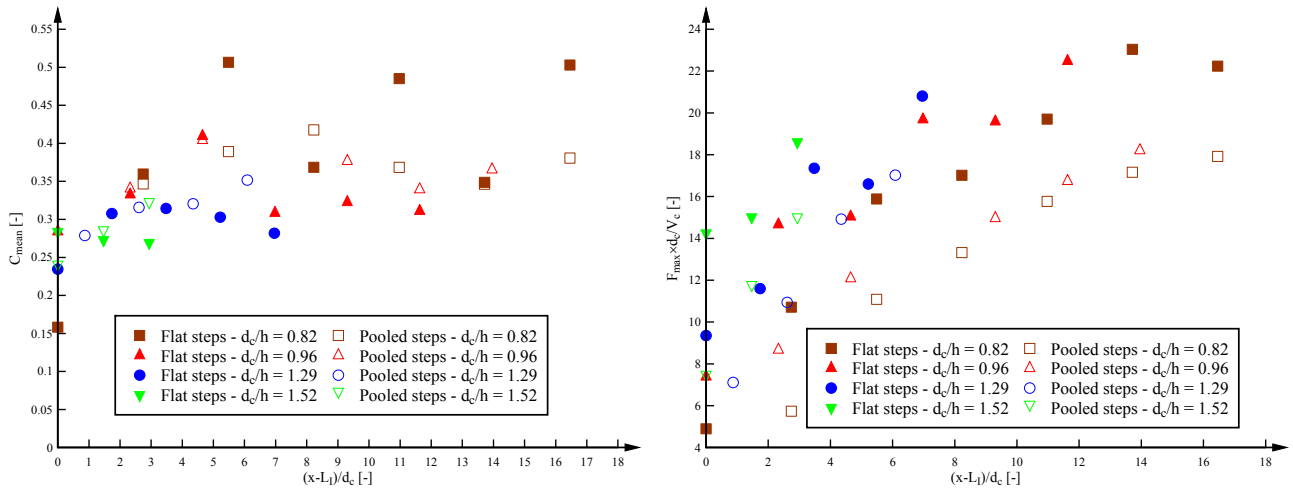

(C) Characteristic dimensionless interfacial velocity V_{90}/V_c

(D) Characteristic maximum turbulence intensity Tu_{max}

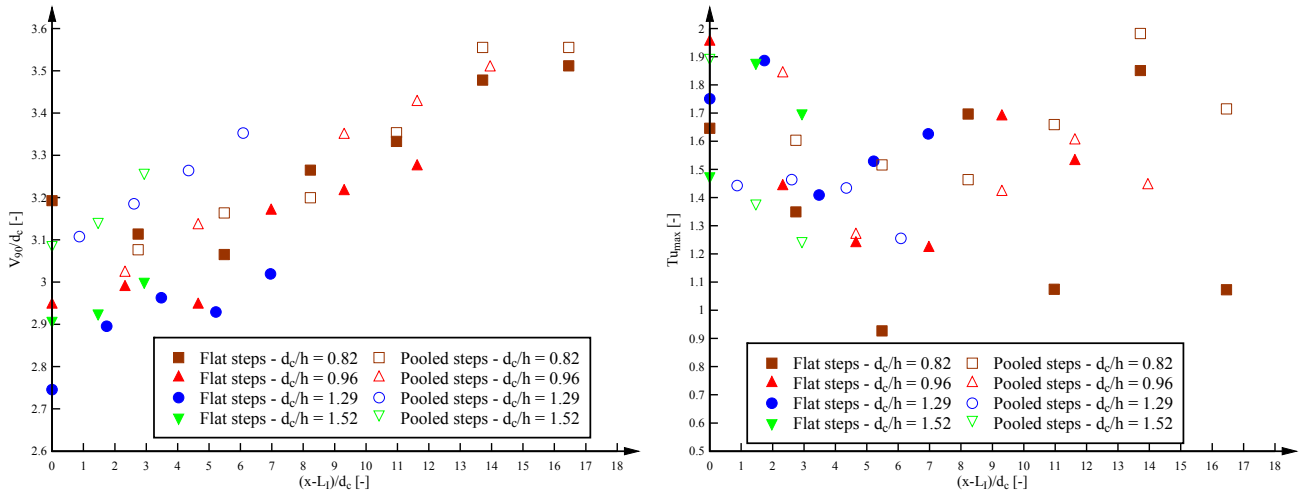

4.3 DISCUSSION

The air-water flow properties on flat and pooled stepped spillways were compared systematically for a range of discharges $0.030 \leq Q \leq 0.113$ m^3/s in the transition and skimming flow regimes. The experiments demonstrated a strong flow aeration for both stepped spillway configurations downstream of the inception point. The comparative results showed similar void fraction distributions and mean air concentrations on the flat and pooled stepped spillways for the same flow rate. The turbulent intensities and the air bubble and water droplet chord sizes showed little difference between the flat and pooled steps. On the other hand, some large bubble count rates and

smaller interfacial velocities were observed on the flat stepped spillway for the same discharge.

The results in terms of interfacial velocities were unexpected. For comparison, smaller interfacial velocities were observed on a 8.9° pooled stepped spillways (FELDER & CHANSON 2012a; FELDER et al. 2012), although the data of KÖKPINAR (2004) on a 30° stepped spillway showed some slightly larger interfacial velocities for the pooled stepped configurations. Table 4-4 summarises the chute geometries tested with these three slopes: 8.9°, 26.6° and 30°.

For all slopes, the data showed larger bubble frequencies on the flat stepped spillways. The largest differences were observed on the 8.9° stepped chute and the smallest on the 30° chute. Further differences were recorded in terms of the turbulence intensities on the 8.9° and 26.6° chutes. On the 8.9° pooled stepped chute, some instationary air-water flow processes were observed associated with larger turbulence levels (FELDER & CHANSON 2012a). In the present study, the turbulence intensities were comparable for both stepped configurations.

The data suggested that some differences between flat and pooled stepped spillway observations might be linked to the difference in slopes and in cavity shapes. Table 4-4 shows indeed the different ratios of pool weir height to step height w/h and weir height to step length w/l. For example, the ratio w/l was identical in the 8.9° and 26.6° slope studies, although the ratio w/h differed.

The comparison of the air-water flow properties suggested the large impact of the channel slope on the air-water flow properties. The flat stepped chute was more exposed to flow instabilities in comparison to the steeper stepped spillways. The instabilities affected the flow velocities and the turbulent energy production processes as shown by FELDER & CHANSON (2012a). It is unknown if a stepped spillway with steep slope (e.g. $\theta = 26.6°$) and a larger rate of pool weir height to step height (e.g. w/h = 1) would be subjected to similar instabilities. The poor weir length l_w might also have a small effect on the air-water flow processes.

Table 4-4 – Experimental investigations of pooled stepped spillway with comparative results between flat and pooled steps

Reference	Slope	h	l	w	l_w	w/l	w/h
	[°]	[m]	[m]	[m]	[m]	[-]	[-]
(1)	(2)	(3)	(4)	(5)	(6)	(7)	(8)
Present study	26.6	0.1	0.2	0.031	0.015	0.155	0.31
FELDER et al. (2012)	8.9	0.05	0.319	0.05	0.015	0.157	1.0
KÖKPINAR (2004)	30	0.06	0.104	0.03	0.026	0.288	0.5

Notes: θ: channel slope; h: step height; l: step length; w: weir height; l_w: pool weir length.

5. AIR-WATER FLOW PROPERTIES ON THE STEPPED SPILLWAYS WITH IN-LINE AND STAGGERED CONFIGURATIONS OF FLAT AND POOLED STEPS

5.1 PRESENTATION

Detailed air-water flow experiments were conducted on the stepped spillway configurations with in-line and staggered configurations of flat and pooled steps (Fig. 5-1). The flow was complex, three-dimensional and some flow instabilities in the form of sidewall standing waves and supercritical shock waves were observed (see section 3.3.4 and 3.5). The transverse variations of flow aeration led to some spatially-varying air-water flow properties in both longitudinal and transverse directions. Therefore the air-water flow measurements were conducted at three transversal locations (z/W = 0.25, 0.5 and 0.75) for each step edge. Fig. 5-1 shows a sketch of the stepped spillway configurations with in-line and staggered steps and highlights the measurement locations.

For all experiments, the measurements in the direction y perpendicular to the spillway slope were performed from the step edge for the flat step section (y = 0) and from the pool weir edge for the pooled section (y = 0). On the channel centreline (z/W = 0.5), Figure 5-2 illustrates the position of the double-tip conductivity probe and the measurement started at the pool weir edge (y = 0). For all experiments, the absolute datum was set at the flat step edge and the air-water flow properties in this section are presented as functions of dimensionless distance perpendicular to the pseudo-bottom formed by the step edges $(y+w)/d_c$.

The air-water flow measurements were performed with a double-tip conductivity probe for $0.016 \leq Q \leq 0.113 m^3/s$ on both stepped spillway configurations. In section 5.2, the air-water flow properties are presented for the stepped spillway with in-line configuration of flat and pooled steps and in section 5.3 for the staggered configuration. A range of air-water flow properties were investigated including the distributions of void fraction, bubble count rate, interfacial velocity and turbulence intensity. The experimental results for the in-line and staggered stepped spillway configurations are compared with the air-water flow observations on flat and pooled stepped spillways respectively (section 4). Furthermore, some longitudinal distributions of characteristic air-water flow parameters are shown. The differences between the in-line and staggered stepped spillway configurations are discussed in section 5.4 and their performances are compared. All air-water flow properties for the stepped spillways with in-line and staggered configurations with flat and pooled steps are presented in Appendix D.

Fig. 5-1 – Sketch of stepped spillways with in-line and staggered configuration of flat and pooled steps (θ = 26.6°) and the three transverse measurement positions (z/W = 0.25, 0.5 and 0.75)

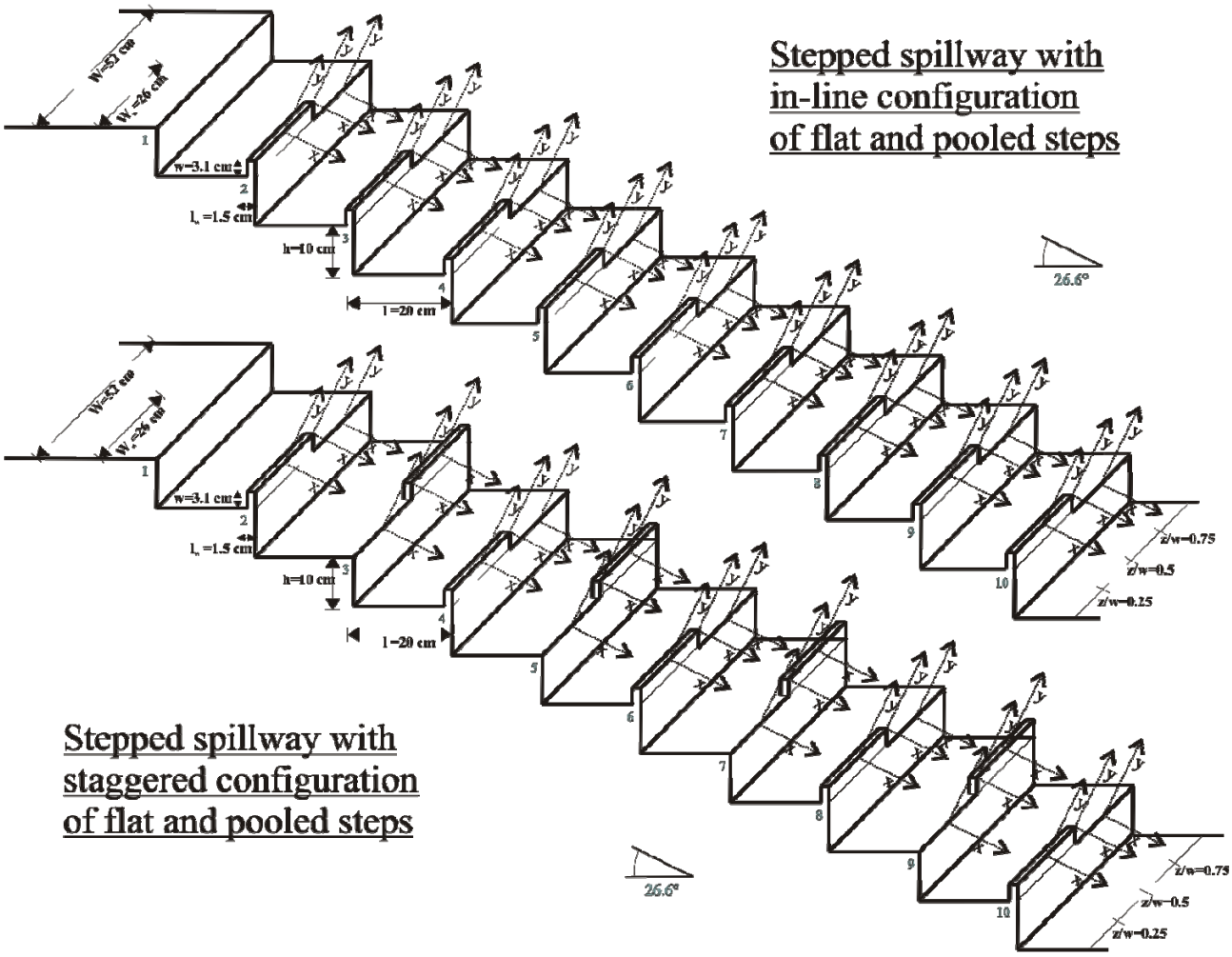

Fig. 5-2 – Position of double-tip conductivity probe (Ø = 0.25 mm) on channel centreline (z/W = 0.5) for the stepped spillways with in-line and staggered configurations of flat and pooled steps (θ = 26.6°)

5.2 AIR-WATER FLOW PROPERTIES ON STEPPED SPILLWAY WITH IN-LINE CONFIGURATION OF FLAT AND POOLED STEPS

5.2.1 Presentation

The experiments on the stepped spillway with in-line configuration of flat and pooled steps were performed with a double-tip conductivity probe at three transverse positions for each step edge in the air-water flow region downstream of the inception point of free-surface aeration. The transverse locations on each step edge comprised the middle of the pooled stepped side (z/W = 0.25), the channel centreline (z/W = 0.5) and the middle of the flat step side (z/W = 0.75) (Fig. 5-1). The experiments were conducted in nappe, transition and skimming flows. Table 5-1 summarises the experimental flow conditions on the stepped spillway with in-line configuration of flat and pooled steps. Some characteristic results are presented in this section. The full data set is presented in Appendix D.

Table 5-1 – Air-water flow measurements with a double-tip conductivity probe (Ø = 0.25 mm) for the stepped spillway with in-line configuration of flat and pooled steps (θ = 26.6°)

Configuration (1)	d_c/h [-] (2)	Q [m^3/s] (3)	Re [-] (4)	Measurement at step edge (5)	Flow regime (6)
Stepped spillway with in-line configuration of flat and pooled steps	0.5	0.016	1.39×10^5	2-10	NA
	0.7	0.030	2.30×10^5	2-10	TRA
	1.15	0.063	4.85×10^5	4-10	SK
	1.45	0.090	6.87×10^5	5-10	SK
	1.7	0.113	8.72×10^5	7-10	SK

Notes: d_c: critical flow depth; h: vertical step height; Q: water discharge; Re: Reynolds number defined in terms of the hydraulic diameter; SK: skimming flow regime; TRA: transition flow regime; NA: nappe flow regime.

5.2.2 Void fraction

Some typical void fraction distributions are illustrated in Figure 5-3 for all step edges downstream of the inception point of air entrainment at the three transverse measurement locations. In Figure 5-3A, the void fraction distribution is presented as a function of y/Y_{90} and compared with the advective diffusion equation for air bubbles (Eq. (4-3), section 4). The void fraction distributions for all transverse positions agreed well with the advective diffusion equation, but some differences in terms of void fraction distributions were observed in the transverse direction (Fig. 5-3A). The

data implied the largest depth-averaged void fraction in the pooled stepped side (lowest curves) and the lowest mean air content on the flat stepped side (upper curves). Some data scatter was observed for all data sets with the largest data scatter for the measurements on the pooled stepped side (Fig. 5-3A).

In Figure 5-3B, the void fraction data for the three transverse positions are shown as a function of $(y+w)/d_c$ for all step edges downstream of the inception point. The data sets were in reasonable agreement despite some scatter (Fig. 5-3B). The void fraction distributions were also compared with the corresponding data on flat and pooled stepped spillways for the same discharge. In Figure 5-3B, these data are only shown at the downstream end of the spillway (step edge 10) on the channel centreline. The void fraction data for the in-line configuration were systematically in between the flat stepped spillway data and the pooled stepped spillway data. In the bubbly flow region ($C< 0.3$), the void fraction data tended to be larger on the flat stepped spillway compared to the data on the flat stepped side on the in-line configuration (Fig. 5-3B). The void fraction distribution for the pooled stepped spillway was above all other distributions including the pooled stepped side on the in-line configured stepped spillway (Fig. 5-3B).

Fig. 5-3 – Void fraction distributions on the stepped spillway with in-line configuration of flat and pooled steps in skimming flows ($\theta = 26.6°$) – Measurements at three transverse locations: z/W = 0.25 (pooled stepped side), z/W = 0.5 (channel centreline), z/W = 0.75 (flat stepped side)
(A) $d_c/h = 1.45$, $Q = 0.090$ m^3/s, $Re = 6.87\times10^5$; Comparison with Eq. (4-3)

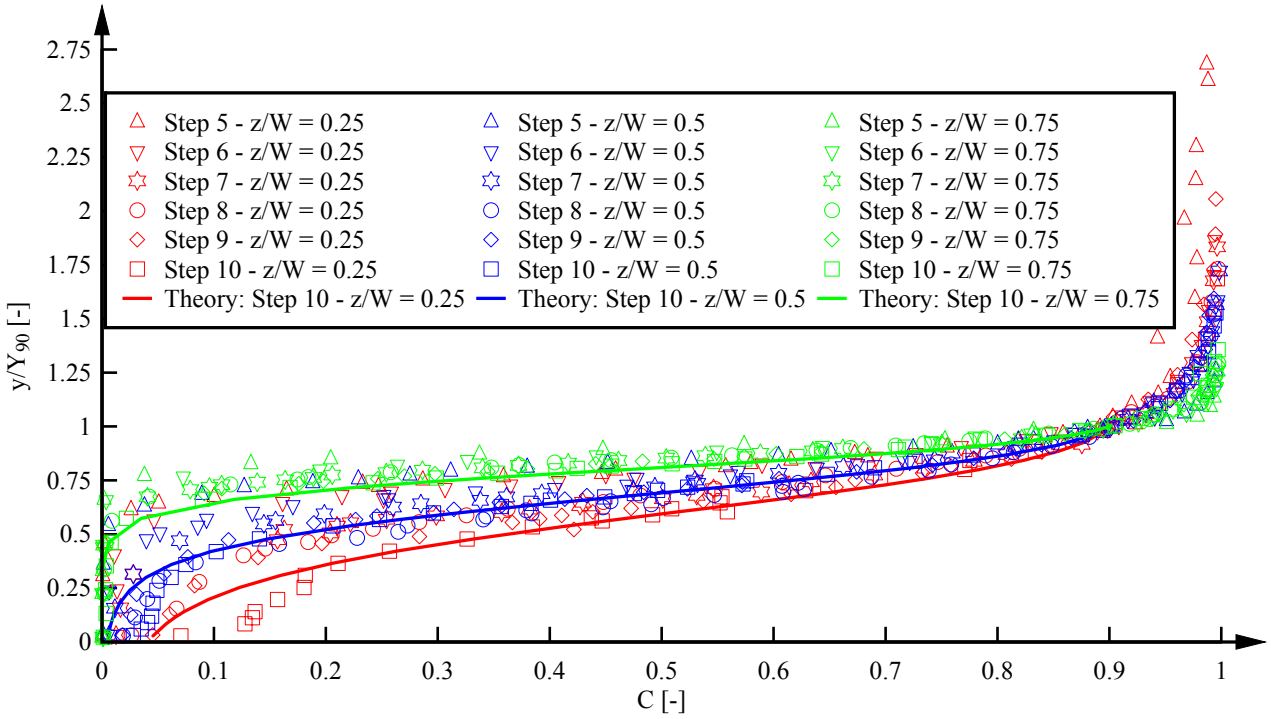

(B) $d_c/h = 1.15$, $Q = 0.063$ m^3/s, $Re = 4.85\times10^5$; Comparison with flat and pooled stepped spillways

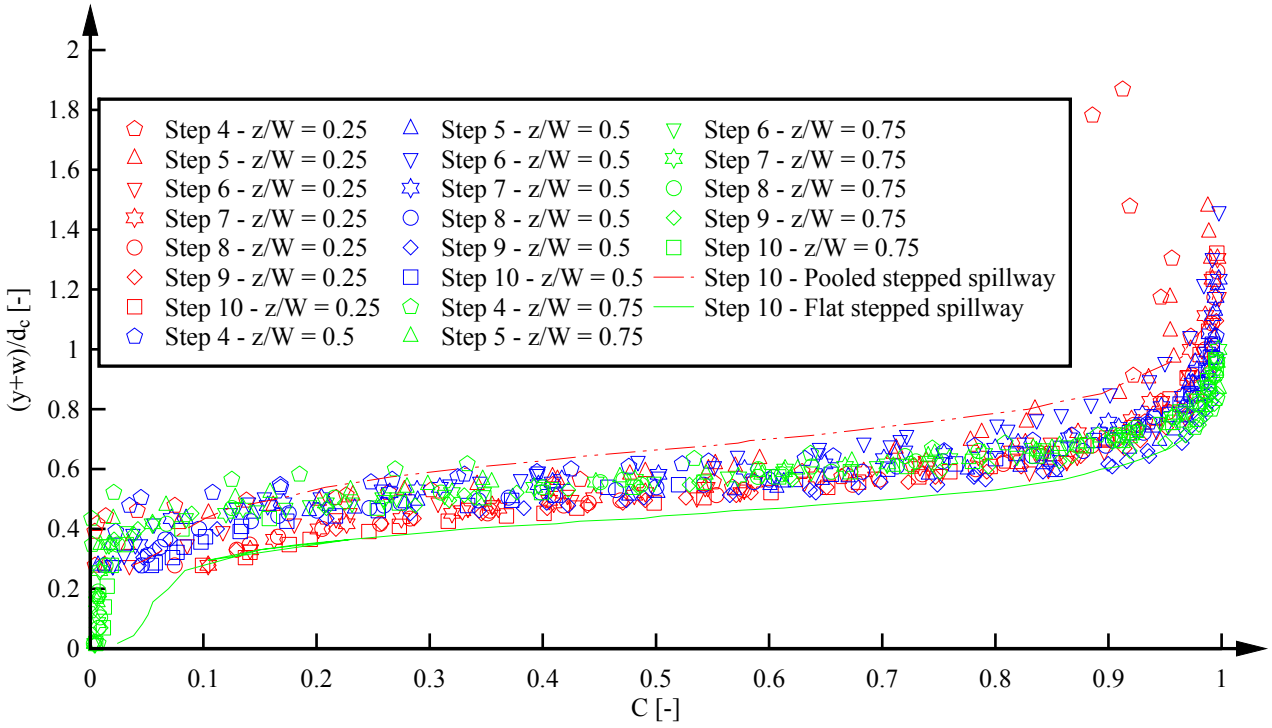

5.2.3 Bubble count rate

The bubble count rate distributions showed characteristic shapes with a maximum bubble count rate in the intermediate flow region ($0.3 < C < 0.7$) and smaller levels of detected bubbles in the lower bubbly and upper spray regions. For all experiments, the maximum bubble count rates increased with increasing distance from the inception point of free-surface aeration. Some typical distributions of dimensionless bubble count rate $F\times d_c/V_c$ are illustrated in Figure 5-4 as functions of y/Y_{90} and $(y+w)/d_c$ for all three transverse measurement positions.

A comparison of bubble count rates in the transverse direction showed the largest bubble count rates in the pooled stepped side and the smallest for the flat stepped spillway side (Fig. 5-4). In Figure 5-4B, the bubble count rate distributions for the stepped spillway with in-line configuration with flat and pooled steps are further compared with some data sets at step edge 10 on the flat and pooled stepped spillways. Some differences were noted between the stepped spillway configurations (Fig. 5-4B). On the flat stepped spillway, the bubble count rates were significantly larger than on the flat stepped side of the in-line configuration for a given flow rate. The bubble count rates on the pooled stepped spillway were smaller compared to those on the pooled stepped side of the in-line stepped spillway for an identical discharge, but comparable in magnitude to the channel centreline data (Fig. 5-4B).

Fig. 5-4 – Dimensionless bubble count rate distributions on the stepped spillway with in-line configuration of flat and pooled steps in skimming flows (θ = 26.6°) – Measurements at three transverse locations: z/W = 0.25 (pooled stepped side), z/W = 0.5 (channel centreline), z/W = 0.75 (flat stepped side)

(A) $d_c/h = 1.70$, $Q = 0.113$ m^3/s, $Re = 8.72\times10^5$

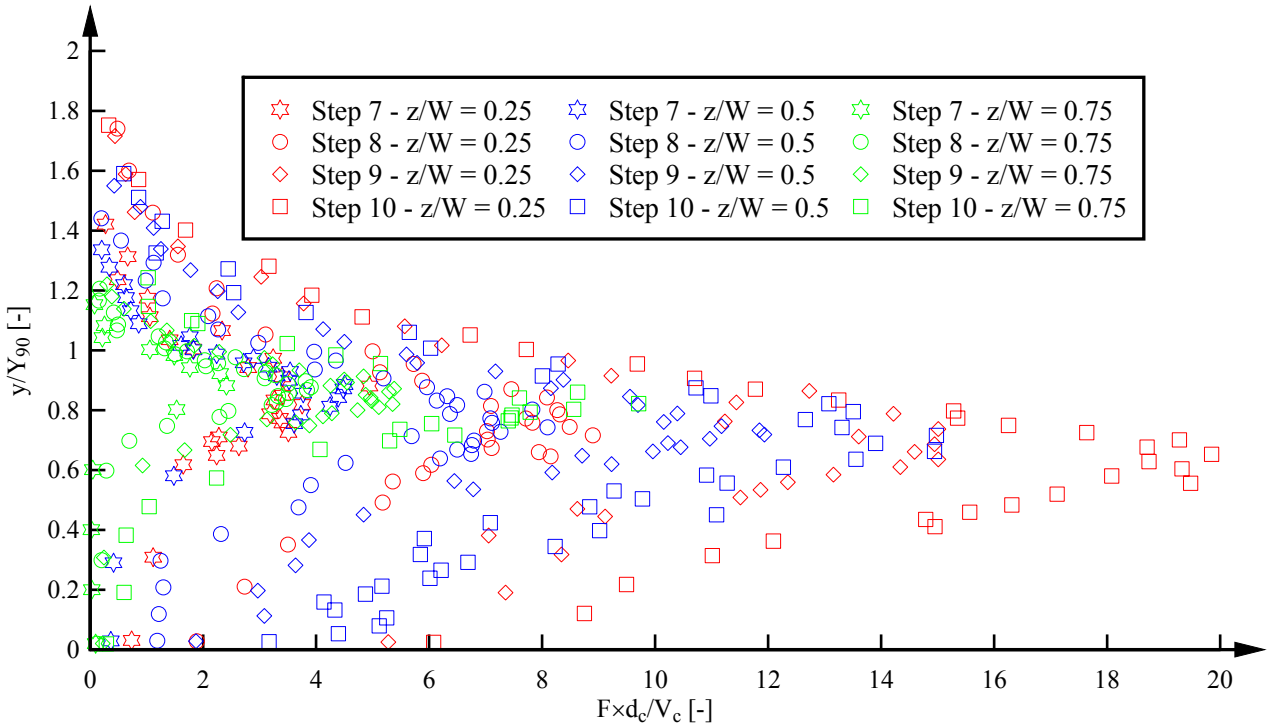

(B) $d_c/h = 1.15$, $Q = 0.063$ m^3/s, $Re = 4.85\times10^5$ - Comparison with flat and pooled stepped spillways

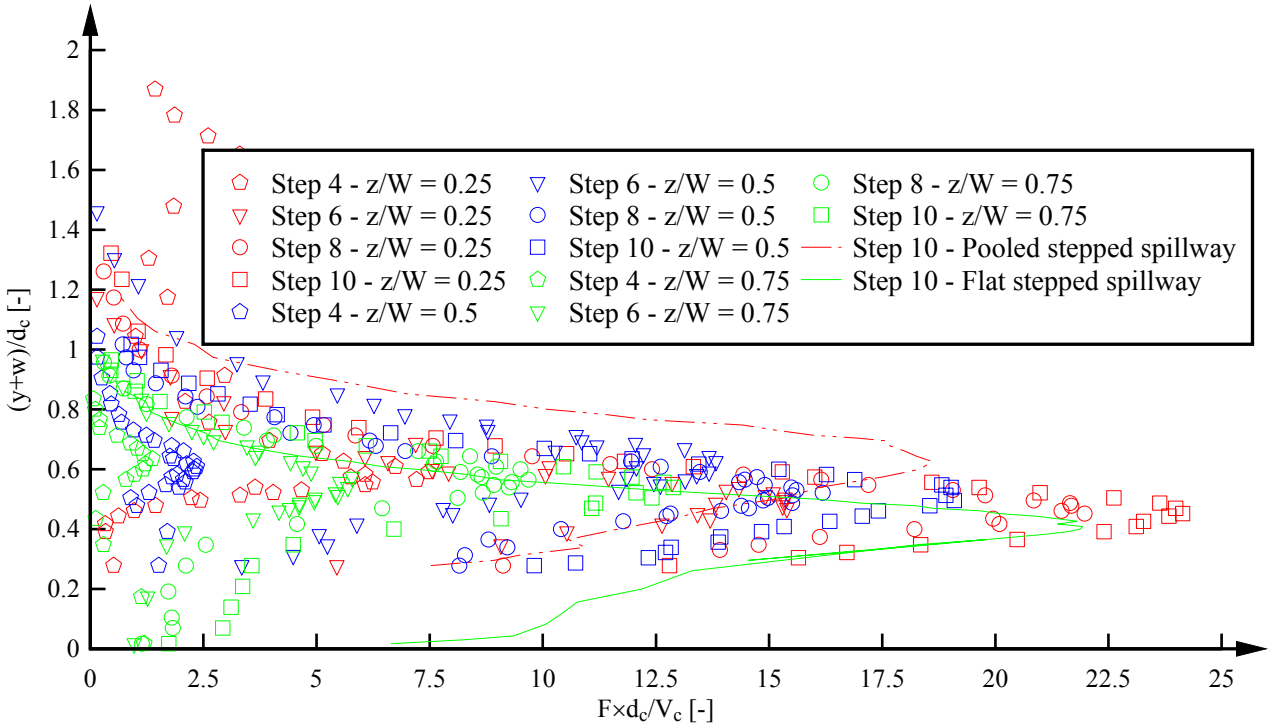

5.2.4 Interfacial velocity

The interfacial velocities were calculated for all data sets and some typical skimming flow data are shown in Figure 5-5. In Figure 5-5A, all dimensionless interfacial velocities V/V_{90} for all skimming flow data sets at the three transverse measurement positions are illustrated as a function of y/Y_{90}. The distributions are compared with a $1/10^{th}$ power law (N = 10) for $y/Y_{90} < 1$ and with a uniform profile for $y/Y_{90} > 1$ (Eq. (4-4) & (4-5), section 4). The interfacial velocity data were in relatively good agreement and compared well with the empirical equations indicating some form of self-similarity. Some scatter was observed on the pooled stepped side for the smallest skimming flow rate. In the upper spray region, some deviation from the uniform profile was observed for the flat and pooled stepped sides (Fig. 5-5A).

In Figure 5-5B, some typical dimensionless interfacial velocity distributions V/V_c are shown as a function of $(y+w)/d_c$ at the three transverse positions and for the corresponding flat and pooled stepped spillway experiments. For all data sets, the interfacial velocities increased with increasing longitudinal distance from the inception point of free-surface aeration. The largest velocities were observed on the flat stepped side and the slowest on the pooled stepped side of the in-line stepped spillway configuration. The velocity distributions showed some differences in the transverse direction. That is, the interfacial velocities on the flat stepped side for the in-line stepped spillway were consistently larger than those observed on the pooled stepped side. Lastly the data implied some discharge concentration on the flat side of the in-line stepped chute.

5.2.5 Turbulence intensity

The turbulence intensity data showed overall some large turbulent levels above the stepped chute with little difference between the transverse measurement locations on the in-line stepped spillway (Fig. 5-6). Figure 5-6 illustrates some typical data at several step edges, where Tu is shown as function of y/Y_{90} and $(y+w)/d_c$ (Fig. 5-6A & 5-6B respectively.) Some data obtained during the flat and pooled stepped spillway experiments are further included for comparison in Figure 5-6B. All data showed the largest turbulence levels in the intermediate flow region ($0.3 < C < 0.7$) and some smaller turbulence in the lower bubbly and upper spray regions. The turbulence intensity distributions for the flat and pooled stepped sides on the in-line stepped spillway showed similar results, with some larger turbulence levels at the first two step edges downstream of the inception point. Further downstream, the turbulence intensities on the flat and pooled stepped sides indicated smaller turbulence levels compared to the centreline data.

Fig. 5-5 – Dimensionless interfacial velocity distributions on the stepped spillway with in-line configuration of flat and pooled steps in skimming flows (θ = 26.6°) – Measurements at three transverse locations: z/W = 0.25 (pooled stepped side), z/W = 0.5 (channel centreline), z/W = 0.75 (flat stepped side)

(A) All skimming flow data sets; Comparison with Eq. (4-4) & (4-5)

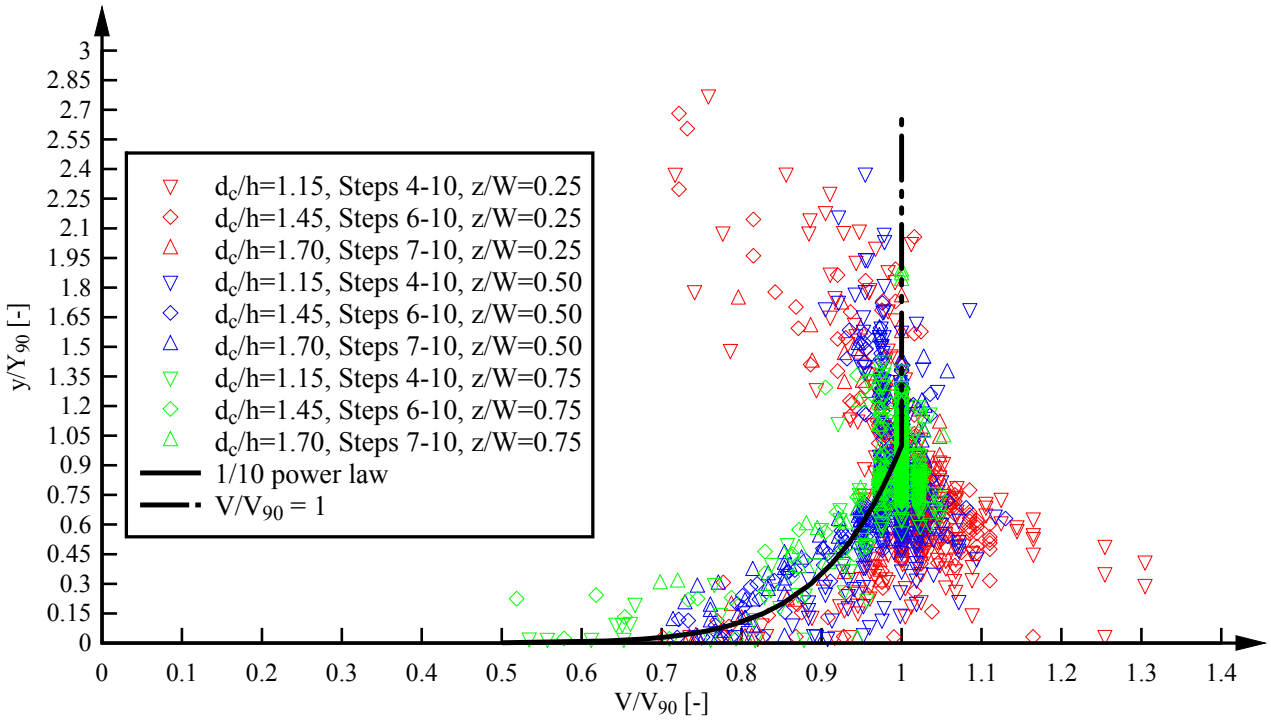

(B) d_c/h = 1.45, Q = 0.090 m^3/s, Re = 6.87×10^5 - Comparison with flat and pooled stepped spillways

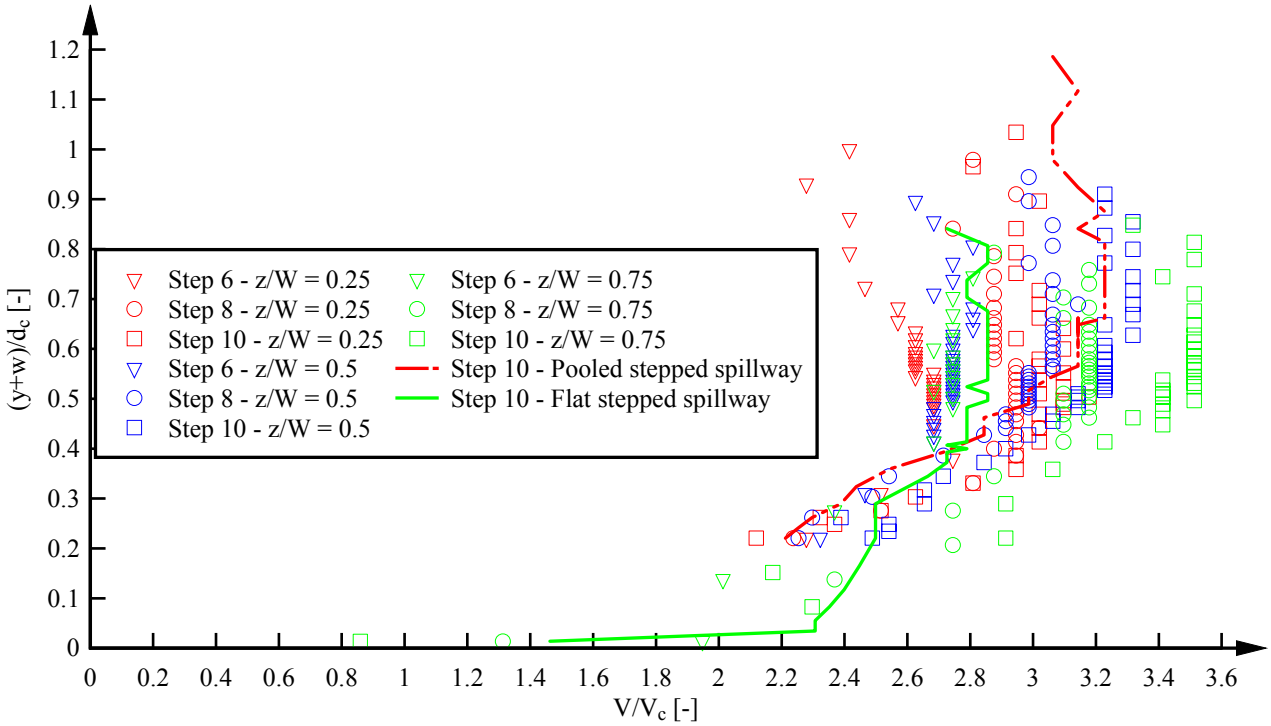

Fig. 5-6 – Turbulence intensity distributions on the stepped spillway with in-line configuration of flat and pooled steps in skimming flows (θ = 26.6°) – Measurements at three transverse locations: z/W = 0.25 (pooled stepped side), z/W = 0.5 (channel centreline), z/W = 0.75 (flat stepped side)
(A) d_c/h = 1.45, Q = 0.090 m^3/s, Re = 6.87×10^5

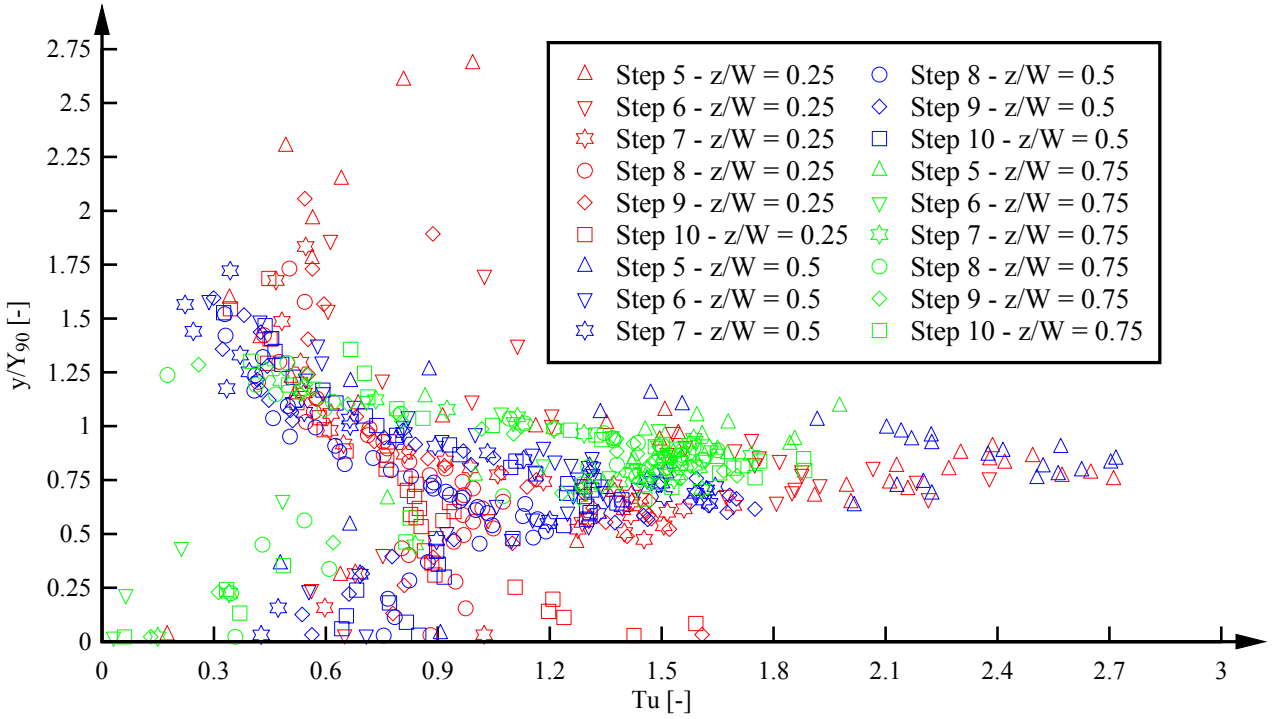

(B) d_c/h = 1.70, Q = 0.113 m^3/s, Re = 8.72×10^5 - Comparison with flat and pooled stepped spillways

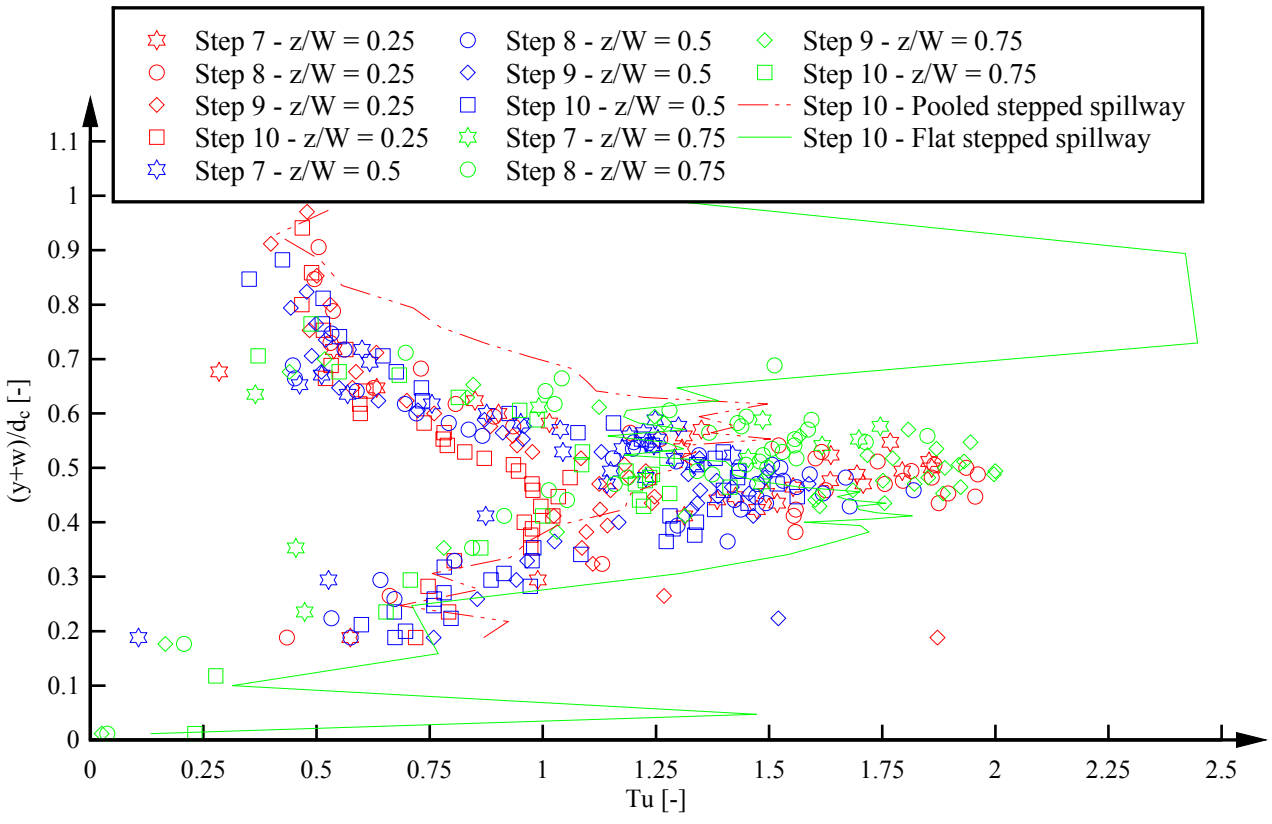

5.2.6 Longitudinal distributions of characteristic air-water flow parameters

Some characteristic air-water flow properties were calculated for all skimming flow data, including the mean air concentration C_{mean}, the characteristic interfacial velocity V_{90} and the maximum bubble count rate F_{max}. Their longitudinal distributions are illustrated in Figure 5-7 for all transverse positions. Note that Figure 5-7 includes both the transverse data and the transverse-averaged data (symbols & lines). The transverse averaging of the data is discussed in Appendix F. The corresponding air-water flow parameters on the flat and pooled stepped spillways are also included in Figure 5-7 for the same flow rates. All the air-water flow parameters are reported in a tabular form in Appendix D, together with further air-water flow parameters and data sets for the nappe and transition flow regimes.

In Figure 5-7A, some longitudinal distributions of mean air concentration C_{mean} are presented for all step edges downstream of the inception point in the skimming flow regime. The observations showed some large differences of mean air content in the transverse direction with the largest values of C_{mean} on the pooled stepped side and the smallest for the flat stepped side. The comparison with flat and pooled stepped spillway data suggested that the transverse averaged data on the in-line stepped spillway yielded some mean void fraction levels close to the flat stepped chute results.

The longitudinal distributions of the characteristic interfacial velocity V_{90} are shown in Figure 5-7B for all skimming flow data at the three transverse positions. The transverse averaged data are also included as well as some flat and pooled stepped spillway data. The results showed some large differences in interfacial velocity V_{90} between the transverse positions at each step edge. The largest velocities V_{90} were observed on the flat stepped side of the in-line configurations of flat and pooled steps and the smallest on the pooled stepped side. This finding was consistent with the velocity profiles shown in Figure 5-5. The transverse averaged velocity V_{90} data compared reasonably well with the data observed on the pooled stepped spillway (Fig. 5-7B).

The maximum bubble count rate values F_{max} for all skimming flow data are presented in Figure 5-7C for all step edges downstream of the inception point. Some significant differences were seen between the transverse positions: much larger bubble count rates were recorded on the pooled stepped side compared to the flat stepped side (Fig. 5-7C). The transverse averaged data were relatively close to the maximum bubble count rate observed on channel centreline as well as to the pooled stepped spillway data.

All data sets showed increasing values C_{mean}, F_{max} and V_{90} with increasing distance from the inception point of air entrainment. That is, uniform equilibrium was not achieved at the chute downstream end for all investigated flow rates.

Fig. 5-7 – Longitudinal distributions of characteristic parameters on the stepped spillway with in-line configuration of flat and pooled steps in skimming flows (θ = 26.6°) – Measurements at three transverse locations: z/W = 0.25 (pooled stepped side), z/W = 0.5 (channel centreline), z/W = 0.75 (flat stepped side) - Comparison with transverse averaged parameters and flat and pooled stepped spillways

(A) Mean air concentration C_{mean}

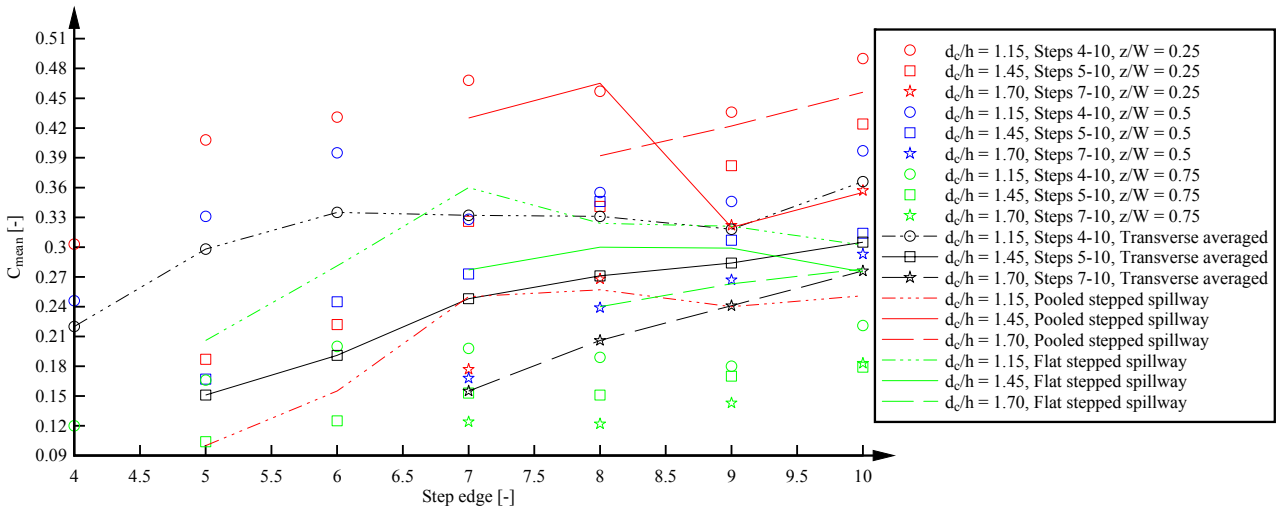

(B) Characteristic interfacial velocity V_{90}

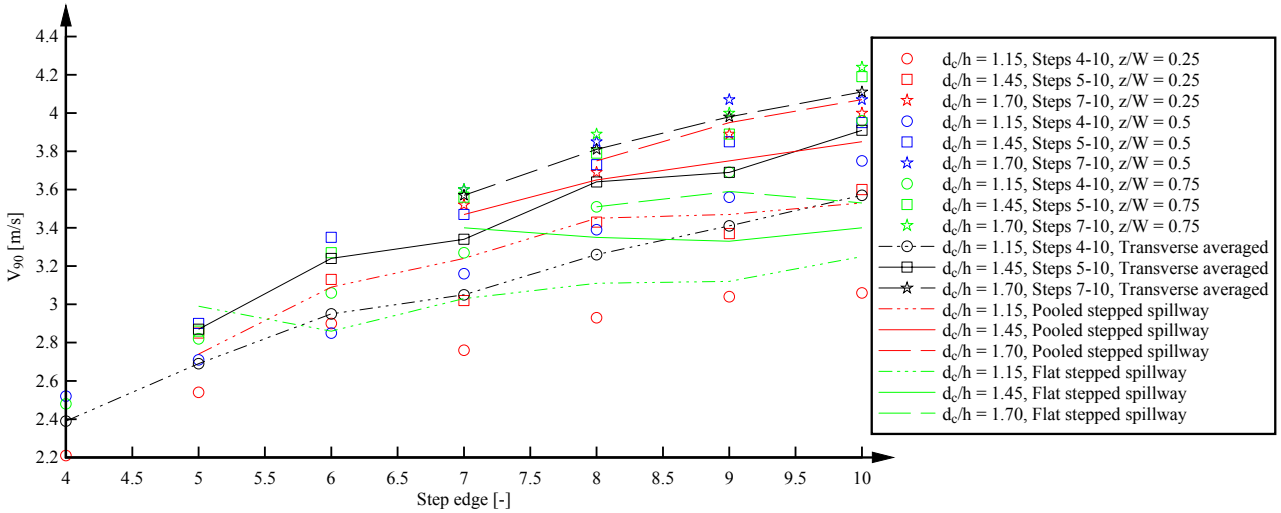

(C) Maximum bubble count rate F_{max}

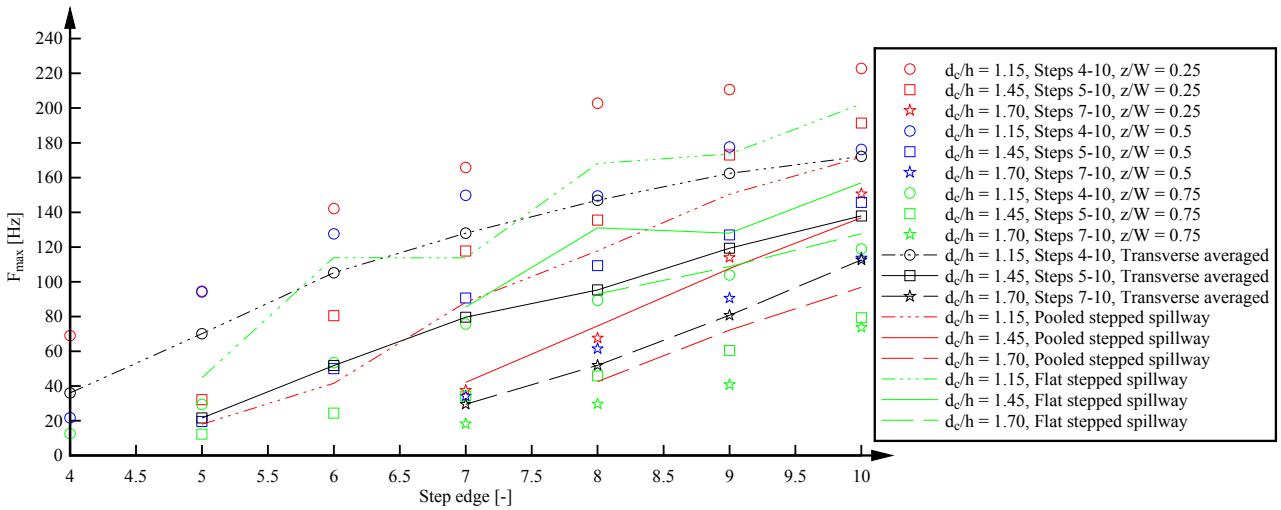

5.2.7 Air-water flow properties in nappe flows

For a discharge in the nappe flow regime ($d_c/h = 0.5$), the air-water flow properties were measured at the three transverse positions and the results are illustrated in Figure 5-8 in dimensionless form as a function of $(y+w)/d_c$. In Figure 5-8, all air-water flow properties reflected the strong three-dimensional and instable nature of the flow, earlier illustrated and discussed in section 3.4.

The void fraction distributions are presented in Figure 5-8A at several step edges downstream of the inception point. For the flat stepped side (z/W = 0.75), the void fraction distributions exhibited similar shapes to those seen in transition flows on flat stepped spillways. On the channel centreline and pooled stepped side, the void fraction distributions showed some scattered profiles. The void fraction profiles seemed close to shaped observed in jets in the nappe flow regime (TOOMBES 2002; TOOMBES & CHANSON 2008a) with high aeration levels for the entire air-water flow column. Similarly, the dimensionless bubble count rate $F \times d_c/V_c$ distributions showed a broad range of shapes as illustrated in Figure 5-8B. The bubble frequency distributions showed profiles with high bubble count rates in the flow region close to the pooled step weir. On the flat stepped side, the bubble count rates were significantly larger and the distributions showed some shapes comparable to those observed on flat stepped spillways with maxima in the intermediate flow region (Fig. 5-8B).

The interfacial velocities on the flat stepped side showed some typical profiles with a shape close to a power law and with increasing velocity with increasing longitudinal distance from the inception point. On the pooled stepped side and channel centreline, the interfacial velocity data showed a slower flow motion. It is believed that the velocity data reflected the strong instabilities of the flow with jets impacting onto the pooled stepped side and the channel centreline. In Figure 5-8C, some typical dimensionless interfacial velocity V/V_c distributions are shown at the three transverse

positions. Figure 5-8C highlights also the significant differences in transverse direction for a given step edge and flow rate, highlighting the three-dimensional nature of the flow.

Some turbulence intensity Tu data are presented in Figure 5-8D. On the flat stepped side, the turbulence intensity distributions showed some typical shapes observed in skimming flows on a flat stepped spillway with some large turbulence levels in the intermediate flow region and smaller values of Tu in the lower bubbly and upper spray regions. On the pooled stepped side and on the channel centreline, the turbulence levels were significantly larger with a lot of data scatter. The large turbulence levels were likely linked with the flow instabilities on the pooled stepped side of the in-line stepped spillway.

Fig. 5-8 – Air-water flow properties on the stepped spillway with in-line configuration of flat and pooled steps in nappe flows (θ = 26.6°) – Measurements at three transverse locations: z/W = 0.25 (pooled stepped side), z/W = 0.5 (channel centreline), z/W = 0.75 (flat stepped side) - Flow conditions: $d_c/h = 0.50$, $Q = 0.016$ m^3/s, $Re = 1.39\times10^5$

(A) Void fraction distributions

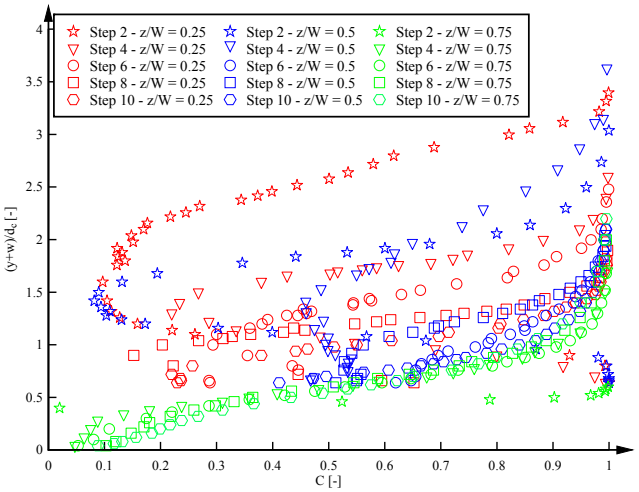

(B) Bubble count rate distributions

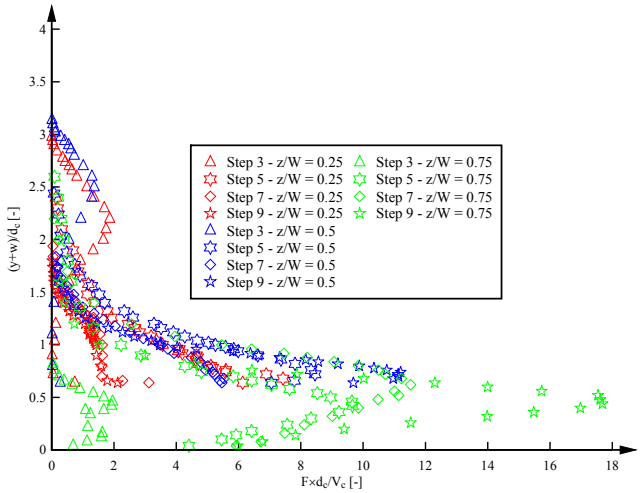

(C) Interfacial velocity distributions

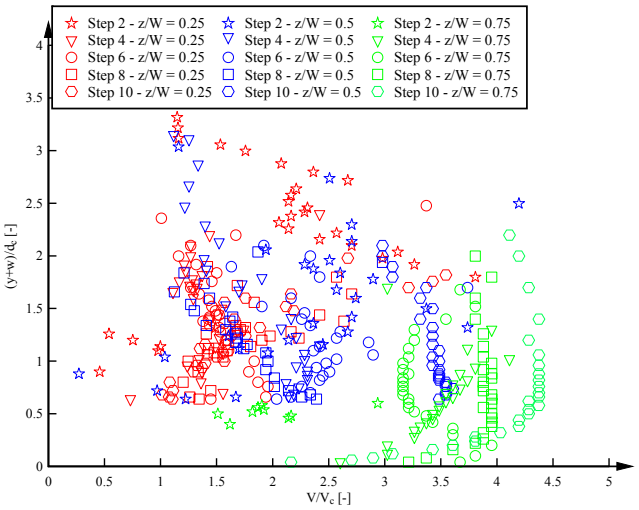

(D) Turbulence intensity distributions

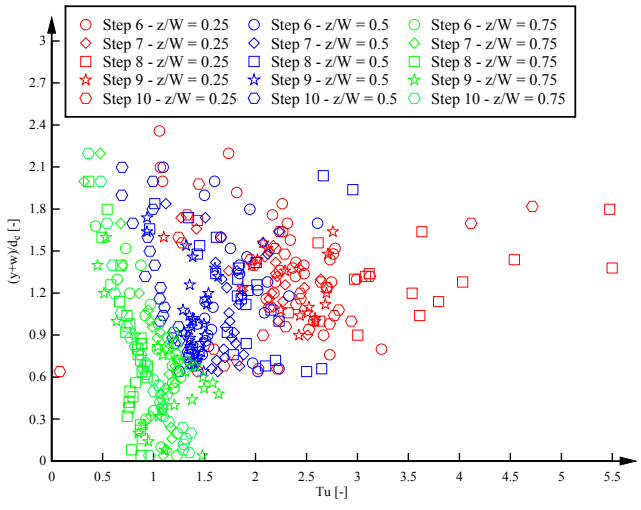

5.2.8 Air-water flow properties in transition flows

The air-water flow properties were also measured in the transition flow regime and some results are presented in Figure 5-9. They are further compared with the corresponding air-water flow property distributions recorded on the channel centreline for the flat and pooled stepped spillways.

The void fraction distributions are illustrated in Figure 5-9A for several step edges downstream of the inception point. The void fraction distributions on the flat stepped side showed a S-shape profile commonly observed in skimming flows. On the pooled stepped side, the distributions of void fraction showed a flat straight profile more typical of a transition flow sub-regime TRA1. The void fraction distributions on the channel centreline showed also some scatter. For the first step edges immediately downstream of the inception point, the void fraction distributions on the channel centreline and pooled stepped side exhibited a profile corresponding to a jet flow, which was consistent with the visual observations.

The dimensionless distributions of bubble count rate $F \times d_c/V_c$ are presented in Figure 5-9B. They showed some bubble frequencies at all transverse positions which were comparable to the flat and pooled stepped spillway observations. Larger bubble frequencies were seen on the flat stepped side of the in-line stepped spillway. On the pooled stepped side, the bubble count rates were significantly smaller and appeared not to increase with longitudinal distance at the downstream end of the channel. The bubble frequencies for the channel centreline were almost identical to the data on the flat and pooled stepped spillways.

The dimensionless distributions of interfacial velocity V/V_c showed some data scatter across the channel width (Fig. 5-9C). On the flat stepped side, some significantly larger velocities were recorded compared to the pooled stepped side. The velocities V/V_c on the flat stepped side were comparable to the velocities on the flat stepped spillway for the same flow rate. The interfacial velocity distributions on the channel centreline showed some large scatter and the velocities were much smaller than on the flat stepped side, as well as the flat and pooled stepped spillways.

The turbulence intensity data exhibited some strong scatter (Fig. 5-9D) with much larger turbulence levels on the first flat and pooled step edges immediately downstream of the inception point. Further downstream, the turbulence levels on the channel centreline and the flat stepped side are in good agreement with the turbulences on the flat and pooled stepped spillways with some maxima in the intermediate flow region. The turbulence intensities for the pooled stepped side showed larger values for the entire flow column.

Fig. 5-9 – Air-water flow properties on the stepped spillway with in-line configuration of flat and pooled steps in transition flow sub-regime TRA1 (θ = 26.6°) – Measurements at three transverse locations: z/W = 0.25 (pooled stepped side), z/W = 0.5 (channel centreline), z/W = 0.75 (flat stepped side) - Flow conditions: $d_c/h = 0.70$, Q = 0.030 m^3/s, Re = 2.30×10^5

(A) Void fraction distributions

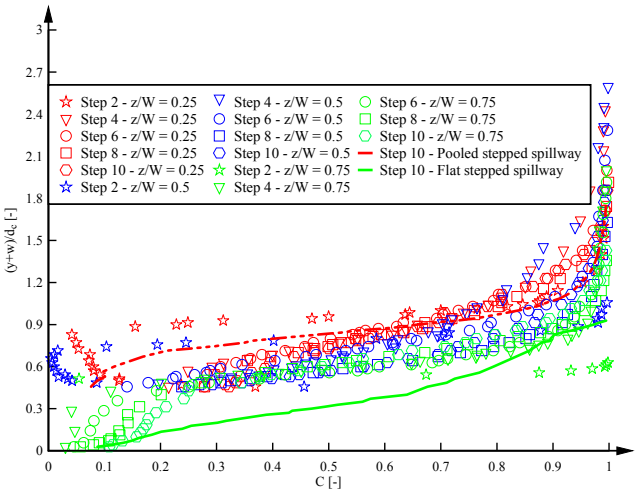

(B) Bubble count rate distributions

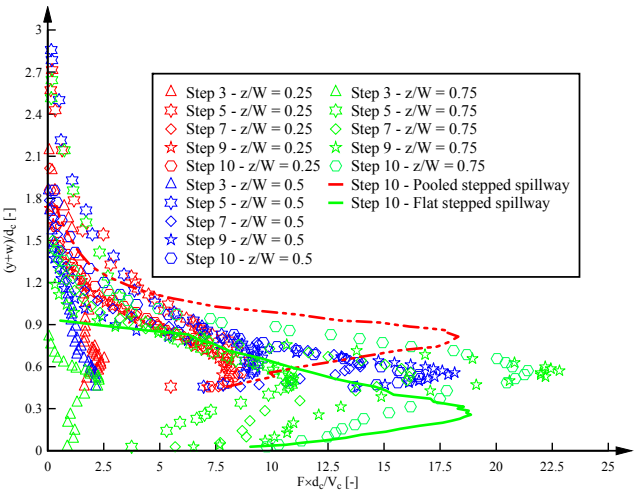

(C) Interfacial velocity distributions

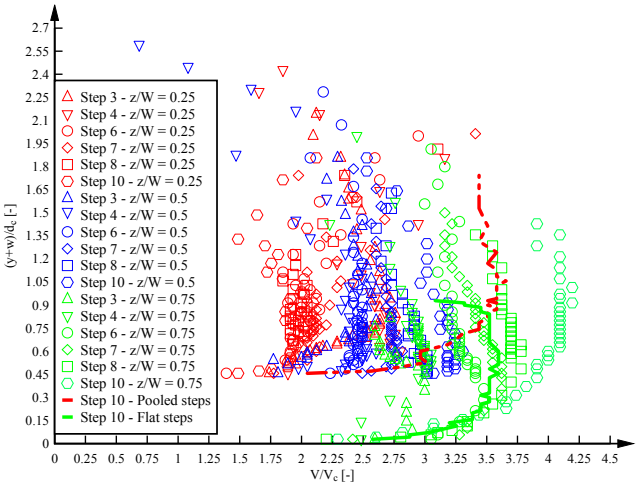

(D) Turbulence intensity distributions

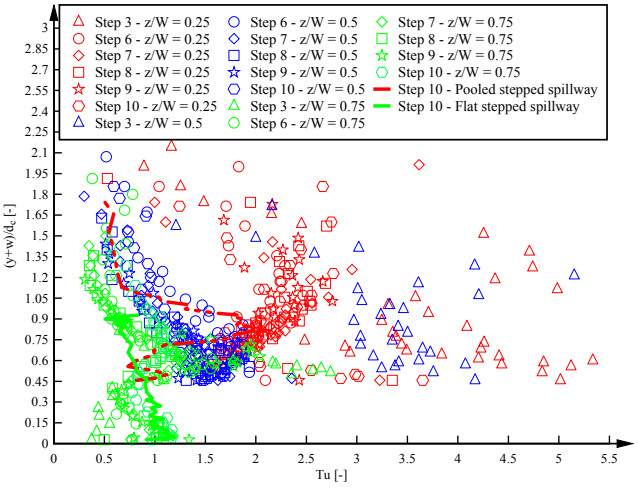

5.3 AIR-WATER FLOW PROPERTIES ON STEPPED SPILLWAY WITH STAGGERED CONFIGURATION OF FLAT AND POOLED STEPS

5.3.1 Presentation

Some experiments were performed on the stepped spillway with staggered configuration of flat and pooled steps with the double-tip conductivity probe at three transverse positions in the air-water flow region. The transverse positions on each step edge comprised z/W = 0.25, z/W = 0.5 and z/W = 0.75. For the flat steps, the first measurement position (y = 0) was defined at the step edge while, for the pooled steps, the first measurement position was the pool weir edge.

The experiments were conducted in transition and skimming flows. Table 5-2 summarises the

experimental flow conditions. The air-water flow properties were calculated and some characteristic results are presented in this section. The full data set is presented in Appendix D.

Table 5-2 – Air-water flow measurements with a double-tip conductivity probe (Ø = 0.25 mm) for the stepped spillway with staggered configuration of flat and pooled steps (θ = 26.6°)

Configuration (1)	d_c/h [-] (2)	Q [m^3/s] (3)	Re [-] (4)	Measurement at step edge (5)	Flow regime (6)
Stepped spillway with staggered configuration of flat and pooled steps	0.7	0.030	2.30×10^5	3-10	TRA
	1.15	0.063	4.85×10^5	5-10	SK
	1.45	0.090	6.87×10^5	6-10	SK
	1.7	0.113	8.72×10^5	7-10	SK

Notes: d_c: critical flow depth; h: vertical step height; Q: water discharge; Re: Reynolds number defined in terms of the hydraulic diameter; SK: skimming flow regime; TRA: transition flow regime.

5.3.2 Void fraction

Some typical void fraction distributions are illustrated in Figure 5-10 for the three transverse positions and at all step edges downstream of the inception point in skimming flows for the staggered stepped spillway configuration. In Figure 5-10A, the distributions of void fraction are shown as a function of y/Y_{90}. In Figure 5-10B, they are presented as a function of $(y+w)/d_c$. Overall the void fraction data reflected the staggered configuration of flat and pooled steps and the shapes of void fraction profiles tended to alternate from step edge to step edge at z/W = 0.25 and z/W = 0.75. On the channel centreline (z/W = 0.5), the void fraction distributions were more uniform along the stepped chute.

The void fraction data for the two outside channel positions were consistently above the channel centreline data indicating a larger mean air concentration on the centre of the spillway (Fig. 5-10A). The void fraction distributions matched closely the advective diffusion equation for air bubbles (Eq. (4-3), section 4) and the theoretical curves are added for some step edges in Figure 5-10A. The data presented in Figure 5-10B illustrated the alternation of flat and pooled steps every second step edge. The void fraction data in the staggered configuration tended to be close to the results observed in the pooled stepped spillway configuration (Fig. 5-10B).

Fig. 5-10 – Void fraction distributions on the stepped spillway with staggered configuration of flat and pooled steps in skimming flows (θ = 26.6°) – Measurements at three transverse positions: z/W = 0.25, z/W = 0.5 (channel centreline) and z/W = 0.75

(A) $d_c/h = 1.70$, Q = 0.113 m^3/s, Re = 8.72×10^5; Comparison with Eq. (4-3)

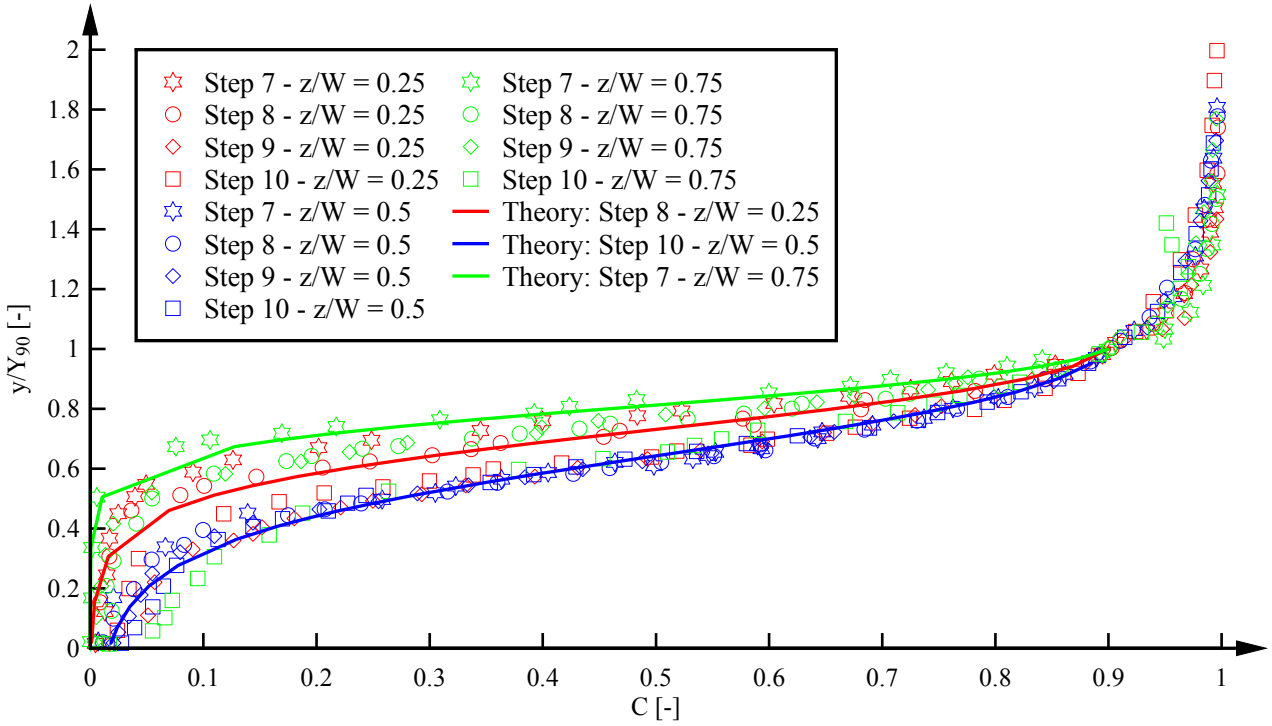

(B) $d_c/h = 1.45$, Q = 0.090 m^3/s, Re = 6.87×10^5; Comparison with flat and pooled stepped spillways

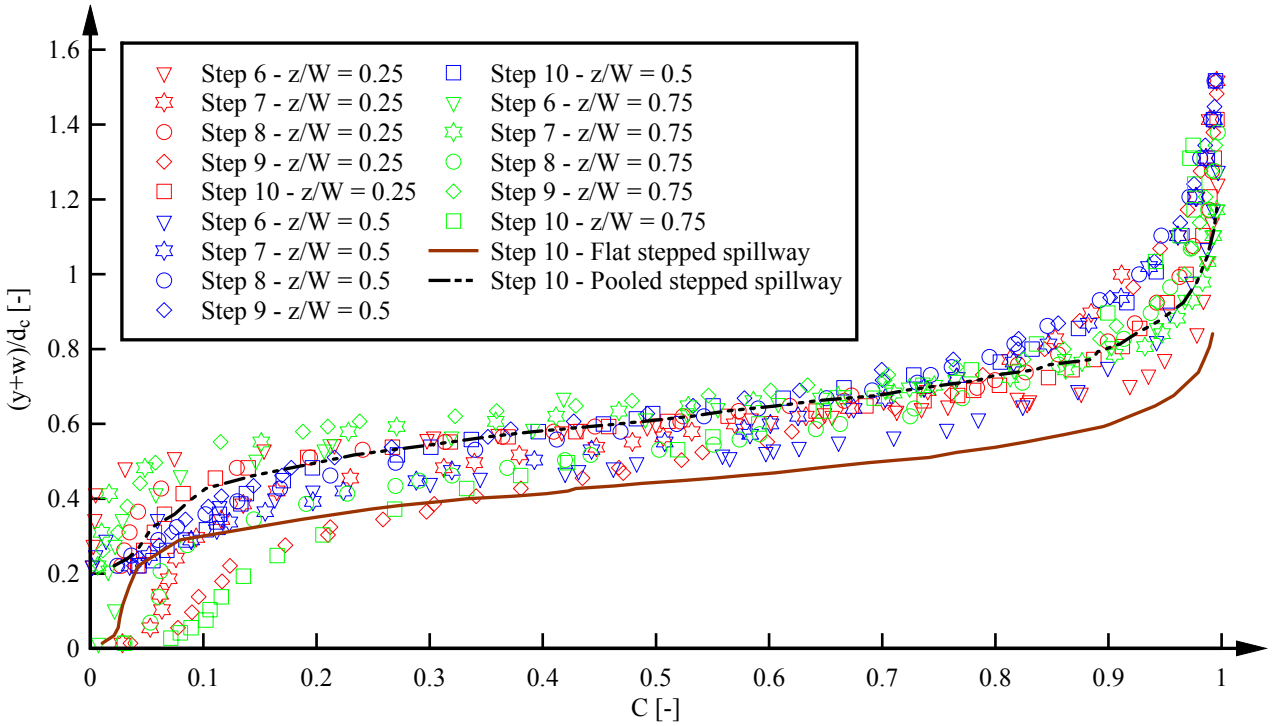

5.3.3 Bubble count rate

The shapes of bubble count rate distributions were typical to those seen in skimming flows with bubble count rate maxima in the intermediate flow region ($0.3 < C < 0.7$) and smaller bubble frequencies in the lower bubbly and upper spray regions. The elevation of the maximum bubble count rate varied in agreement with the alternation of flat and pooled steps every second step edge (Fig. 5-11A). Some differences were also visible between the three transverse positions, showing some larger numbers of entrained bubbles on the pooled steps and the smallest bubble count rate on channel centreline. For all experiments, the maximum bubble count rate increased with increasing downstream distance from the inception point. The comparison with the flat and stepped spillway data showed some much larger bubble count rates at all transverse positions on the stepped spillway with staggered configuration of flat and pooled steps (Fig. 5-11B). Some typical dimensionless bubble count rate $F \times d_c/V_c$ distributions are illustrated in Figure 5-11 as functions of y/Y_{90} and $(y+w)/d_c$, for the skimming flow experiments.

Fig. 5-11 – Dimensionless bubble count rate distributions on the stepped spillway with staggered configuration of flat and pooled steps in skimming flows ($\theta = 26.6°$) – Measurements at three transverse positions: z/W = 0.25, z/W = 0.5 (channel centreline) and z/W = 0.75
(A) $d_c/h = 1.15$, $Q = 0.063$ m^3/s, $Re = 4.85 \times 10^5$

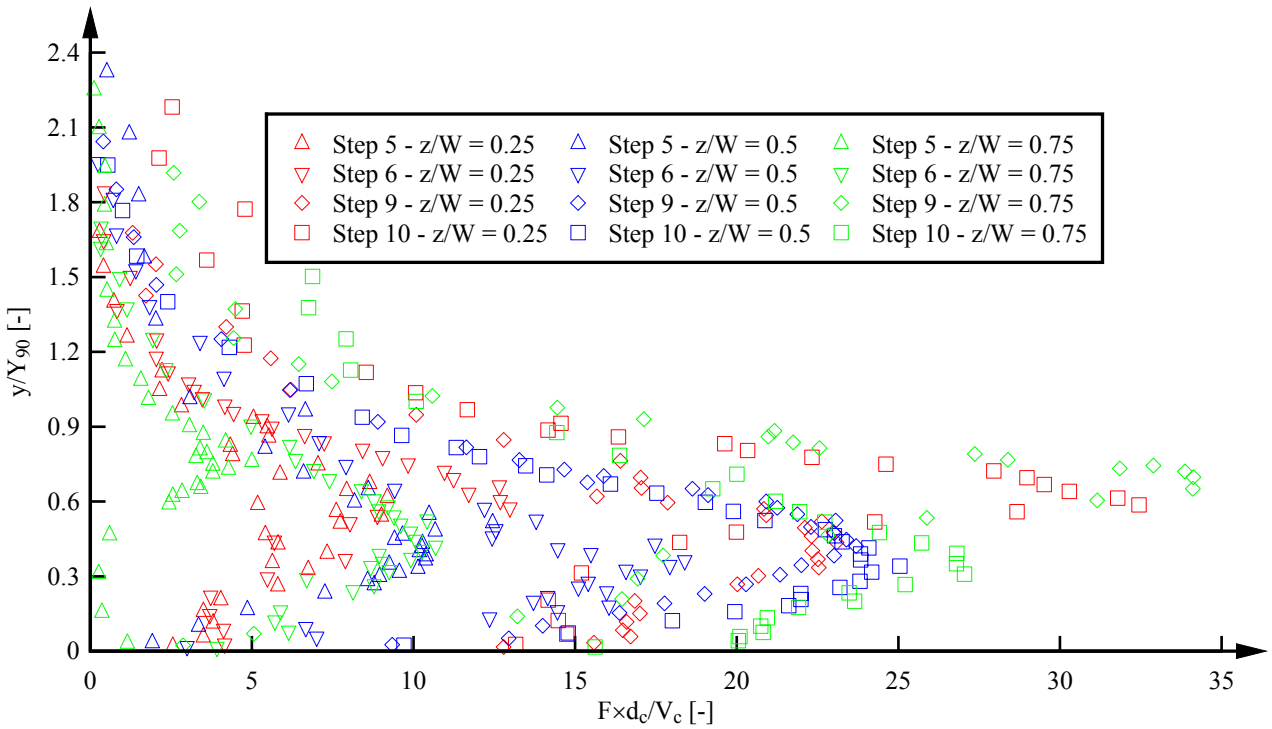

(B) d_c/h = 1.70, Q = 0.113 m^3/s, Re = 8.72×10^5 - Comparison with flat and pooled stepped spillways

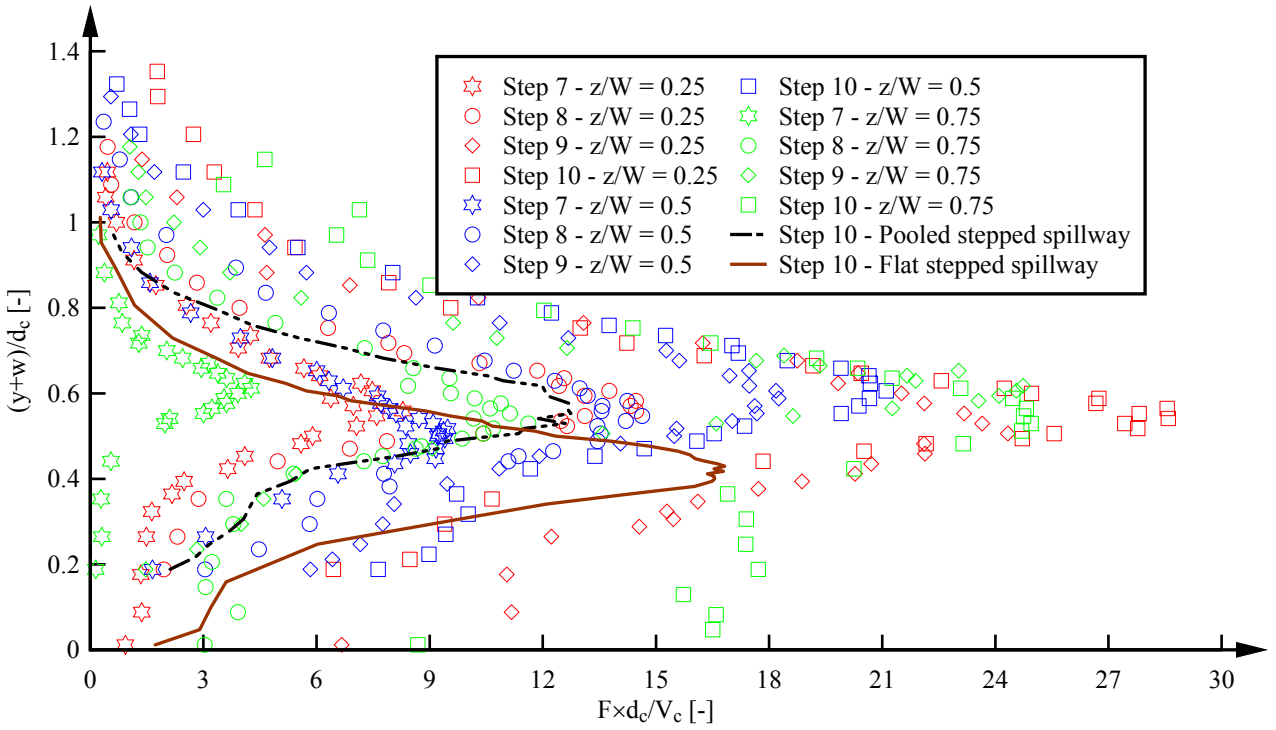

5.3.4 Interfacial velocity

The interfacial velocities were calculated for all skimming flow discharges at the three transverse positions. Figure 5-12 presents some dimensionless results. For all interfacial velocities, some differences were observed between successive step edges at all transverse positions. In Figure 5-12A, the dimensionless interfacial velocities V/V_{90} are shown as functions of y/Y_{90} and the data are compared with the $1/10^{th}$ power law (Eq. (4-4), section 4). On the staggered stepped spillway, the velocity were in reasonably close agreement with the power law, despite some scatter especially for the data on the channel centreline.

The dimensionless interfacial velocity V/V_c data are illustrated in Figure 5-12B as a function of $(y+w)/d_c$. At a given step edge, the data showed some larger interfacial velocities on channel centreline. Further the interfacial velocities at z/W = 0.75 tended to be larger than those at z/W = 0.25. This difference might be linked with the first step cavity configuration, being a flat step for z/W = 0.75 and a pooled step edge for z/W = 0.25. The corresponding interfacial velocities for the flat and pooled stepped spillways were added in Figure 5-12B. Overall the channel centreline velocities for the staggered stepped spillway were comparable to the pooled stepped spillway velocities.

Fig. 5-12 – Dimensionless interfacial velocity distributions on the stepped spillway with staggered configuration of flat and pooled steps in skimming flows (θ = 26.6°) – Measurements at three transverse positions: z/W = 0.25, z/W = 0.5 (channel centreline) and z/W = 0.75

(A) All skimming flow data sets; Comparison with Eq. (4-4) & (4-5)

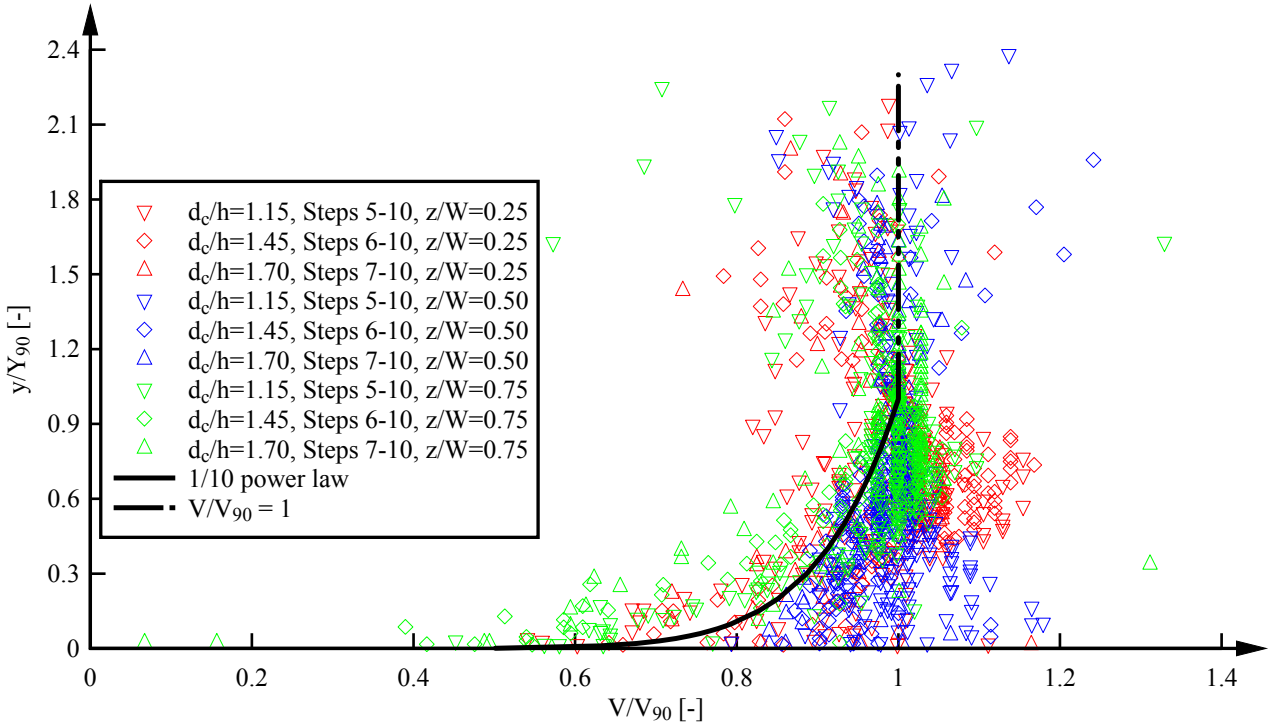

(B) d_c/h = 1.45, Q = 0.090 m^3/s, Re = 6.87×10^5 - Comparison with flat and pooled stepped spillways

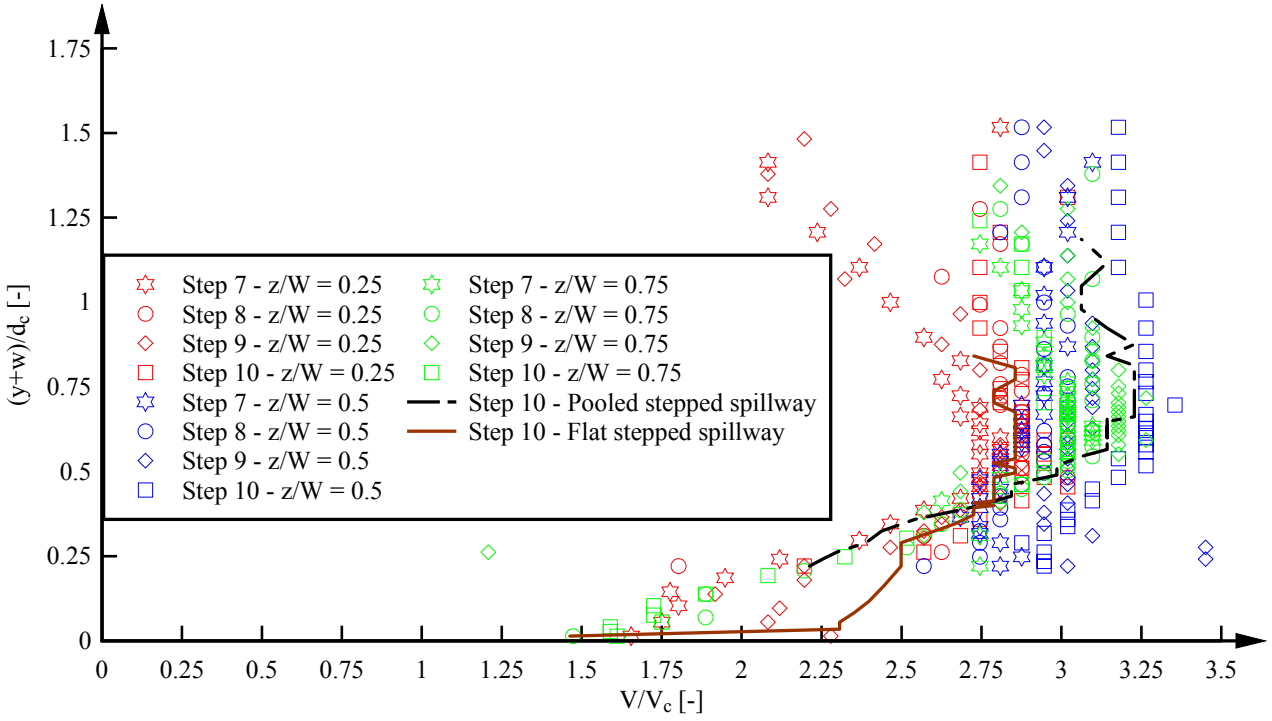

5.3.5 Turbulence intensity

Some typical turbulence intensity distributions are illustrated in Figure 5-13 as functions of y/Y_{90} and $(y+w)/d_c$. All distributions showed some large turbulence levels in the intermediate flow region ($0.3 < C < 0.7$) and smaller values in the lower bubbly and upper spray regions. However the distributions of turbulence intensities exhibited some shapes which differed between the flat and pooled sides of the staggered stepped chute. The differences were mostly seen immediately downstream of the inception point and lesser transverse differences were seen further downstream.

5.3.6 Longitudinal distributions of characteristic air-water flow parameters

Some longitudinal distributions of characteristic air-water flow parameters are presented in Figure 5-14 for the skimming flow data sets. All characteristic air-water flow parameters are listed in a tabular manner in Appendix D.

The mean air concentration C_{mean} is shown in Figure 5-14A at the three transverse positions for all step edges downstream of the inception point. The transverse averaged data are added. The mean air concentrations showed some strong variations from step edge to step edge linked with the alternation of flat and pooled steps on each outside. On the channel centreline, the mean void fraction C_{mean} data were the largest highlighting the strong local aeration. The mean void fraction data for the flat and pooled stepped spillways are included in Figure 5-14A. Overall, the transverse averaged mean air concentration on the staggered stepped spillway exhibited larger values than those observed on flat and pooled stepped spillway configurations for the same flow rate.

The characteristic interfacial velocity V_{90} data are shown in Figure 5-14B. The interfacial velocities showed some longitudinal variation from step edge to step edge linked with the alternation of flat and pooled steps. With increasing distance from the inception point, the interfacial velocities increased for all experiments. Some velocity differences were observed between the different transverse positions with some scatter for all data sets. Overall the characteristic velocity V_{90} was the largest on the channel centreline, while the data at $z/W = 0.75$ were mostly greater than those at $z/W = 0.25$. The finding was consistent with the velocity profile observations (Fig. 5-12B). The transverse averaged velocities V_{90} showed a relatively close agreement with the centreline interfacial velocity data. A comparison indicated a relatively close agreement between the transverse averaged data and the flat stepped spillway for the smallest skimming flows rates. For the largest flow rates, the transverse averaged values of V_{90} were closer to the pooled stepped spillway data (Fig. 5-14B).

Fig. 5-13 – Turbulence intensity distributions on the stepped spillway with staggered configuration of flat and pooled steps in skimming flows (θ = 26.6°) – Measurements at three transverse positions: z/W = 0.25, z/W = 0.5 (channel centreline) and z/W = 0.75

(A) $d_c/h = 1.70$, $Q = 0.113$ m^3/s, $Re = 8.72\times10^5$

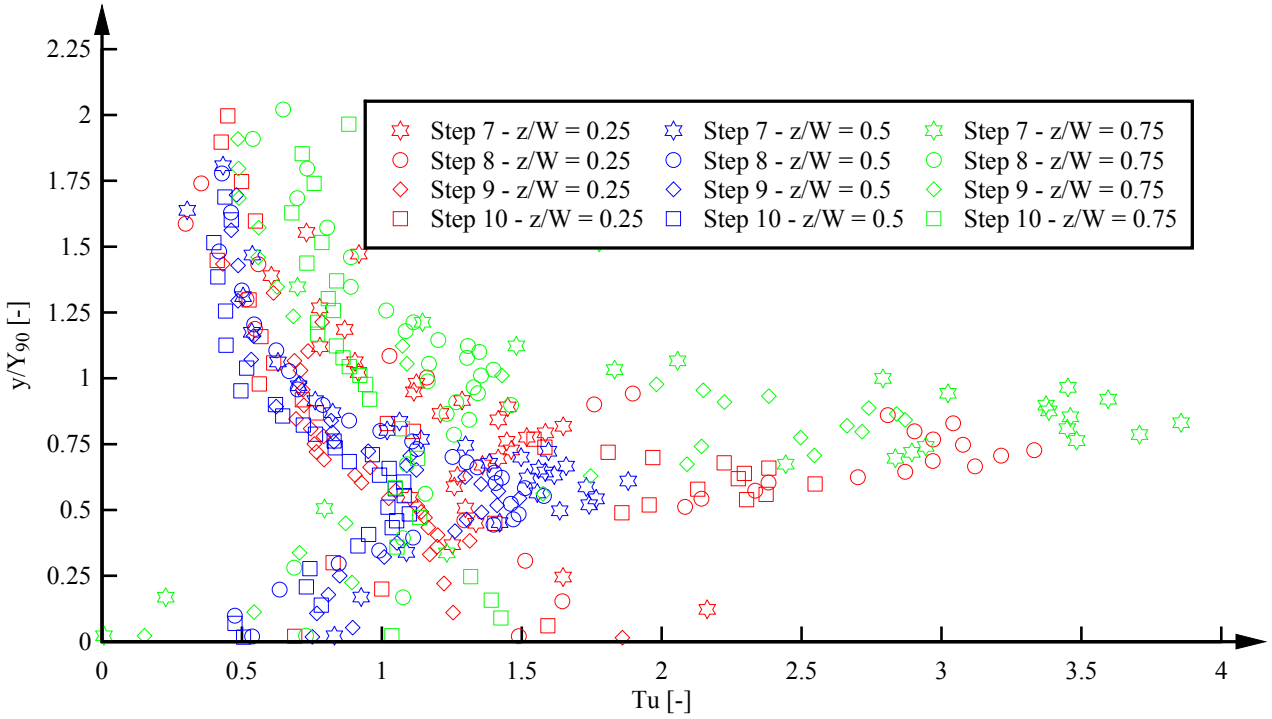

(B) $d_c/h = 1.15$, $Q = 0.063$ m^3/s, $Re = 4.85\times10^5$, Comparison with flat and pooled stepped spillways

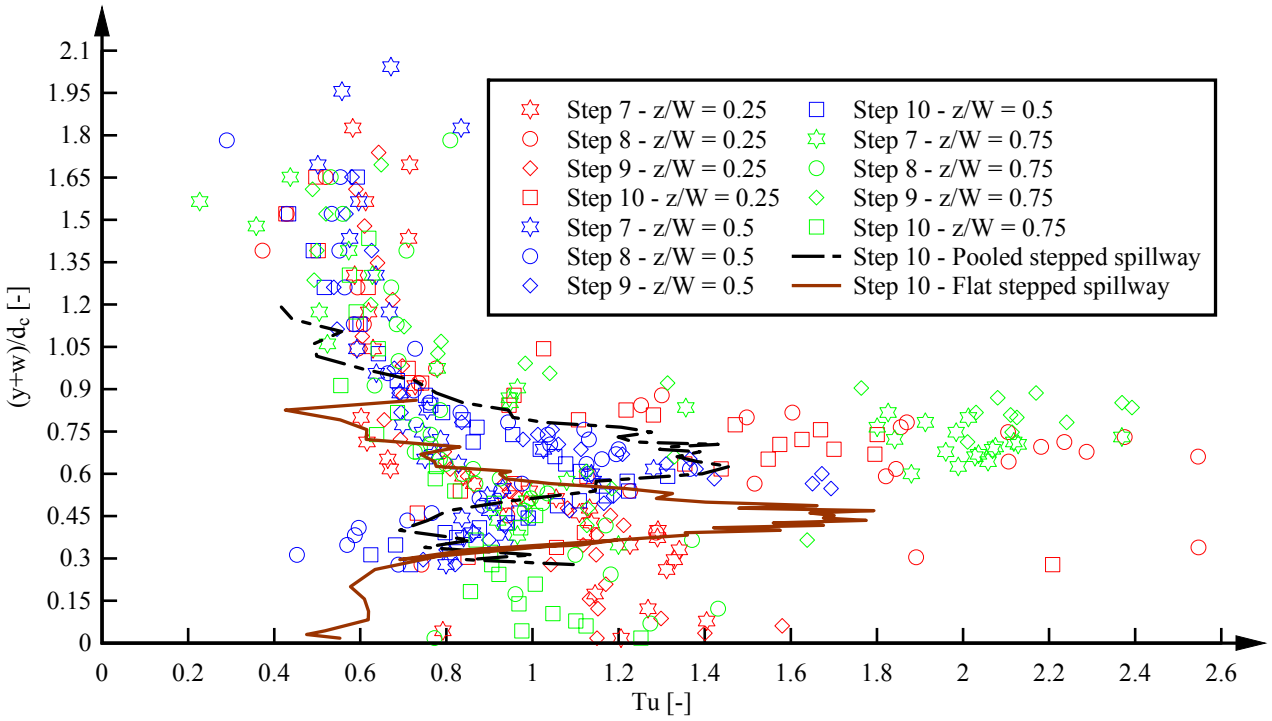

The longitudinal distributions of maximum bubble count rate F_{max} are presented in Figure 5-14C for the three transverse positions together with the transverse averaged data. The largest bubble count

rate data were observed at z/W = 0.25 and the smallest at z/W = 0.75 for all skimming flow data sets. The differences might be linked with the different first step cavity geometry: i.e., pooled step at z/W = 0.25 and flat step for z/W = 0.75. The transverse averaged values of F_{max} were slightly smaller compared to the maximum bubble count rates on the channel centreline. The data for the flat and pooled stepped spillway configurations are included in Figure 5-14C. Overall the transverse averaged data showed relatively close agreement with the pooled stepped spillway data. For all data sets, the bubble count rates increased with increasing downstream distance from the inception point and no uniform equilibrium was achieved in the present configuration.

Fig. 5-14 – Longitudinal distributions of characteristic parameters on the stepped spillway with staggered configuration of flat and pooled steps in skimming flows (θ = 26.6°) – Measurements at three transverse positions: z/W = 0.25, z/W = 0.5 (channel centreline) and z/W = 0.75 Comparison with transverse averaged parameters and flat and pooled stepped spillways

(A) Mean air concentration C_{mean}

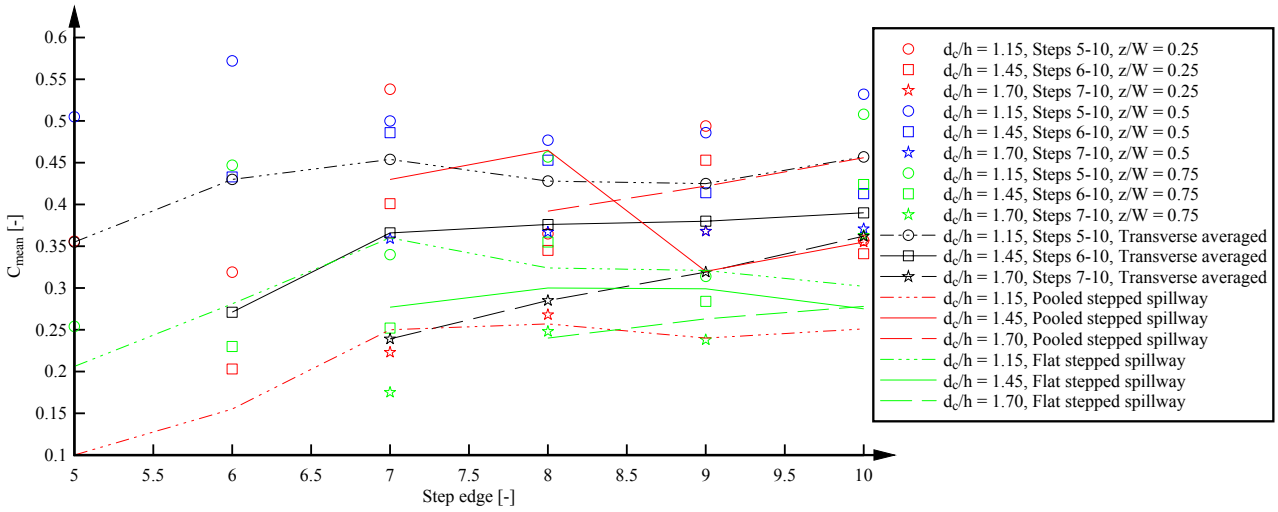

(B) Characteristic interfacial velocity V_{90}

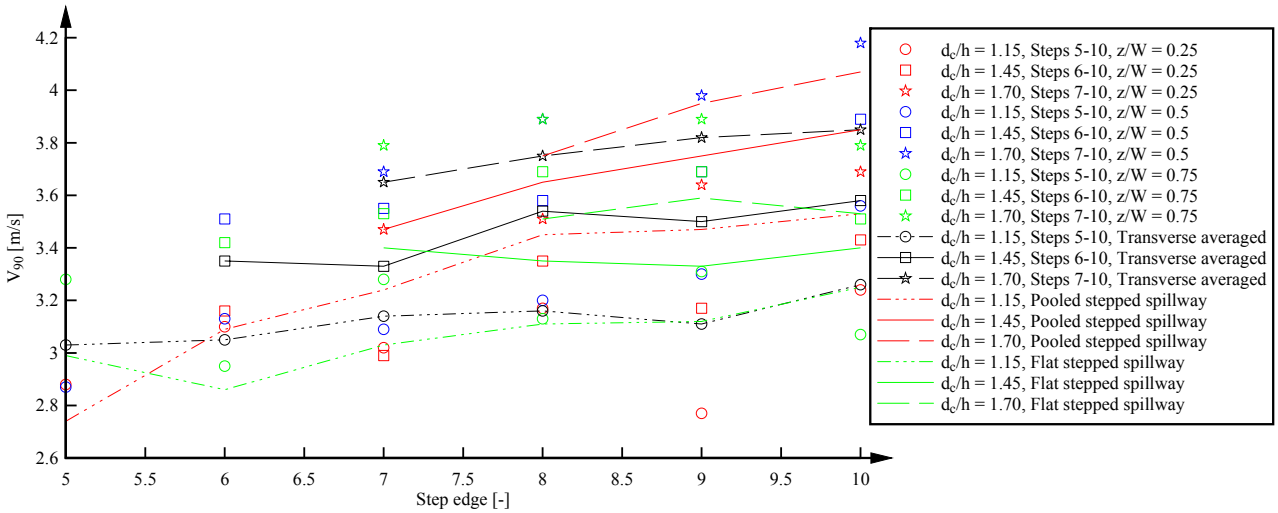

(C) Maximum bubble count rate F_{max}

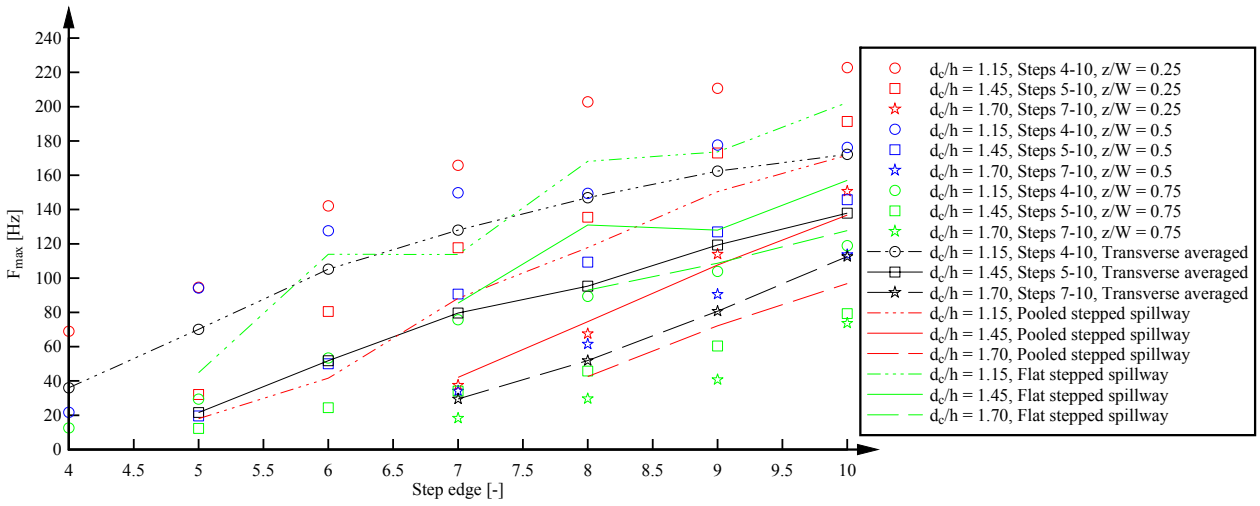

5.3.7 Air-water flow properties in transition flows

For a transition flow rate ($d_c/h = 0.7$), some detailed air-water flow measurements were performed at all step edges downstream of the inception point. The resulting distributions of void fraction C, bubble count rate F, interfacial velocity V and turbulence intensity Tu are illustrated in Figure 5-15 as functions of $(y+w)/d_c$. The flat and pooled stepped spillway data at the downstream end are added for comparison (Fig. 5-15). All the data presented a range of scatter reflecting the existence of flow instabilities as well as the wavy three-dimensional flow patterns in the transition flow.

The void fraction distributions showed some profiles typical of transition flows with some flat shape (Fig. 5-15A). The alternation of flat and pooled steps induced some rapid changes in void fraction distribution shapes with downstream distance.

In Figure 5-15B, some typical distributions of dimensionless bubble count rate $F \times d_c/V_c$ are presented. The data showed some strong variations in the longitudinal and transverse directions. Close to the inception point of air entrainment, the shapes of bubble count rate distributions differed from most profiles observed next to the downstream end of the staggered configuration. At the downstream end, some larger bubble count rates were observed in the intermediate flow region ($0.3 < C < 0.7$) as seen on flat and pooled stepped spillways (Fig. 5-15B). Interestingly the bubble count rates on the channel centreline did not increase with increasing downstream distance. At $z/W = 0.25$ and 0.75, the bubble count rates were slightly larger, but the data did not show a typical increase in bubble count rates with increasing downstream distance as observed with other stepped configurations.

The dimensionless distributions of interfacial velocity V/V_c are shown in Figure 5-15C at the three transverse positions. Some strong data was observed with the largest interfacial velocities for $z/W = 0.75$, corresponding to the flat stepped side of the staggered stepped spillway at the first step cavity.

The interfacial velocities for z/W = 0.25 and on channel centreline were quantitatively close, and smaller than the velocities observed on both flat and pooled stepped spillways (Fig. 5-15C).

The distributions of the turbulence intensities are illustrated in Figure 5-15D for all data sets in the transition flow rate. The largest turbulence levels were recorded for the pooled step edges just downstream of the inception point. Overall the turbulence intensities were slightly larger compared to those observed in skimming flows and transition flows on the flat and pooled stepped spillways. The turbulence intensity distributions changed with downstream distance in a manner reflecting the alternations of flat and pooled steps on the staggered stepped chute, while the centreline data were almost uniform.

Fig. 5-15 – Air-water flow properties on the stepped spillway with stepped spillway with staggered configuration of flat and pooled steps in skimming flows (θ = 26.6°) – Measurements at three transverse positions: z/W = 0.25, z/W = 0.5 (channel centreline) and z/W = 0.75: $d_c/h = 0.70$, Q = 0.030 m^3/s, Re = 2.30×10^5

(A) Void fraction distributions

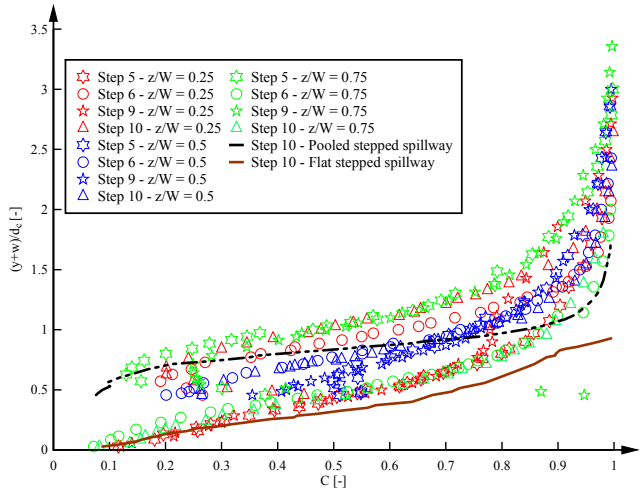

(B) Bubble count rate distributions

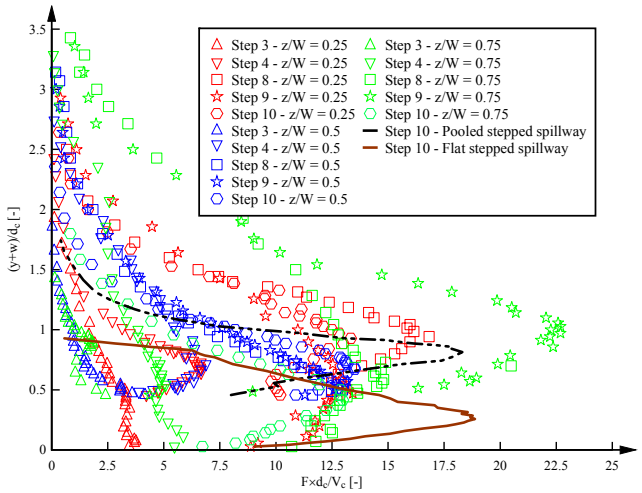

(C) Interfacial velocity distributions

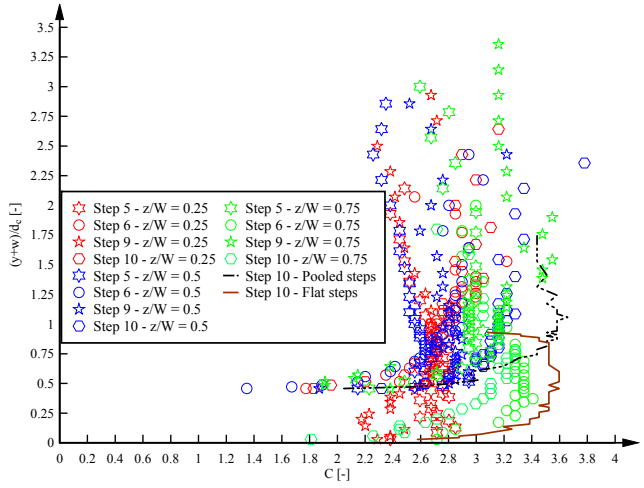

(D) Turbulence intensity distributions

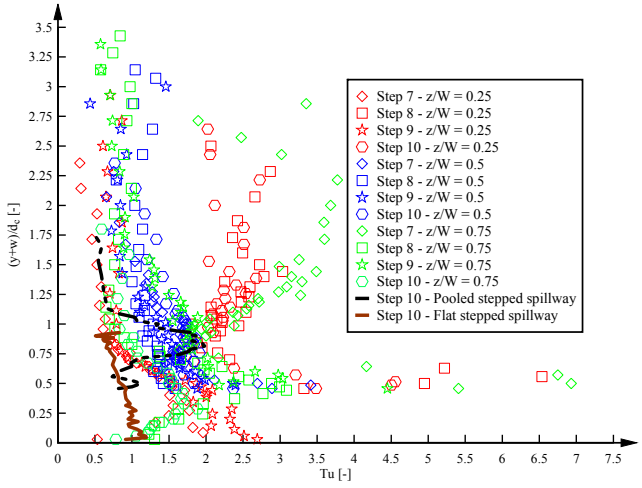

5.4 SUMMARY AND DISCUSSION

Some extensive air-water flow measurements were conducted on the stepped spillways with in-line and staggered configurations of flat and pooled steps. Most experiments were performed in the skimming flow regime, although a few experiments were conducted in transition and nappe flows. The flows were highly three-dimensional and the measurements were conducted at three transverse positions at each step edge downstream of the inception point.

The physical experiments highlighted the complexity of the air-water flow and its three-dimensional nature. For all flow rates, some differences in air-water flow properties were recorded between the three transverse locations. With increasing discharges and increasing distance downstream of the inception point the differences tended to become lesser. In skimming flows, the void fraction and interfacial velocity distributions for both stepped spillways agreed well with the advective diffusion equation of air-bubbles and the power law respectively for all measurement locations. Some strong turbulence levels were observed reflecting the existence of flow instabilities and flow singularities on the complex stepped spillway configurations.

For the smaller flow rates in the nappe and transition flow regimes, some strong instabilities and data scatter were observed, with significant differences in air-water flow properties across the chute. The differences in air-water flow properties across the channel width were observed for all discharges in both in-line and staggered stepped spillway configurations. Overall these complex stepped spillway designs cannot be recommended for a typical stepped spillway design because of the flow instabilities.

6. ENERGY DISSIPATION AND FLOW RESISTANCE ON THE STEPPED SPILLWAYS

6.1 RESIDUAL HEAD AND ENERGY DISSIPATION

For the design engineers, it is critical to quantify accurately the rate of energy dissipation above the stepped chute and the residual energy at the downstream end of the stepped spillway. In this section, the rate of energy dissipation and the residual energy were estimated for all stepped spillway configurations. The data were calculated based upon the detailed air-water flow measurements with the double-tip conductivity probe. The rate of energy dissipation $\Delta H/H_{max}$ expressed the percentage of total energy loss along the stepped spillway relative to the upstream total head H_{max}:

$$H_{max} = \frac{3}{2} \times d_c + H_{dam} \quad (6\text{-}1)$$

where H_{dam} is the dam height and d_c the critical flow depth. The total head loss ΔH was estimated as: $\Delta H = H_{max} - H_{res}$ in which the residual head H_{res} was:

$$H_{res} = d \times \cos\theta + \frac{U_w{}^2}{2 \times g} + w = \int_0^{Y_{90}} (1 - C) \times \cos\theta \times dy + \frac{q_w{}^2}{2 \times g \times \left(\int_0^{Y_{90}} (1 - C) \times dy \right)^2} + w \quad (6\text{-}2)$$

where d is the equivalent clear water flow depth, θ the channel slope, U_w the flow velocity ($U_w = q/d$), w the pool weir height (w = 0 for a flat step), q is the water discharge per unit width. Note that the effects of velocity correction coefficient were neglected in first approximation, Equations (6-1) and (6-2) apply to the flat and pooled stepped spillways and the calculations were performed at the last step edge (i.e. step edge 10).

For the stepped spillways with in-line and staggered configurations of flat and pooled stepped steps, the residual head was averaged in the transverse direction:

$$H_{res} = 0.375 \times \left(d_{local} \times \cos\theta + \frac{U_{local}{}^2}{2 \times g} + w \right)_{0.25} + 0.25 \times \left(d_{local} \times \cos\theta + \frac{U_{local}{}^2}{2 \times g} + w \right)_{0.5} + 0.375 \times \left(d_{local} \times \cos\theta + \frac{U_{local}{}^2}{2 \times g} + w \right)_{0.75} \quad (6\text{-}3)$$

where the subscripts 0.25, 0.5 and 0.75 refer to the three transverse measurement locations, d_{local} is the local equivalent clear water flow depth and U_{local} is the local flow velocity estimated as $U_{local} = q_{local}/d_{local}$ with:

$$q_{local} = \int_0^{Y_{90}} V \times (1 - C) \times dy \quad (6\text{-}4)$$

A sensitivity analysis of the transverse averaging method was conducted and some details are

presented in Appendix F.

The data in terms of rate of energy dissipation are presented in Figure 6-1 as a function of the dimensionless drop in elevation between the broad-crested weir and the measured step edge Δz_o. In Figure 6-1, the present data are compared with the experimental data of FELDER et al. (2012) down 8.9° flat and pooled stepped spillways, and some reanalysed data of THORWARTH (2008) and KÖKPINAR (2004) on stepped spillways with 14.6° and 30° slope respectively (Table 6-1). The present data (θ = 26.6°) showed a larger rate of energy dissipation on the flat stepped spillway compared to the other configurations in the skimming flow regime. In the transition flows, the pooled stepped spillway showed the largest rate of energy dissipation (Fig. 6-1).

Fig. 6-1 - Rate of energy dissipation at the downstream end of the flat and pooled stepped chutes - Comparison of results between the present stepped spillway configurations, data of FELDER et al. (2012) and re-analysed data of THORWARTH (2008) and KÖKPINAR (2004)

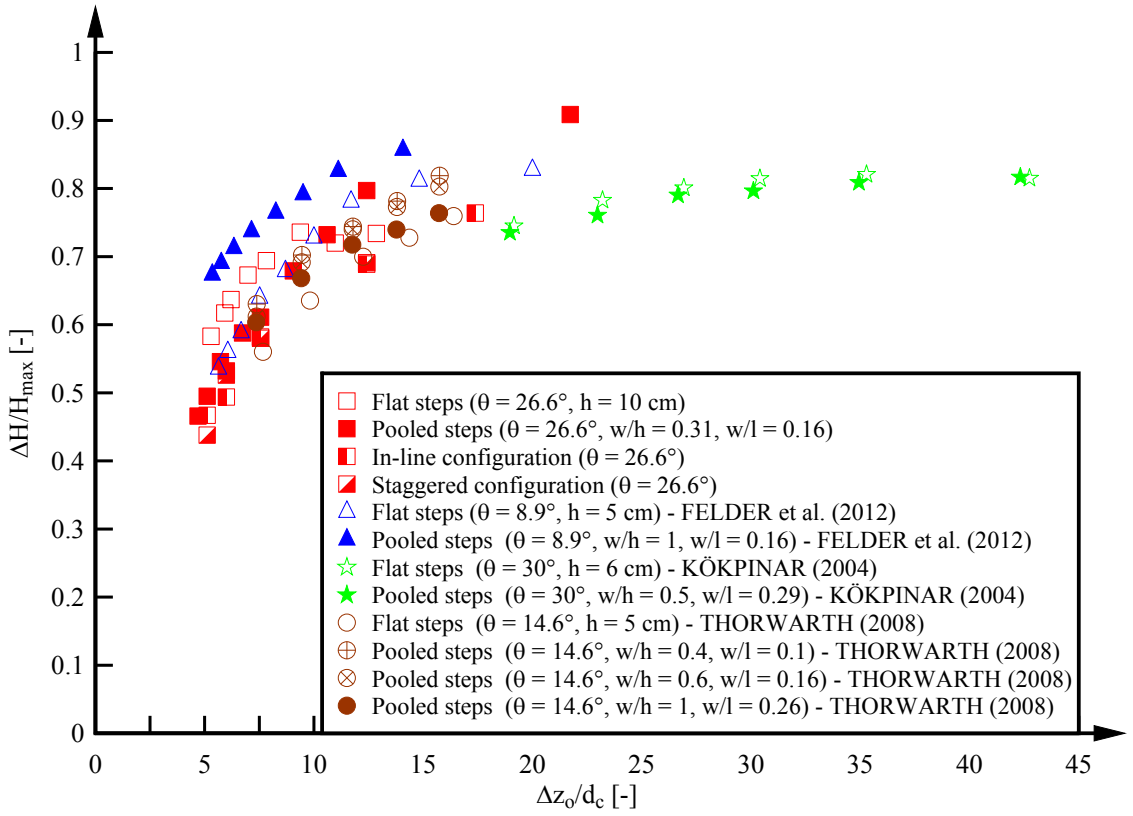

The present findings contradicted the observations by FELDER et al. (2012) and THORWARTH (2008) on 8.9° and 14.6° stepped chutes: these studies observed the largest rate of energy dissipation rates on the pooled stepped spillway configurations. THORWARTH (2008) investigated different ratios of pool weir height w to step height h, and pool weir height w to step length l. The re-analysed data (θ = 8.9° & 14.6°) showed larger energy dissipation for all pooled stepped spillway

experiments. The re-analysis of KÖKPINAR's (2004) data showed on the other hand little difference between the flat and pooled stepped spillway performances. The data of KÖKPINAR (2004) showed a smaller decrease in energy dissipation rate with increasing discharge, compared to all other data sets (Fig. 6-1). On a 30º slope, TAKAHASHI et al. (2008) showed comparatively larger rate of energy dissipation on the flat stepped chute than on the pooled steps, and the finding was observed systematically for a range of relative pool heights ($0.2 < w/h < 1$).

Table 6-1 - Experimental studies of flat and pooled stepped spillways: pooled step configuration details

Reference (1)	Slope [º] (2)	h [m] (3)	w/h (4)	w/l (5)	W [m] (6)
KÖKPINAR (2004)	30.0	0.06	0.50	0.288	0.50
THORWARTH (2008)	14.6	0.05	0.4 0.6 1	0.105 0.156 0.261	0.50
TAKAHASHI et al. (2008)	30	0.20	0.2 - 1	0.11 - 0.58	0.40
FELDER et al. (2012)	8.9	0.05	1.0	0.157	0.50
Present study	26.6	0.10	0.31	0.155	0.52

The residual head data are illustrated in Figure 6-2, in which the present data are compared with earlier studies (Table 6-1). The dimensionless residual head H_{res}/d_c is shown as a function of the dimensionless discharge d_c/h (Fig. 6-2). The present data showed the smallest residual head for the flat stepped spillway: i.e., $H_{res}/d_c \approx 3.1$ in the skimming flow regime. On the pooled stepped spillway, the residual head was larger: i.e., $H_{res}/d_c \approx 3.7$. For the stepped spillways with in-line and staggered configurations of flat and pooled steps, larger residual head data were obtained, with a significant data scatter.

The data of FELDER et al. (2012) and THORWARTH (2008) showed smaller residual heads on the pooled stepped spillways with 8.9° and 14.6° slopes, while the dimensionless residual head remained almost constant for the investigated discharges (Fig. 6-2). The data of KÖKPINAR (2004) yielded some much larger residual energy for both flat and pooled stepped spillways down the 30° slope. The authors do not have a physical explanation to date. However the residual head for the flat stepped spillway was smaller for all discharges. This observation was in agreement with the present findings of smaller residual head for the flat stepped spillway.

Overall the present analysis implied that the chute slope had a large impact upon the energy dissipation performances. On the steeper slopes (26.6° and 30°), a smaller residual energy was

achieved on the flat stepped spillway configuration, while the residual energy was smaller for the pooled stepped spillway configuration on the flat slopes (8.9° and 14.6°).

Fig. 6-2 - Dimensionless residual energy at the downstream end of flat and pooled stepped chutes - Comparison of present results with data of FELDER et al. (2012) and re-analysed data of THORWARTH (2008), KÖKPINAR (2004)

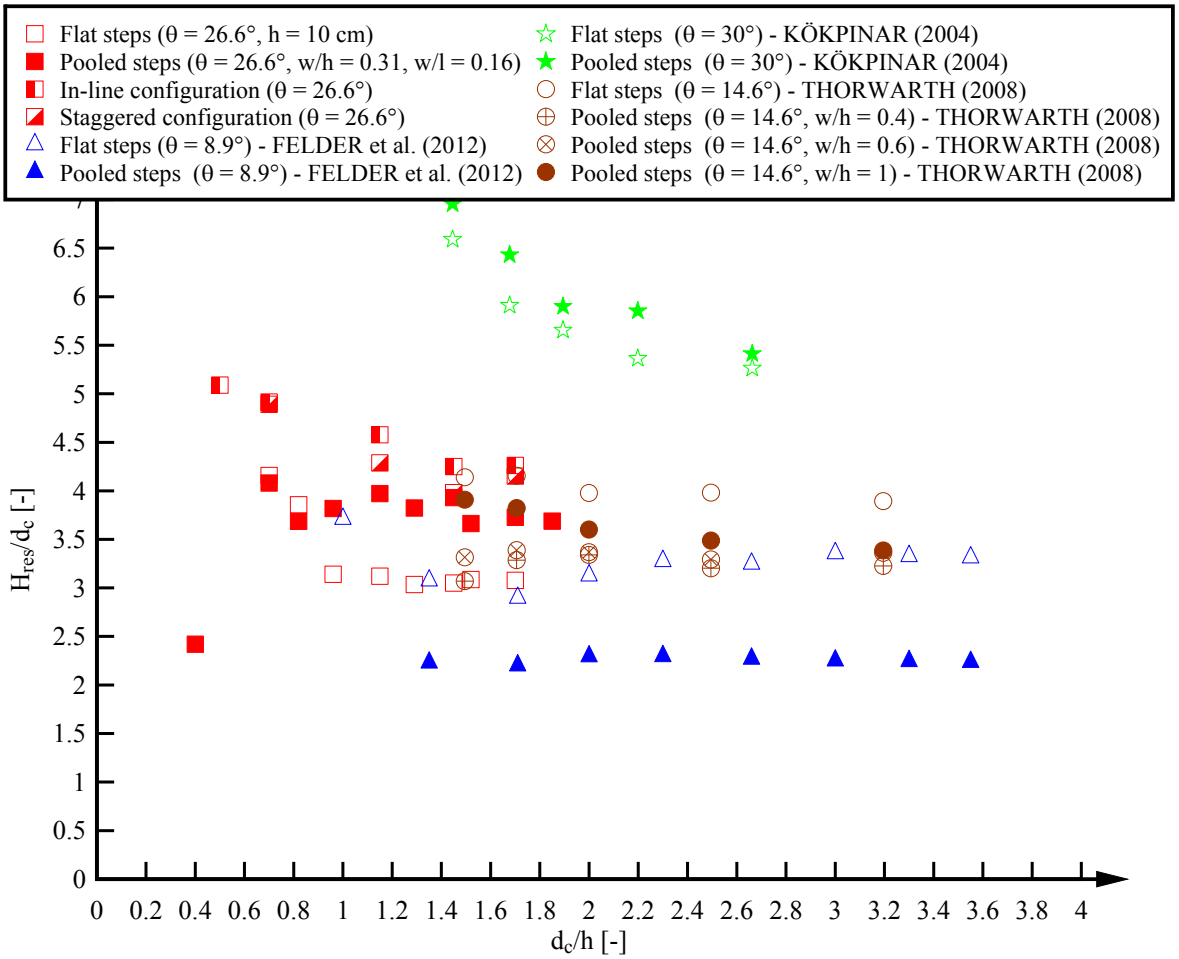

6.2 FLOW RESISTANCE

On stepped spillways, some significant form losses are caused by the steps (CHANSON 2001). Some additional flow resistance might be caused by the pool weir on pooled stepped spillways. The flow resistance is commonly expressed in the form of a Darcy-Weisbach friction factor f_e (RAJARATNAM 1990; CHANSON 2001). The friction factor on a stepped spillway is a average dimensionless shear stress between the air-water main stream and the step cavities. Herein the Darcy-Weisbach friction factor was calculated as:

$$f_e = \frac{8 \times \tau_0}{\rho_w \times U_w^2} = \frac{8 \times g \times S_f \times \left(\int_{y=0}^{Y_{90}} (1-C)\,dy \right)}{U_w^2} = \frac{8 \times g \times S_f \times d}{U_w^2} \quad (6\text{-}4)$$

where the friction slope equals $S_f = - \partial H/\partial x$, H is the total head, x is the distance in flow direction, C is the void fraction, Y_{90} is the flow depth where C = 90%, d is the equivalent clear water flow depth and U_w is the flow velocity (CHANSON 2001; CHANSON et al. 2002). Equation (6-4) was used to calculate the equivalent Darcy-Weisbach friction factors for the flat and pooled stepped spillway configurations. For the in-line and staggered configurations of flat and pooled stepped steps, the friction factor was based upon a transverse averaging of the air-water flow properties:

$$f_e = 0.375 \times \left(\frac{8 \times g \times S_f \times d_{local}}{U_{local}^2} \right)_{0.25} + 0.25 \times \left(\frac{8 \times g \times S_f \times d_{local}}{U_{local}^2} \right)_{0.5} + 0.375 \times \left(\frac{8 \times g \times S_f \times d_{local}}{U_{local}^2} \right)_{0.75} \quad (6\text{-}5)$$

where the subscripts 0.25, 0.5 and 0.75 refer to z/W, and d_{local} and U_{local} are the clear-water flow depth and flow velocity at the transverse location z/W. Further details on the transverse averaging approach are presented in Appendix F.

The friction factor results are illustrated in Figure 6-3 as a function of the dimensionless step cavity roughness height $(h+w)\times\cos\theta/D_H$, where D_H is the hydraulic diameter. For the stepped spillways with in-line and staggered configuration of flat and pooled steps, the step roughness cavity height was averaged in the transverse direction. All present data showed some scatter within typically $0.15 < f_e < 0.28$ for the skimming flows (Fig. 6-3). There was no clear trend in terms of flow resistance. Larger friction factors were observed for the smallest flow rates for all stepped spillway configurations: i.e., $f_e \approx 0.3$ (small flow rates).

The present data were compared with earlier studies on flat slopes (Fig. 6-3). On flat slopes (8.9° and 14.6°), the friction factors were significantly smaller on the flat stepped spillways compared to the pooled stepped spillways. That is, the friction factor on the flat stepped spillways was $f_e \approx 0.1$. For the 14.6° pooled stepped spillway, $f_e \approx 0.19$ and while $f_e \geq 0.3$ on the 8.9° pooled stepped spillway.

In the present study ($\theta = 26.6°$), the pooled weir did not increase the flow resistance, contrarily to earlier flat slope observations. That is, the present data showed little effect of the pools upon the friction factor despite some data scatter. Although the weir height did not affect the flow resistance for the slope of 26.6°, it would be interesting to investigate the effect of larger weir height for the same channel slope.

Fig. 6-3 - Darcy friction factors on flat and pooled stepped spillways - Comparison between present data and data of THORWARTH (2008) and FELDER et al. (2012)

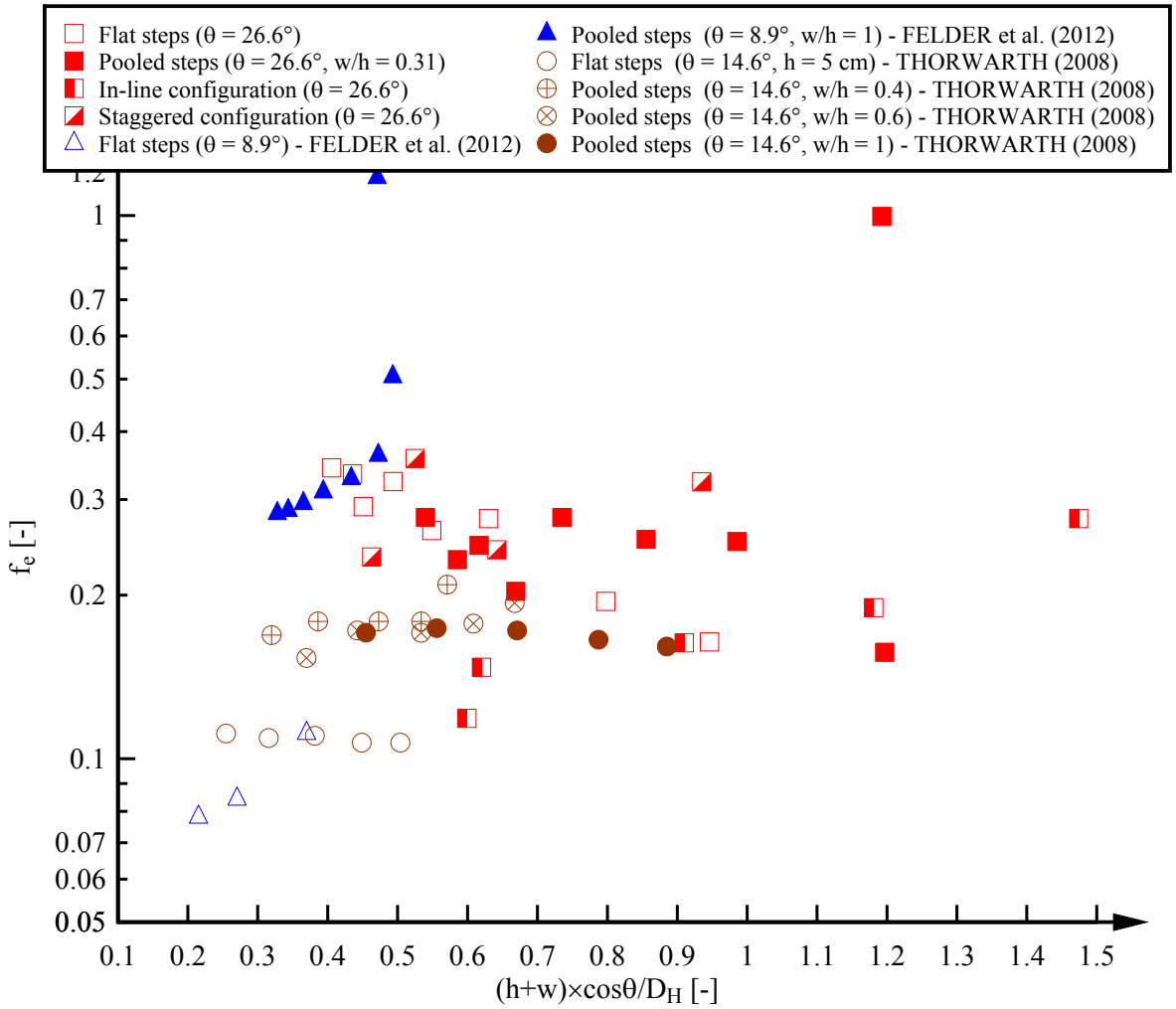

6.3 DISCUSSION

The present results indicated that the rate of energy dissipation was smaller on the pooled stepped spillway compared to the flat steps while the residual energy was larger. This finding was in contrast to experimental observations on 14.6° and 8.9° stepped chutes (THORWARTH (2008, FELDER et al. 2012). That is, the channel slope had a significant effect on the energy dissipation and the effect of the pool weir appeared to be reduced on steeper stepped chutes. On pooled stepped spillways with flat slopes (θ = 8.9º & 14.6º), some instabilities were observed and these might have enhanced the energy dissipation performances. The studies of THORWARTH (2008) ad TAKAHASHI et al. (2008) showed that the pool weir height did not affect the rate of energy dissipation significantly.

The interpretation of the experimental results for the stepped spillway configurations with in-line and staggered flat and pooled steps was more difficult. The flow was highly three-dimensional and, the residual energy varied significantly in the transverse direction. While some transverse averaging

was used herein to compare the energy dissipation performances, the residual energy at some transverse locations was much larger compared to the averaged values. Simply the present findings for the staggered and in-line stepped spillway configurations should not be used for design guidelines and can only provide a rough estimate of the average energy dissipation rate. These stepped spillway configurations are further affected by some flow instabilities and they should not be considered as a design option. If such complex in-line or staggered stepped spillway design is to be used, the present study demonstrated that a rigorous physical study is necessary to investigate in greater details the flow properties.

7. CONCLUSION

A physical study was performed on a relatively large size stepped spillway channel with a 26.6° slope and 0.10 m high steps. Different stepped chute configurations were tested. These were a spillway chute with flat horizontal steps, a pooled stepped spillway with 0.031 m high pool weirs, and two stepped spillway configurations with in-line and staggered arrangements of flat and pooled steps. Note that the test section length was moderate and uniform equilibrium flow conditions were not achieved at the downstream end of the chute for all investigated flow conditions.

For all stepped spillways, some visual observations of the flow patterns were performed for discharges $0.002 \leq Q \leq 0.155$ m^3/s. The flat stepped spillway showed some typical flow patterns with nappe, transition and skimming flow regimes depending upon the flow rate. Some similar flow regimes were observed on the pooled stepped spillway, although some pulsating flow was seen for some nappe flow rates associated with the downstream propagation of small instabilities. On the in-line and staggered configurations of flat and pooled steps, the flow was highly three-dimensional. Some strong instabilities and three-dimensional flow motion were documented. Standing sidewall waves and shock waves were observed along the sidewalls and on the channel centreline respectively, and these instabilities were associated with some strong splashing.

For all stepped spillway configurations some detailed air-water flow measurements were conducted downstream of the inception point of free-surface aeration. For the stepped spillways with in-line and staggered configurations of flat and pooled steps, the measurements were conducted at three transverse locations to document the three-dimensional nature of the flow. On the flat and pooled stepped spillway configurations, additional measurements were conducted with an array of two single-tip conductivity probes to estimate the integral turbulent time and length scales.

The experimental data showed similar void fraction distributions and mean air concentrations on both flat and pooled stepped spillways. The turbulence levels, and the air bubble and water droplet chord sizes, were also comparable between the two configurations. On the other hand, some larger bubble frequencies and integral turbulent length scales were observed on the flat stepped spillway, while larger velocities were recorded on the pooled stepped chute for identical flow rates. The measurements on the stepped spillways of in-line and staggered configurations of flat and pooled steps presented some significant transverse differences in terms of air-water flow properties between the flat and pooled stepped sides.

The rate of energy dissipation, residual head and Darcy-Weisbach friction factor were calculated based upon the air-water flow properties. The results showed that the rate of energy dissipation was smaller on the pooled stepped spillway compared to that on the flat stepped chute. Conversely the residual energy was larger at the downstream end of the pooled stepped chute. The experimental

data for the stepped spillway configuration with in-line and staggered configurations of flat and pooled steps showed large differences in the transverse direction, although the transverse averaged rates of energy dissipation and residual energy for the in-line and staggered configurations compared reasonably well with the observations on the pooled stepped spillway.

Altogether the present study demonstrated that, on a 26.6° stepped chute, the designs with pooled steps and in-line and staggered configurations of flat and pooled steps did not provide any advantageous performances in terms of energy dissipation and flow aeration, while they were affected by flow instabilities and three-dimensional patterns leading to some flow concentration. Another outcome is that some detailed investigations for complex stepped spillway designs are strongly recommended before any implementation in a prototype environment.

8. ACKNOWLEDGEMENTS

The authors thank Professor Daniel B. BUNG (FH Aachen University of Applied Sciences, Germany) and Dr Michael PFISTER (EPFL ENAC IIC LCH, Switzerland) for their detailed review of the report. The writers thank Jason VAN DER GEVEL and Stewart MATTHEWS (The University of Queensland) for their technical assistance. Some helpful discussion with Dr Masayuki TAKAHASHI (Nihon University, Japan), is acknowledged. The first writer acknowledges the financial support through a University of Queensland research scholarship. The financial support of the Australian Research Council is acknowledged (Grants ARC DP0878922 & DP120100481).

APPENDIX A – PHOTOGRAPHS OF STEPPED SPILLWAY CONFIGURATIONS AND FLOW PATTERNS

Visual observations were conducted for the stepped spillway configurations in the present study for a wide range of discharges (Table A-1). Table A-1 lists the experimental flow conditions for the visual observations of the flow pattern for the stepped spillway configurations. The experiments were conducted for flow rates of up to Q = 0.155 m^3/s and for Reynolds numbers between 1.4×10^4 and 1.2×10^6 (Table A-1). Herein most experiments were performed with Re > 1×10^5 for which scale effects might be considered small (FELDER & CHANSON 2009a).

In this Appendix, photographs are presented of the experimental setup for the different stepped spillway configurations (Fig. A-1 to A-4). This Appendix comprises also a collection of photographs showing the flow patterns for a range of different flow rates for the configurations. For each stepped spillway configuration, a compilation of photographs is presented for the different flow regimes: i.e., nappe, transition and skimming flows. Furthermore, some details about some instabilities and special features of the flow pattern are shown in several series of photographs. The flow patterns for the flat stepped spillway are illustrated in Figure A-5 to A-7, for the pooled stepped spillway in Figures A-8 to A-12, for the stepped spillway with in-line configuration of flat and pooled steps in Figures A-13 to A-19 and for the stepped spillway with staggered configuration of flat and pooled steps in Figures A-20 to A-25.

Table A-1 – Experimental flow conditions for the visual observations of the flow patterns for the stepped spillway configurations (θ = 26.6°)

Configuration (1)	d_c/h [-] (2)	Q [m^3/s] (3)	Re [-] (4)
Flat stepped spillway	0.12 – 2.02	0.002 - 0.148	1.6×10^4 –1.1×10^6
Pooled stepped spillway	0.11 – 1.94	0.002 - 0.139	1.5×10^4 –1.1×10^6
Stepped spillway with in-line configuration of flat and pooled steps	0.11 – 2.01	0.002 - 0.146	1.4×10^4 –1.1×10^6
Stepped spillway with staggered configuration of flat and pooled steps	0.15 – 2.09	0.003 - 0.155	2.3×10^4 –1.2×10^6

Notes: θ: channel slope; d_c: critical flow depth; h: step height; Q: water discharge; Re: Reynolds number defined in terms of the hydraulic diameter.

Fig. A-1 – Photos of the experimental setup of the flat stepped spillway (θ = 26.6°)

Fig. A-2 – Photos of the experimental setup of the pooled stepped spillway (θ = 26.6°)

Fig. A-3 – Photos of the experimental setup of the stepped spillway with in-line configuration of flat and pooled steps (θ = 26.6°)

Fig. A-4 – Photos of the experimental setup of the stepped spillway with staggered configuration of flat and pooled steps (θ = 26.6°)

Fig. A-5 – Nappe flow regime on the flat stepped spillway (θ = 26.6°)

(A) $d_c/h = 0.018$, $Q = 0.004$ m^3/s, $Re = 3.1\times10^4$

(B) $d_c/h = 0.018$, $Q = 0.004$ m^3/s, $Re = 3.1\times10^4$

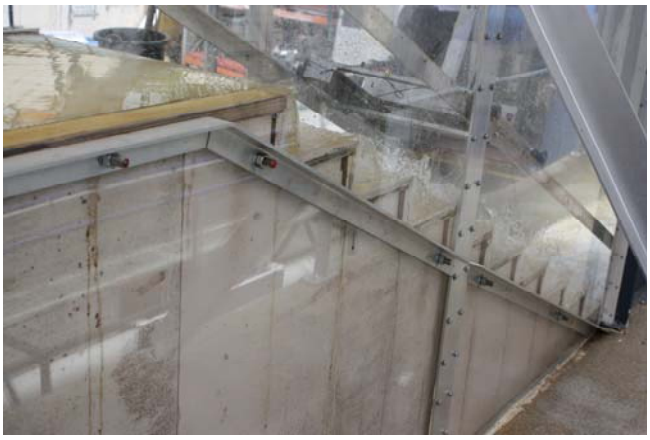

(C) $d_c/h = 0.33$, $Q = 0.010$ m^3/s, $Re = 7.5\times10^4$

(D) $d_c/h = 0.33$, $Q = 0.010$ m^3/s, $Re = 7.5\times10^4$

(E) $d_c/h = 0.49$, $Q = 0.018$ m^3/s, $Re = 1.4\times10^5$

(F) $d_c/h = 0.49$, $Q = 0.018$ m^3/s, $Re = 1.4\times10^5$

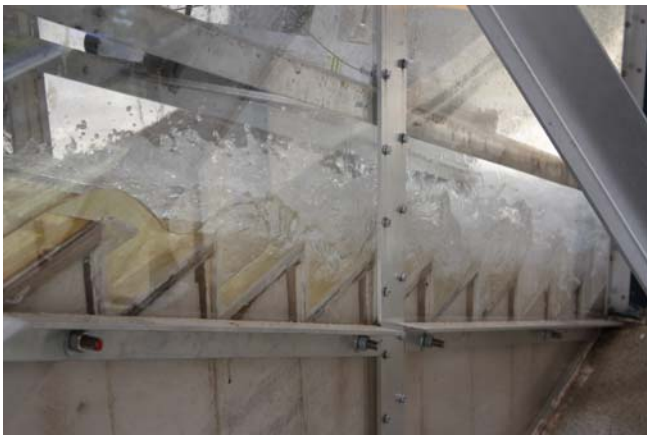

Fig. A-6 – Transition flow regime on the flat stepped spillway (θ = 26.6°)

(A) $d_c/h = 0.57$, $Q = 0.022$ m^3/s, $Re = 1.7\times10^5$

(B) $d_c/h = 0.57$, $Q = 0.022$ m^3/s, $Re = 1.7\times10^5$

(C) $d_c/h = 0.66$, $Q = 0.027$ m^3/s, $Re = 2.1\times10^5$

(D) $d_c/h = 0.66$, $Q = 0.027$ m^3/s, $Re = 2.1\times10^5$

(E) $d_c/h = 0.80$, $Q = 0.037$ m^3/s, $Re = 2.8\times10^5$

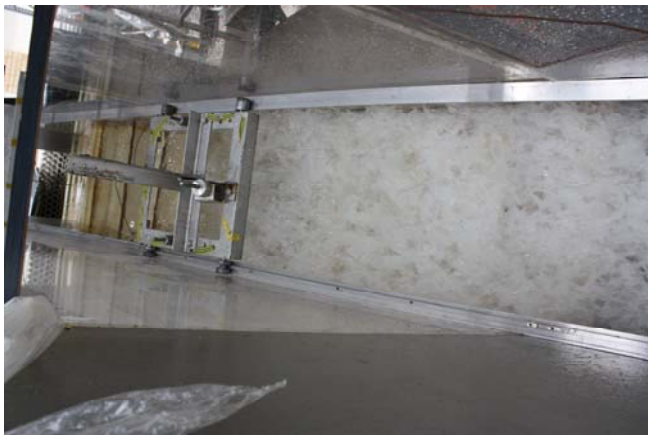

(F) $d_c/h = 0.84$, $Q = 0.039$ m^3/s, $Re = 3.0\times10^5$

Fig. A-7 – Skimming flow regime on the flat stepped spillway ($\theta = 26.6°$)

(A) $d_c/h = 0.97$, $Q = 0.049$ m^3/s, $Re = 3.8\times10^5$

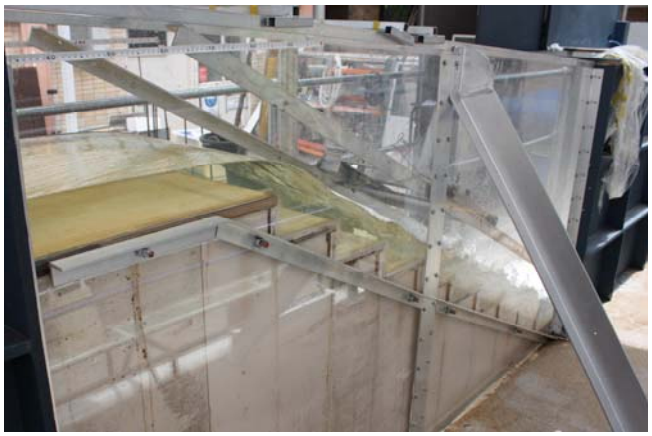

(B) $d_c/h = 1.25$, $Q = 0.072$ m^3/s, $Re = 5.5\times10^5$

(C) $d_c/h = 1.37$, $Q = 0.083$ m^3/s, $Re = 6.3\times10^5$

(D) $d_c/h = 1.51$, $Q = 0.095$ m^3/s, $Re = 7.3\times10^5$

(E) $d_c/h = 1.73$, $Q = 0.117$ m^3/s, $Re = 8.9\times10^5$

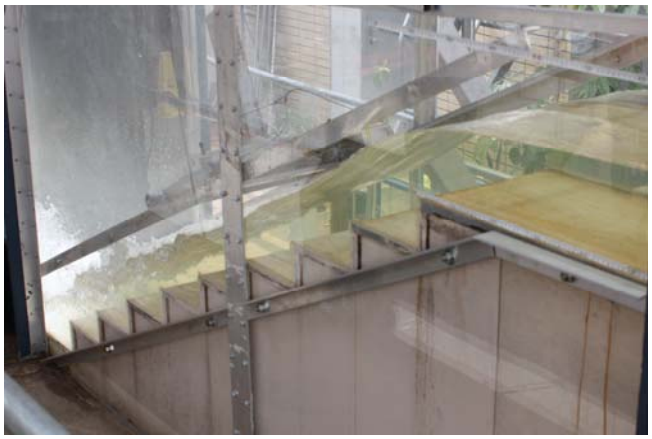

(F) $d_c/h = 1.73$, $Q = 0.117$ m^3/s, $Re = 8.9\times10^5$

Fig. A-8 – Nappe flow regime on the pooled stepped spillway (θ = 26.6°. w = 3.1 cm)

(A) $d_c/h = 0.26$, $Q = 0.007$ m^3/s, $Re = 5.1\times10^4$

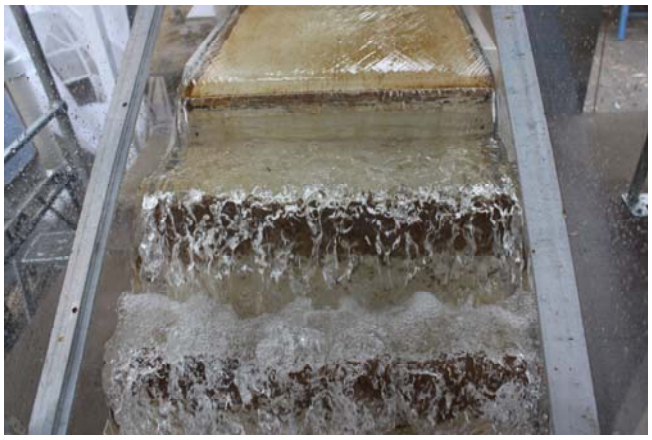

(B) $d_c/h = 0.26$, $Q = 0.007$ m^3/s, $Re = 5.1\times10^4$

(C) $d_c/h = 0.33$, $Q = 0.010$ m^3/s, $Re = 7.5\times10^4$

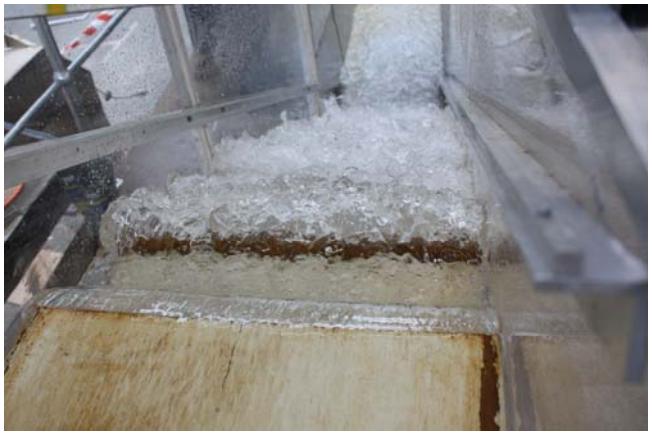

(D) $d_c/h = 0.33$, $Q = 0.010$ m^3/s, $Re = 7.5\times10^4$

(E) $d_c/h = 0.36$, $Q = 0.011$ m^3/s, $Re = 8.3\times10^4$

(F) $d_c/h = 0.36$, $Q = 0.011$ m^3/s, $Re = 8.3\times10^4$

Fig. A-9 – Pulsations in first step cavity in the nappe flow regime on the pooled stepped spillway (θ = 26.6°, w = 3.1 cm): d_c/h = 0.40, Q = 0.013 m^3/s, Re = 1×10^5 (order from top left to bottom right)

Fig. A-10 – Transition flow regime on the pooled stepped spillway ($\theta = 26.6°$. w = 3.1 cm)

(A) $d_c/h = 0.53$, $Q = 0.020$ m^3/s, $Re = 1.5\times10^5$

(B) $d_c/h = 0.53$, $Q = 0.020$ m^3/s, $Re = 1.5\times10^5$

(C) $d_c/h = 0.71$, $Q = 0.031$ m^3/s, $Re = 2.4\times10^5$

(D) $d_c/h = 0.77$, $Q = 0.035$ m^3/s, $Re = 2.6\times10^5$

(E) $d_c/h = 0.77$, $Q = 0.035$ m^3/s, $Re = 2.6\times10^5$

(F) $d_c/h = 0.88$, $Q = 0.043$ m^3/s, $Re = 3.3\times10^5$

Fig. A-11 – Small instabilities in the transition flow regime on the pooled stepped spillway (θ = 26.6°. w = 3.1 cm): d_c/h = 0.88, Q = 0.043 m^3/s, Re = 3.3×10^5 (order from top left to bottom right)

Fig. A-12 – Skimming flow regime on the pooled stepped spillway (θ = 26.6°. w = 3.1 cm)

(A) $d_c/h = 1.27$, $Q = 0.074$ m^3/s, $Re = 5.6\times10^5$

(B) $d_c/h = 1.27$, $Q = 0.074$ m^3/s, $Re = 5.6\times10^5$

(C) $d_c/h = 1.52$, $Q = 0.096$ m^3/s, $Re = 7.4\times10^5$

(D) $d_c/h = 1.77$, $Q = 0.121$ m^3/s, $Re = 9.3\times10^5$

(E) $d_c/h = 1.94$, $Q = 0.139$ m^3/s, $Re = 1.1\times10^6$

(F) $d_c/h = 1.94$, $Q = 0.139$ m^3/s, $Re = 1.1\times10^6$

Fig. A-13 – Nappe flow regime on the stepped spillway with in-line configuration of flat and pooled (w = 3.1 cm) steps (θ = 26.6°)

(A) $d_c/h = 0.18$, $Q = 0.004\ m^3/s$, $Re = 3.1 \times 10^4$

(B) $d_c/h = 0.18$, $Q = 0.004\ m^3/s$, $Re = 0.3 \times 10^4$

(C) $d_c/h = 0.23$, $Q = 0.006\ m^3/s$, $Re = 4.4 \times 10^4$

(D) $d_c/h = 0.23$, $Q = 0.006\ m^3/s$, $Re = 4.4 \times 10^4$

(E) $d_c/h = 0.31$, $Q = 0.009 m^3/s$, $Re = 6.8 \times 10^4$

(F) $d_c/h = 0.31$, $Q = 0.009 m^3/s$, $Re = 6.8 \times 10^4$

Fig. A-14 – Nappe flow regime on the stepped spillway with in-line configuration of flat and pooled (w = 3.1 cm) steps (θ = 26.6°)

(A) $d_c/h = 0.39$, $Q = 0.013 m^3/s$, $Re = 9.6 \times 10^4$

(B) $d_c/h = 0.39$, $Q = 0.013 m^3/s$, $Re = 9.6 \times 10^4$

(C) $d_c/h = 0.39$, $Q = 0.013 m^3/s$, $Re = 9.6 \times 10^4$

(D) $d_c/h = 0.39$, $Q = 0.013 m^3/s$, $Re = 9.6 \times 10^4$

Fig. A-15 –Nappe flows (pooled step side) and transition flows (flat side) on the stepped spillway with in-line configuration of flat and pooled (w = 3.1 cm) steps (θ = 26.6°) for $0.46 \leq d_c/h \leq 0.55$

(A) $d_c/h = 0.46$, $Q = 0.016 m^3/s$, $Re = 1.2 \times 10^5$

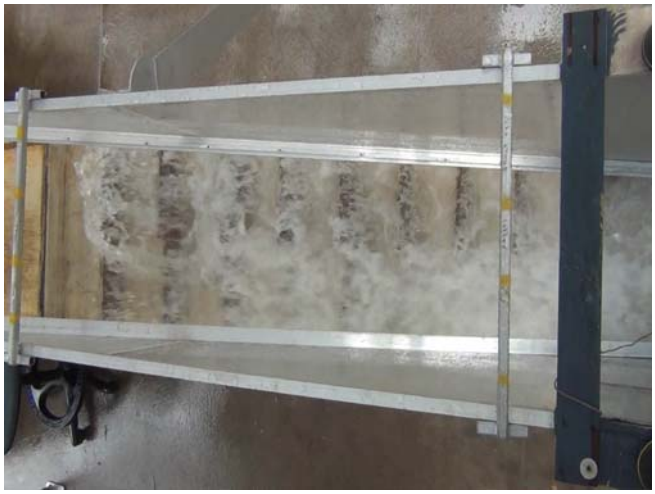

(B) $d_c/h = 0.46$, $Q = 0.016 m^3/s$, $Re = 1.2 \times 10^5$

(C) $d_c/h = 0.46$, $Q = 0.016 m^3/s$, $Re = 1.2 \times 10^5$

(D) $d_c/h = 0.46$, $Q = 0.016 m^3/s$, $Re = 1.2310^5$

(E) dc/h = 0.50, Q = 0.018 m3/s, $Re = 1.4 \times 10^5$

(F) dc/h = 0.50, Q = 0.018 m3/s, $Re = 1.4 \times 10^5$

Fig. A-16 – Nappe flows (pooled step side) and transition flows (flat side) on the stepped spillway with in-line configuration of flat and pooled (w = 3.1 cm) steps (θ = 26.6°) for $0.46 \leq d_c/h \leq 0.55$

(A) dc/h = 0.50, Q = 0.018 m3/s, Re = 1.4×10^5 (B) dc/h = 0.50, Q = 0.018 m3/s, Re = 1.4×10^5

(C) dc/h = 0.55, Q = 0.021 m3/s, Re = 1.6×10^5 (D) dc/h = 0.55, Q = 0.021 m3/s, Re = 1.6×10^5

(E) dc/h = 0.55, Q = 0.021 m3/s, Re = 1.6×10^5 (F) dc/h = 0.55, Q = 0.021 m3/s, Re = 1.6×10^5

Fig. A-17 – Transition flow regime on the stepped spillway with in-line configuration of flat and pooled (w = 3.1 cm) steps (θ = 26.6°)

(A) $d_c/h = 0.57$, $Q = 0.022$ m^3/s, $Re = 1.7\times10^5$

(B) $d_c/h = 0.57$, $Q = 0.022$ m^3/s, $Re = 1.7\times10^5$

(C) $d_c/h = 0.65$, $Q = 0.027$ m^3/s, $Re = 2.1\times10^4$

(D) $d_c/h = 0.65$, $Q = 0.027$ m^3/s, $Re = 2.1\times10^4$

(E) $d_c/h = 0.70$, $Q = 0.030$ m^3/s, $Re = 2.30\times10^5$

(F) $d_c/h = 0.70$, $Q = 0.030$ m^3/s, $Re = 2.30\times10^5$

Fig. A-18 – Skimming flow regime on the stepped spillway with in-line configuration of flat and pooled (w = 3.1 cm) steps (θ = 26.6°)

(A) $d_c/h = 1.15$, $Q = 0.063$ m^3/s, $Re = 4.9\times10^5$

(B) $d_c/h = 1.15$, $Q = 0.063$ m^3/s, $Re = 4.9\times10^5$

(C) $d_c/h = 1.15$, $Q = 0.063$ m^3/s, $Re = 4.9\times10^5$

(D) $d_c/h = 1.45$, $Q = 0.092$ m^3/s, $Re = 6.9\times105$

(E) $d_c/h = 1.45$, $Q = 0.092$ m^3/s, $Re = 6.9\times105$

(F) $d_c/h = 1.45$, $Q = 0.092$ m^3/s, $Re = 6.9\times10^5$

Fig. A-19 – Transition and skimming flow regime on the stepped spillway with in-line configuration of flat and pooled (w = 3.1 cm) steps (θ = 26.6°)

(A) $d_c/h = 0.7$, $Q = 0.0301$ m^3/s, $Re = 2.3\times10^5$

(B) $d_c/h = 0.75$, $Q = 0.0337$ m^3/s, $Re = 2.6\times10^5$

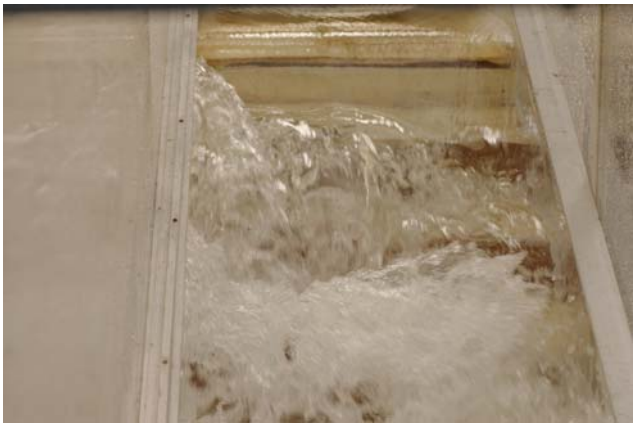

(C) $d_c/h = 1.28$, $Q = 0.0742$ m^3/s, $Re = 5.7\times10^5$

(D) $d_c/h = 1.28$, $Q = 0.0742$ m^3/s, $Re = 5.7\times10^5$

(E) $d_c/h = 1.92$, $Q = 0.138$ m^3/s, $Re = 10.5\times10^5$

(F) $d_c/h = 1.92$, $Q = 0.138$ m^3/s, $Re = 10.5\times10^5$

Fig. A-20 – Nappe flow regime stepped spillway with staggered configuration of flat and pooled (w = 3.1 cm) steps (θ = 26.6°)

(A) $d_c/h = 0.15$, $Q = 0.003$ m^3/s, $Re = 2.3\times10^4$

(B) $d_c/h = 0.15$, $Q = 0.003$ m^3/s, $Re = 2.3\times10^4$

(C) $d_c/h = 0.29$, $Q = 0.009$ m^3/s, $Re = 6.2\times10^4$

(D) $d_c/h = 0.29$, $Q = 0.009$ m^3/s, $Re = 6.2\times10^4$

(E) $d_c/h = 0.39$, $Q = 0.011$ m^3/s, $Re = 9.6\times10^4$

(F) $d_c/h = 0.39$, $Q = 0.011$ m^3/s, $Re = 9.6\times10^4$

Fig. A-21 – Nappe flow regime stepped spillway with staggered configuration of flat and pooled (w = 3.1 cm) steps (θ = 26.6°)

(A) $d_c/h = 0.44$, $Q = 0.015$ m^3/s, $Re = 1.15\times10^5$

(B) $d_c/h = 0.44$, $Q = 0.015$ m^3/s, $Re = 1.15\times10^5$

(C) $d_c/h = 0.56$, $Q = 0.020$ m^3/s, $Re = 1.64\times10^5$

(D) $d_c/h = 0.56$, $Q = 0.020$ m^3/s, $Re = 1.64\times10^5$

(E) $d_c/h = 0.56$, $Q = 0.020$ m^3/s, $Re = 1.64\times10^5$

(F) $d_c/h = 0.56$, $Q = 0.020$ m^3/s, $Re = 1.64\times10^5$

Fig. A-22 – Transition flow regime on the stepped spillway with staggered configuration of flat and pooled (w = 3.1 cm) steps (θ = 26.6°)

(A) $d_c/h = 0.59$, $Q = 0.023 m^3/s$, $Re = 1.8 \times 10^5$

(B) $d_c/h = 0.59$, $Q = 0.023 m^3/s$, $Re = 1.8 \times 10^5$

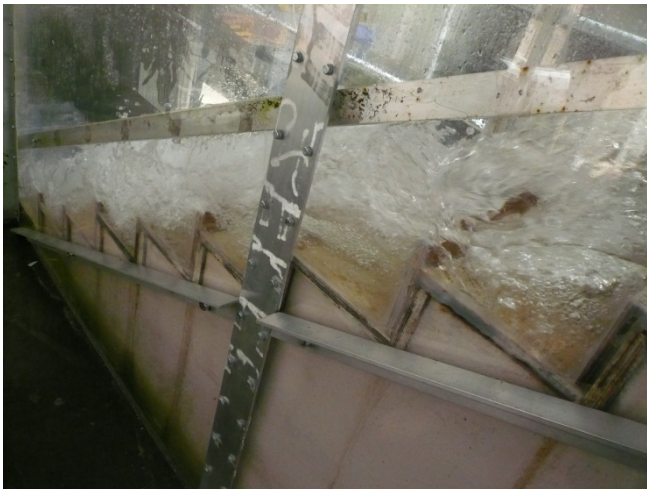

(C) $d_c/h = 0.59$, $Q = 0.023 m^3/s$, $Re = 1.8 \times 10^5$

(D) $d_c/h = 0.59$, $Q = 0.023 m^3/s$, $Re = 1.8 \times 10^5$

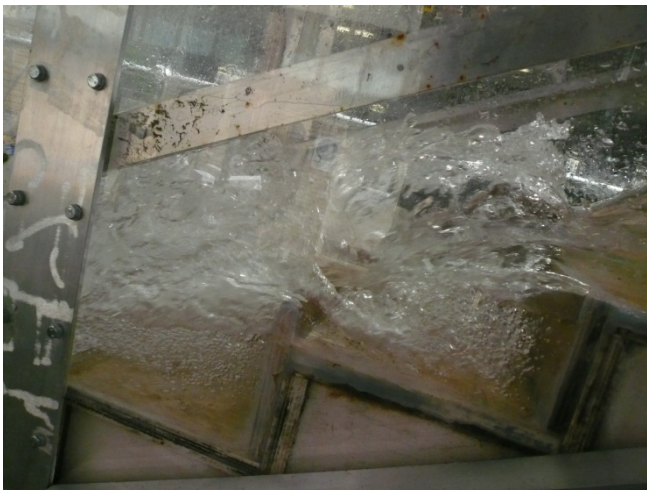

(E) $dc/h = 0.66$, $Q = 0.028\ m^3/s$, $Re = 2.1 \times 10^5$

(F) $d_c/h = 0.66$, $Q = 0.028\ m^3/s$, $Re = 2.1 \times 10^5$

Fig. A-23 – Transition flow regime on the stepped spillway with staggered configuration of flat and pooled (w = 3.1 cm) steps (θ = 26.6°)

(A) $d_c/h = 0.66$, $Q = 0.028$ m^3/s, $Re = 2.1\times10^5$

(B) $d_c/h = 0.66$, $Q = 0.028$ m^3/s, $Re = 2.1\times10^5$

(C) $d_c/h = 0.74$, $Q = 0.033$ m^3/s, $Re = 2.5\times10^5$

(D) $d_c/h = 0.74$, $Q = 0.033$ m^3/s, $Re = 2.5\times10^5$

(E) $d_c/h = 0.81$, $Q = 0.038$ m^3/s, $Re = 2.9\times10^5$

(F) $d_c/h = 0.81$, $Q = 0.038$ m^3/s, $Re = 2.9\times10^5$

Fig. A-24 – Transition flow on the stepped spillway with staggered configuration of flat and pooled (w = 3.1 cm) steps (θ = 26.6°)

(A) $d_c/h = 0.86$, $Q = 0.041$ m^3/s, $Re = 3.1\times10^5$ (B) $d_c/h = 0.86$, $Q = 0.041$ m^3/s, $Re = 3.1\times10^5$

Fig. A-25 – Skimming flow regime on the stepped spillway with staggered configuration of flat and pooled (w = 3.1 cm) steps (θ = 26.6°)

(A) $d_c/h = 0.92$, $Q = 0.045 m^3/s$, $Re = 3.5 \times 10^5$

(B) $d_c/h = 0.92$, $Q = 0.045 m^3/s$, $Re = 3.5 \times 10^5$

(C) $d_c/h = 1.42$, $Q = 0.087\ m^3/s$, $Re = 6.7 \times 10^5$

(D) $d_c/h = 1.42$, $Q = 0.087\ m^3/s$, $Re = 6.7 \times 10^5$

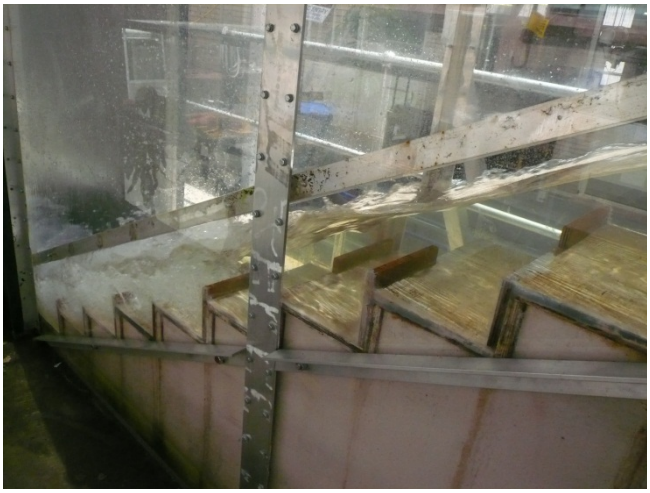

(E) $d_c/h = 1.80$, $Q = 0.124\ m^3/s$, $Re = 9.5 \times 10^5$

(F) $d_c/h = 1.80$, $Q = 0.124\ m^3/s$, $Re = 9.5 \times 10^5$

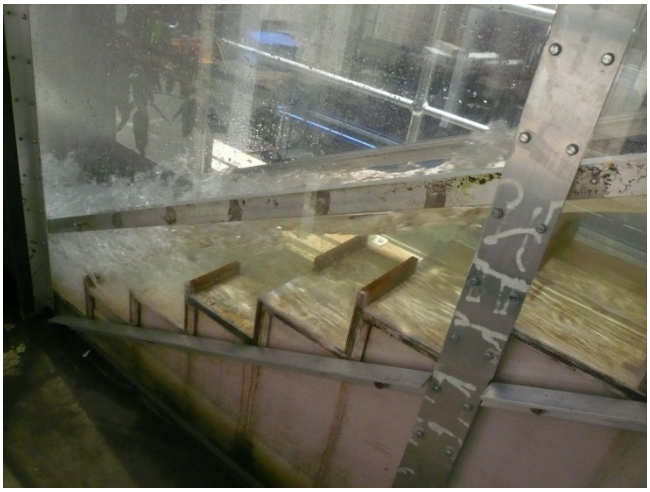

APPENDIX B – CAVITY EJECTIONS ON FLAT AND POOLED STEPPED SPILLWAYS

B.1 PRESENTATION

In skimming flow, the water skims over a pseudo-bottom formed by the step edges. The recirculation process in the step cavities is maintained by the transmission of shear stress of the main flow and unsteady momentum exchanges by the main stream and cavity flows (RAJARATNAM 1990). In the present study, some cavities showed some distinct ejection processes with inward and outward cavity flow motion. These occurred at irregular time intervals and led to some additional air entrainment. The total entrained air in the cavities was enhanced by both the interfacial free-surface aeration and singular ejection processes. In previous studies, it was suggested, that the initiating mechanism takes place in the fully-developed main stream flow, not in the cavity itself (ELAVARASAN et al. 1995; DJENIDI et al. 1999; CHANSON et al. 2002). Velocity differences and vortices next to step edges may be the cause for cavity ejections (FELDER & CHANSON 2008).

In the present study, the cavity ejections were documented thoroughly on the flat and pooled stepped spillways for three flow rates in the skimming flow regime (Table B-1). Table B-1 summarises the flow conditions for the cavity ejection observations. The flow visualisations were recorded with a HD video camera Sony^{TM} HDR-XR160E (Standard HQ HD quality 25 fps).

Table B-1 - Experimental flow conditions for the visual observations of cavity ejection frequencies for the flat and pooled stepped spillways ($\theta = 26.6°$)

Configuration (1)	d_c/h [-] (2)	Q [m^3/s] (3)	Re [-] (4)	Investigated step cavities (5)	Inception point (6)
Flat stepped spillway	1.15	0.063	4.85×10^5	5 to 10	5 to 6
	1.33	0.079	6.04×10^5	5 to 10	6
	1.45	0.090	6.87×10^5	6 to 10	7
	1.70	0.113	8.72×10^5	7 to 10	8 to 9
Pooled stepped spillway	1.15	0.063	4.85×10^5	4 to 10	5 to 6
	1.33	0.079	6.04×10^5	5 to 10	6 to 7
	1.45	0.090	6.87×10^5	6 to 10	7
	1.70	0.113	8.72×10^5	7 to 10	8

Notes: d_c: critical flow depth; h: vertical step height; Q: water discharge; Re: Reynolds number defined in terms of the hydraulic diameter.

B.2 CAVITY EJECTION DEFINITION AND VIDEO ANALYSIS

Detailed visual observations of cavity ejection processes were conducted for the flat and pooled stepped spillway configurations (Table B-1). The recirculation processes were observed for each step cavity at and downstream of the inception point of free-surface aeration. The clear-water surface upstream of the inception point appeared two-dimensional and parallel to the pseudo-bottom formed by the step edges and pooled weir edges respectively. Close to the inception point, the surface showed an irregular flapping mechanism ([1]) which led to some waving behaviour. Within the flapping surface patterns, the surface tended to lean inward the cavity at irregular intervals and caused an air packet ejection which was advected in the form of smaller and uniform shaped bubbles within the step cavities. This pattern was consistent with previous observations on flat stepped spillways (CHAMANI 2000; TOOMBES & CHANSON 2007).

With increasing discharge, the flapping mechanisms of the free-surface became less distinct. Visually, the flow resistance caused by the next downstream step, or pool edge, yielded some ejection processes close to the respective step or pool edge. Figure B-1 illustrates the flapping mechanism and the cavity ejection processes on the flat and pooled stepped spillways, while Figure B-2 presents some photographic sequences. The cavity ejection processes were similar in appearance for the flat and pooled steps, although some slight differences could be seen. A comparative analysis between ejections in cavities on the flat and pooled stepped spillways is discussed later in this appendix. The ejections of air packets may yield to some larger air concentrations in the cavities. The air-water flow properties in step cavities were discussed by MATOS et al. (2001), GONZALEZ & CHANSON (2004) and FELDER & CHANSON (2011a).

In the present study, a frame-by-frame video analysis was performed for the flat and pooled stepped spillways for all step cavities at and downstream of the inception point of free-surface aeration. The video duration was 60 s. The count of cavity ejections yielded information about the cavity ejection rate or frequency F_{ej} [Hz]. The analysis was performed for skimming flows with dimensionless flow rates of d_c/h=1.15, 1.33, 1.45 and 1.70, where d_c is the critical flow depth and h is the step height. The distribution of ejected air packets in the cavity was performed at 5 detection locations illustrated in Figure B-3. Figure B-3 shows the positions for the cavity ejection analyses for the flat stepped spillway configuration. The positions were identical for the experiments on the pooled stepped spillway configuration. For both stepped spillway configurations, an ejection was counted when an air packet passed the red sections marked in Figure B-3. Please note, that the ejection video analysis was conducted manually in a frame-by-frame analysis and therefore some human error was present in the overall results.

[1] The flapping mechanism was discussed by CHAMANI (2000) and CHANSON (2001).

Fig B-1 - Sketches of the ejection processes in step cavities on the flat and pooled stepped spillways ($\theta = 26.6°$)

(A) Ejection Process for low flow rates

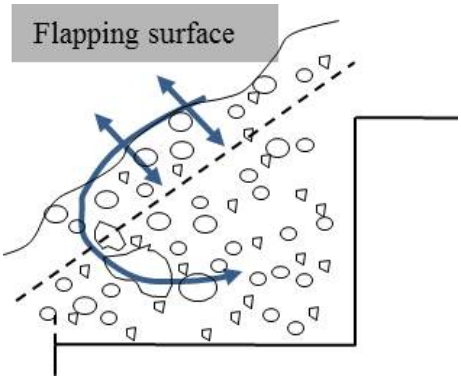

(B) Ejection Process for larger flow rates

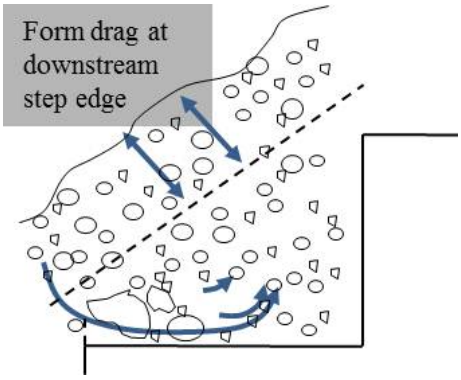

Fig B-2 - Photographs of sequential cavity ejections - (A1) to (A3): Flat stepped spillway configuration; (B1) to (B3): Pooled stepped spillway configuration; For each sequence, time between frames = 1/10 s

(A1) Flapping surface

(A2) Ejection process in cavity

(A3) Distribution of air packet in cavity

(B1) Visible flow resistance close to pool weir

(B2) Ejection process in cavity

(B3) Distribution of air packet in cavity

Fig B-3 - Recording positions for the cavity ejection video analysis on the flat and pooled stepped spillways ($\theta = 26.6°$)

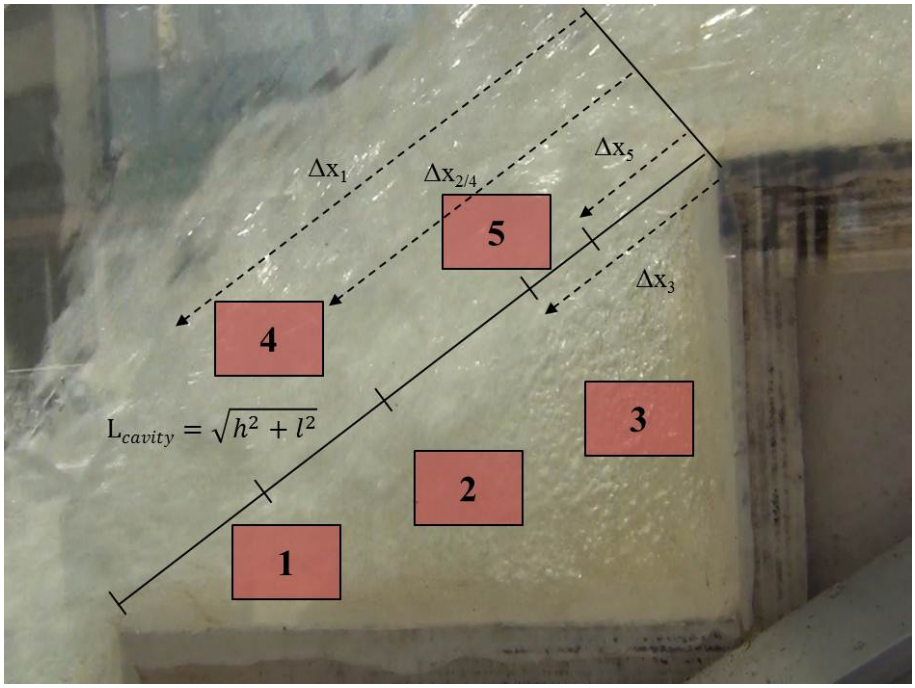

B.3 CAVITY EJECTION FREQUENCIES ON THE FLAT AND POOLED STEPPED SPILLWAYS

A summary of the ejection frequencies is given in Table B-2 for the flat stepped spillway and Table B-3 for the pooled stepped spillway respectively. In Table B-2, n is the number of detected air packets per position and $F_{ej}=n/t$ is the averaged ejection frequency. The shaded data correspond to the largest ejection frequencies for a given discharge.

The dimensionless cavity ejection frequency data $F_{ej}\times d_c/V_c$ are plotted in Figure B-4 as a function of the dimensionless longitudinal distance from the upstream end of the channel x/d_c for all data sets ([2]). The data in Figure B-4 include both flat and pooled stepped configurations in the skimming flow regime. The results indicated that the largest ejection frequencies could be seen at position 1 and 2 for both the flat and pooled stepped spillways. They decreased with further distance from the inception point of air entrainment for all skimming flow discharges. They fluctuated between adjacent step edges. The frequencies on the flat stepped spillway were consistently higher than on the pooled stepped spillway, which may suggest an influence by the pools on the irregular occurrence of ejections in the cavity. With the pooled stepped configuration, the ejection process might be affected by the larger inertia of the large cavity volume.

[2] Herein, x = 0 at the downstream end of the broad-crested weir (i.e. first step edge).

Table B-2 - Summary of cavity ejection frequencies on the flat stepped spillway (θ = 26.6°)

			Position 1		Position 2		Position 3		Position 4		Position 5	
d_c/h [-]	Cavity position	t [s]	n [-]	F_{ej} [Hz]	n [-]	F_{ej} [Hz]	n [-]	F_{ej} [Hz]	n [-]	F_{ej} [Hz]	n [-]	F_{ej} [Hz]
(1)	(2)	(3)	(4)	(5)	(6)	(7)	(8)	(9)	(10)	(11)	(12)	(13)
1.15	5 to 6	60	45	0.75	42	0.70	23	0.38	45	0.75	18	0.30
	6 to 7		49	0.82	35	0.58	19	0.32	38	0.63	23	0.38
	7 to 8		24	0.40	41	0.68	31	0.52	37	0.62	25	0.42
	8 to 9		55	0.92	48	0.80	49	0.82	43	0.72	30	0.50
	9 to 10		66	1.10	55	0.92	40	0.67	55	0.92	36	0.60
1.33	5 to 6	60	49	0.82	34	0.57	17	0.28	32	0.53	23	0.38
	6 to 7		51	0.85	35	0.58	21	0.35	37	0.62	22	0.37
	7 to 8		41	0.68	36	0.60	37	0.62	33	0.55	27	0.45
	8 to 9		31	0.52	32	0.53	16	0.27	22	0.37	18	0.30
	9 to 10		43	0.72	41	0.68	36	0.60	20	0.33	14	0.23
1.45	6 to 7	60	39	0.65	23	0.38	15	0.25	15	0.25	8	0.13
	7 to 8		36	0.60	33	0.55	34	0.57	42	0.70	30	0.50
	8 to 9		28	0.47	22	0.37	19	0.32	21	0.35	13	0.22
	9 to 10		35	0.58	28	0.47	38	0.63	20	0.33	16	0.27
1.70	7 to 8	60	43	0.72	12	0.20	13	0.22	27	0.45	8	0.13
	8 to 9		28	0.47	17	0.28	16	0.27	13	0.22	12	0.20
	9 to 10		22	0.37	27	0.45	29	0.48	10	0.17	9	0.15

Notes: F_{ej}: average cavity ejection frequency; t: video duration; n: ejection count; Shaded data: largest ejection frequency for a given discharge.

Table B-3 – Summary of cavity ejection frequencies on the pooled stepped spillway (θ = 26.6°)

			Position 1		Position 2		Position 3		Position 4		Position 5	
d_c/h [-]	Cavity position	t [s]	n [-]	F_{ej} [Hz]	n [-]	F_{ej} [Hz]	n [-]	F_{ej} [Hz]	n [-]	F_{ej} [Hz]	n [-]	F_{ej} [Hz]
(1)	(2)	(3)	(4)	(5)	(6)	(7)	(8)	(9)	(10)	(11)	(12)	(13)
1.15	4 to 5	60	38	0.63	36	0.60	21	0.35	26	0.43	22	0.37
	5 to 6		50	0.83	43	0.72	16	0.27	19	0.32	26	0.43
	6 to 7		24	0.40	36	0.60	9	0.15	14	0.23	9	0.15
	7 to 8		15	0.25	30	0.50	13	0.22	12	0.20	23	0.38
	8 to 9		32	0.53	35	0.58	8	0.13	18	0.30	28	0.47
	9 to 10		45	0.75	61	1.02	19	0.32	23	0.38	33	0.55
1.33	5 to 6	60	22	0.37	39	0.65	24	0.40	35	0.58	41	0.68
	6 to 7		24	0.40	30	0.50	21	0.35	27	0.45	29	0.48
	7 to 8		22	0.37	81	1.35	35	0.58	56	0.93	92	1.53
	8 to 9		37	0.62	38	0.63	16	0.27	16	0.27	13	0.22
	9 to 10		25	0.42	27	0.45	16	0.27	12	0.20	18	0.30
1.45	6 to 7	60	32	0.53	33	0.55	10	0.17	26	0.43	13	0.22
	7 to 8		21	0.35	46	0.77	24	0.40	29	0.48	23	0.38
	8 to 9		46	0.77	48	0.80	10	0.17	21	0.35	30	0.50
	9 to 10		46	0.77	63	1.05	26	0.43	27	0.45	15	0.25
1.70	7 to 8	60	33	0.55	40	0.67	16	0.27	30	0.50	27	0.45
	8 to 9		23	0.38	30	0.50	8	0.13	15	0.25	13	0.22
	9 to 10		26	0.43	28	0.47	25	0.42	14	0.23	10	0.17

Notes: F_{ej}: average cavity ejection frequency; t: video duration; n: ejection count; Shaded data: largest ejection frequency for a given discharge.

Fig B-4 - Dimensionless cavity ejection frequencies $(F_{ej}\times d_c)/V_c$ on the flat and pooled stepped spillways ($\theta = 26.6°$) in skimming flows

(A) $d_c/h=1.15$, $Q=0.063$ m^3/s, $Re=4.86\times10^5$ (B) $d_c/h=1.33$, $Q=0.079$ m^3/s, $Re=6.04\times10^5$

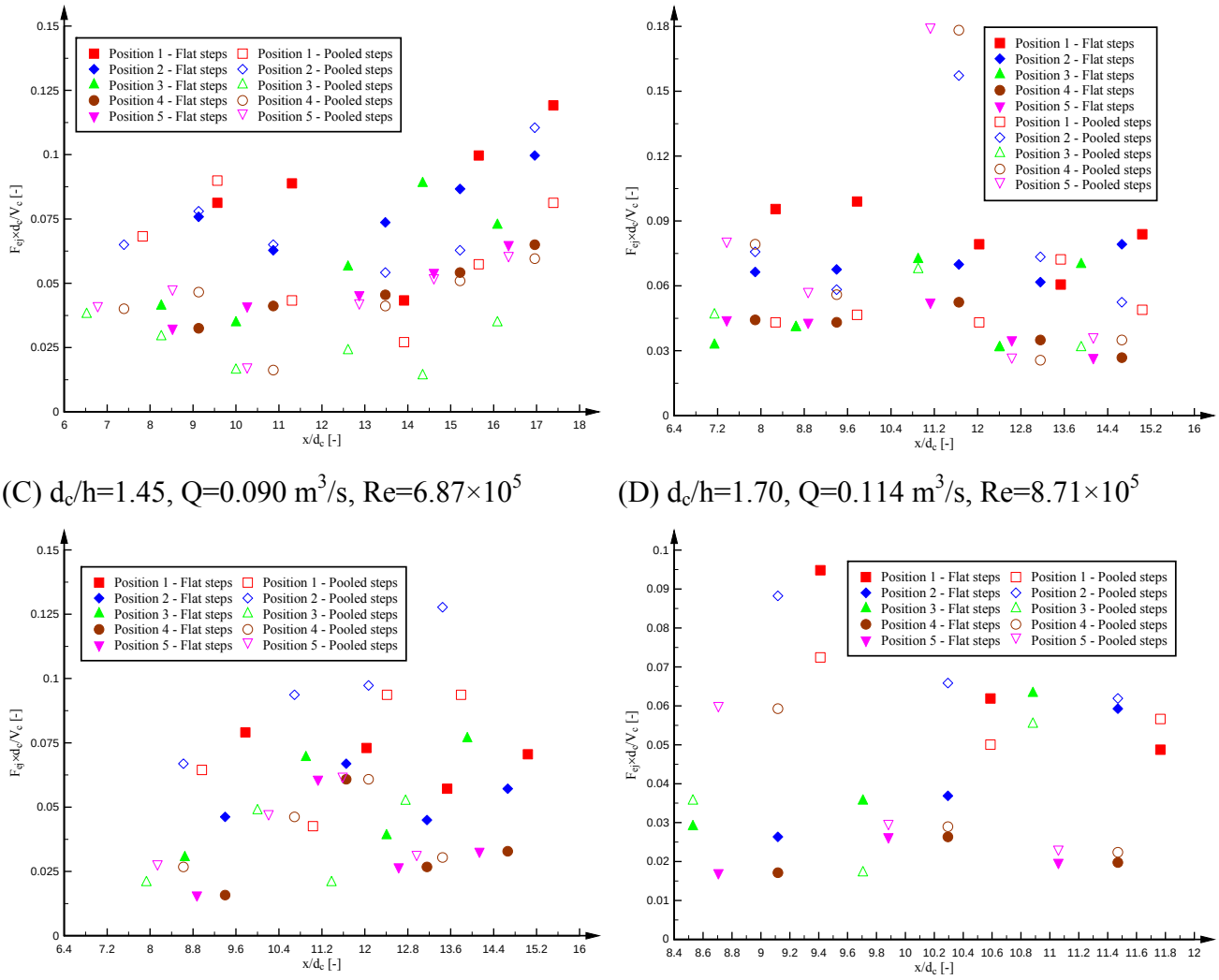

(C) $d_c/h=1.45$, $Q=0.090$ m^3/s, $Re=6.87\times10^5$ (D) $d_c/h=1.70$, $Q=0.114$ m^3/s, $Re=8.71\times10^5$

A local distinct peak could be observed for $d_c/h=1.33$ at $x/d_c=11.5$ for the pooled stepped spillway which corresponded to locations 2, 4 and 5 at the cavity between step edge 7 and 8 (Fig. B-4B). The cavity ejection frequencies were up to 2 times higher than those for adjacent cavities. This peak highlighted the irregular occurrence of ejections for some specific flow situations, and the entire reason for the local maximum remained unclear.

Figure B-5 shows the relationship between the Reynolds number Re and the dimensionless cavity ejection frequency $F_{ej}\times d_c/V_c$. The square and circle symbols indicate the average frequencies for a

given Reynolds number. The ejection processes in the cavities may be associated with regions of high shear stress along the cavity region and the Reynolds number was closely linked to turbulence properties. The results showed that the ejection frequencies decreased with increasing Reynolds numbers.

Fig. B-5 - Relationship between average dimensionless cavity ejection frequencies $F_{ej} \times d_c/V_c$ and Reynolds number Re for the flat and pooled stepped spillway configurations (θ = 26.6°) in skimming flows

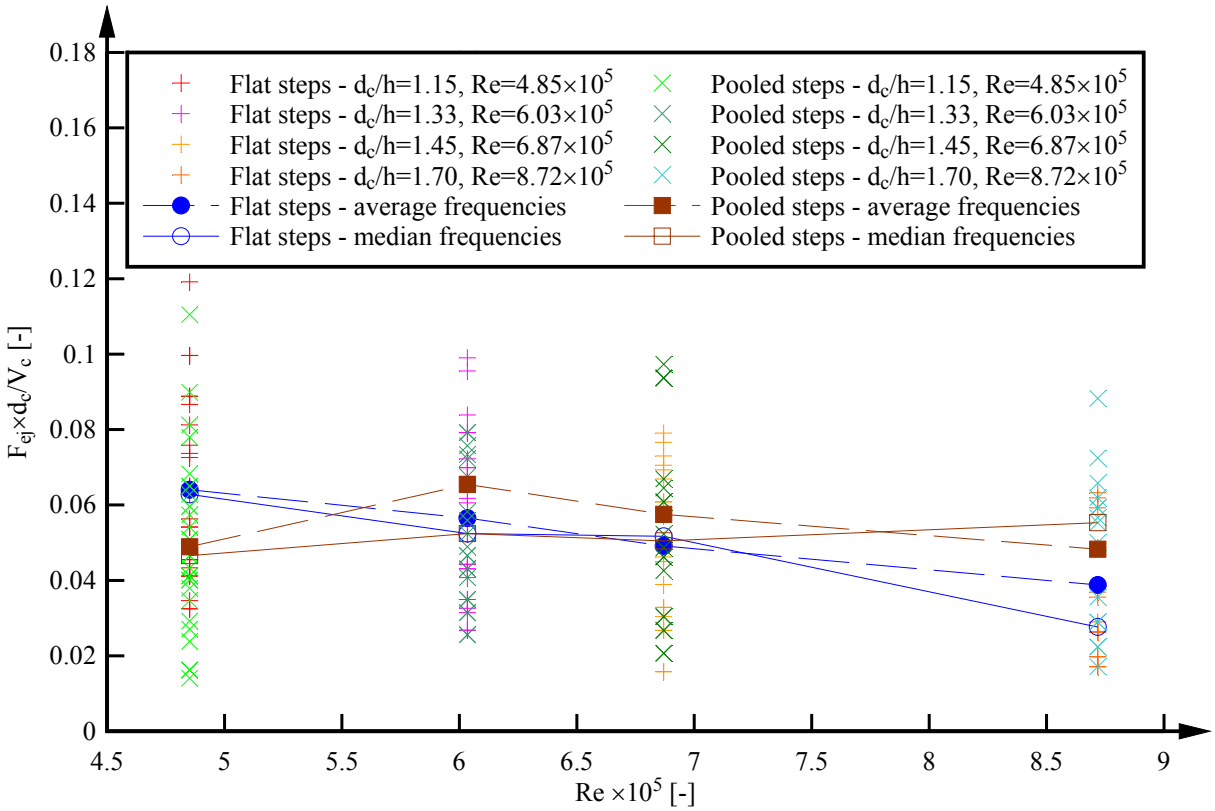

B.4 RELATIONSHIP OF CAVITY EJECTION FEQUENCY AND DARCY FRICTION FACTOR

CHANSON & TOOMBES (2001) analysed the ejection processes in skimming flow on stepped spillways based upon energy considerations. The reasoning assumed that all the energy losses took place by viscous dissipation in the cavity, with some energy exchange between the main stream and the recirculation by irregular fluid ejection. The results yielded an expression of the averaged ejection frequency F_{ej} as a function of the Darcy-Weisbach friction factor f_e:

$$\frac{F_{ej} \times (h \times \cos\theta)}{U_w} \approx \frac{f_e}{2 \times \lambda \times \eta} \qquad \text{(B-1)}$$

where U_w is the flow velocity, h is the vertical step height, θ is the angle between the pseudo-bottom formed by the step edges and the horizontal, λ is the ratio of average fluid ejection volume

to total cavity volume, and η is the ratio of average ejection period to burst duration. Equation (B-1) was developed for a wide chute with flat horizontal steps assuming a gradually-varied flow motion close to uniform equilibrium. CHANSON et al. (2002) reported that the ratio λ of average fluid ejection volume to total cavity volume was λ ~ 0.5 and the ratio η of average ejection period to burst duration was η ~ 7, yielding:

$$\frac{F_{ej} \times (h \times \cos\theta)}{U_w} \approx \frac{f_e}{5} \quad \text{(B-2)}$$

More generally the reasoning may be extended to a pooled stepped chute:

$$\frac{F_{ej} \times (h \times \cos\theta)}{U_w} \approx \frac{f_e}{2 \times \lambda \times \eta \times \left(1 + 2 \times \frac{w}{h}\right)} \quad \text{(B-3)}$$

where w is the pool height. Equation (B-3) is valid for a wide chute with horizontal steps and vertical pool walls.

In the present study, the air-water flow properties were recorded with detailed double-tip conductivity probe measurements for both the flat and pooled stepped spillway configurations with three flow rates in the skimming flow regime. The mean flow velocity U_w was calculated for all step edges as well as the friction factors f_e for the air-water flow downstream of the inception point. The latter was estimated as:

$$f_e = \frac{8 \times \tau_0}{\rho_w \times U_w^2} = \frac{8 \times g \times S_f \times \left(\int_{y=0}^{Y_{90}} (1-C)\,dy \right)}{U_w^2} = \frac{8 \times g \times S_f \times d}{U_w^2} \quad \text{(B-4)}$$

where the friction slope S_f equals $S_f = - \partial H/\partial x$, H is the total head, τ_o is the boundary shear stress, x is the distance in the flow direction, ρ_w is the water density; C is the void fraction, Y_{90} is the flow depth where C = 90%, d is the equivalent clear water flow depth and U_w is the flow velocity (CHANSON 2001).

The relationship between Darcy-Weisbach friction factors and dimensionless cavity ejection frequency $F_{ej} \times ((h+w) \times \cos\theta)/U_W$ was tested herein for the flat and pooled stepped spillway configurations. Some results are presented in Figure B-6, and the best fit correlations are listed in Table B-4. The present data were qualitatively comparable to Equation (B-3), but they differed quantitatively (Table B-4, column 6). The results of the present video analysis suggested that the dimensionless cavity ejection $F_{ej} \times ((h+w) \times \cos\theta)/U_W$ ranged between $f_e/25$ and $f_e/12$. The cavity ejection frequency tended to decrease with increasing discharges (Table B-4).

Herein the average ejection period to burst duration was on average $\eta = \tau_{ejection}/\tau_{burst} \sim 3.5$. The present video analysis did not yield information about the average fluid ejection volume.

Fig. B-6 - Dimensionless cavity ejection frequency $F_{ej}\times(h\times\cos\theta)/U_W$ as a function of the longitudinal distance x/d_c from the crest with flat steps and pooled steps

(A) $d_c/h=1.15$

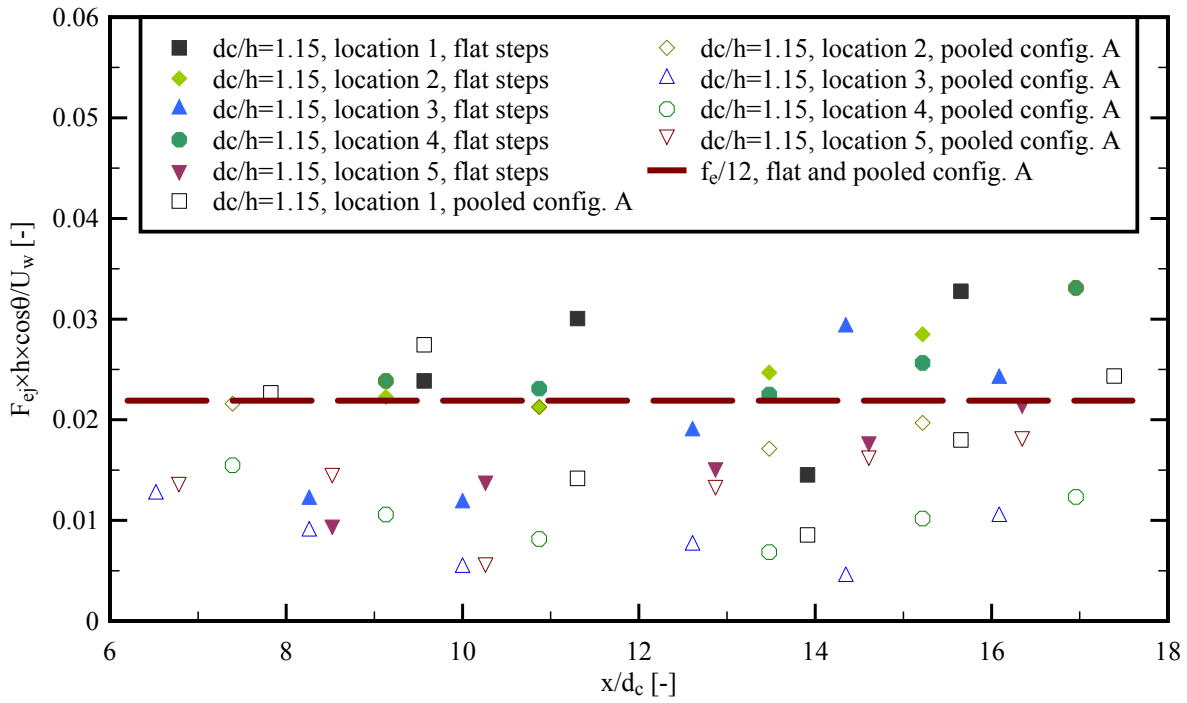

(B) $d_c/h=1.45$

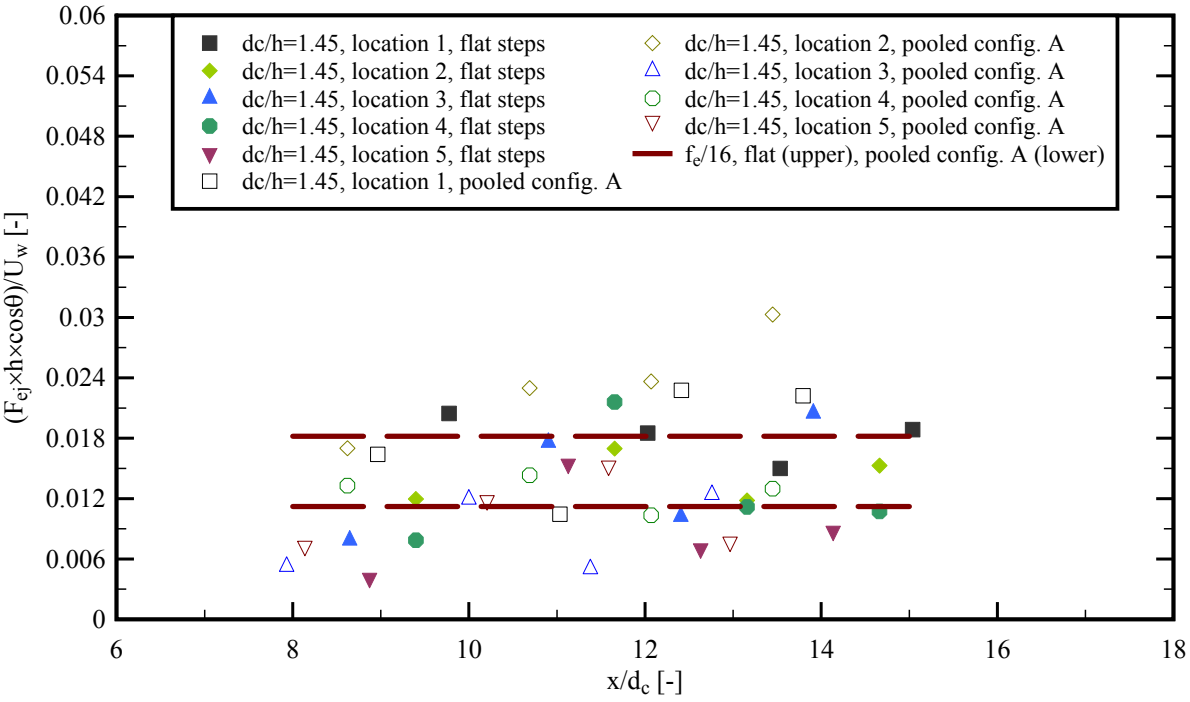

(C) $d_c/h=1.70$

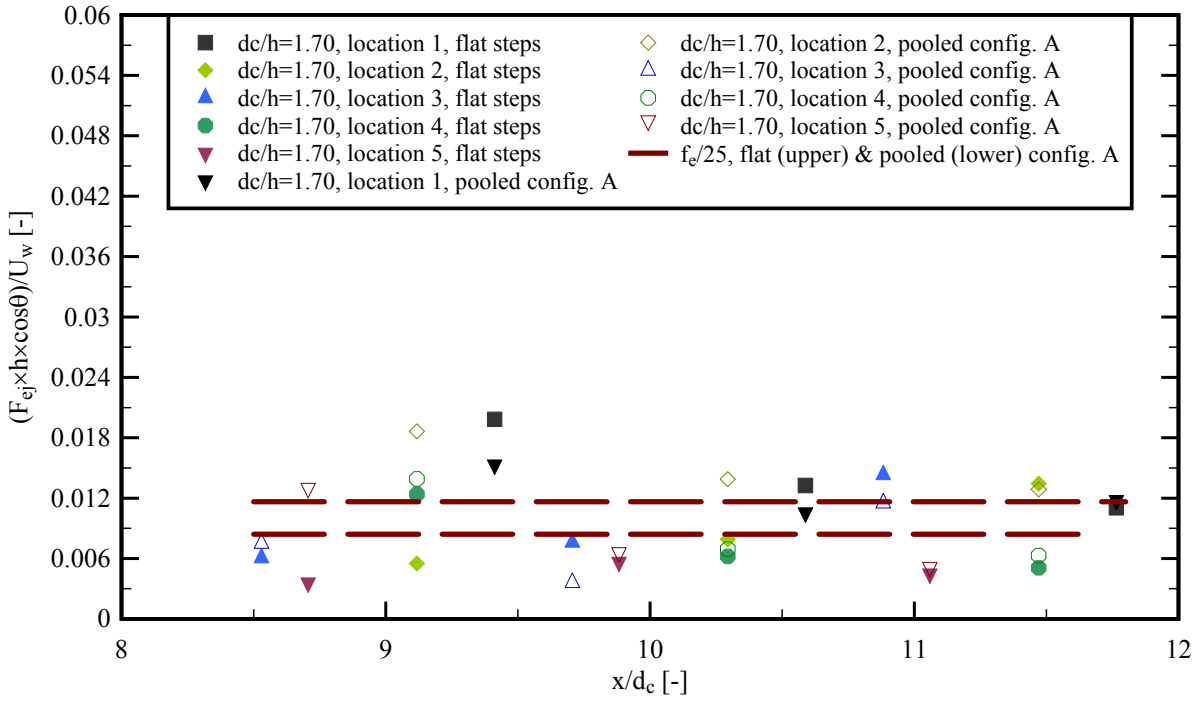

Table B-4 - Relationship between Darcy-Weisbach friction factors and dimensionless cavity ejection frequency $F_{ej}\times((h+w)\times\cos\theta)/U_W$ for the flat and pooled stepped spillway configurations ($\theta = 26.6°$)

Configuration (1)	d_c/h [-] (2)	Q [m^3/s] (3)	Re [-] (4)	f_e [-] (5)	$F_{ej}\times((h+w)\times\cos\theta)/U_W \approx$ (6)
Flat stepped spillway	1.15	0.063	4.85×10^5	0.263	$f_e/12$
	1.45	0.090	6.87×10^5	0.291	$f_e/16$
	1.70	0.113	8.72×10^5	0.343	$f_e/25$
Pooled stepped spillway	1.15	0.063	4.85×10^5	0.278	$f_e/12$
	1.45	0.090	6.87×10^5	0.247	$f_e/16$
	1.70	0.113	8.72×10^5	0.278	$f_e/25$

Notes: d_c: critical flow depth; h: vertical step height; Q: water discharge; Re: Reynolds number defined in terms of the hydraulic diameter; f_e: Darcy-Weisbach friction factor; F_{ej}: cavity ejection frequency; h: step height; w: pool weir height; U_w: mean flow velocity.

B.5 SUMMARY AND DISCUSSION

Three-dimensional flow patterns on stepped spillways are highly complex and not trivial to describe. The physical processes are not sufficiently understood. Three-dimensional flow behaviour

could be observed for the flat and pooled stepped spillways in the present study and no significant differences in the flow patterns was observed across the channel width.

The cavity ejection processes were investigated in a video analysis for the skimming flow regime on both stepped spillway configurations. Some differences in terms of frequencies and size of entrained air packets were observed. The pool weirs had an influence on the ejection and seemed to disturb a clear development of the mixing layer downstream of each pool edge for lower discharges. With increasing discharges, the ejection frequencies became more similar between the two stepped spillways. Some relationships to the turbulent dissipation were compared and showed some contributions. It may be associated that a clear mixing layer with large shear stress leading to a more constant turbulent dissipation on each adjacent step edge. The flat steps configuration showed some high energy dissipation along the channel, which may relate to some of the described processes. A clear validation was not possible by video analysis and air-water flow measurements. Some further investigations of the region of high shear stress along the cavity may lead to some coherence with previous research of processes in cavities at stepped hydraulics (e.g. GONZALEZ & CHANSON 2004; FELDER & CHANSON 2009b).

APPENDIX C –AIR-WATER FLOW PROPERTIES ON FLAT AND POOLED STEPPED SPILLWAYS

C.1 PRESENTATION

In this appendix, the air-water flow properties for the flat and pooled stepped spillway experiments of the present study are presented. The results comprise the distributions of void fraction, bubble count rate, interfacial velocity, turbulence intensity, auto- and cross-correlation time scales and maximum cross-correlation values. In section C.2, the results for the flat stepped spillway experiments are presented (Fig. C-1 to C-8) and section C.3 contains the air-water flow properties for the pooled stepped spillway (Fig. C-9 to C-18). In section C.4, some air bubble and water droplet chord sizes for the flat and pooled stepped spillways are presented (Fig. C-19 to C-26).

Table C-1 summarises some basic air-water flow parameters for all experiments on the flat stepped spillway while Table C-2 regroups the characteristic parameters for the pooled stepped spillway experiments.

Notation

C	void fraction defined as the volume of air per unit volume of air and water;
C_{mean}	depth-average void fraction defined in terms of Y_{90}: $C_{mean} = 1 - d/Y_{90}$;
D_H	hydraulic diameter (m);
d	equivalent clear water flow depth (m);
d_c	critical flow depth (m);
F	air bubble count rate (Hz) defined as the number of detected air bubbles per unit time;
F_{max}	maximum bubble count rate in a cross-section (Hz);
h	vertical step height (m);
l	horizontal step length (m);
Q	water discharge (m^3/s);
q_w	water discharge per unit width (m^2/s);
Re	Reynolds number defined in terms of the hydraulic diameter: $Re = \rho_w \times U_w \times D_H/\mu_w$;
R_{xx}	normalised auto-correlation function (reference) probe;
R_{xy}	normalised cross-correlation function between two probe output signals;
$(R_{xy})_{max}$	maximum cross-correlation between two probe output signals;
Tu	turbulence intensity;
Tu_{max}	maximum turbulence intensity in a cross-section;
T_{xx}	auto-correlation integral time scale (s);
T_{xy}	cross-correlation integral time scale (s);
U_w	mean flow velocity (m/s): $U_w = q_w/d$;
V	interfacial velocity (m/s);
V_c	critical flow velocity (m/s);

V_{90}	characteristic interfacial velocity (m/s) where the void fraction is 90%;
w	weir height in pooled stepped spillway configuration (m), also called pool height;
Y_{90}	characteristic depth (m) where the void fraction is 90%;
y	distance (m) measured normal to the invert (or channel bed);
θ	angle between pseudo-bottom formed by the step edges and the horizontal;
Ø	probe sensor diameter (m).

Table C-1 – Characteristic air-water flow parameters for the measurements on the flat stepped spillway (θ = 26.6°) with a double-tip conductivity probe (Ø = 0.25 mm)

d_c/h [-] (1)	Q [m^3/s] (2)	Re [-] (3)	Step edge (4)	C_{mean} [-] (5)	F_{max} [Hz] (6)	V_{90} [m/s] (7)	U_w [m/s] (8)	d [m] (9)	Y_{90} [m] (10)	Tu_{max} [-] (11)
0.70	0.030	2.30×10^5	4	0.276	68.6	2.85	1.97	0.0294	0.0406	1.18
			5	0.678	119.8	2.47	2.35	0.0247	0.0768	1.37
			6	0.467	179.8	2.70	2.50	0.0232	0.0435	1.39
			7	0.592	193.8	2.70	2.35	0.0247	0.0605	1.15
			8	0.470	237.4	2.77	2.04	0.0284	0.0535	1.05
			9	0.373	251.8	2.92	2.11	0.0274	0.0438	1.64
			10	0.561	223.3	2.92	2.29	0.0253	0.0576	1.19
0.82	0.038	2.90×10^5	4	0.158	53.6	2.85	2.26	0.0323	0.0383	1.65
			5	0.360	117.4	2.78	2.13	0.0342	0.0535	1.35
			6	0.507	174.2	2.74	2.46	0.0296	0.0600	0.93
			7	0.369	186.6	2.92	2.32	0.0314	0.0497	1.70
			8	0.485	216.1	2.98	2.55	0.0286	0.0556	1.07
			9	0.349	252.6	3.11	2.21	0.0330	0.0507	1.85
			10	0.503	243.8	3.14	2.37	0.0307	0.0618	1.07
0.96	0.049	3.71×10^5	5	0.284	74.6	2.86	2.27	0.0412	0.0575	1.95
			6	0.333	148.0	2.90	2.48	0.0377	0.0565	1.44
			7	0.409	151.9	2.86	2.21	0.0423	0.0716	1.24
			8	0.308	198.7	3.08	2.23	0.0418	0.0605	1.22
			9	0.323	197.8	3.12	2.19	0.0426	0.0629	1.69
			10	0.311	226.9	3.18	2.28	0.0409	0.0594	1.53
1.15	0.063	4.85×10^5	5	0.206	44.8	2.99	2.46	0.0496	0.0624	2.42
			6	0.281	113.9	2.86	2.81	0.0434	0.0604	1.56
			7	0.360	113.8	3.03	2.44	0.0501	0.0782	1.88
			8	0.324	168.1	3.11	2.46	0.0496	0.0734	1.34
			9	0.321	173.6	3.12	2.51	0.0486	0.0717	1.59
			10	0.302	202.4	3.25	2.48	0.0491	0.0704	1.79
1.29	0.075	5.73×10^5	6	0.235	81.7	3.08	2.84	0.0508	0.0664	1.75
			7	0.308	101.3	3.25	2.57	0.0562	0.0812	1.89
			8	0.314	151.5	3.33	2.66	0.0543	0.0792	1.41
			9	0.303	144.9	3.29	2.52	0.0572	0.0820	1.53
			10	0.282	181.6	3.39	2.58	0.0559	0.0778	1.63
1.45	0.090	6.87×10^5	7	0.277	85.4	3.40	2.84	0.0609	0.0842	1.74
			8	0.300	131.0	3.35	2.90	0.0597	0.0852	1.44
			9	0.299	128.0	3.33	2.80	0.0617	0.0881	1.61
			10	0.275	157.0	3.40	2.75	0.0629	0.0867	1.78
1.52	0.097	7.39×10^5	8	0.284	114.3	3.55	3.03	0.0615	0.0858	1.48
			9	0.273	120.4	3.58	2.87	0.0649	0.0893	1.88
			10	0.269	149.2	3.67	2.84	0.0655	0.0897	1.70
1.70	0.113	8.72×10^5	8	0.240	93.0	3.51	3.25	0.0676	0.0889	1.64
			9	0.263	108.7	3.59	3.17	0.0692	0.0940	1.41
			10	0.278	127.7	3.53	3.00	0.0733	0.1015	1.82

Table C-2 – Characteristic air-water flow parameters for the measurements on the pooled stepped spillway (θ = 26.6°, w = 3.1 cm) with a double-tip conductivity probe (Ø = 0.25 mm)

d_c/h [-] (1)	Q [m^3/s] (2)	Re [-] (3)	Step edge (4)	C_{mean} [-] (5)	F_{max} [Hz] (6)	V_{90} [m/s] (7)	U_w [m/s] (8)	d [m] (9)	Y_{90} [m] (10)	Tu_{max} [-] (11)
0.40	0.013	9.95×10^4	2	0.487	16.4	0.84	0.58	0.0432	0.0843	2.47
			3	0.435	47.9	1.61	1.25	0.0200	0.0354	1.50
			4	0.592	55.4	0.98	0.83	0.0303	0.0743	3.24
			5	0.472	70.0	1.54	1.13	0.0222	0.0421	1.89
			6	0.594	65.7	1.25	0.87	0.0287	0.0706	3.07
			7	0.493	76.4	1.74	1.14	0.0220	0.0434	1.94
			8	0.593	77.9	1.46	0.89	0.0280	0.0688	2.97
			9	0.518	87.5	1.88	1.15	0.0217	0.0450	1.84
			10	0.613	85.5	1.60	0.89	0.0280	0.0724	3.80
0.70	0.030	2.30×10^5	4	0.325	25.3	2.60	2.51	0.0231	0.0342	3.30
			5	0.636	104.2	2.63	2.16	0.0269	0.0739	1.49
			6	0.644	145.9	2.69	2.07	0.0281	0.0789	1.77
			7	0.644	168.0	2.69	2.07	0.0281	0.0788	1.83
			8	0.638	194.4	2.82	2.13	0.0273	0.0753	1.81
			9	0.631	204.6	2.85	2.10	0.0276	0.0748	2.05
			10	0.637	216.6	3.00	2.13	0.0272	0.0750	1.98
0.82	0.038	2.90×10^5	4	0.347	62.9	2.75	2.18	0.0334	0.0511	1.60
			5	0.389	121.6	2.83	2.28	0.0319	0.0523	1.52
			6	0.418	146.0	2.86	2.06	0.0354	0.0607	1.46
			7	0.368	172.9	3.00	2.18	0.0334	0.0528	1.66
			8	0.346	188.2	3.18	2.16	0.0337	0.0516	1.98
			9	0.381	196.4	3.18	2.17	0.0336	0.0543	1.71
			10	0.347	62.9	2.75	2.18	0.0334	0.0511	1.60
0.96	0.049	3.71×10^5	5	0.340	87.6	2.93	2.48	0.0376	0.0570	1.84
			6	0.404	122.0	3.04	2.24	0.0416	0.0699	1.27
			7	0.377	151.1	3.25	2.35	0.0398	0.0638	1.42
			8	0.339	169.0	3.33	2.35	0.0398	0.0602	1.60
			9	0.365	183.8	3.40	2.43	0.0384	0.0605	1.44
			10	0.340	87.6	2.93	2.48	0.0376	0.0570	1.84
1.15	0.063	4.85×10^5	5	0.100	18.0	2.74	2.48	0.0492	0.0880	1.77
			6	0.155	41.6	3.09	2.70	0.0452	0.0890	2.63
			7	0.250	88.2	3.24	2.52	0.0484	0.1045	1.58
			8	0.257	117.8	3.45	2.61	0.0468	0.1033	1.50
			9	0.240	150.4	3.47	2.63	0.0464	0.1004	1.54
			10	0.251	171.7	3.53	2.75	0.0443	0.0993	1.46
1.29	0.075	5.73×10^5	6	0.279	62.1	3.49	2.66	0.0543	0.0753	1.44
			7	0.316	95.5	3.58	2.74	0.0527	0.0770	1.46
			8	0.321	130.3	3.66	2.72	0.0531	0.0781	1.43
			9	0.352	148.6	3.76	2.85	0.0506	0.0780	1.26
			10	0.279	62.1	3.49	2.66	0.0543	0.0753	1.44
1.45	0.090	6.87×10^5	7	0.430	42.1	3.47	2.89	0.0598	0.1049	2.10
			8	0.465	74.6	3.65	3.00	0.0577	0.1079	1.90
			9	0.320	107.6	3.75	3.03	0.0571	0.0840	1.61
			10	0.355	136.8	3.85	3.10	0.0558	0.0865	1.38
1.52	0.097	7.39×10^5	8	0.236	58.8	3.76	3.02	0.0616	0.0807	1.88
			9	0.282	93.2	3.83	2.95	0.0630	0.0877	1.37
			10	0.318	119.2	3.97	3.04	0.0612	0.0898	1.23
1.70	0.113	8.72×10^5	8	0.392	42.6	3.75	3.21	0.0683	0.1122	1.86
			9	0.422	72.2	3.95	3.22	0.0682	0.1179	1.65
			10	0.456	96.8	4.07	3.26	0.0672	0.1236	1.50

1.85	0.130	9.89×10^5	10	0.234	79.1	4.21	3.39	0.0735	0.0960	1.43

C.2 AIR-WATER FLOW PROPERTIES ON THE FLAT STEPPED SPILLWAY

This section presents the vertical distributions of air-water flow properties for the experiments with a double-tip conductivity probe on the flat stepped spillway. Table C-3 summarises the experimental flow conditions the flow regime and the inception point of air entrainment for the flat stepped spillway experiments. Table C-4 details the data set presented in this section and it indicates the respective position of the six graphs in Figures C-1 to C-8. All air-water flow distributions are presented in terms of the dimensionless distance perpendicular to the pseudo-bottom formed by the step edges y/d_c. The pseudo-bottom was defined as the zero position, i.e. $y = 0$.

Table C-3 - Air-water flow measurements with a double-tip conductivity probe (Ø = 0.25 mm) for the flat stepped spillways ($\theta = 26.6°$, h = 5 cm)

Configuration (1)	d_c/h [-] (2)	Q [m^3/s] (3)	Re [-] (4)	Measurement at step edge (5)	Inception point step edge (6)	Flow regime (7)
Flat stepped spillway	0.7	0.030	2.30×10^5	4-10	3 to 4	TRA1
	0.82	0.038	2.90×10^5	4-10	4	TRA
	0.96	0.049	3.71×10^5	5-10	5	SK
	1.15	0.063	4.85×10^5	5-10	5 to 6	SK
	1.29	0.075	5.73×10^5	6-10	6	SK
	1.45	0.090	6.87×10^5	7-10	7	SK
	1.52	0.097	7.39×10^5	8-10	8	SK
	1.7	0.113	8.72×10^5	8-10	8 to 9	SK

Notes: d_c: critical flow depth; h: vertical step height; Q: water discharge; Re: Reynolds number defined in terms of the hydraulic diameter; SK: skimming flow regime; TRA: transition flow regime.

Table C-4 - Summary of the air-water flow properties on the flat stepped spillway and positioning in the following figures (Fig. C-1 to C-8); Illustration as functions of y/d_c

Void fraction C	Dimensionless bubble count rate $F \times d_c/V_c$
Dimensionless interfacial velocity V/V_c	Turbulence intensity Tu
Dimensionless auto-correlation time scale $T_{xx} \times \sqrt{g/d_c}$	Dimensionless cross-correlation time scale $T_{xy} \times \sqrt{g/d_c}$
Maximum cross-correlation in a cross-section $(R_{xy})_{max}$	

Notes: y: distance normal to the pseudo bottom; C: void fraction; F: bubble count rate; d_c: critical flow depth; V_c: critical flow velocity; V: interfacial velocity; Tu: turbulence intensity; T_{xx}: auto-correlation time scale; T_{xy}: cross-correlation time scale; $(R_{xy})_{max}$: maximum cross-correlation.

Fig. C-1 – Air-water flow properties on the flat stepped spillway (θ = 26.6°) as functions of y/d_c – Transition flow sub-regime TRA1: $d_c/h = 0.7$, $Q = 0.030$ m^3/s, $Re = 2.30\times10^5$; Step edges 4-10

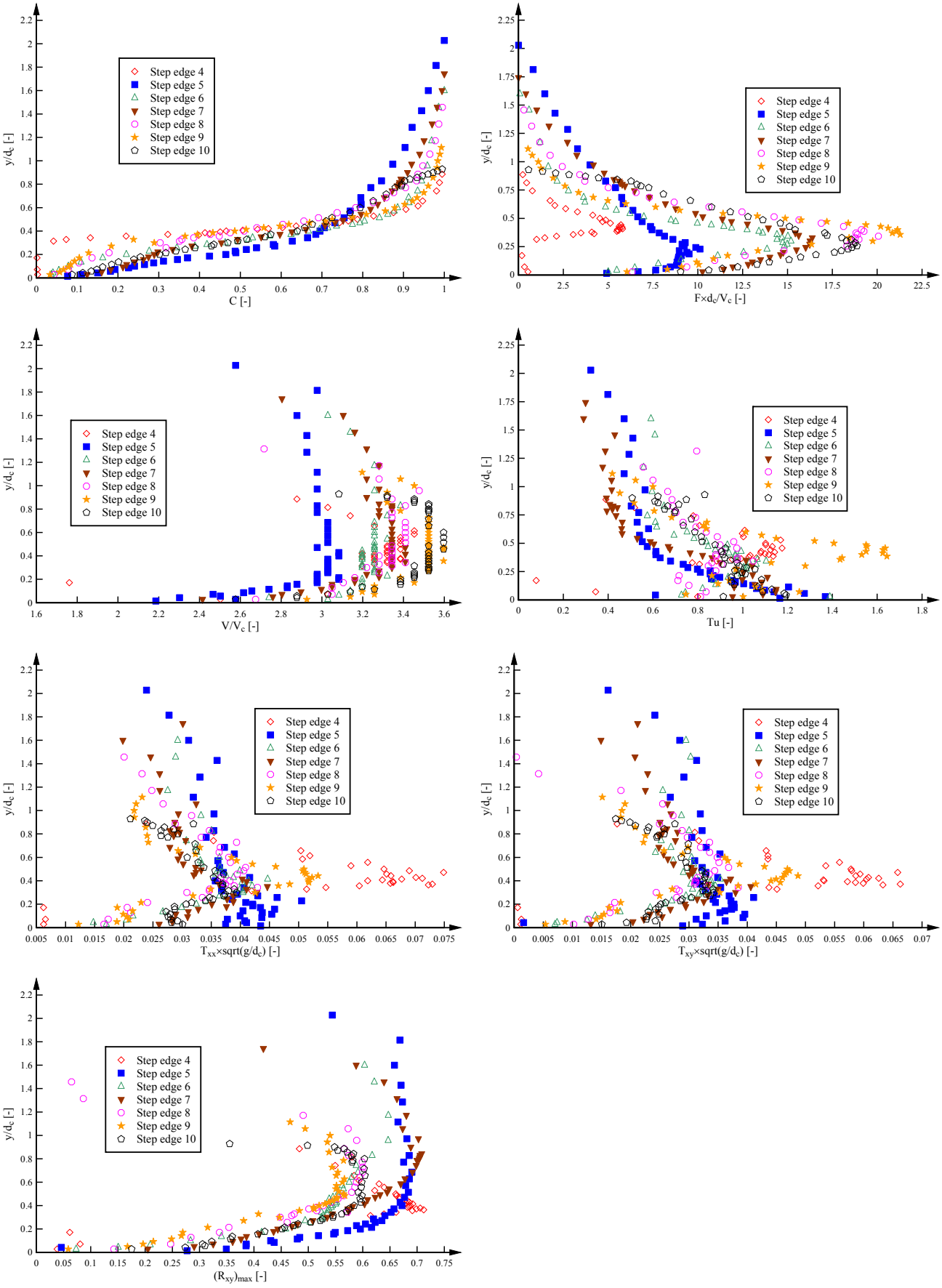

Fig. C-2 – Air-water flow properties on the flat stepped spillway (θ = 26.6°) as functions of y/d_c – Transition flow: $d_c/h = 0.82$, $Q = 0.038$ m^3/s, $Re = 2.90\times10^5$; Step edges 4-10

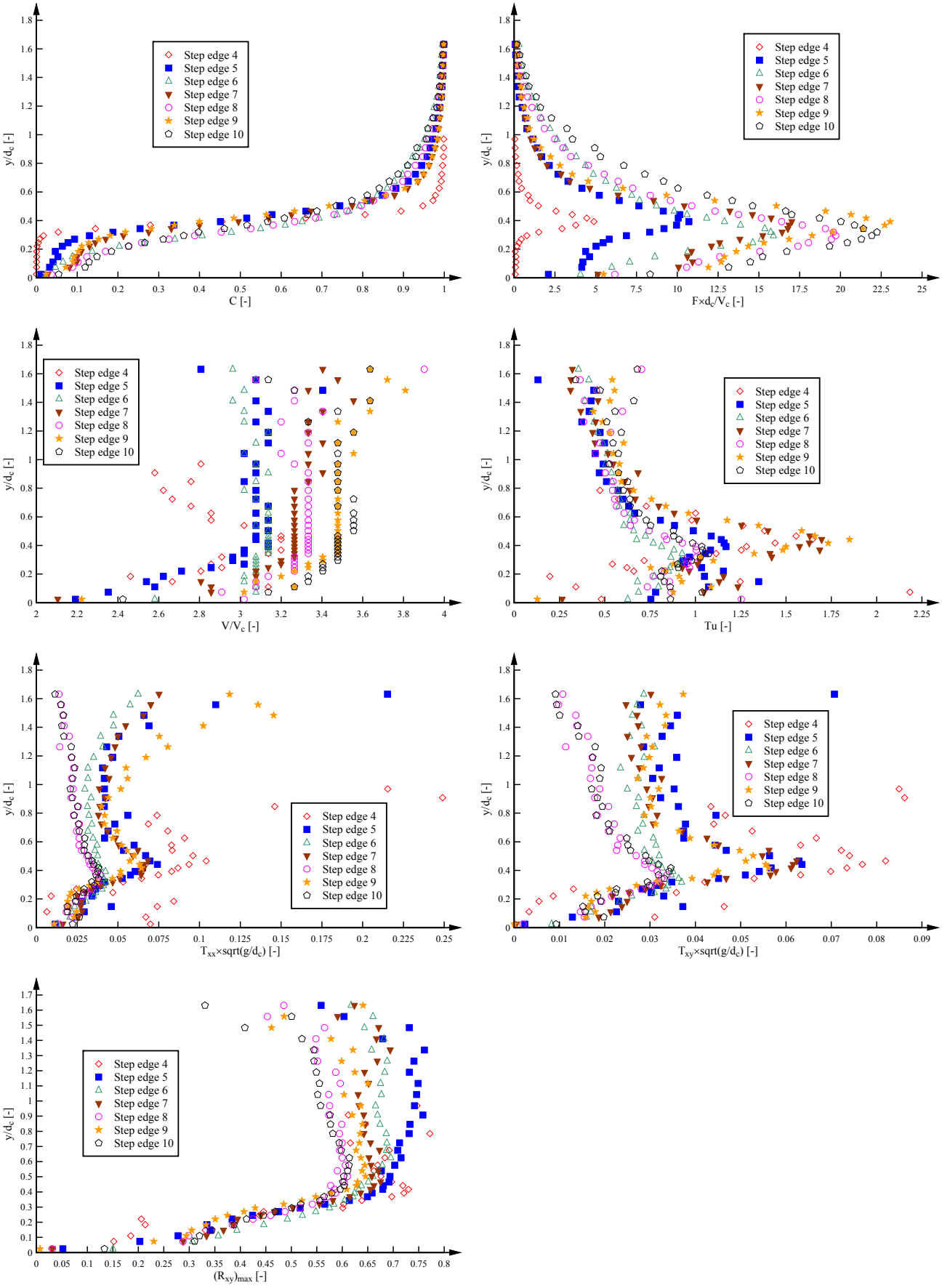

Fig. C-3 – Air-water flow properties on the flat stepped spillway (θ = 26.6°) as functions of y/d_c – Skimming flow: $d_c/h = 0.96$, $Q = 0.049$ m^3/s, $Re = 3.71\times10^5$; Step edges 5-10

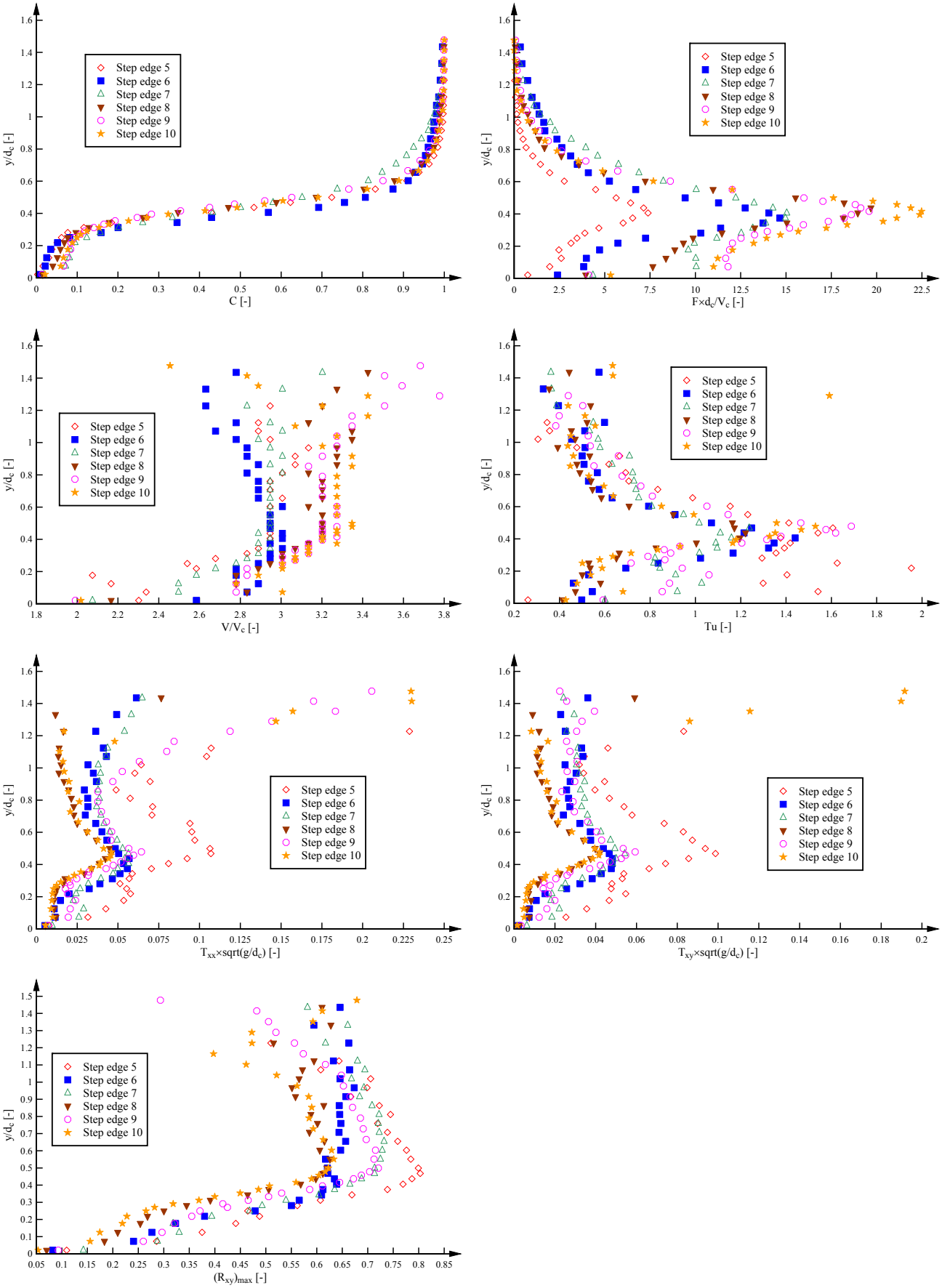

Fig. C-4 – Air-water flow properties on the flat stepped spillway (θ = 26.6°) as functions of y/d_c – Skimming flow: $d_c/h = 1.15$, $Q = 0.063$ m^3/s, $Re = 4.85\times10^5$; Step edges 5-10

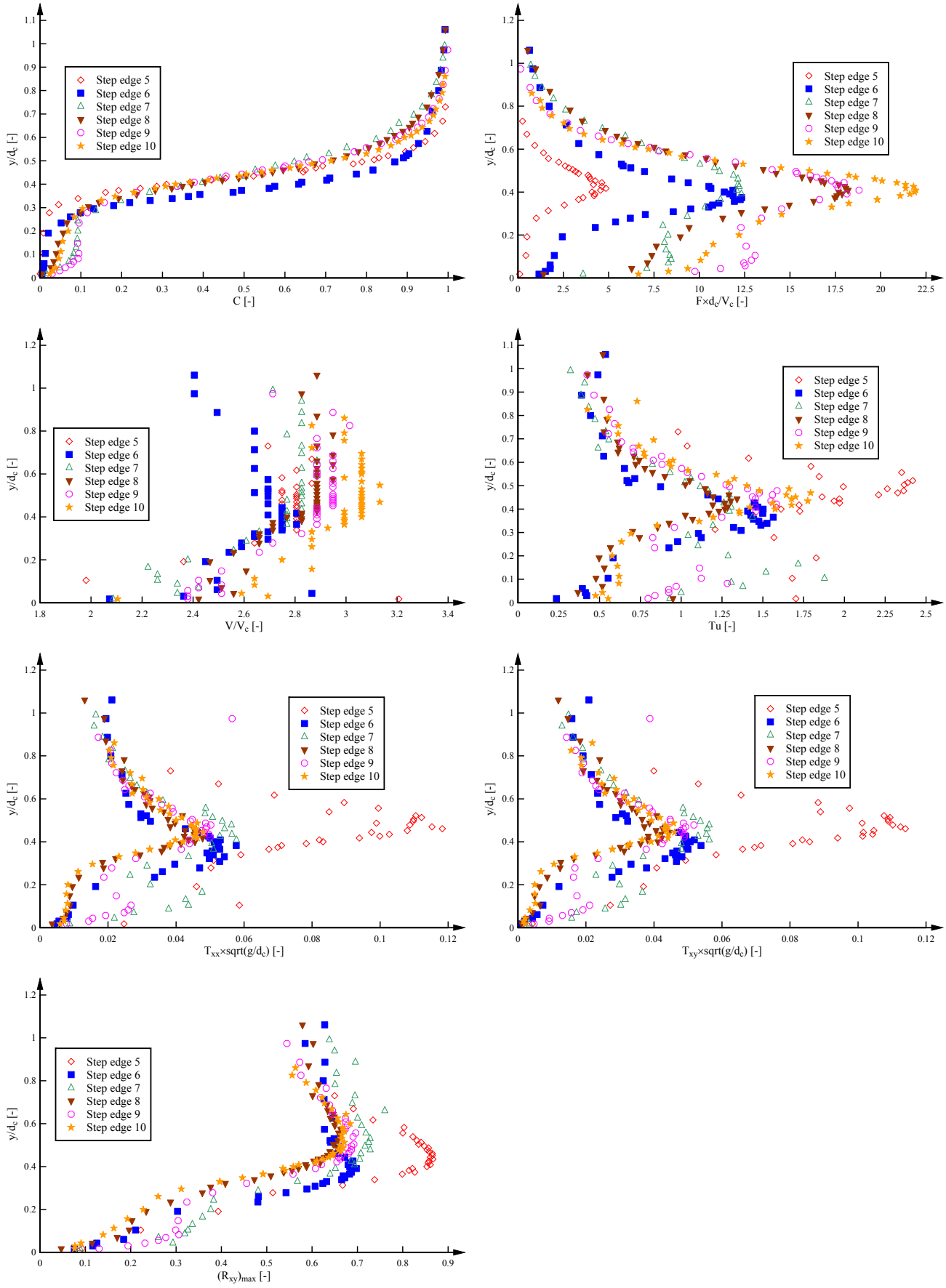

Fig. C-5 – Air-water flow properties on the flat stepped spillway (θ = 26.6°) as functions of y/d_c – Skimming flow: $d_c/h = 1.29$, $Q = 0.075$ m^3/s, $Re = 5.73\times10^5$; Step edges 6-10

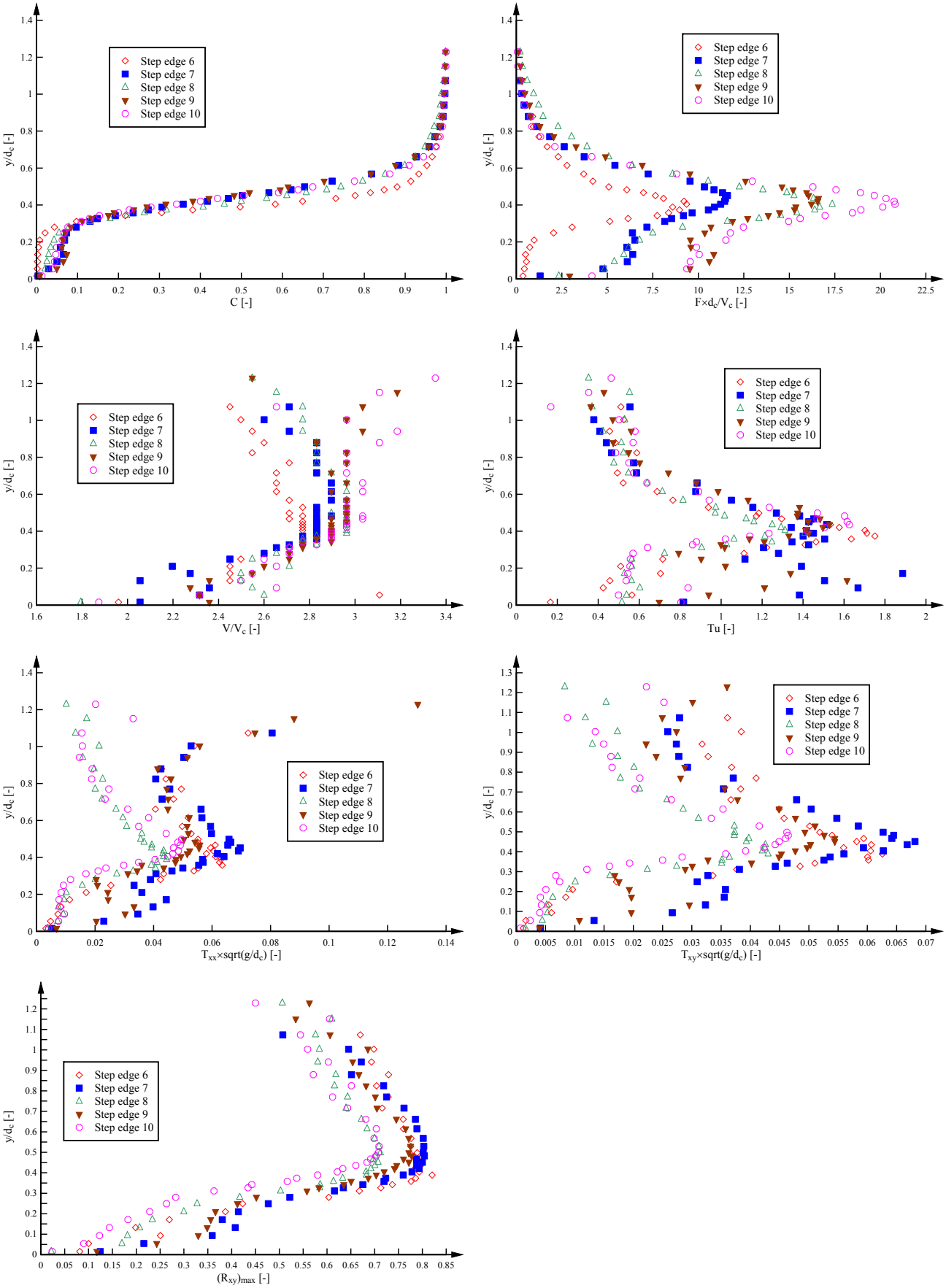

Fig. C-6 – Air-water flow properties on the flat stepped spillway (θ = 26.6°) as functions of y/d_c – Skimming flow: $d_c/h = 1.45$, $Q = 0.090$ m^3/s, $Re = 6.87\times10^5$; Step edges 7-10

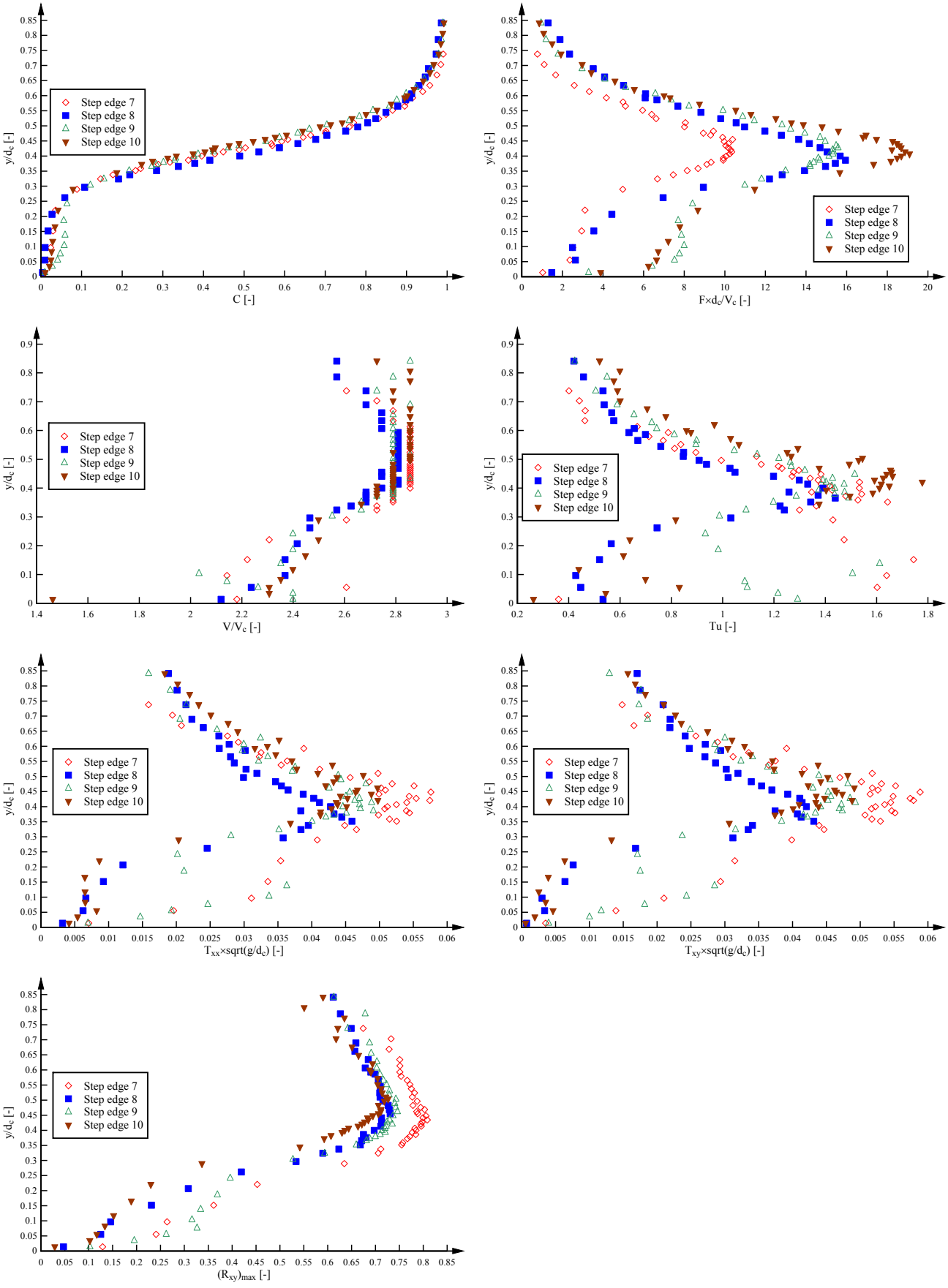

Fig. C-7 – Air-water flow properties on the flat stepped spillway (θ = 26.6°) as functions of y/d_c – Skimming flow: $d_c/h = 1.52$, $Q = 0.097$ m^3/s, $Re = 7.39\times10^5$; Step edges 8-10

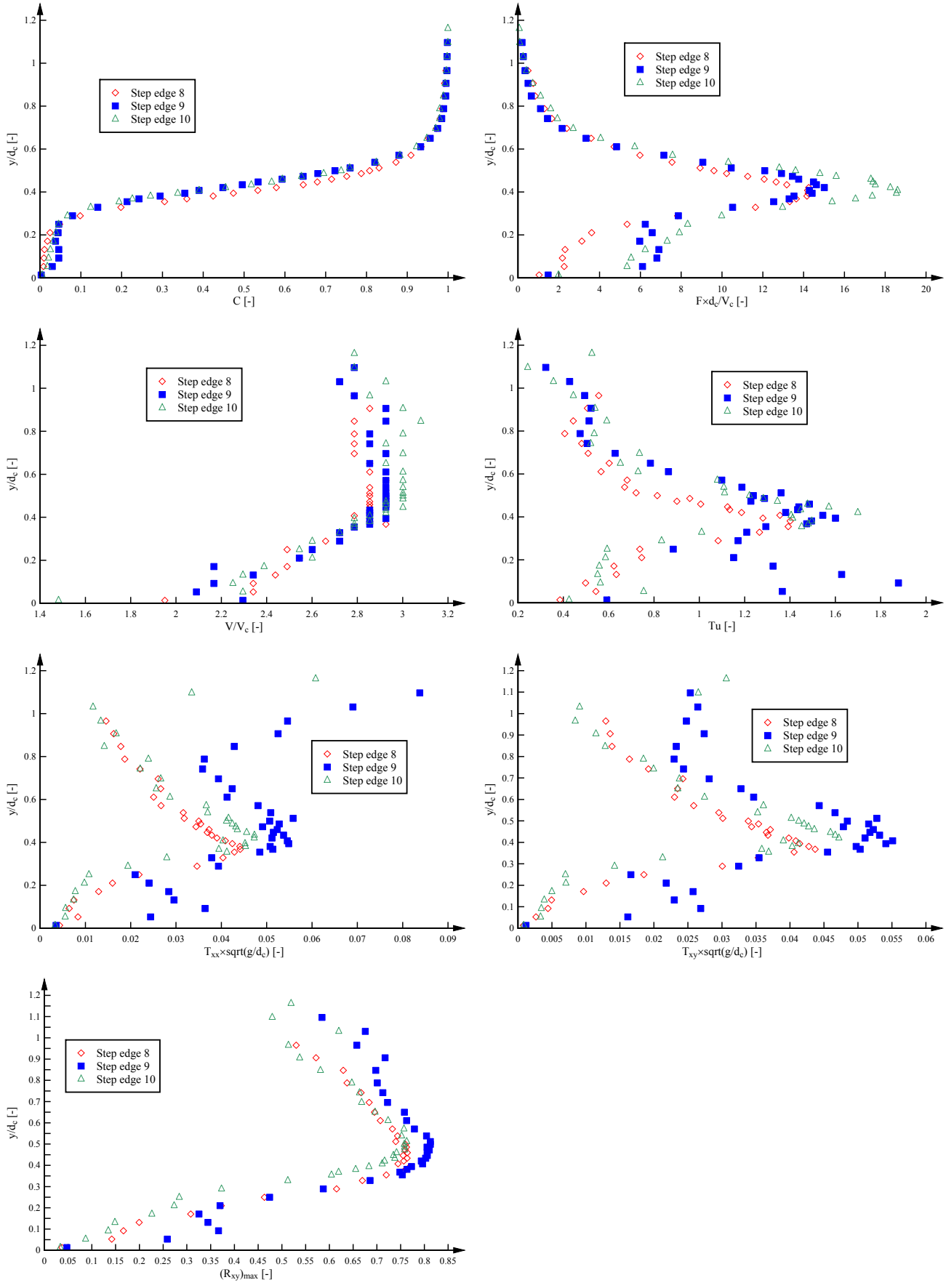

Fig. C-8 – Air-water flow properties on the flat stepped spillway (θ = 26.6°) as functions of y/d_c – Skimming flow: $d_c/h = 1.70$, $Q = 0.113$ m^3/s, $Re = 8.72\times10^5$; Step edges 8-10

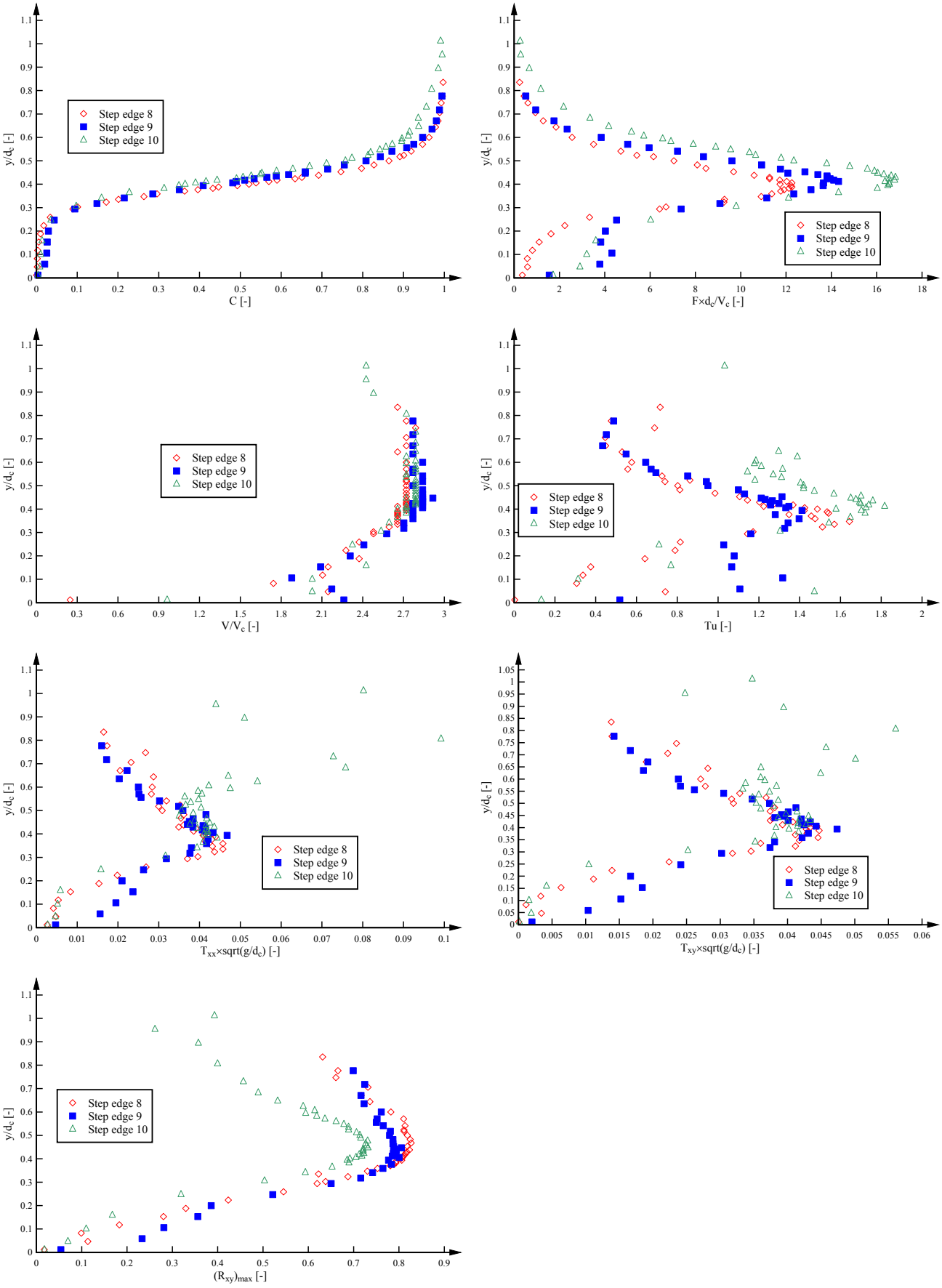

C.3 AIR-WATER FLOW PROPERTIES ON THE POOLED STEPPED SPILLWAY

This section presents the air-water flow properties for the experiments with a double-tip conductivity probe on the pooled stepped spillway and Table C-5 lists the experimental flow conditions. Table C-6 summarises the presented data in this section and it indicates the respective position of the six graphs in Figures C-9 to C-18. All air-water flow distributions are presented in terms of the dimensionless distance from the pool weir height $(y+w)/d_c$. The weir pool edge was defined as the zero position for the measurements with the conductivity probe, i.e. y = 0.

Table C-5 - Air-water flow measurements with a double-tip conductivity probe (Ø = 0.25 mm) for the pooled stepped spillways (θ = 26.6°, h = 5 cm, w = 3.1 cm)

Configuration (1)	d_c/h [-] (2)	Q [m^3/s] (3)	Re [-] (4)	Measurement at step edge (5)	Inception point step edge (6)	Flow regime (7)
Pooled stepped spillway	0.4	0.013	9.95×10^4	2-10	2	NA
	0.7	0.030	2.30×10^5	4-10	4	TRA
	0.82	0.038	2.90×10^5	5-10	4 to 5	TRA
	0.96	0.049	3.71×10^5	6-10	5 to 6	TRA/SK
	1.15	0.063	4.85×10^5	5-10	5 to 6	SK
	1.29	0.075	5.73×10^5	7-10	6 to 7	SK
	1.45	0.090	6.87×10^5	7-10	7	SK
	1.52	0.097	7.39×10^5	8-10	8	SK
	1.7	0.113	8.72×10^5	8-10	8	SK
	1.85	0.130	9.89×10^5	10	9 to 10	SK

Notes: d_c: critical flow depth; h: vertical step height; Q: water discharge; Re: Reynolds number; SK: skimming flow regime; TRA: transition flow regime; NA: nappe flow regime.

Table C-6 - Summary of the air-water flow properties on the flat stepped spillway and positioning in the following figures (Fig. C-9 to C-18); Illustration as functions of $(y+w)/d_c$

Void fraction C	Dimensionless bubble count rate $F\times d_c/V_c$
Dimensionless interfacial velocity V/V_c	Turbulence intensity Tu
Dimensionless auto-correlation time scale $T_{xx}\times\sqrt{g/d_c}$	Dimensionless cross-correlation time scale $T_{xy}\times\sqrt{g/d_c}$
Maximum cross-correlation in a cross-section $(R_{xy})_{max}$	

Notes: y: distance normal to the pseudo bottom; C: void fraction; F: bubble count rate; d_c: critical flow depth; V_c: critical flow velocity; V: interfacial velocity; Tu: turbulence intensity; T_{xx}: auto-correlation time scale; T_{xy}: cross-correlation time scale; $(R_{xy})_{max}$: maximum cross-correlation auto-correlation time scale; w: pool weir height.

Fig. C-9 – Air-water flow properties on the pooled stepped spillway (θ = 26.6°) as functions of $(y+w)/d_c$ – Nappe flow: $d_c/h = 0.4$, $Q = 0.013$ m^3/s, $Re = 9.95\times10^4$; Step edges 2-10

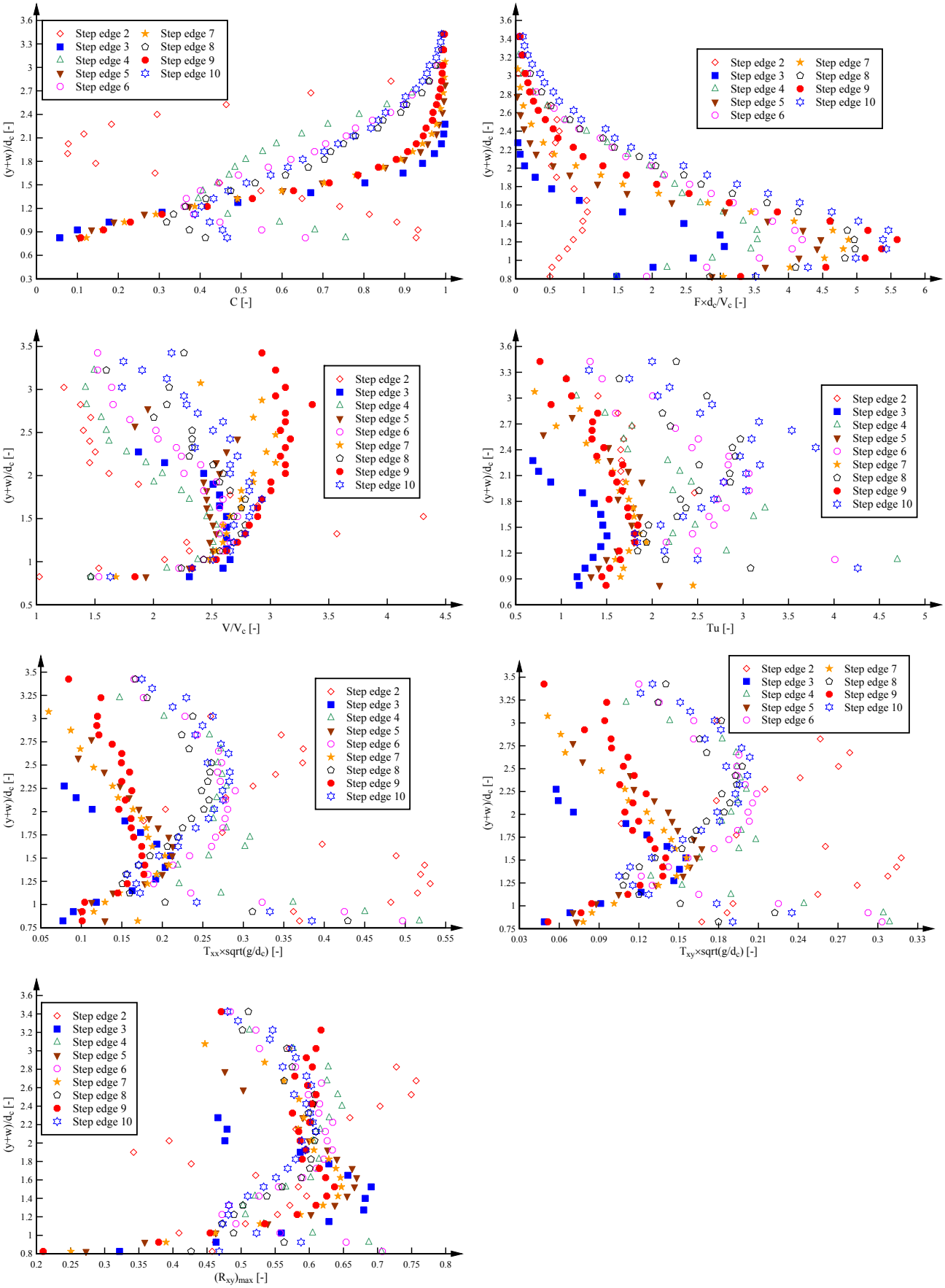

Fig. C-10 – Air-water flow properties on the pooled stepped spillway (θ = 26.6°) as functions of $(y+w)/d_c$ – Transition flow: $d_c/h = 0.7$, $Q = 0.030$ m^3/s, $Re = 2.30\times10^5$; Step edges 4-10

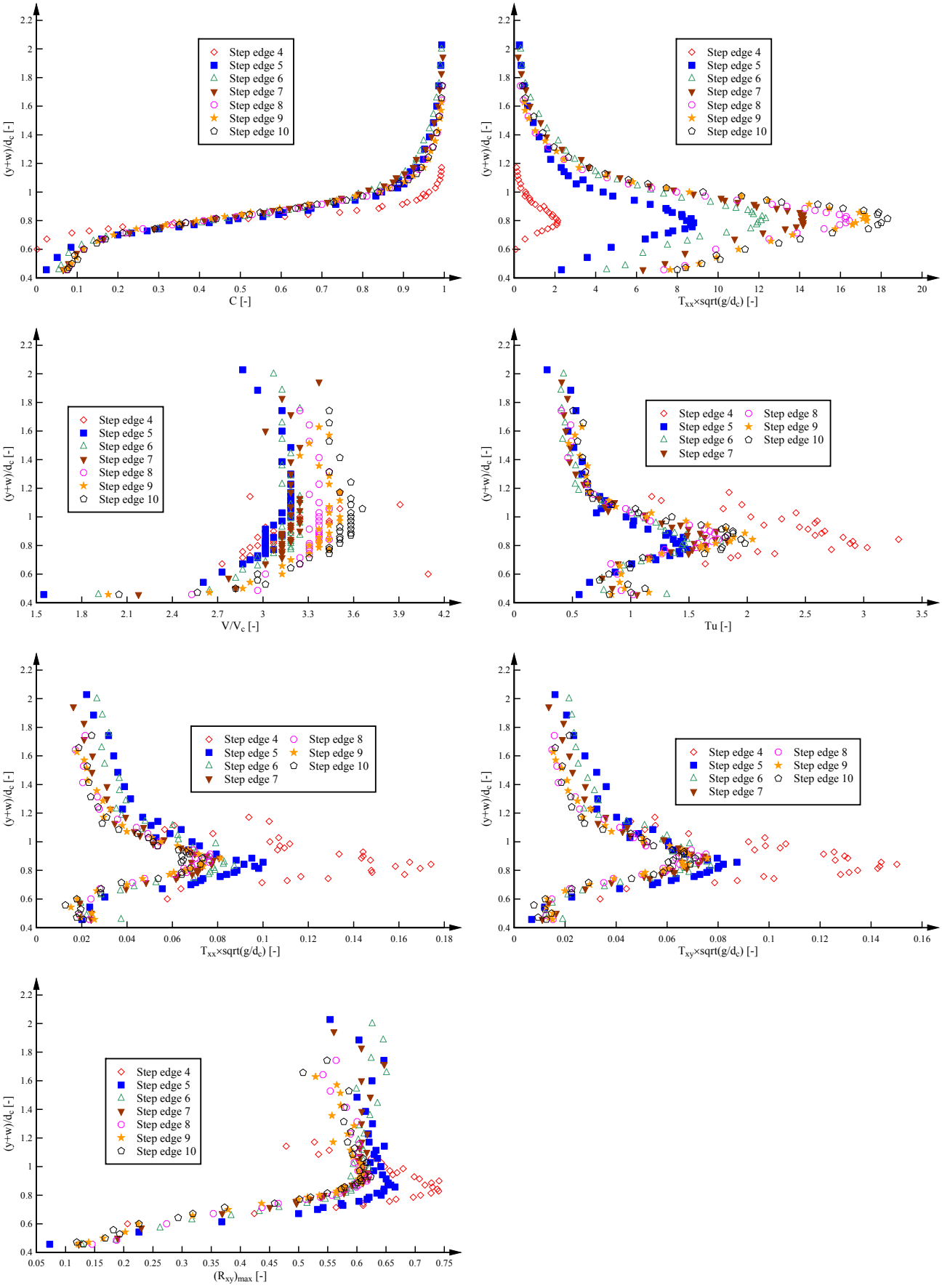

Fig. C-11 – Air-water flow properties on the pooled stepped spillway (θ = 26.6°) as functions of $(y+w)/d_c$ – Transition flow: $d_c/h = 0.82$, $Q = 0.038$ m^3/s, $Re = 2.90\times10^5$; Step edges 5-10

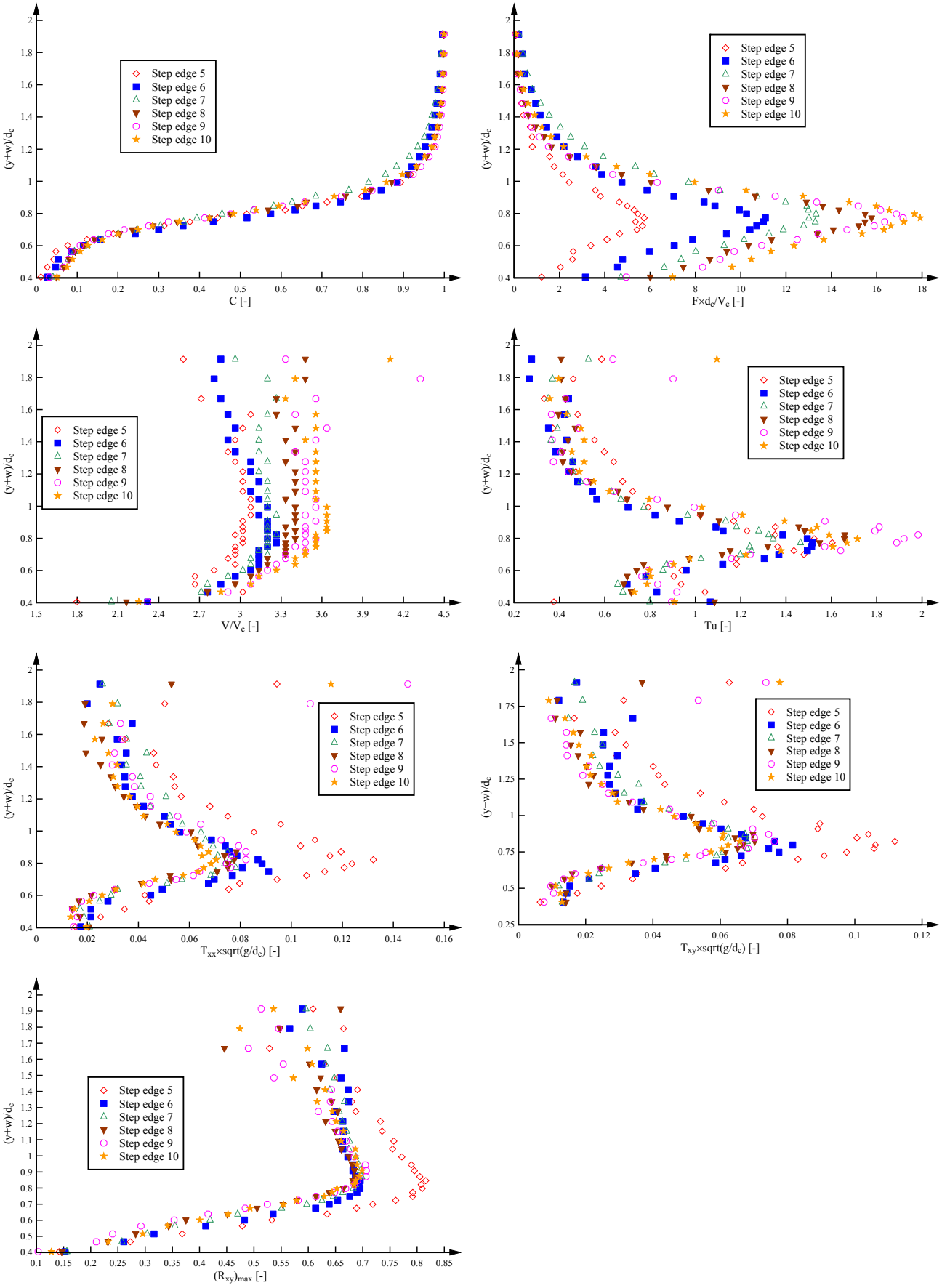

Fig. C-12 – Air-water flow properties on the pooled stepped spillway (θ = 26.6°) as functions of $(y+w)/d_c$ – Skimming flow: $d_c/h = 0.96$, $Q = 0.049$ m^3/s, $Re = 3.71\times10^5$; Step edges 6-10

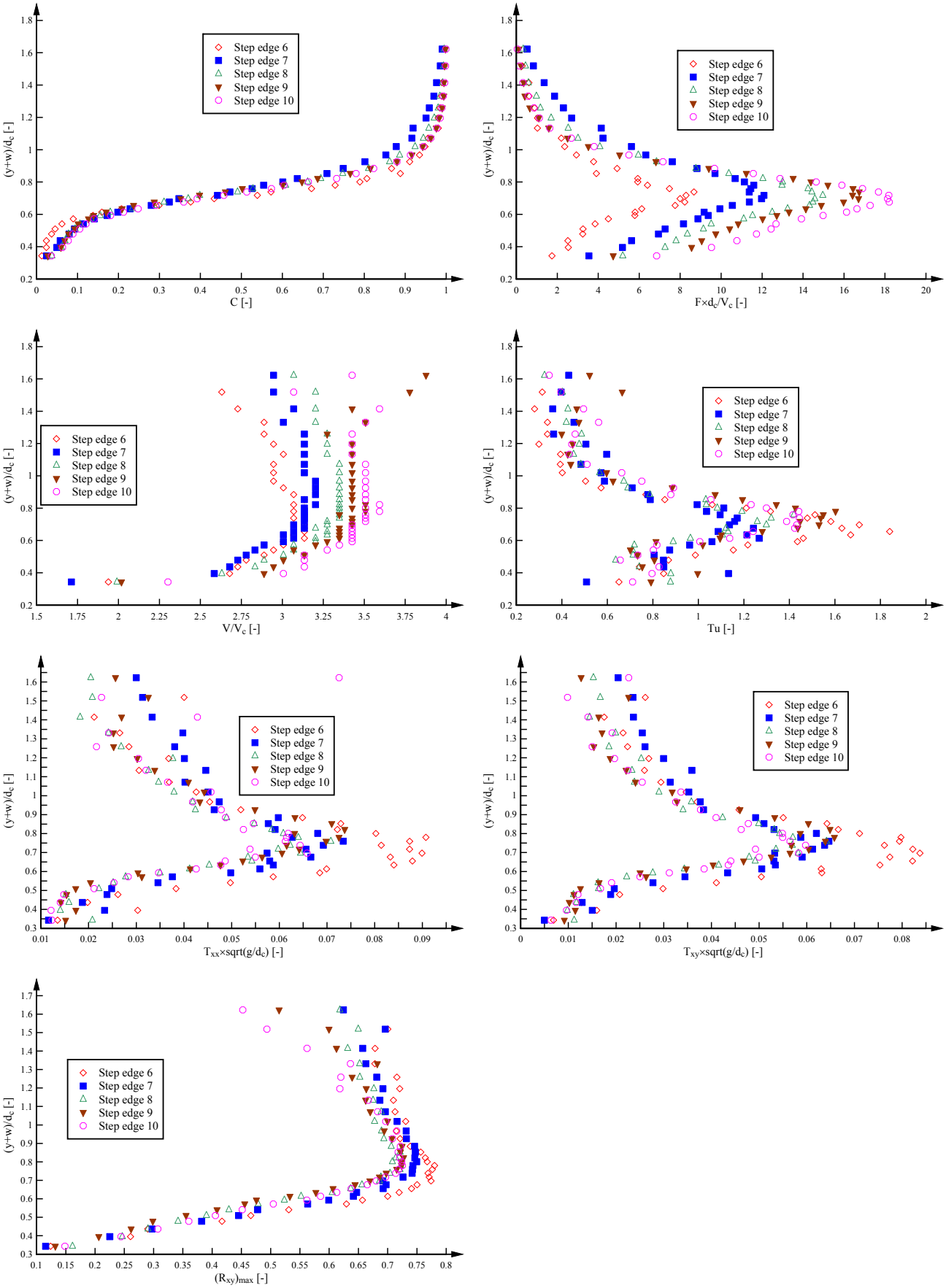

Fig. C-13 – Air-water flow properties on the pooled stepped spillway (θ = 26.6°) as functions of $(y+w)/d_c$ – Skimming flow: $d_c/h = 1.15$, $Q = 0.063$ m^3/s, $Re = 4.85\times10^5$; Step edges 5-10

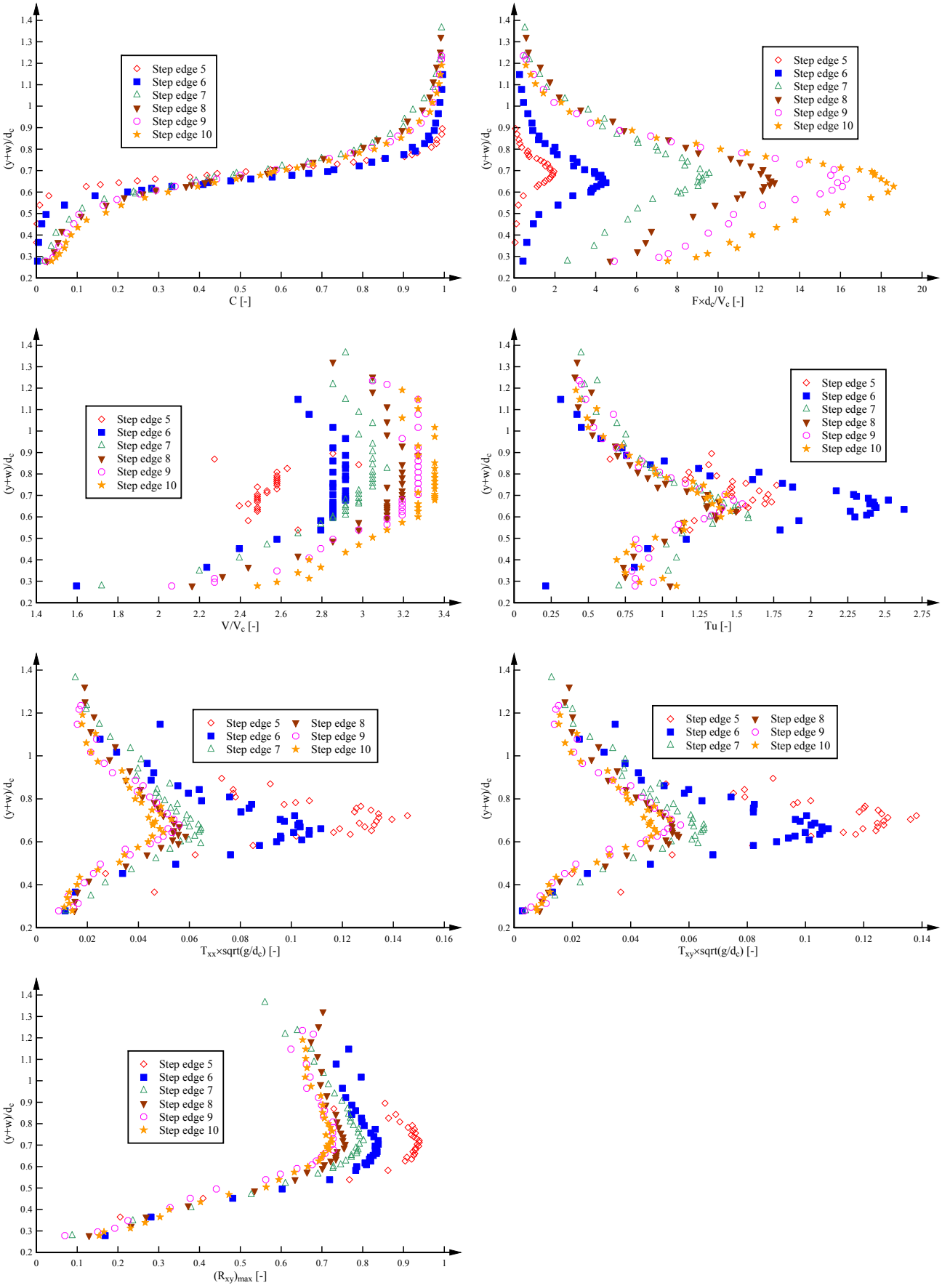

Fig. C-14 – Air-water flow properties on the pooled stepped spillway (θ = 26.6°) as functions of $(y+w)/d_c$ – Skimming flow: $d_c/h = 1.29$, $Q = 0.075$ m^3/s, $Re = 5.73\times10^5$; Step edges 7-10

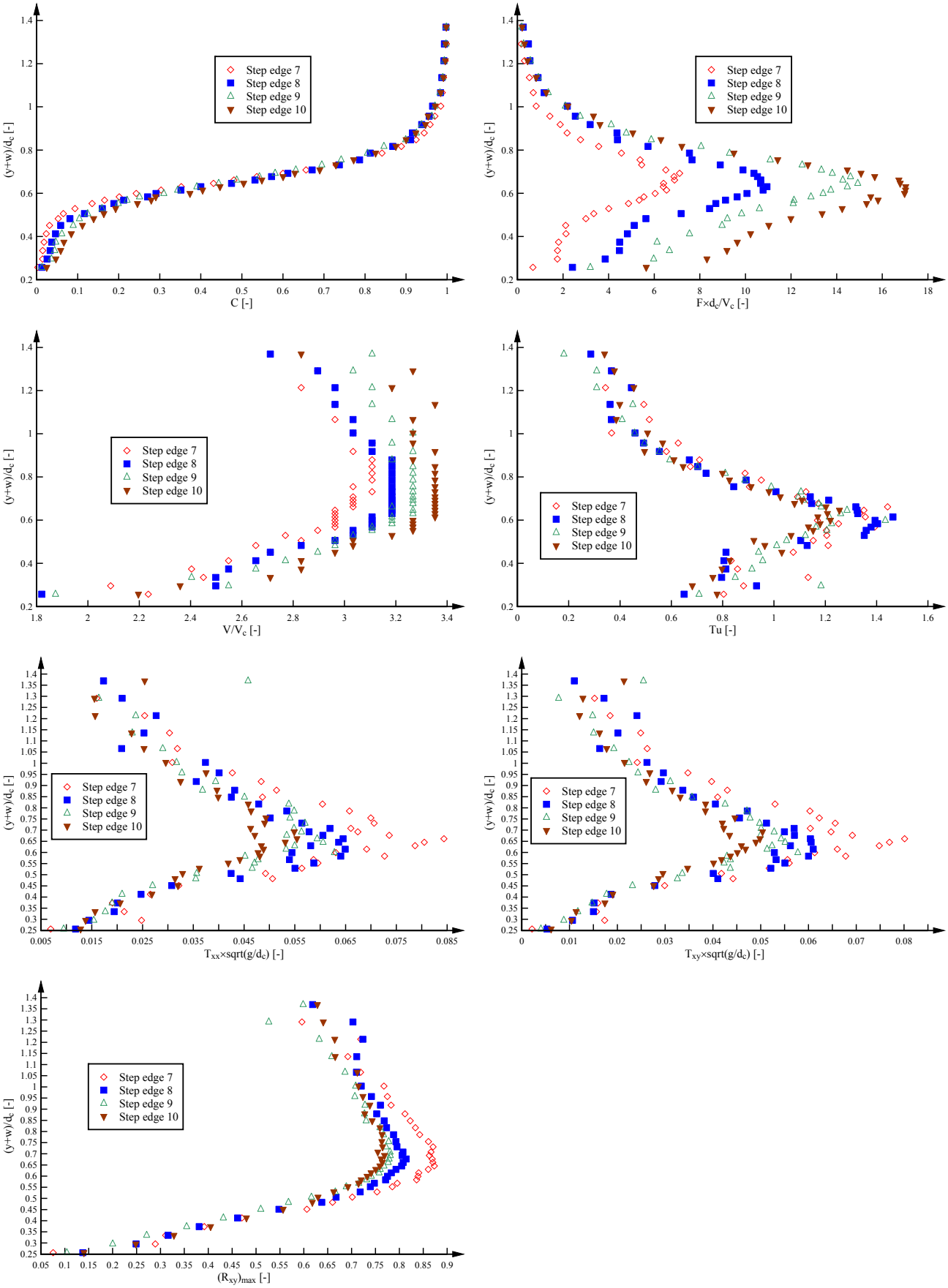

Fig. C-15 – Air-water flow properties on the pooled stepped spillway (θ = 26.6°) as functions of $(y+w)/d_c$ – Skimming flow: $d_c/h = 1.45$, $Q = 0.090$ m^3/s, $Re = 6.87\times10^5$; Step edges 7-10

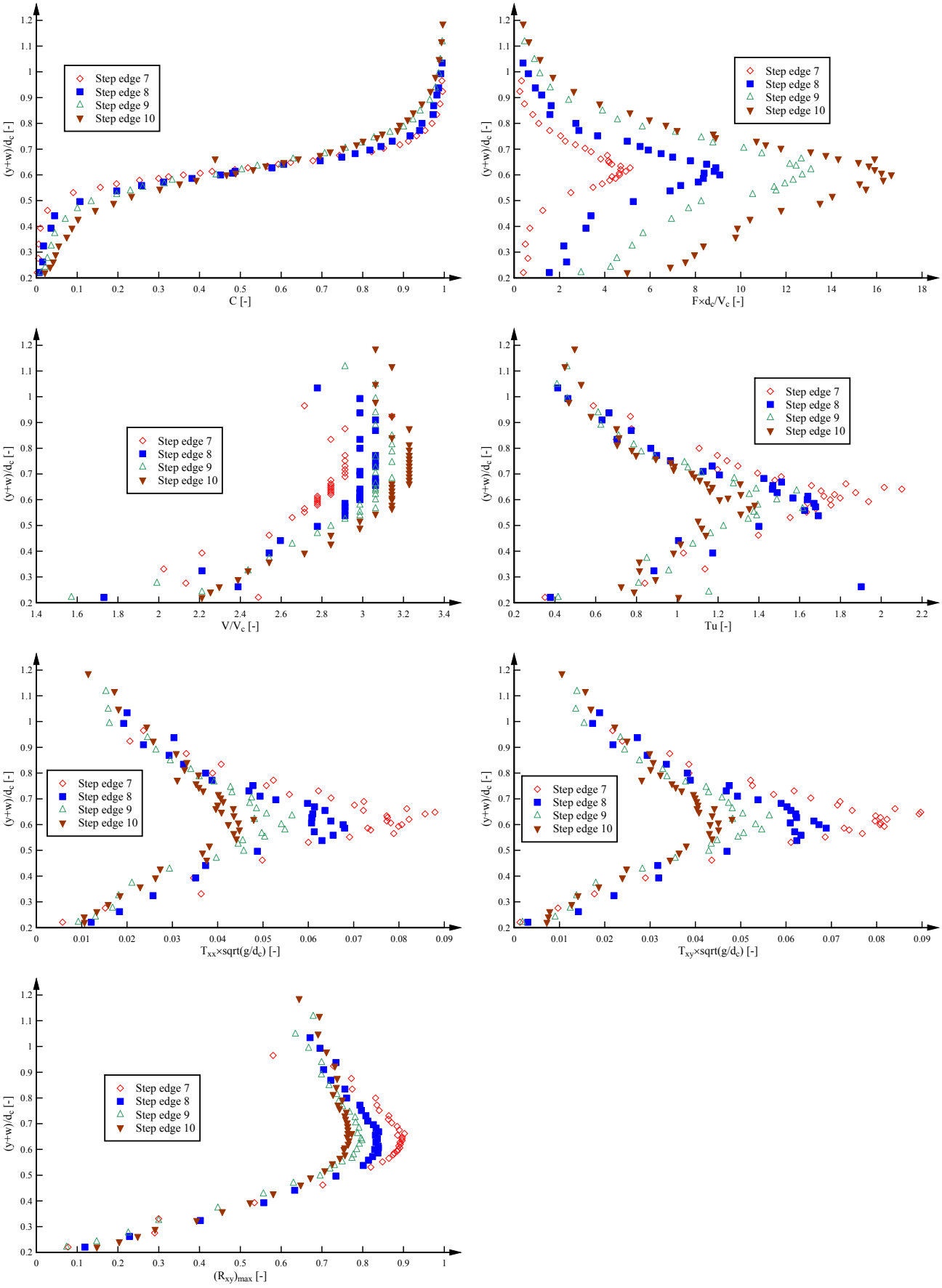

Fig. C-16 – Air-water flow properties on the pooled stepped spillway (θ = 26.6°) as functions of $(y+w)/d_c$ – Skimming flow: $d_c/h = 1.52$, $Q = 0.097$ m^3/s, $Re = 7.39\times10^5$; Step edges 8-10

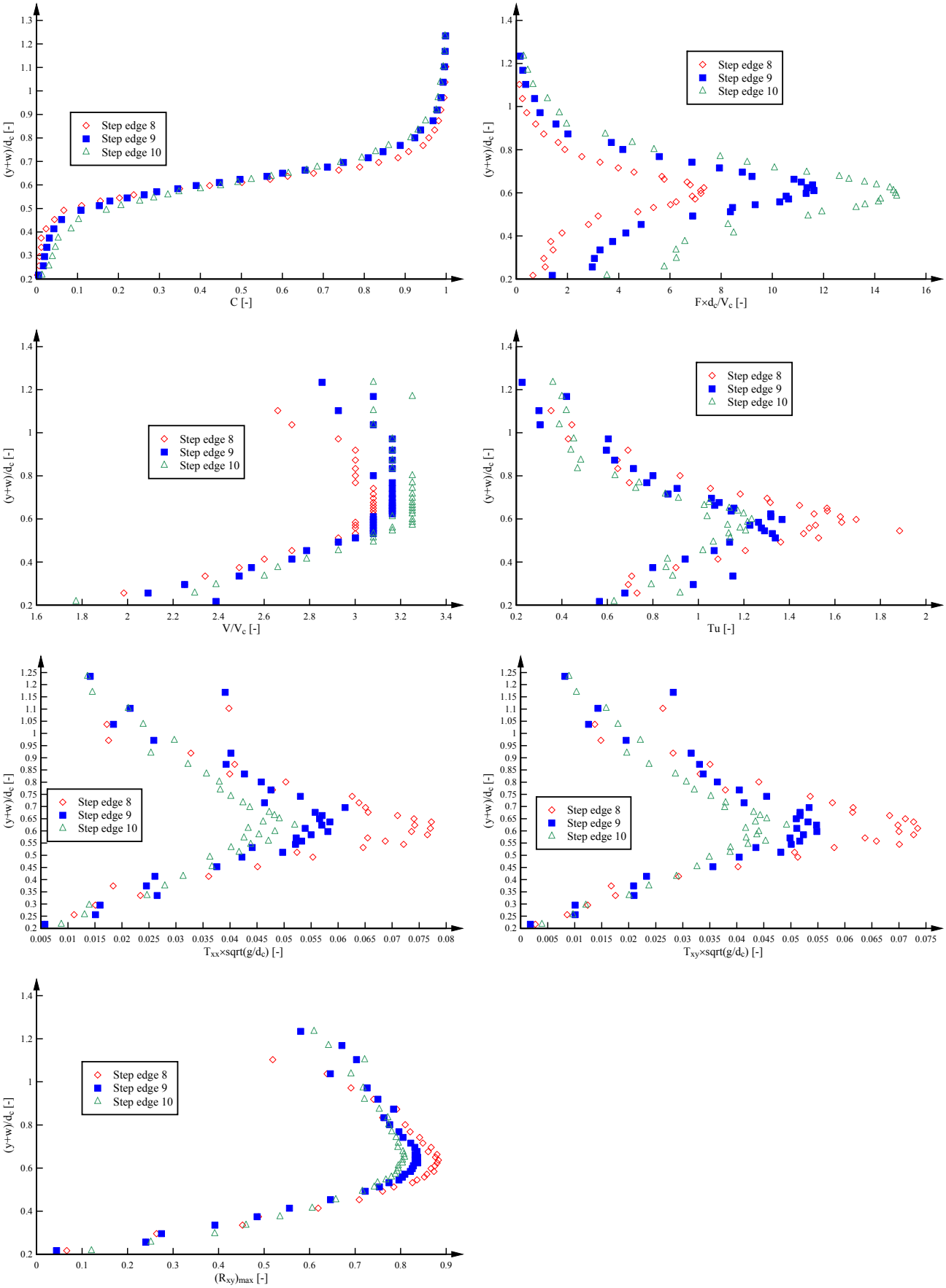

Fig. C-17 – Air-water flow properties on the pooled stepped spillway (θ = 26.6°) as functions of $(y+w)/d_c$ – Skimming flow: $d_c/h = 1.70$, $Q = 0.113$ m^3/s, $Re = 8.72\times10^5$; Step edges 8-10

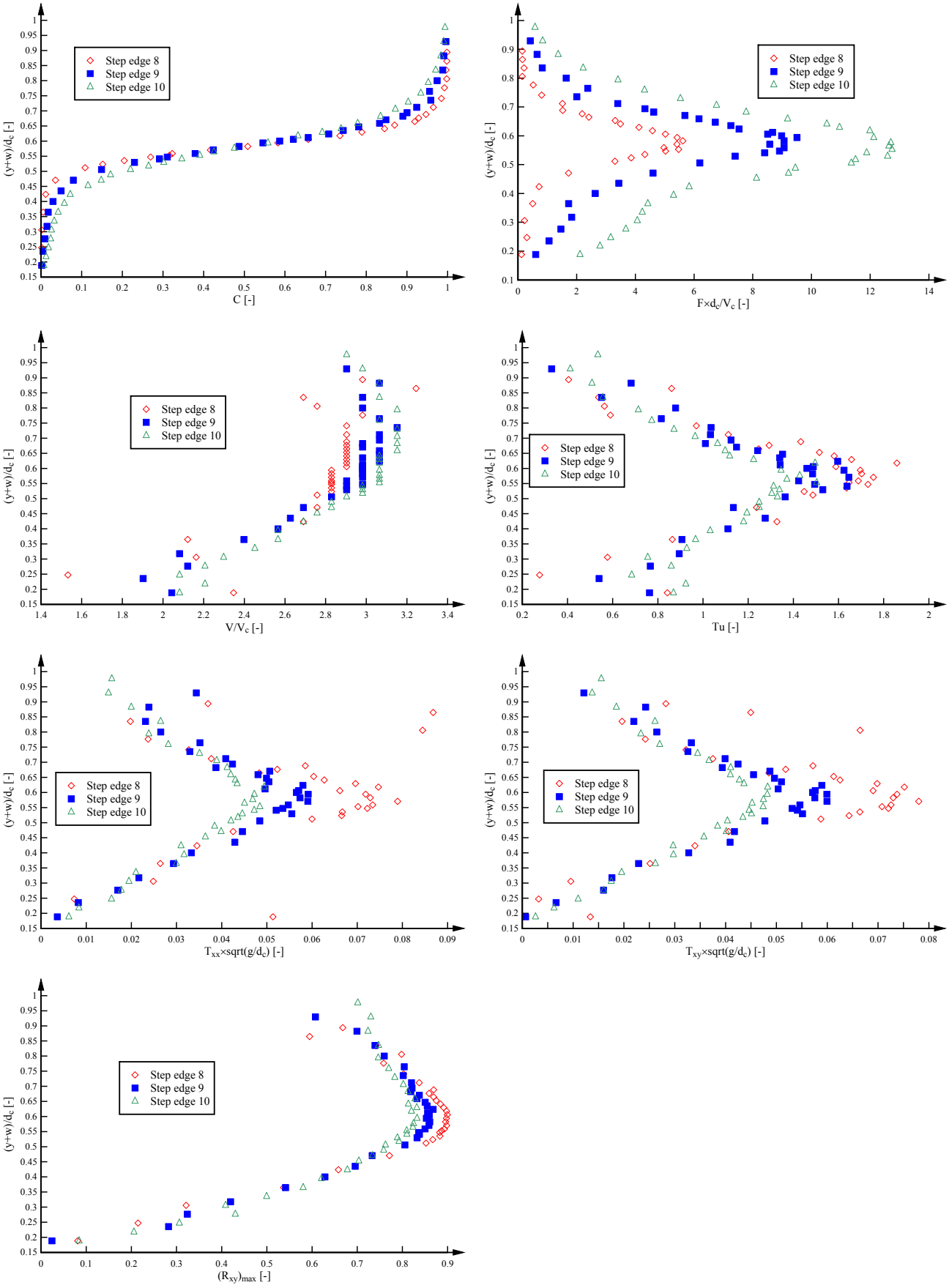

Fig. C-18 – Air-water flow properties on the pooled stepped spillway (θ = 26.6°) as functions of $(y+w)/d_c$ – Skimming flow: $d_c/h = 1.85$, $Q = 0.130$ m^3/s, $Re = 9.89\times10^5$; Step edge 10

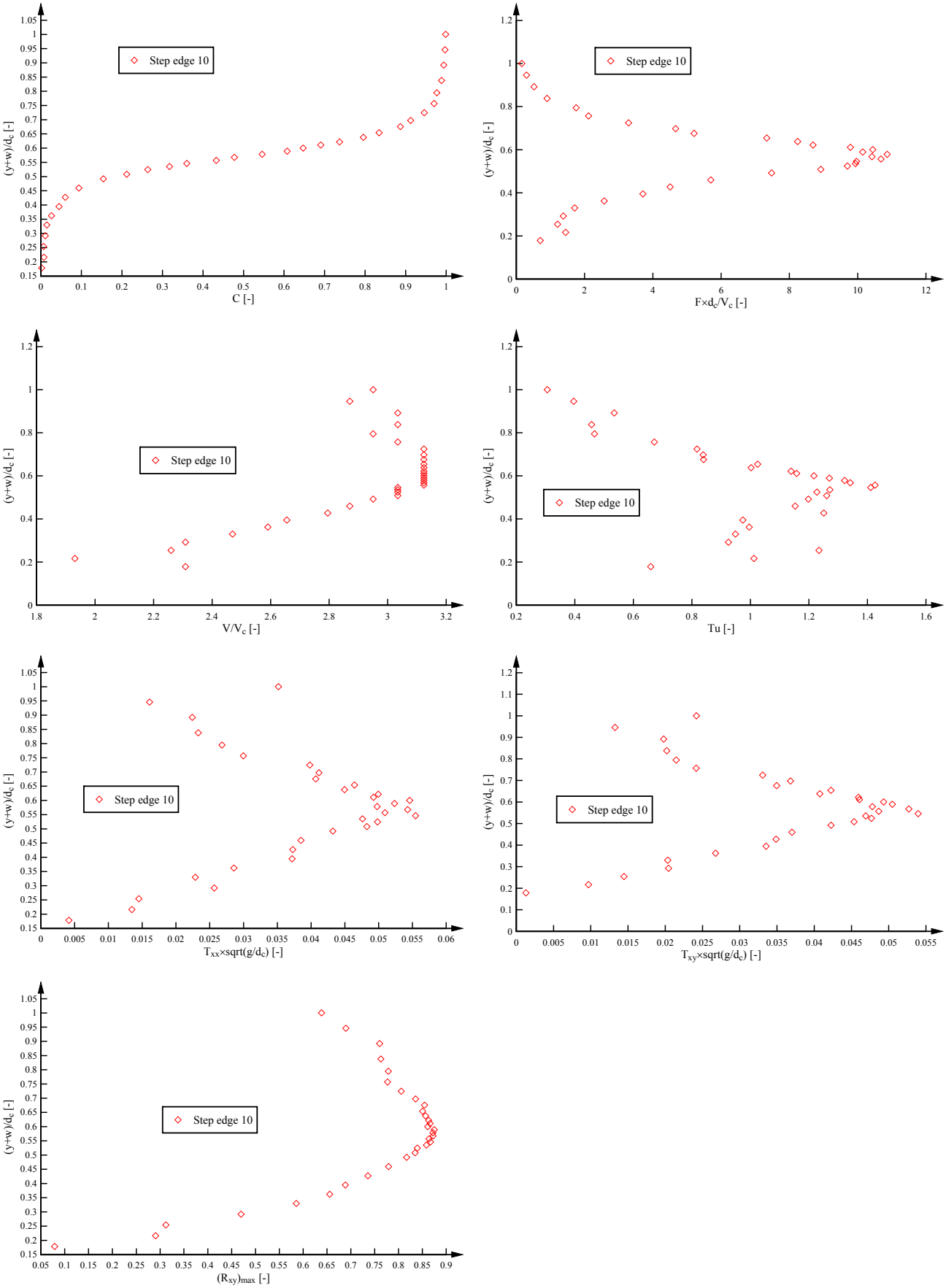

C.4 COMPARISON OF AIR BUBBLE AND WATER DROPLET CHORD SIZES ON THE FLAT AND POOLED STEPPED SPILLWAYS:

Fig. C-19 Comparison of probability distribution functions of air bubble chord sizes on the flat and pooled stepped spillways: $d_c/h = 0.82$, $Q = 0.038$ m^3/s, $Re = 2.90\times10^5$

(A) Step edge 9

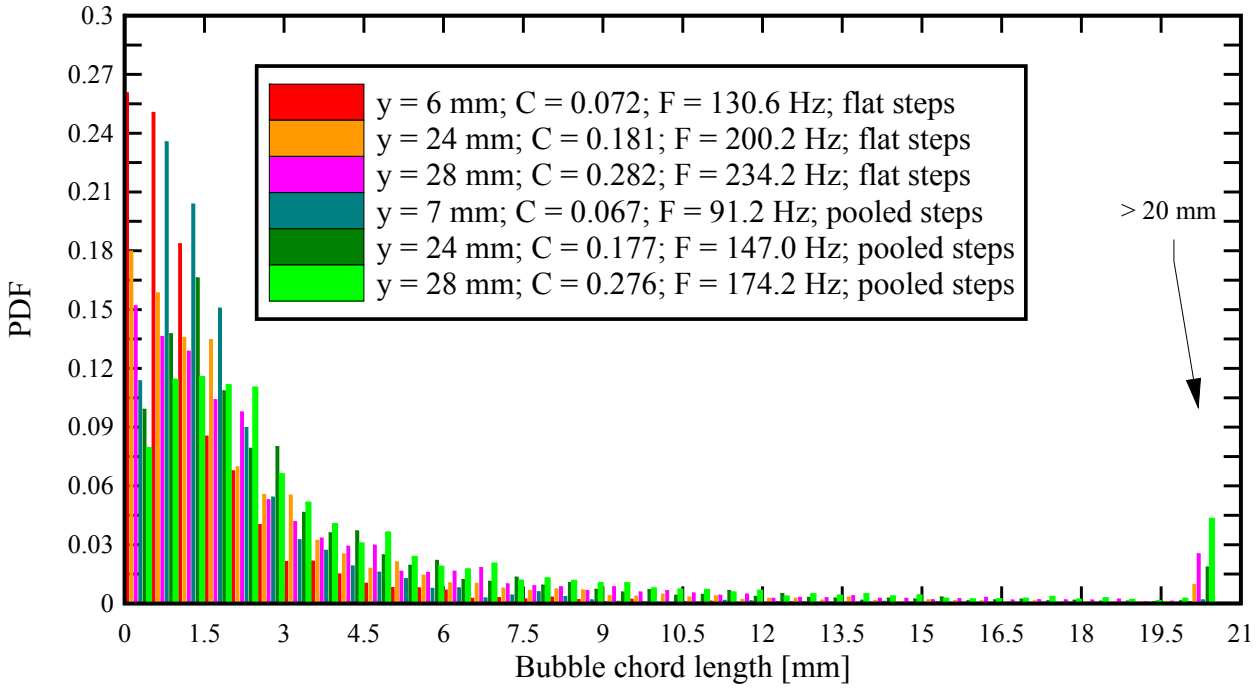

(B) Step edge 10

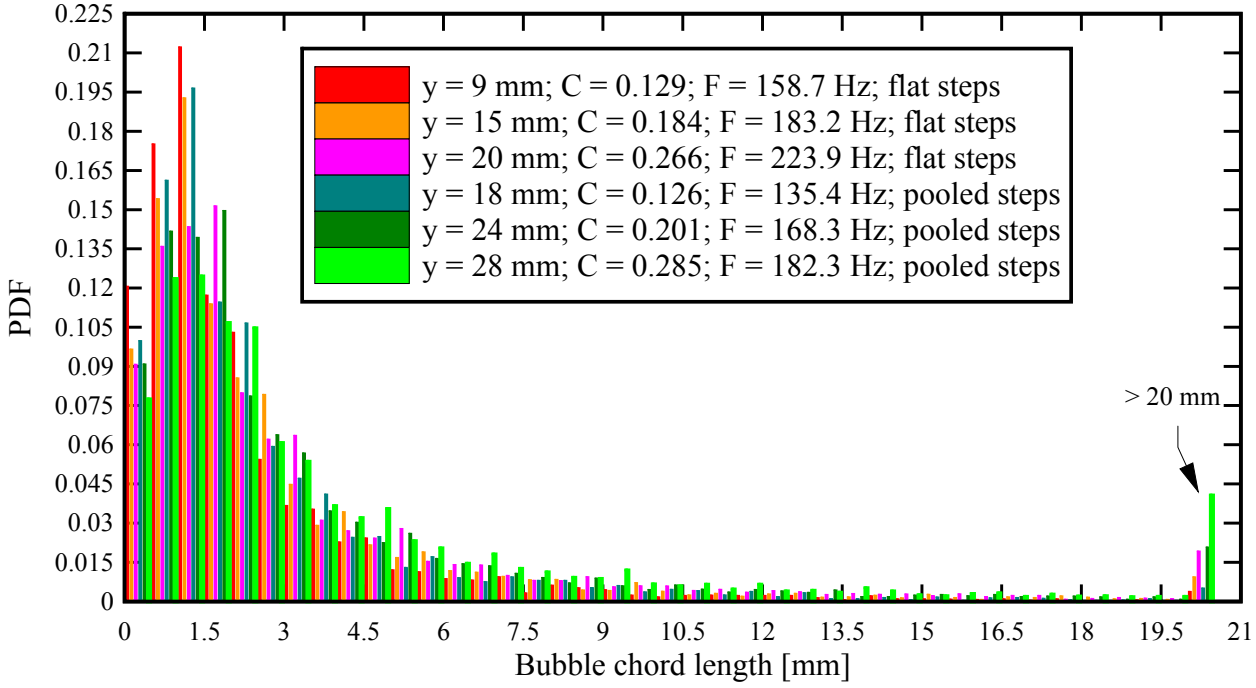

Fig. C-20 Comparison of probability distribution functions of air bubble chord sizes on the flat and pooled stepped spillways: $d_c/h = 0.96$, $Q = 0.049$ m^3/s, $Re = 3.71 \times 10^5$

(A) Step edge 9

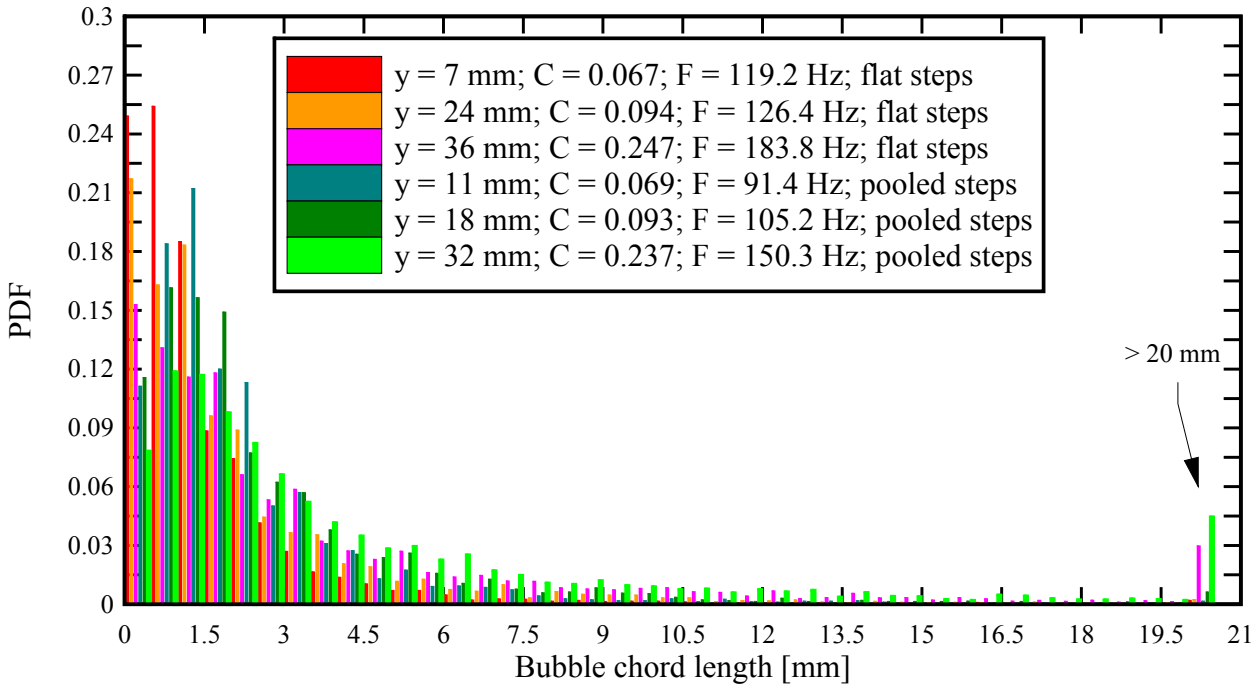

(B) Step edge 10

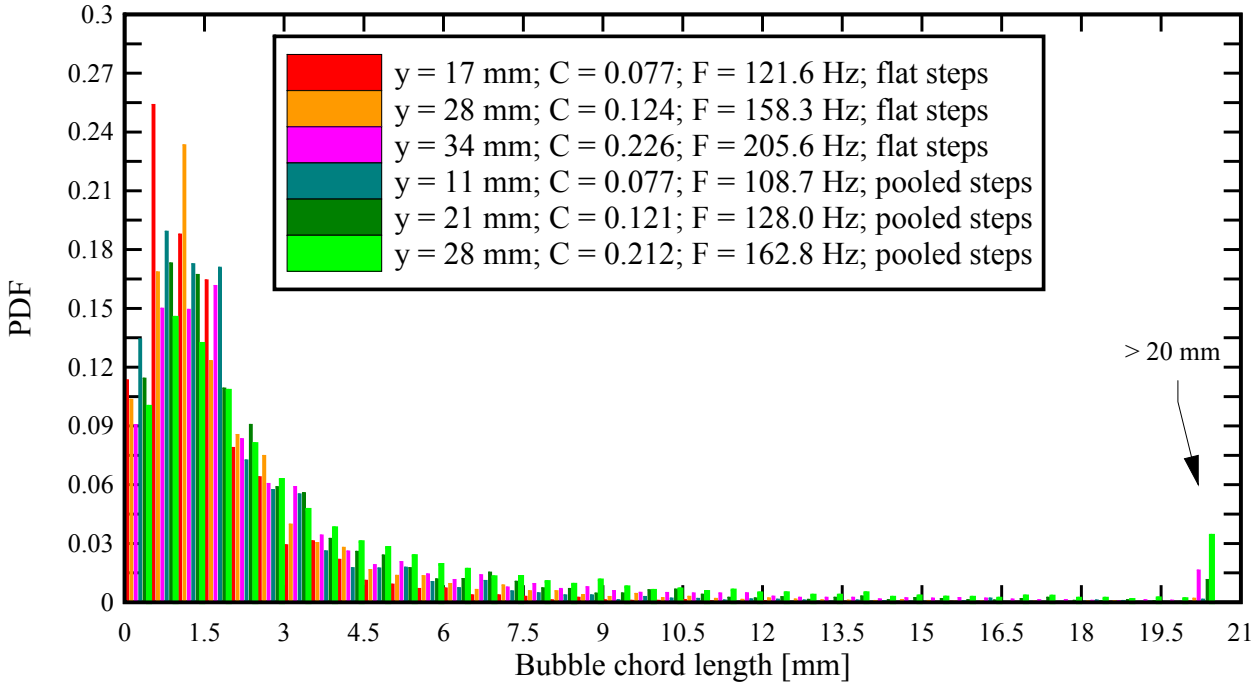

Fig. C-21 Comparison of probability distribution functions of air bubble chord sizes on the flat and pooled stepped spillways: $d_c/h = 1.29$, $Q = 0.075$ m^3/s, $Re = 5.73\times10^5$

(A) Step edge 9

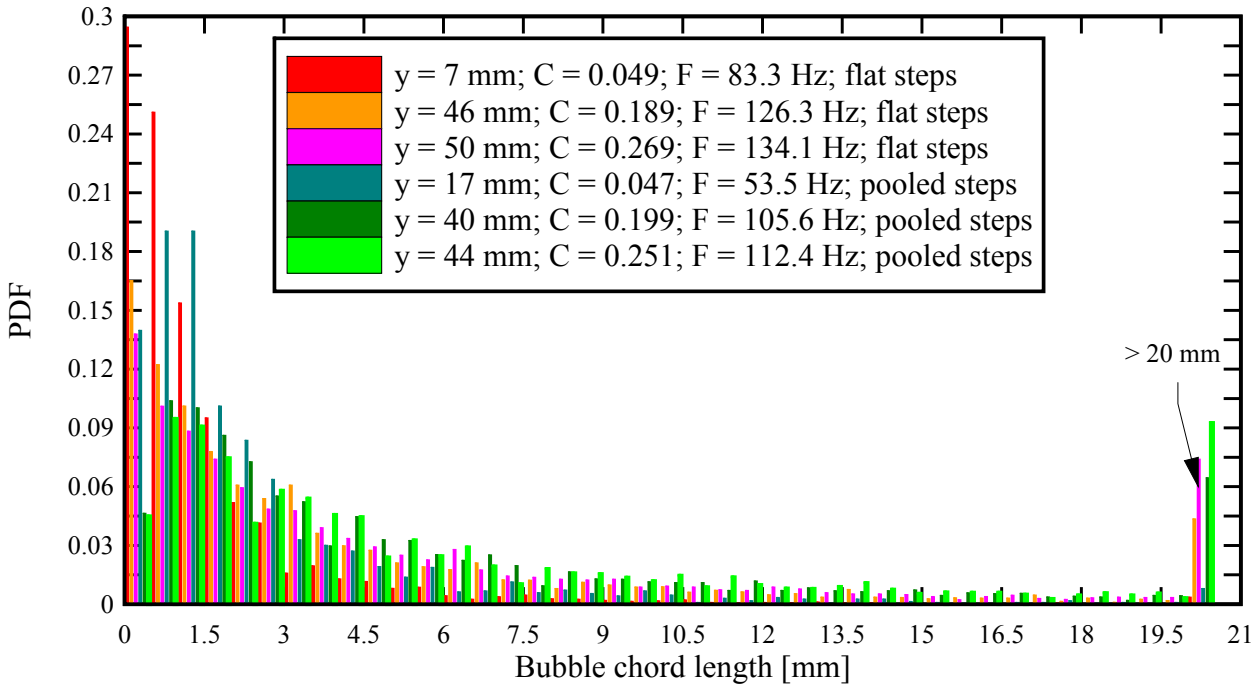

(B) Step edge 10

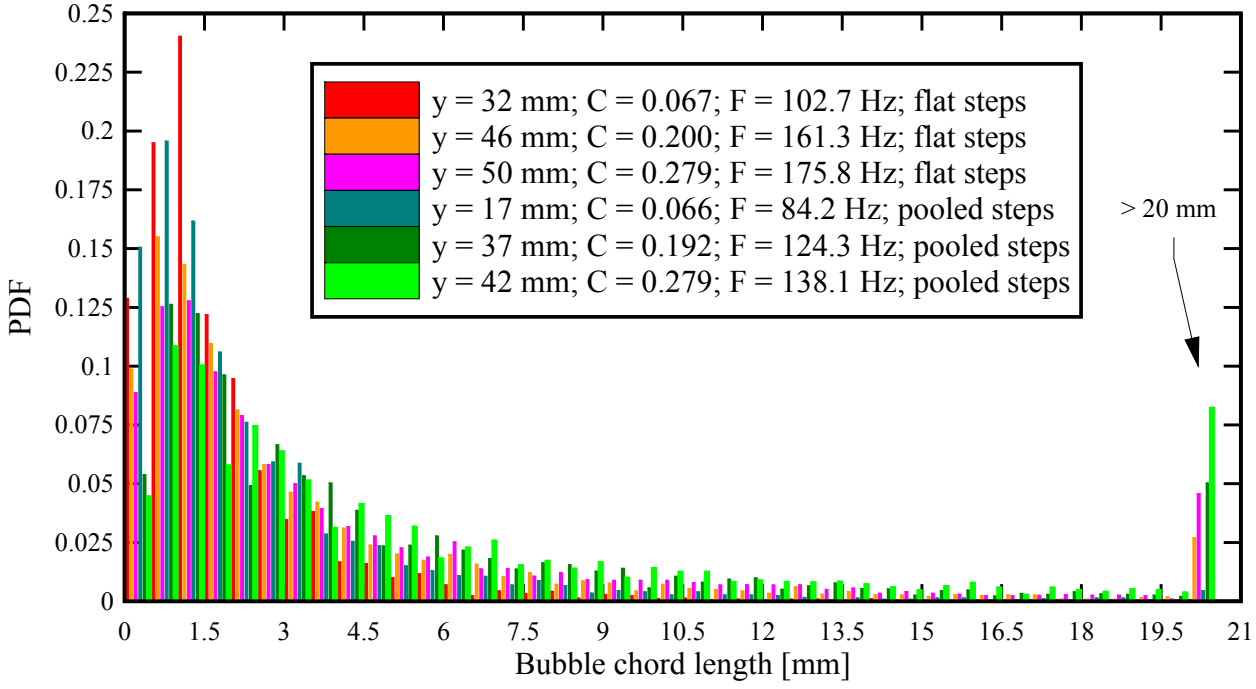

Fig. C-22 Comparison of probability distribution functions of air bubble chord sizes on the flat and pooled stepped spillways: $d_c/h = 1.52$, $Q = 0.097$ m^3/s, $Re = 7.39\times10^5$ - Step edge 10

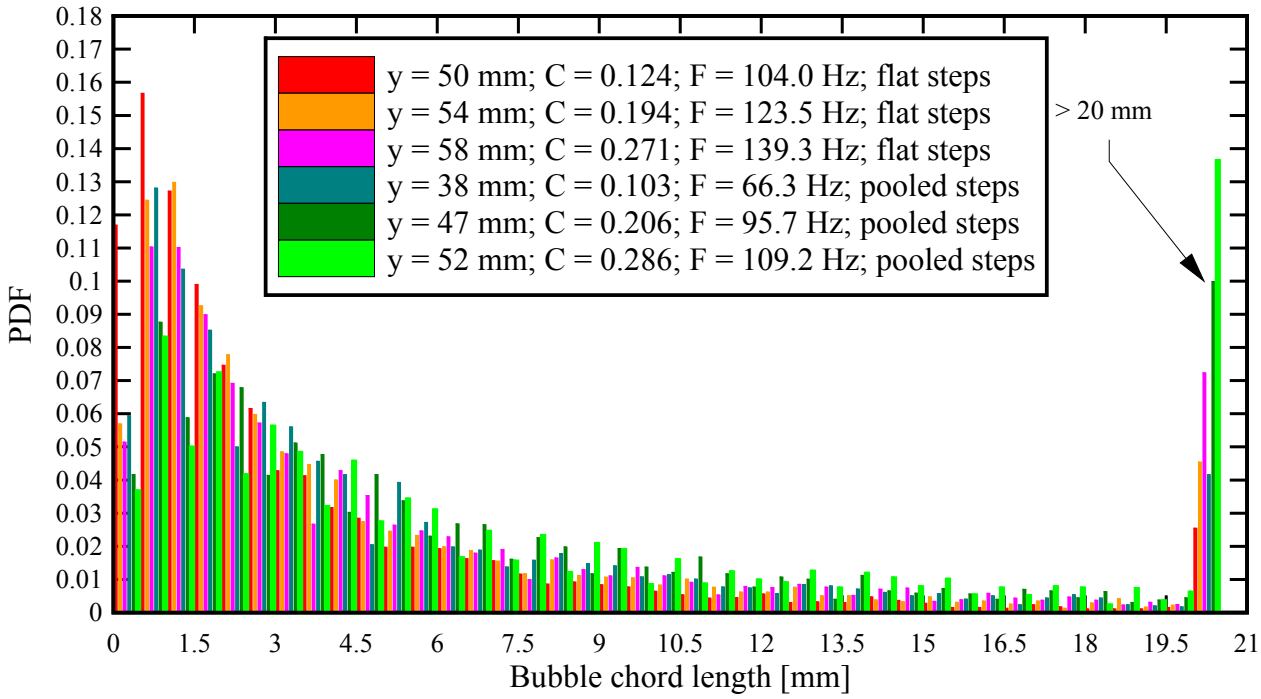

Fig. C-23 Comparison of probability distribution functions of water droplet chord sizes on the flat and pooled stepped spillways: $d_c/h = 0.82$, $Q = 0.038$ m^3/s, $Re = 2.90\times10^5$

(A) Step edge 9

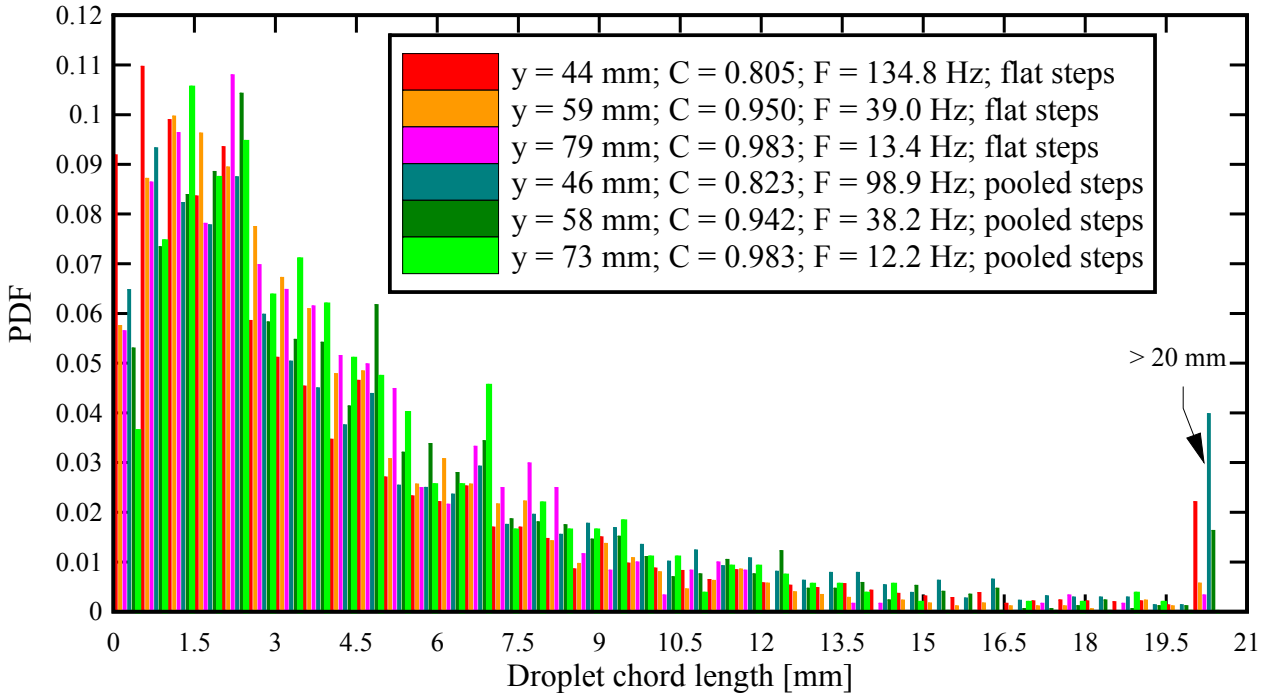

(B) Step edge 10

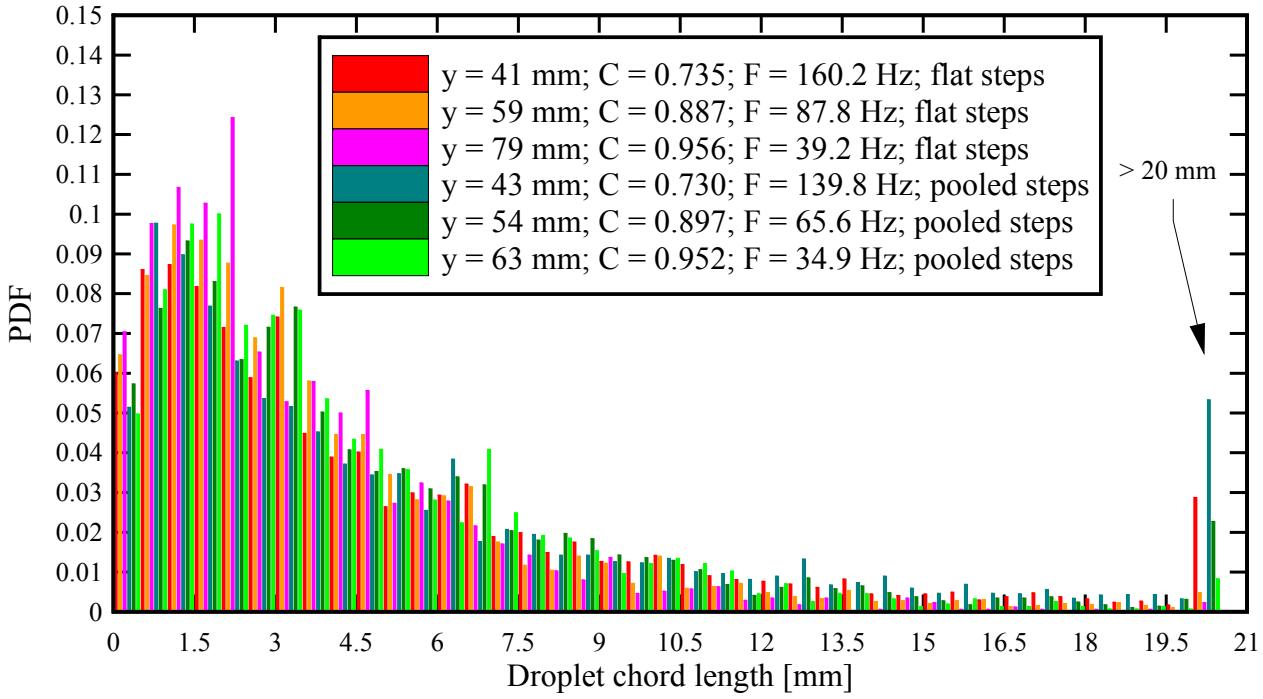

Fig. C-24 Comparison of probability distribution functions of water droplet chord sizes on the flat and pooled stepped spillways: $d_c/h = 0.96$, $Q = 0.049$ m^3/s, $Re = 3.71\times10^5$

(A) Step edge 9

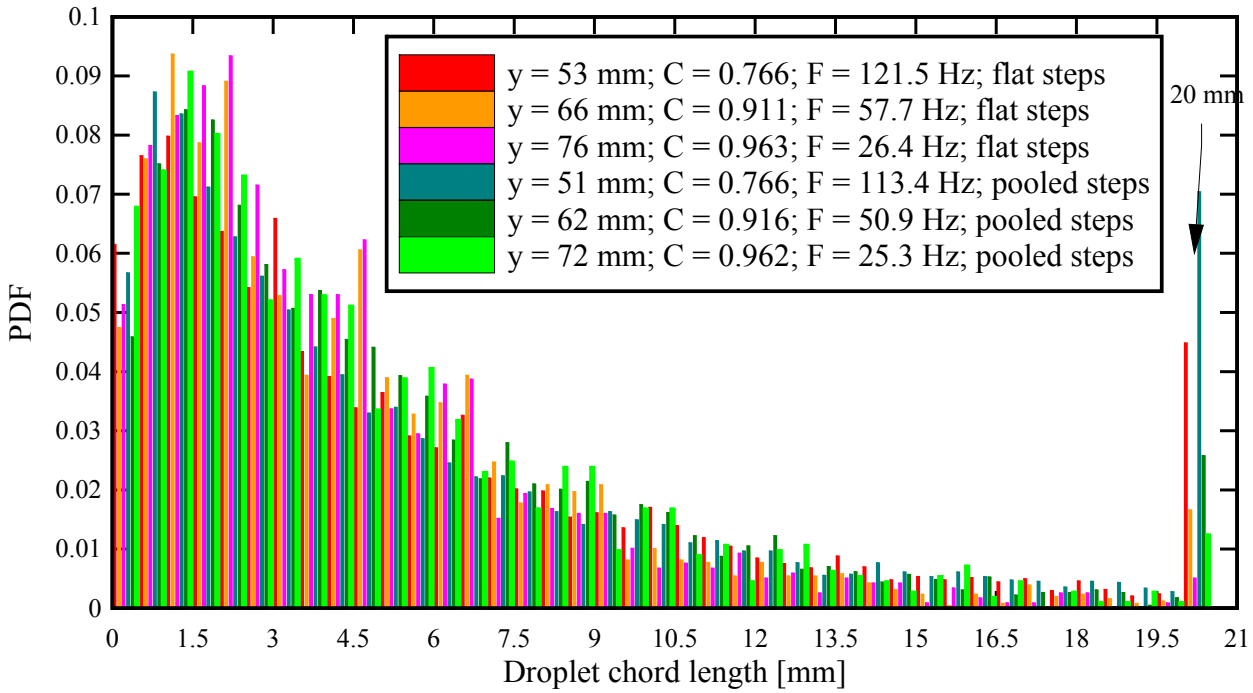

(B) Step edge 10

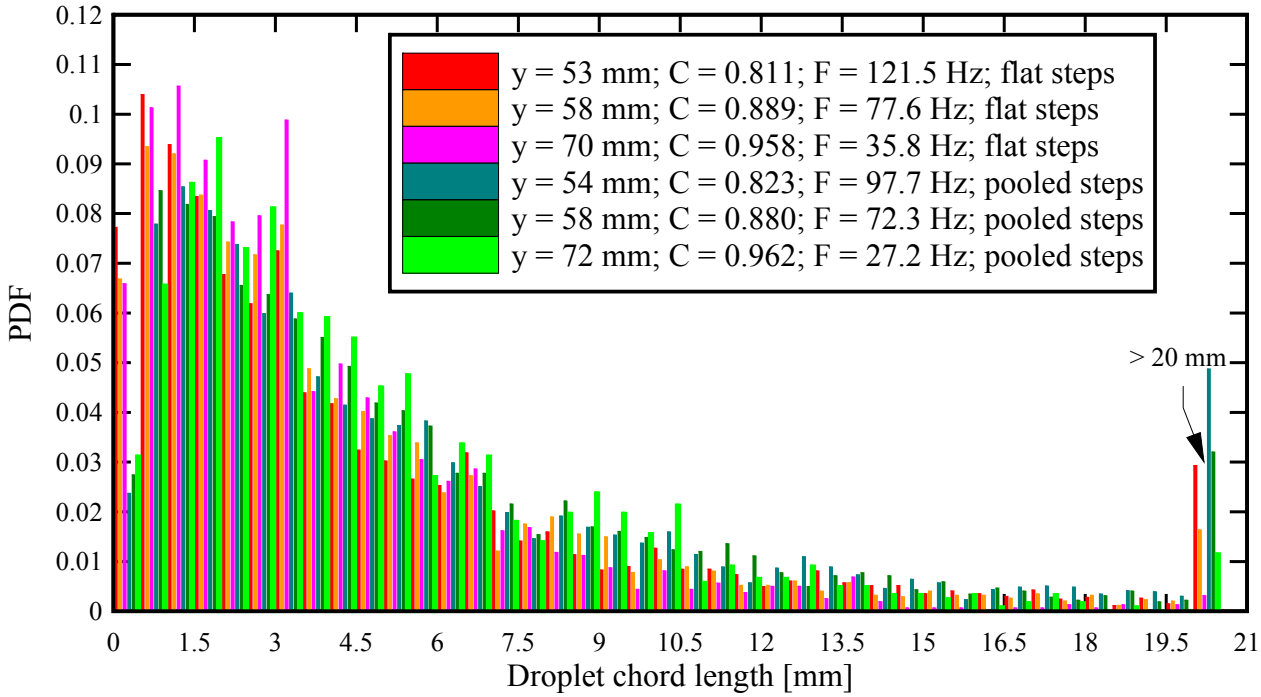

Fig. C-25 Comparison of probability distribution functions of water droplet chord sizes on the flat and pooled stepped spillways: $d_c/h = 1.29$, $Q = 0.075$ m^3/s, $Re = 5.73\times10^5$

(A) Step edge 9

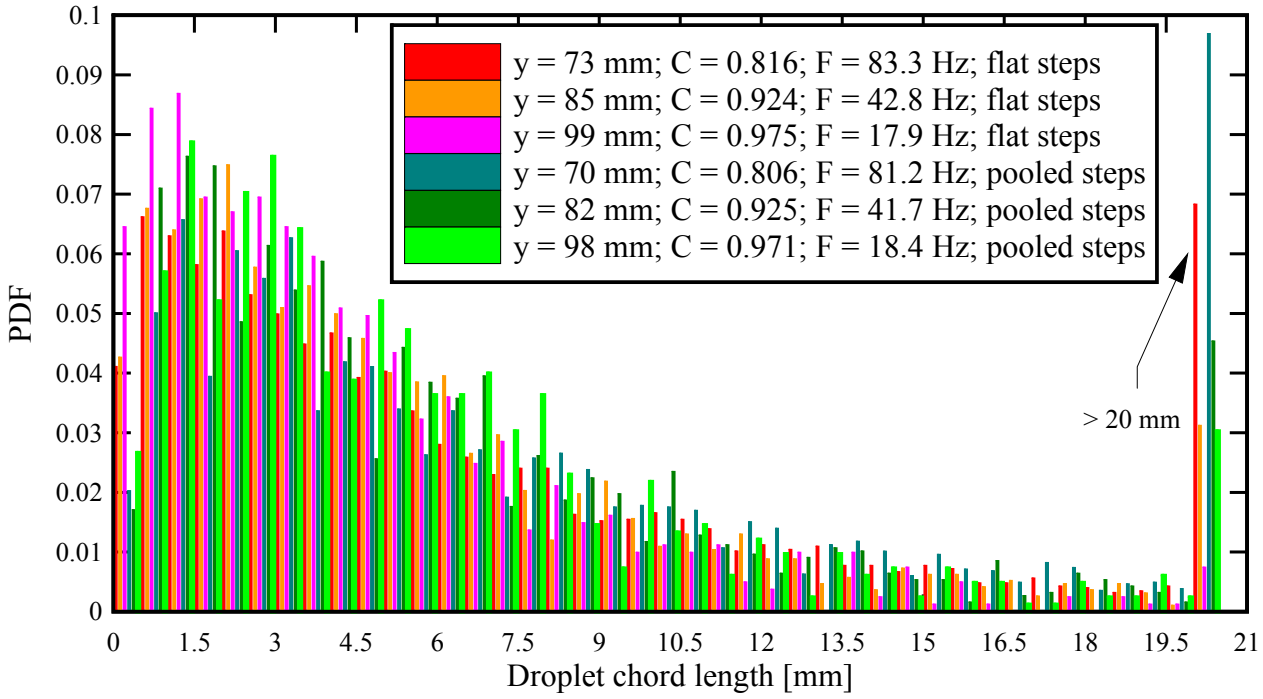

(B) Step edge 10

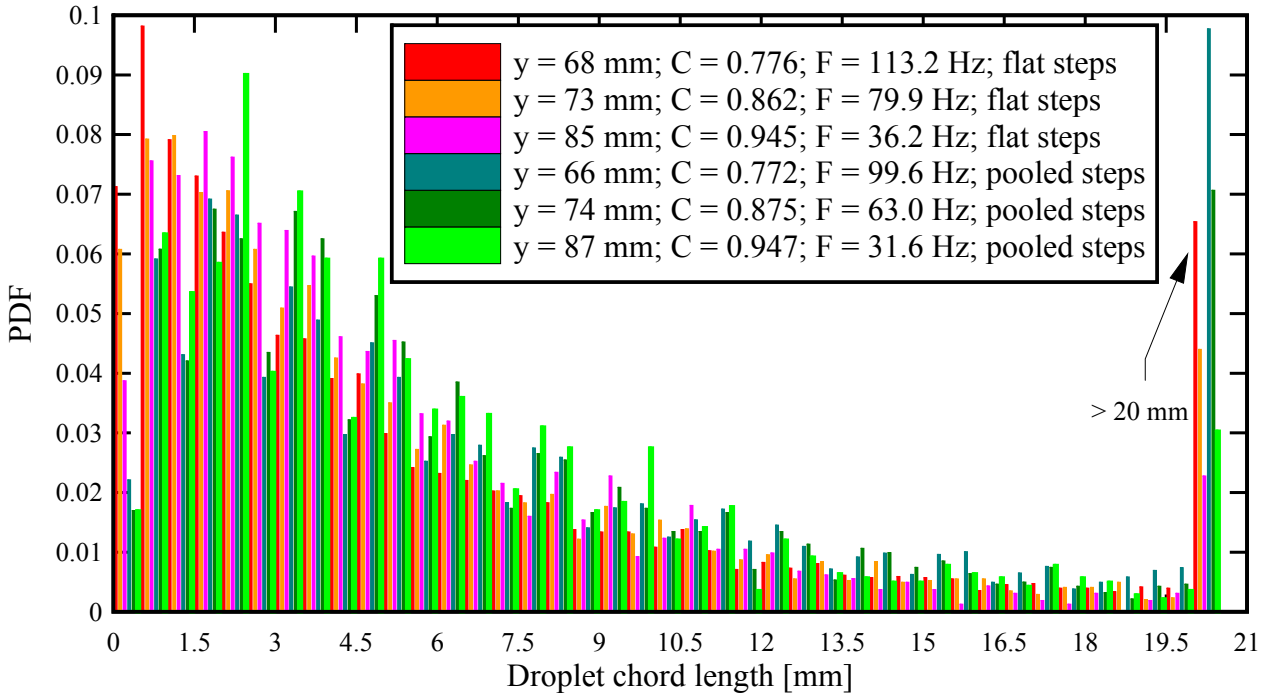

Fig. C-26 Comparison of probability distribution functions of water droplet chord sizes on the flat and pooled stepped spillways: $d_c/h = 1.52$, $Q = 0.097$ m^3/s, $Re = 7.39\times10^5$ - Step edge 10

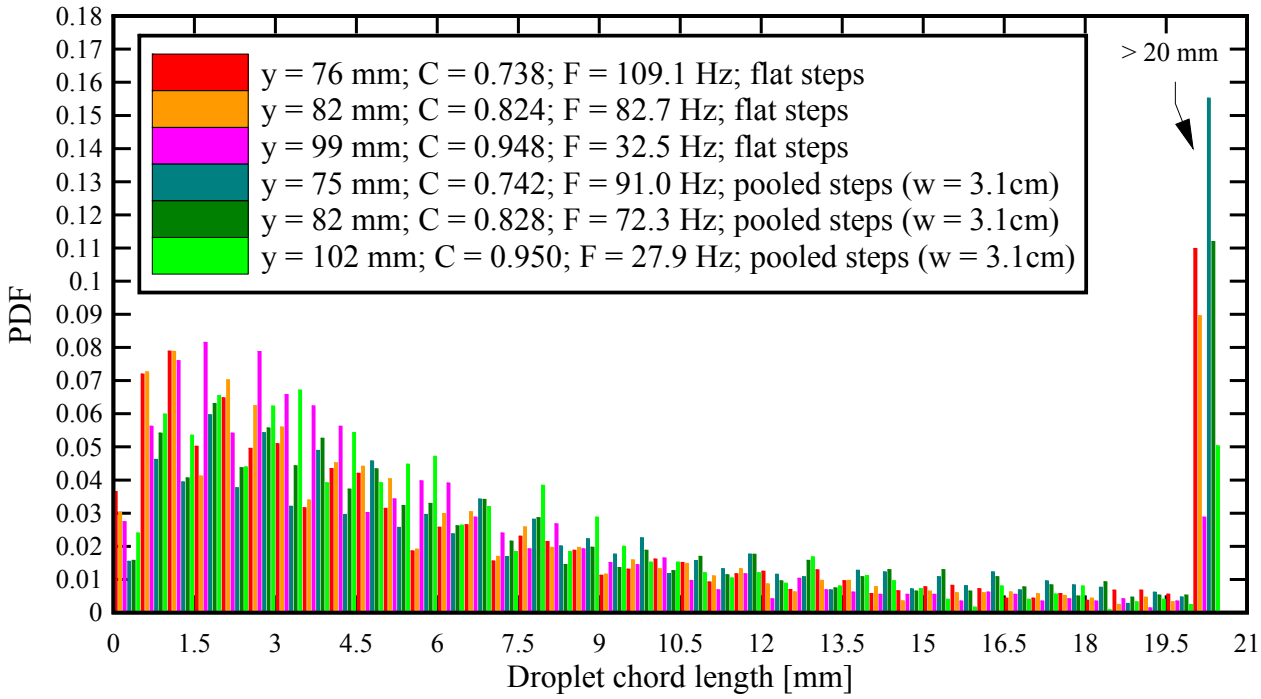

APPENDIX D –AIR-WATER FLOW PROPERTIES ON THE STEPPED SPILLWAYS WITH IN-LINE AND STAGGERED CONFIGURATIONS OF FLAT AND POOLED STEPS

D.1 PRESENTATION

In this appendix, the air-water flow properties for the stepped spillway with in-line and staggered configurations of flat and pooled steps for all experiments of the present study are presented. The results comprise the distributions of void fraction, bubble count rate, interfacial velocity and turbulence intensity at the three transverse measurement positions (z/W = 0.25, 0.5, 0.75) at each step edge. Figure D-1 shows a sketch of the stepped spillway configurations with in-line and staggered flat and pooled steps highlighting the measurement positions.

In section D.2, the results for the stepped spillway with in-line configuration are presented (Fig. D-2 to D-16) and section D.3 contains the air-water flow properties for the stepped spillway with staggered configuration of flat and pooled steps (Fig. D-17 to D-28). Furthermore some characteristic air-water flow parameters for all experiments on the in-line stepped spillway configuration and on the staggered stepped spillway configuration are presented in sections D.2 and D.3 respectively.

Notation

C	void fraction defined as the volume of air per unit volume of air and water;
C_{mean}	depth-average void fraction defined in terms of Y_{90}: $C_{mean} = 1 - d/Y_{90}$;
D_H	hydraulic diameter (m);
d	equivalent clear water flow depth (m);
d_c	critical flow depth (m);
F	air bubble count rate (Hz) defined as the number of detected air bubbles per unit time;
F_{max}	maximum bubble count rate in a cross-section (Hz);
h	vertical step height (m);
l	horizontal step length (m);
l_w	pool weir length (m);
Q	water discharge (m^3/s);
q	water discharge per unit width (m^2/s);
q_{local}	local flow rate per unit width (m^2/s);
Re	Reynolds number defined in terms of the hydraulic diameter: $Re = \rho \times U \times D_H/\mu$;
Tu	turbulence intensity;
Tu_{max}	maximum turbulence intensity in a cross-section;
U_{local}	mean flow velocity (m/s): $U_{local} = q_{local}/d$;
V	interfacial velocity (m/s);
V_c	critical flow velocity (m/s);

V_{90}	characteristic interfacial velocity (m/s) where the void fraction is 90%;
W	channel width (m);
W_w	widths of the pooled and flat part in the staggered and in-line configurations of flat and pooled steps (m);
w	weir height in pooled stepped spillway configuration (m), also called pool height;
Y_{90}	characteristic depth (m) where the void fraction is 90%;
y	distance (m) measured normal to the invert (or channel bed);
z	transverse distance (m) in the channel;
μ	dynamic viscosity (Pa.s);
ρ	density (kg/m^3);
θ	angle between pseudo-bottom formed by the step edges and the horizontal;
Ø	probe sensor diameter (m).

Fig. D-1 – Sketch of stepped spillways with in-line and staggered configuration of flat and pooled steps (θ = 26.6°) and the three transverse measurement positions (z/W = 0.25, 0.5 and 0.75)

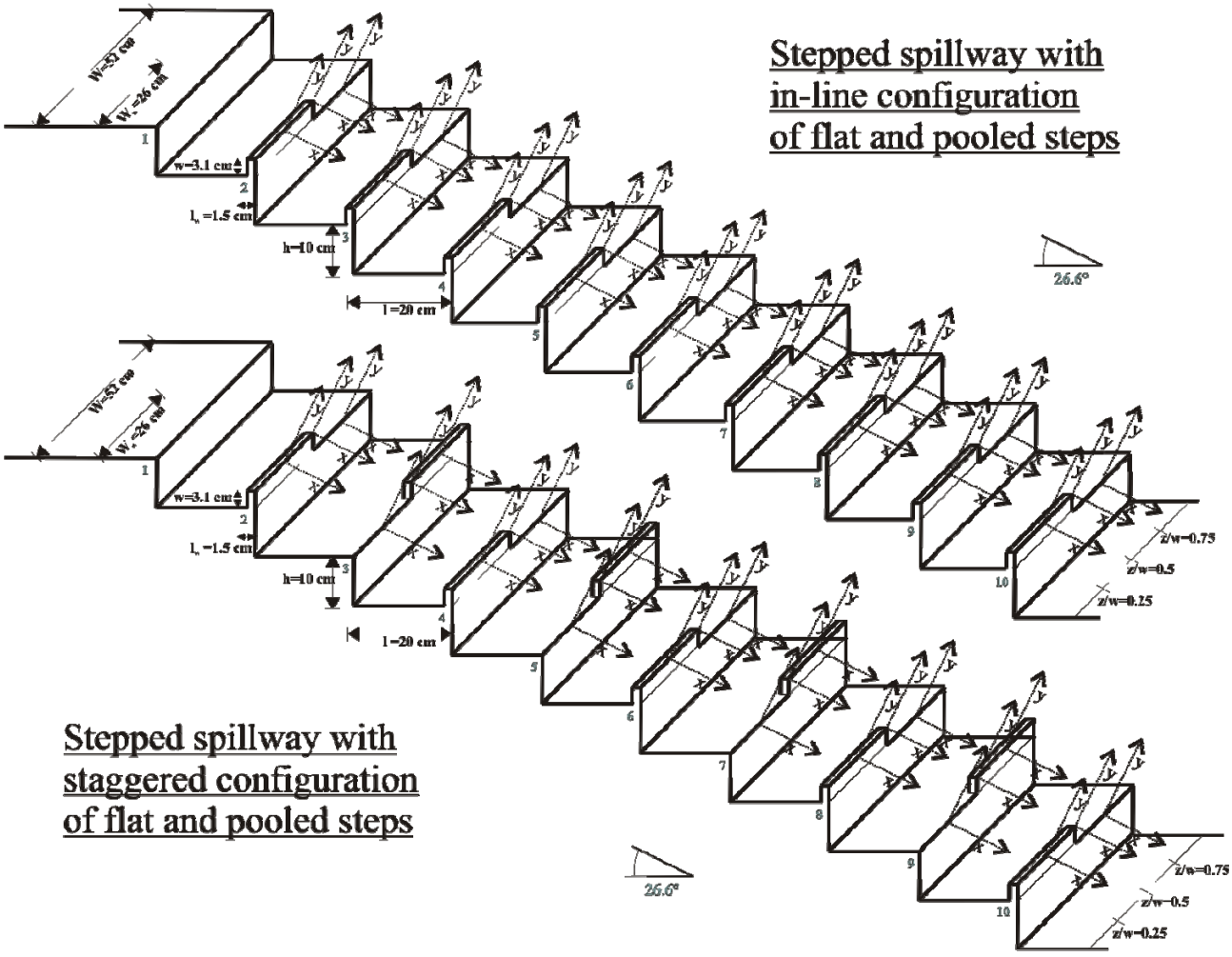

D.2 AIR-WATER FLOW PROPERTIES ON STEPPED SPILLWAY WITH IN-LINE CONFIGURATION OF FLAT AND POOLED STEPS

This section presents the air-water flow properties for the experiments with a double-tip conductivity probe on the stepped spillway with in-line configuration of flat and pooled steps. Table D-1 lists the experimental flow condition for the experiments including the flow regimes.

In section D.2.1, some characteristic air-water flow parameters are presented for all discharges. The parameters are shown for three transverse positions at each step edge and the transverse averaged values are also included (see Appendix F for definition and discussion). Section D.2.2 presents the air-water flow properties for all experiments on the stepped spillway with in-line configuration of flat and pooled steps including the void fraction C, the dimensionless bubble count rate $F \times d_c/V_c$, dimensionless interfacial velocity V/V_c and turbulence intensity Tu. All air-water flow distributions are presented in terms of the dimensionless distance perpendicular to the pseudo bottom formed by the flat step edges $(y+w)/d_c$.

Table D-1 – Air-water flow measurements with a double-tip conductivity probe (Ø = 0.25 mm) for the stepped spillway with in-line configuration of flat and pooled steps (θ = 26.6°)

Configuration (1)	d_c/h [-] (2)	Q [m^3/s] (3)	Re [-] (4)	Measurement at step edge (5)	Flow regime (6)
Stepped spillway with in-line configuration of flat and pooled steps	0.5	0.016	1.39×10^5	2-10	NA
	0.7	0.030	2.30×10^5	2-10	TRA
	1.15	0.063	4.85×10^5	4-10	SK
	1.45	0.090	6.87×10^5	5-10	SK
	1.7	0.113	8.72×10^5	7-10	SK

Notes: d_c: critical flow depth; h: vertical step height; Q: water discharge; Re: Reynolds number defined in terms of the hydraulic diameter; SK: skimming flow regime; TRA: transition flow regime; NA: nappe flow regime.

D.2.1 Longitudinal distributions of characteristic air-water flow parameters on the stepped spillway with in-line configuration of flat and pooled steps

Table D-2 – Mean air concentration C_{mean} measured at three transverse positions and transverse averaged calculation on the stepped spillway with in-line configuration of flat and pooled steps (θ = 26.6°); Measurements with a double-tip conductivity probe (Ø = 0.25 mm)

d_c/h [-] (1)	Q [m^3/s] (2)	Re [-] (3)	Step edge (4)	C_{mean} at z/W = 0.25 [-] (5)	C_{mean} at z/W = 0.5 [-] (6)	C_{mean} at z/W = 0.75 [-] (7)	C_{mean} (Transverse averaged) [-] (8)
0.50	0.016	1.39×10^5	2	0.419	0.540	0.108	0.333
			3	0.810	0.899	0.240	0.619
			4	0.581	0.609	0.408	0.523
			5	0.635	0.675	0.465	0.581
			6	0.502	0.747	0.419	0.532
			7	0.495	0.620	0.430	0.502
			8	0.471	0.646	0.460	0.511
			9	0.480	0.622	0.403	0.487
			10	0.508	0.700	0.513	0.558
0.7	0.030	2.30×10^5	2	0.294	0.212	0.098	0.200
			3	0.639	0.720	0.156	0.478
			4	0.606	0.687	0.267	0.499
			5	0.709	0.654	0.460	0.602
			6	0.567	0.563	0.345	0.483
			7	0.565	0.554	0.354	0.483
			8	0.571	0.612	0.357	0.501
			9	0.565	0.573	0.307	0.470
			10	0.605	0.661	0.415	0.548
1.15	0.063	4.85×10^5	4	0.303	0.246	0.120	0.220
			5	0.408	0.331	0.166	0.298
			6	0.431	0.395	0.200	0.335
			7	0.468	0.328	0.198	0.332
			8	0.457	0.355	0.189	0.331
			9	0.436	0.346	0.180	0.318
			10	0.490	0.397	0.221	0.366
1.45	0.090	6.87×10^5	5	0.187	0.167	0.104	0.151
			6	0.222	0.245	0.125	0.191
			7	0.326	0.273	0.153	0.248
			8	0.341	0.346	0.151	0.271
			9	0.382	0.307	0.170	0.284
			10	0.424	0.314	0.179	0.305
1.70	0.113	8.72×10^5	7	0.177	0.168	0.124	0.155
			8	0.268	0.239	0.122	0.206
			9	0.322	0.267	0.143	0.241
			10	0.357	0.293	0.183	0.276

Notes: d_c: critical flow depth; h: vertical step height; Q: water discharge; Re: Reynolds number defined in terms of the hydraulic diameter; C_{mean}: mean air concentration; z/W = 0.25: pooled stepped side; z/W = 0.75: flat stepped side; Transverse averaging method defined in Appendix F.

Table D-3 – Maximum bubble count rate F_{max} measured at three transverse positions and transverse averaged calculation on the stepped spillway with in-line configuration of flat and pooled steps (θ = 26.6°); Measurements with a double-tip conductivity probe (Ø = 0.25 mm)

d_c/h [-] (1)	Q [m^3/s] (2)	Re [-] (3)	Step edge (4)	F_{max} at z/W = 0.25 [Hz] (5)	F_{max} at z/W = 0.5 [Hz] (6)	F_{max} at z/W = 0.75 [Hz] (7)	F_{max} (Transverse averaged) [Hz] (8)
0.50	0.016	1.39×10^5	2	103.9	35.2	20.0	55.3
			3	89.4	19.1	27.4	48.6
			4	43.7	76.5	97.7	72.2
			5	20.8	118.3	135.2	88.1
			6	29.6	88.4	162.3	94.1
			7	34.1	77.4	161.3	92.6
			8	103.9	81.8	204.6	136.1
			9	89.4	156.8	247.4	165.5
			10	43.7	172.5	207.4	137.3
0.7	0.030	2.30×10^5	2	36.8	23.0	8.8	22.9
			3	29.8	25.7	27.2	27.8
			4	96.6	87.0	58.9	80.1
			5	106.6	113.0	129.4	116.8
			6	96.6	127.9	174.5	133.6
			7	100.4	166.4	191.6	151.1
			8	93.4	177.9	217.9	161.2
			9	95.4	214.7	270.0	190.7
			10	102.0	196.6	253.3	182.4
1.15	0.063	4.85×10^5	4	69.0	21.7	12.6	36.0
			5	94.6	94.2	29.4	70.1
			6	142.1	127.6	53.4	105.2
			7	165.8	149.8	75.7	128.0
			8	202.8	149.4	89.4	146.9
			9	210.7	177.6	103.9	162.4
			10	222.8	176.2	118.9	172.2
1.45	0.090	6.87×10^5	5	32.1	19.6	12.3	21.6
			6	80.5	50.0	24.4	51.8
			7	117.7	90.7	34.1	79.6
			8	135.5	109.3	45.8	95.3
			9	173.0	127.0	60.4	119.3
			10	191.4	145.7	79.3	137.9
1.70	0.113	8.72×10^5	7	37.5	34.2	18.3	29.5
			8	67.6	61.5	29.7	51.9
			9	114.0	90.6	40.8	80.7
			10	150.7	113.7	73.7	112.6

Notes: d_c: critical flow depth; h: vertical step height; Q: water discharge; Re: Reynolds number defined in terms of the hydraulic diameter; F_{max}: maximum bubble count rate; z/W = 0.25: pooled stepped side; z/W = 0.75: flat stepped side; Transverse averaging method defined in Appendix F.

Table D-4 – Characteristic interfacial velocity V_{90} measured at three transverse positions and transverse averaged calculation on the stepped spillway with in-line configuration of flat and pooled steps (θ = 26.6°); Measurements with a double-tip conductivity probe (Ø = 0.25 mm)

d_c/h [-] (1)	Q [m^3/s] (2)	Re [-] (3)	Step edge (4)	V_{90} at z/W = 0.25 [m/s] (5)	V_{90} at z/W = 0.5 [m/s] (6)	V_{90} at z/W = 0.75 [m/s] (7)	V_{90} (Transverse averaged) [m/s] (8)
0.50	0.016	1.39×10^5	2	0.89	1.89	1.07	1.21
			3	1.64	1.83	2.01	1.83
			4	0.89	0.87	2.83	1.61
			5	1.79	1.92	2.18	1.97
			6	1.04	1.72	2.22	1.65
			7	0.90	1.38	2.20	1.51
			8	2.60	0.98	2.72	2.24
			9	0.96	2.20	3.04	2.05
			10	1.30	2.41	3.02	2.22
0.7	0.030	2.30×10^5	2	1.69	1.62	2.08	1.82
			3	1.96	2.01	2.23	2.07
			4	2.32	1.68	2.38	2.18
			5	2.04	2.05	2.32	2.15
			6	1.72	2.03	2.67	2.15
			7	1.80	2.23	2.82	2.29
			8	1.62	2.37	3.00	2.33
			9	1.40	2.54	3.27	2.39
			10	1.45	2.49	3.39	2.44
1.15	0.063	4.85×10^5	4	2.21	2.52	2.48	2.39
			5	2.54	2.71	2.82	2.69
			6	2.90	2.85	3.06	2.95
			7	2.76	3.16	3.27	3.05
			8	2.93	3.39	3.51	3.26
			9	3.04	3.56	3.69	3.41
			10	3.06	3.75	3.96	3.57
1.45	0.090	6.87×10^5	5	2.85	2.90	2.86	2.87
			6	3.13	3.35	3.27	3.24
			7	3.02	3.47	3.56	3.34
			8	3.43	3.73	3.79	3.64
			9	3.37	3.85	3.89	3.69
			10	3.60	3.95	4.19	3.91
1.70	0.113	8.72×10^5	7	3.52	3.60	3.60	3.57
			8	3.69	3.85	3.89	3.81
			9	3.89	4.07	4.00	3.98
			10	4.00	4.07	4.24	4.11

Notes: d_c: critical flow depth; h: vertical step height; Q: water discharge; Re: Reynolds number defined in terms of the hydraulic diameter; V_{90}: characteristic interfacial velocity where C = 90%; z/W = 0.25: pooled stepped side; z/W = 0.75: flat stepped side; Transverse averaging method defined in Appendix F.

Table D-5 – Local discharge per unit width q_{local} for measurement at three transverse positions and transverse averaged calculation on the stepped spillway with in-line configuration of flat and pooled steps (θ = 26.6°); Measurements with a double-tip conductivity probe (Ø = 0.25 mm)

d_c/h [-] (1)	Q [m^3/s] (2)	Re [-] (3)	Step edge (4)	q_{local} at z/W = 0.25 [m^2/s] (5)	q_{local} at z/W = 0.5 [m^2/s] (6)	q_{local} at z/W = 0.75 [m^2/s] (7)	q_{local} (Transverse averaged) [m^2/s] (11)
0.50	0.016	1.39×10^5	2	0.1500	0.0662	0.0255	0.0824
			3	0.0334	0.0189	0.0448	0.0341
			4	0.0301	0.0521	0.0664	0.0492
			5	0.0185	0.0209	0.0524	0.0318
			6	0.0352	0.0150	0.0699	0.0432
			7	0.0190	0.0180	0.0735	0.0392
			8	0.0232	0.0208	0.0764	0.0426
			9	0.0208	0.0186	0.0698	0.0386
			10	0.0146	0.0199	0.0730	0.0378
0.7	0.030	2.30×10^5	2	0.0576	0.0498	0.0177	0.0407
			3	0.0625	0.0381	0.0834	0.0642
			4	0.0539	0.0448	0.0905	0.0654
			5	0.0412	0.0411	0.1003	0.0633
			6	0.0429	0.0399	0.1053	0.0656
			7	0.0371	0.0377	0.1106	0.0648
			8	0.0349	0.0296	0.1134	0.0630
			9	0.0366	0.0316	0.1223	0.0675
			10	0.0359	0.0363	0.1155	0.0659
1.15	0.063	4.85×10^5	4	0.0951	0.0934	0.1661	0.1213
			5	0.1032	0.0862	0.1730	0.1251
			6	0.0858	0.1163	0.1754	0.1270
			7	0.0823	0.1095	0.1947	0.1313
			8	0.0760	0.1011	0.1971	0.1277
			9	0.0741	0.0930	0.2022	0.1269
			10	0.0747	0.1050	0.1828	0.1228
1.45	0.090	6.87×10^5	5	0.1452	0.1387	0.0626	0.1126
			6	0.1475	0.1458	0.2240	0.1758
			7	0.1403	0.1479	0.2225	0.1730
			8	0.1395	0.1459	0.2326	0.1760
			9	0.1295	0.1485	0.2416	0.1763
			10	0.1360	0.1545	0.2369	0.1785
1.70	0.113	8.72×10^5	7	0.1773	0.1584	0.1676	0.1689
			8	0.1799	0.1720	0.2509	0.2046
			9	0.1883	0.1781	0.2512	0.2093
			10	0.1952	0.1883	0.2971	0.2317

Notes: d_c: critical flow depth; h: vertical step height; Q: water discharge; Re: Reynolds number defined in terms of the hydraulic diameter; q_{local}: local discharge per unit width; z/W = 0.25: pooled stepped side; z/W = 0.75: flat stepped side; Transverse averaging method defined in Appendix F.

Table D-6 – Local mean flow velocity U_{local} for measurement at three transverse positions and transverse averaged calculation on the stepped spillway with in-line configuration of flat and pooled steps (θ = 26.6°); Measurements with a double-tip conductivity probe (Ø = 0.25 mm)

d_c/h [-] (1)	Q [m^3/s] (2)	Re [-] (3)	Step edge (4)	U_{local} at z/W = 0.25 [m/s] (5)	U_{local} at z/W = 0.5 [m/s] (6)	U_{local} at z/W = 0.75 [m/s] (7)	U_{local} (Transverse averaged) [m/s] (11)
0.50	0.016	1.39×10^5	2	2.06	1.75	1.15	1.64
			3	1.61	1.57	1.99	1.74
			4	1.01	1.32	2.24	1.55
			5	1.40	1.77	2.18	1.79
			6	1.16	1.66	2.48	1.78
			7	0.83	1.40	2.22	1.49
			8	1.02	1.36	2.63	1.71
			9	0.97	2.13	2.93	2.00
			10	0.83	2.42	2.61	1.90
0.7	0.030	2.30×10^5	2	1.68	2.06	0.50	1.33
			3	1.93	1.90	2.38	2.09
			4	2.05	1.96	2.26	2.11
			5	1.91	1.91	2.54	2.15
			6	1.69	1.98	2.75	2.16
			7	1.69	2.23	2.84	2.26
			8	1.51	2.46	2.88	2.26
			9	1.52	2.60	3.16	2.41
			10	1.56	2.60	2.97	2.35
1.15	0.063	4.85×10^5	4	2.70	2.33	2.29	2.45
			5	2.59	2.79	2.59	2.64
			6	2.91	2.84	2.75	2.83
			7	2.77	3.02	3.02	2.93
			8	2.78	3.21	3.06	2.99
			9	2.87	3.46	3.27	3.17
			10	2.86	3.40	2.96	3.03
1.45	0.090	6.87×10^5	5	2.74	3.00	0.77	2.07
			6	3.07	3.06	2.80	2.97
			7	3.29	3.19	2.95	3.14
			8	3.27	3.17	3.08	3.17
			9	3.42	3.38	3.34	3.38
			10	3.31	3.37	3.18	3.28
1.70	0.113	8.72×10^5	7	3.33	2.76	1.92	2.66
			8	3.45	3.36	2.85	3.20
			9	3.53	3.42	3.00	3.30
			10	3.67	3.53	3.48	3.56

Notes: d_c: critical flow depth; h: vertical step height; Q: water discharge; Re: Reynolds number defined in terms of the hydraulic diameter; U_{local}: local velocity per unit width; z/W = 0.25: pooled stepped side; z/W = 0.75: flat stepped side; Transverse averaging method defined in Appendix F

Table D-7 – Characteristic flow depth Y_{90} for measurement at three transverse positions and transverse averaged calculation on the stepped spillway with in-line configuration of flat and pooled steps (θ = 26.6°); Measurements with a double-tip conductivity probe (Ø = 0.25 mm)

d_c/h [-] (1)	Q [m^3/s] (2)	Re [-] (3)	Step edge (4)	Y_{90} at z/W = 0.25 [m] (5)	Y_{90} at z/W = 0.5 [m] (6)	Y_{90} at z/W = 0.75 [m] (7)	Y_{90} (Transverse averaged) [m] (11)
0.50	0.016	1.39×10^5	2	0.1251	0.0821	0.0250	0.0768
			3	0.1091	0.1185	0.0297	0.0817
			4	0.0713	0.1005	0.0501	0.0707
			5	0.0362	0.0362	0.0449	0.0395
			6	0.0609	0.0356	0.0484	0.0499
			7	0.0453	0.0340	0.0581	0.0473
			8	0.0430	0.0431	0.0538	0.0471
			9	0.0413	0.0231	0.0400	0.0363
			10	0.0358	0.0273	0.0573	0.0417
0.7	0.030	2.30×10^5	2	0.0487	0.0307	0.0394	0.0407
			3	0.0894	0.0715	0.0415	0.0670
			4	0.0668	0.0730	0.0545	0.0637
			5	0.0744	0.0622	0.0733	0.0709
			6	0.0587	0.0461	0.0584	0.0554
			7	0.0506	0.0378	0.0603	0.0510
			8	0.0538	0.0310	0.0613	0.0509
			9	0.0552	0.0284	0.0558	0.0487
			10	0.0582	0.0412	0.0665	0.0571
1.15	0.063	4.85×10^5	4	0.0504	0.0531	0.0823	0.0630
			5	0.0672	0.0462	0.0801	0.0668
			6	0.0517	0.0677	0.0798	0.0662
			7	0.0558	0.0539	0.0805	0.0646
			8	0.0504	0.0487	0.0795	0.0609
			9	0.0459	0.0410	0.0753	0.0557
			10	0.0512	0.0512	0.0792	0.0617
1.45	0.090	6.87×10^5	5	0.0653	0.0556	0.0907	0.0724
			6	0.0617	0.0631	0.0914	0.0732
			7	0.0632	0.0639	0.0891	0.0731
			8	0.0647	0.0704	0.0889	0.0752
			9	0.0613	0.0633	0.0871	0.0715
			10	0.0712	0.0668	0.0907	0.0774
1.70	0.113	8.72×10^5	7	0.0647	0.0689	0.0998	0.0789
			8	0.0712	0.0673	0.1003	0.0811
			9	0.0787	0.0710	0.0975	0.0838
			10	0.0828	0.0755	0.1047	0.0892

Notes: d_c: critical flow depth; h: vertical step height; Q: water discharge; Re: Reynolds number defined in terms of the hydraulic diameter; Y_{90}: characteristic flow depth where C = 90%; z/W = 0.25: pooled stepped side; z/W = 0.75: flat stepped side; Transverse averaging method defined in Appendix F.

Table D-8 – Maximum turbulence intensity Tu_{max} for measurement at three transverse positions and transverse averaged calculation on the stepped spillway with in-line configuration of flat and pooled steps (θ = 26.6°); Measurements with a double-tip conductivity probe (Ø = 0.25 mm)

d_c/h [-] (1)	Q [m^3/s] (2)	Re [-] (3)	Step edge (4)	Tu_{max} at z/W = 0.25 [-] (5)	Tu_{max} at z/W = 0.5 [-] (6)	Tu_{max} at z/W = 0.75 [-] (7)	Tu_{max} (Transverse averaged) [-] (11)
0.50	0.016	1.39×10^5	2	6.10	4.77	2.31	4.35
			3	4.28	2.86	0.85	2.64
			4	3.57	2.65	1.74	2.65
			5	2.64	1.57	1.02	1.77
			6	3.24	2.33	1.27	2.27
			7	2.64	1.88	1.33	1.96
			8	5.50	2.65	0.94	3.08
			9	2.71	1.63	1.64	2.04
			10	2.94	1.45	1.37	1.98
0.7	0.030	2.30×10^5	2	8.46	5.99	5.16	6.61
			3	5.34	5.15	2.74	4.32
			4	6.22	6.02	2.40	4.74
			5	4.13	1.90	0.99	2.40
			6	2.47	1.94	1.59	2.01
			7	3.23	2.35	1.35	2.31
			8	3.35	1.94	1.21	2.20
			9	2.76	1.90	2.04	2.28
			10	3.65	1.68	1.24	2.25
1.15	0.063	4.85×10^5	4	4.10	1.82	1.69	2.63
			5	1.74	2.21	2.33	2.08
			6	1.40	1.05	1.82	1.47
			7	1.54	1.60	1.71	1.62
			8	1.41	1.45	1.29	1.38
			9	1.86	2.20	2.12	2.04
			10	1.34	1.60	1.48	1.46
1.45	0.090	6.87×10^5	5	2.71	2.72	1.86	2.39
			6	2.39	1.47	1.63	1.88
			7	1.69	1.64	1.74	1.70
			8	1.07	1.19	1.65	1.32
			9	1.52	1.75	1.70	1.65
			10	1.59	1.39	1.88	1.65
1.70	0.113	8.72×10^5	7	1.86	1.42	1.75	1.71
			8	1.96	1.82	1.85	1.88
			9	1.25	1.59	2.00	1.62
			10	1.06	1.56	1.41	1.32

Notes: d_c: critical flow depth; h: vertical step height; Q: water discharge; Re: Reynolds number defined in terms of the hydraulic diameter; Tu_{max}: maximum turbulence intensity in a cross-section; z/W = 0.25: pooled stepped side; z/W = 0.75: flat stepped side; Transverse averaging method defined in Appendix F.

D.2.2 Air-water flow properties on the stepped spillway with in-line configuration of flat and pooled steps

Table D-9 summarises the presented data in this section and it indicates the respective position of the graphs in Figures D-2 to D-16. All air-water flow distributions are presented in terms of the dimensionless distance perpendicular to the pseudo bottom formed by the step edges $(y+w)/d_c$. The pseudo bottom formed by the flat step edges was defined as the zero position, i.e. y = 0.

Table D-9 - Summary of the air-water flow properties on the stepped spillway with in-line configuration of flat and pooled steps and positioning in the following figures (Fig. D-2 to D-16); Illustration as functions of $(y+w)/d_c$

Void fraction C	Dimensionless bubble count rate $F \times d_c/V_c$
Dimensionless interfacial velocity V/V_c	Turbulence intensity Tu

Notes: y: distance normal to the pseudo bottom; C: void fraction; F: bubble count rate; d_c: critical flow depth; V_c: critical flow velocity; V: interfacial velocity; Tu: turbulence intensity.

Fig. D-2 – Air-water flow properties on the stepped spillway with in-line configuration of flat and pooled steps (θ = 26.6°) as functions of $(y+w)/d_c$ – Nappe flows: $d_c/h = 0.50$, Q = 0.016 m^3/s, Re = 1.39×10^5; Step edges 2-10; Transverse position z/W = 0.25 (pooled steps side)

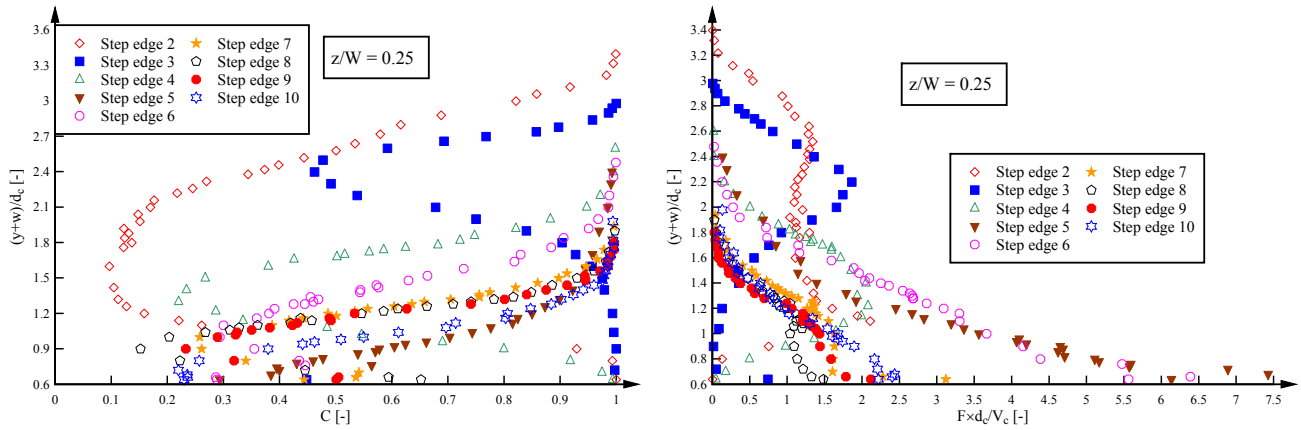

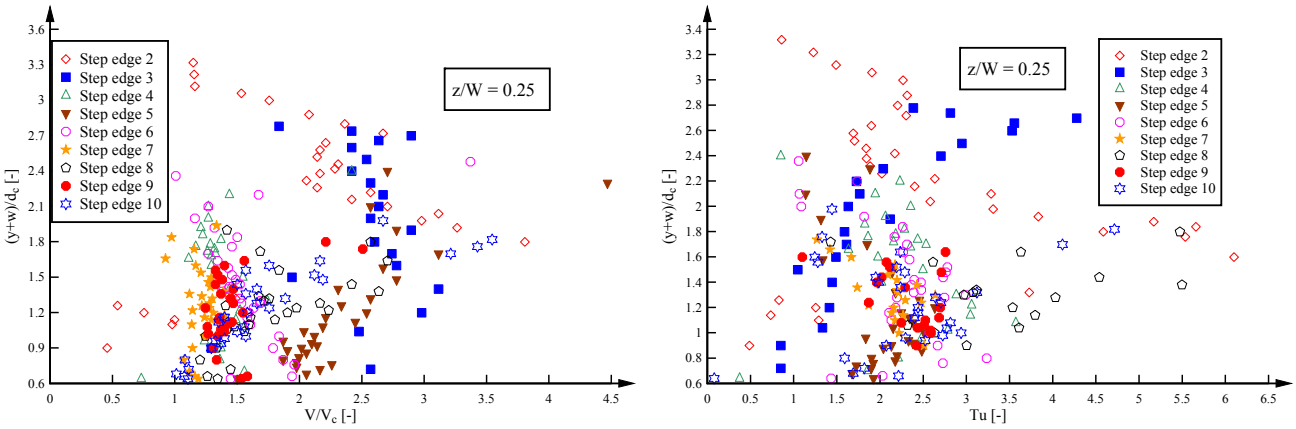

Fig. D-3 – Air-water flow properties on the stepped spillway with in-line configuration of flat and pooled steps (θ = 26.6°) as functions of $(y+w)/d_c$ – Nappe flows: $d_c/h = 0.50$, $Q = 0.016$ m^3/s, $Re = 1.39\times10^5$; Step edges 2-10; Transverse position z/W = 0.5 (channel centreline)

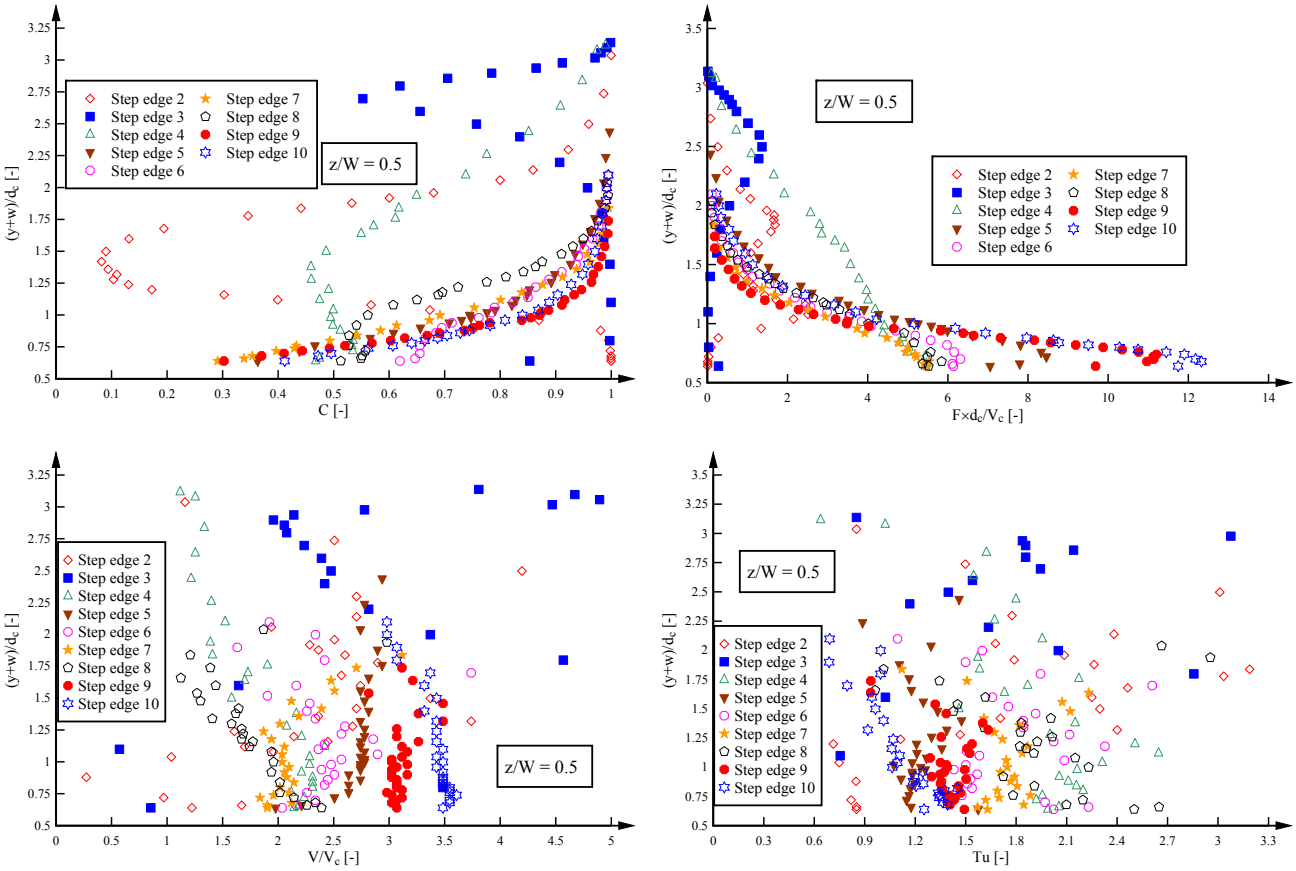

Fig. D-4 – Air-water flow properties on the stepped spillway with in-line configuration of flat and pooled steps (θ = 26.6°) as functions of $(y+w)/d_c$ – Nappe flows: $d_c/h = 0.50$, $Q = 0.016$ m^3/s, $Re = 1.39\times10^5$; Step edges 2-10; Transverse position z/W = 0.75 (flat steps side)

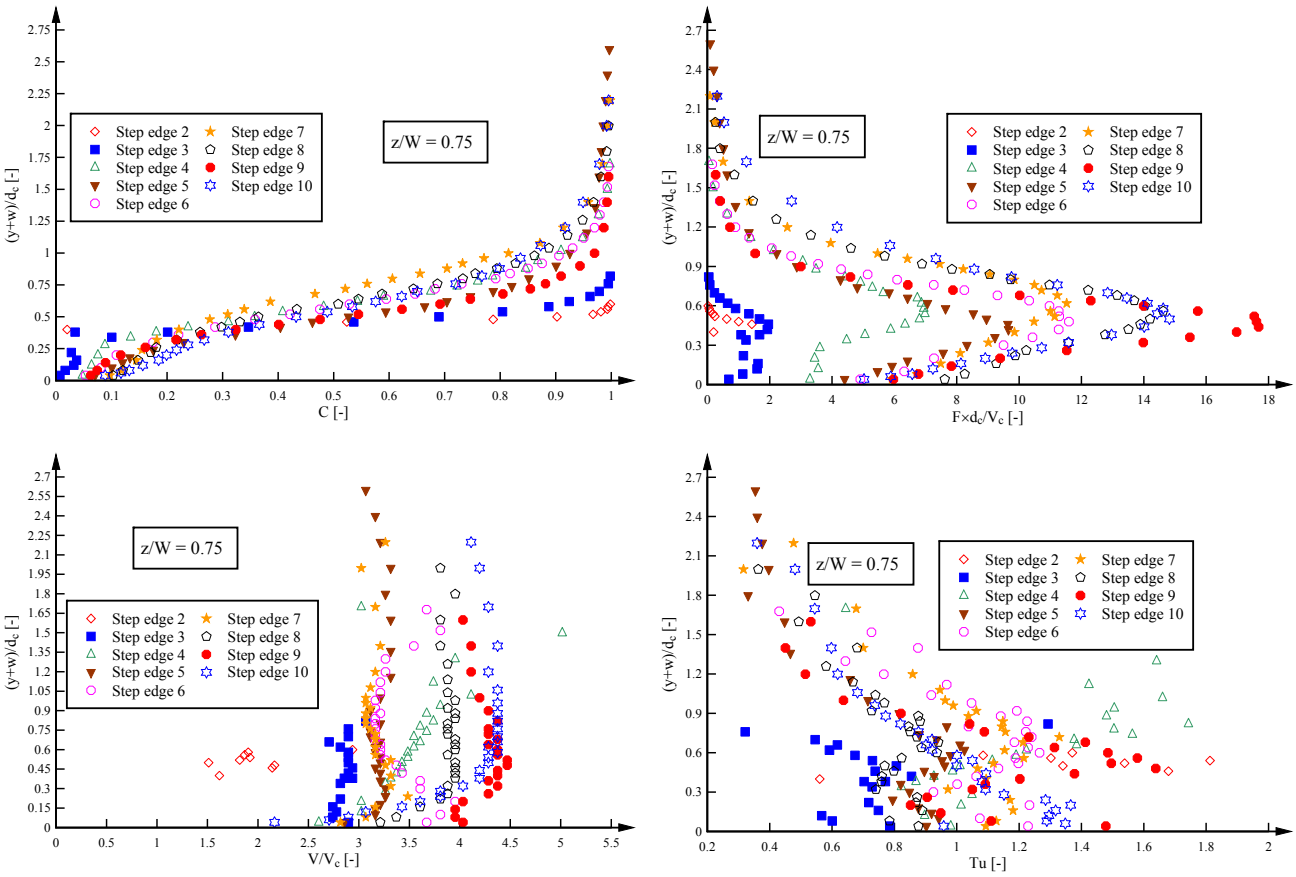

Fig. D-5 – Air-water flow properties on the stepped spillway with in-line configuration of flat and pooled steps (θ = 26.6°) as functions of $(y+w)/d_c$ – Transition flows: $d_c/h = 0.70$, $Q = 0.030$ m^3/s, $Re = 2.30\times10^5$; Step edges 2-10; Transverse position z/W = 0.25 (pooled steps side)

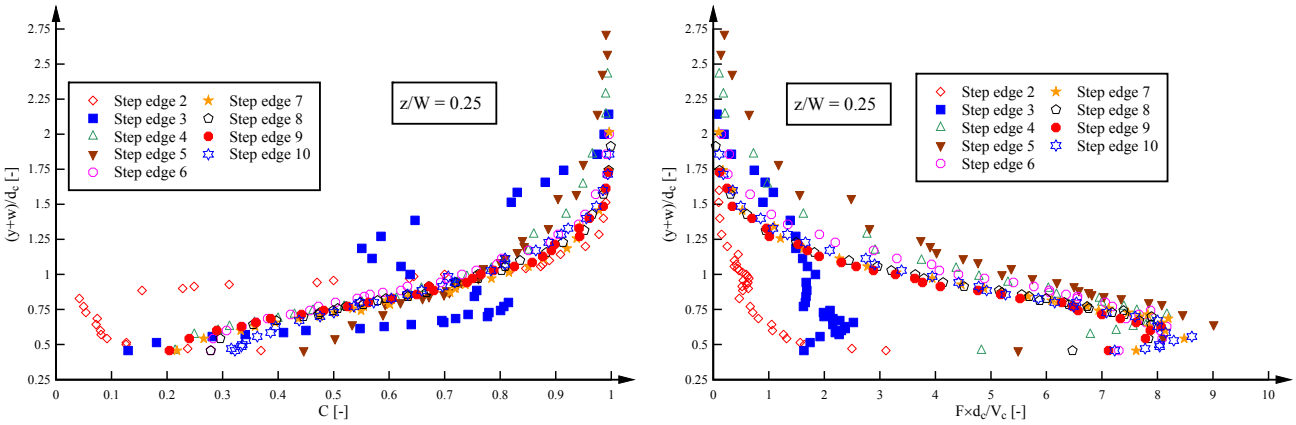

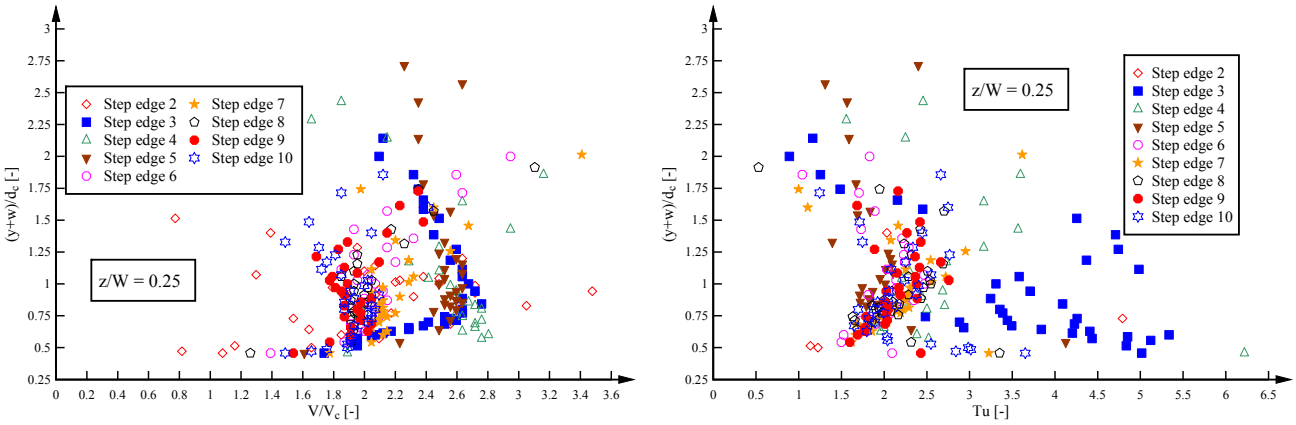

Fig. D-6 – Air-water flow properties on the stepped spillway with in-line configuration of flat and pooled steps (θ = 26.6°) as functions of $(y+w)/d_c$ – Transition flows: $d_c/h = 0.70$, $Q = 0.030$ m^3/s, $Re = 2.30 \times 10^5$; Step edges 2-10; Transverse position z/W = 0.5 (channel centreline)

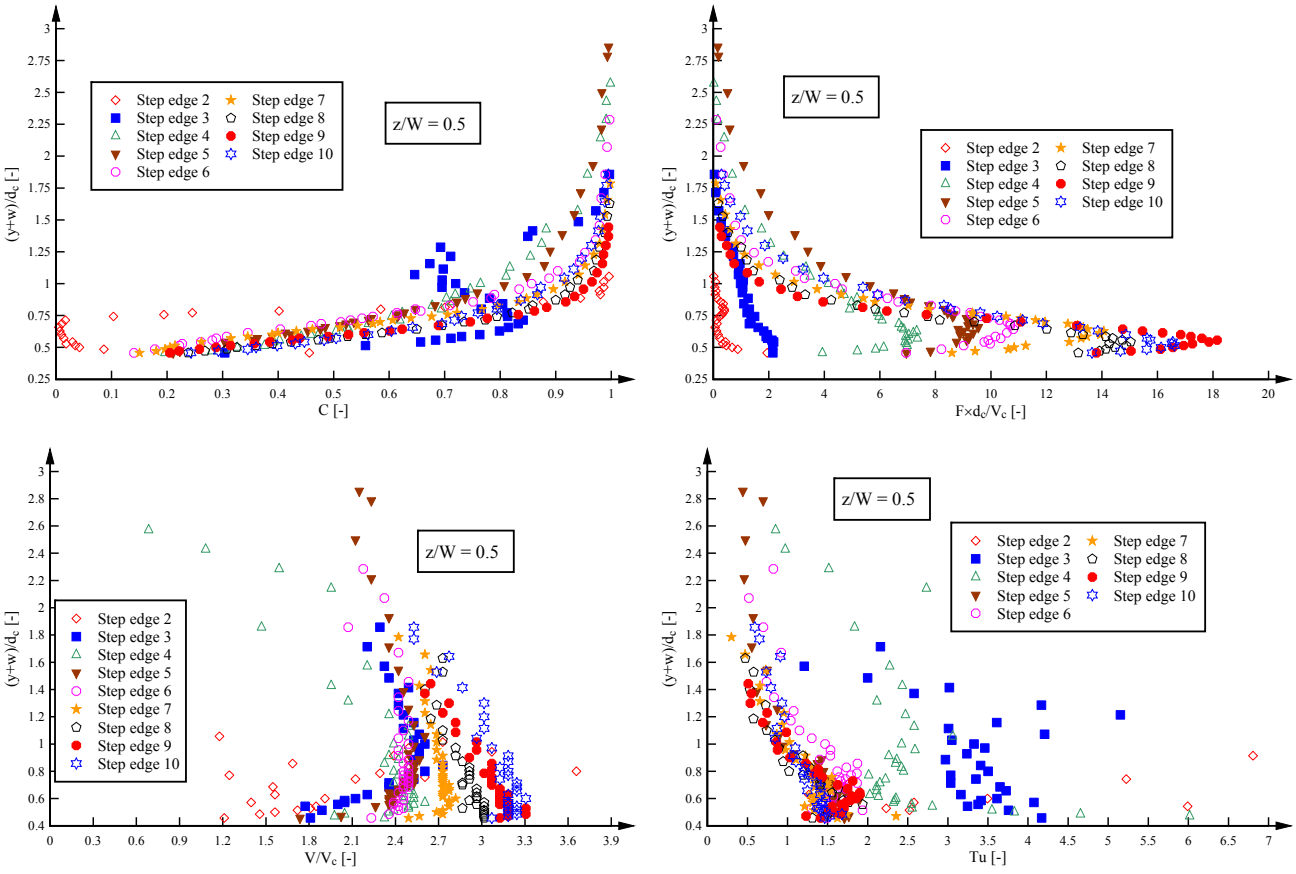

Fig. D-7 – Air-water flow properties on the stepped spillway with in-line configuration of flat and pooled steps (θ = 26.6°) as functions of $(y+w)/d_c$ – Transition flows: $d_c/h = 0.70$, $Q = 0.030$ m^3/s, $Re = 2.30\times10^5$; Step edges 2-10; Transverse position z/W = 0.75 (flat steps side)

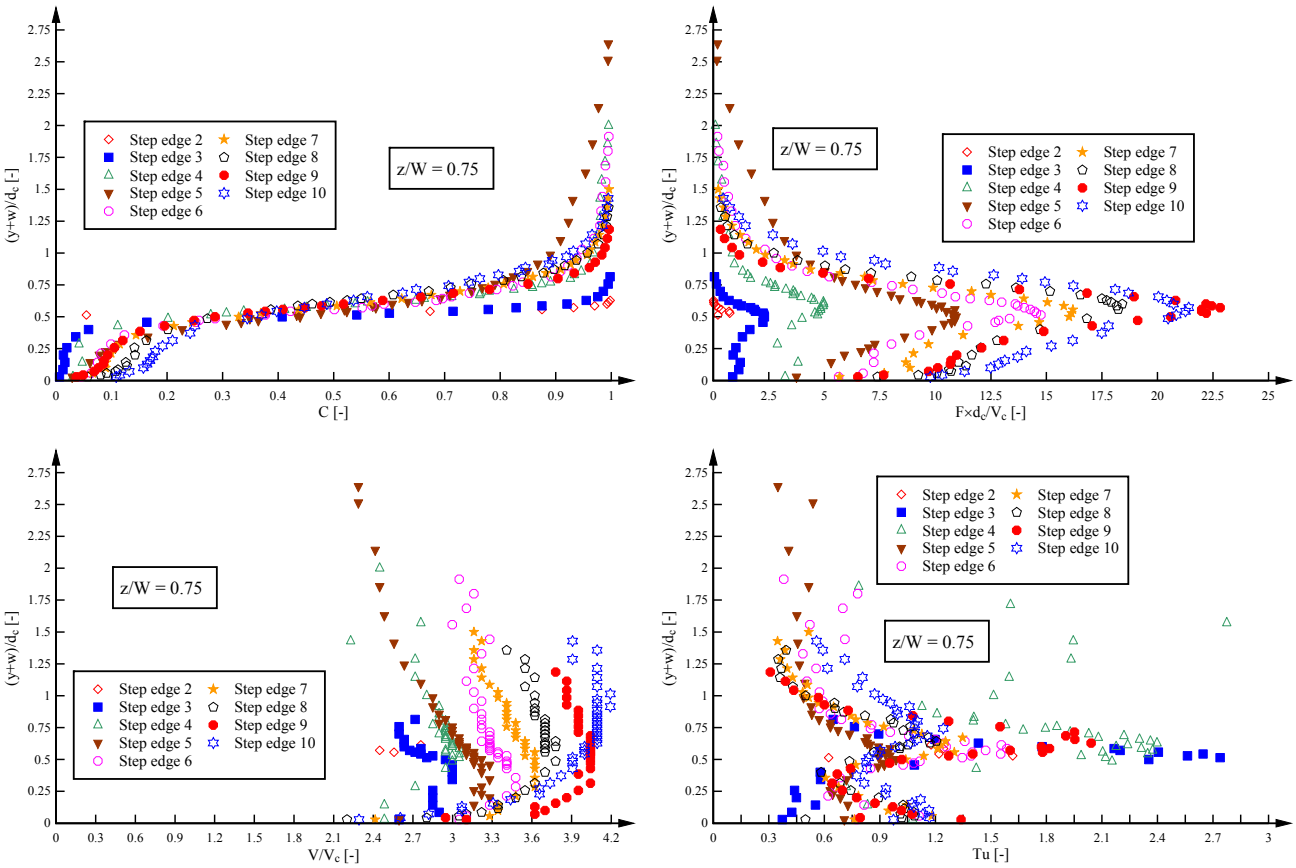

Fig. D-8 – Air-water flow properties on the stepped spillway with in-line configuration of flat and pooled steps (θ = 26.6°) as functions of $(y+w)/d_c$ – Skimming flows: $d_c/h = 1.15$, $Q = 0.063$ m^3/s, $Re = 4.85\times10^5$; Step edges 4-10; Transverse position z/W = 0.25 (pooled steps side)

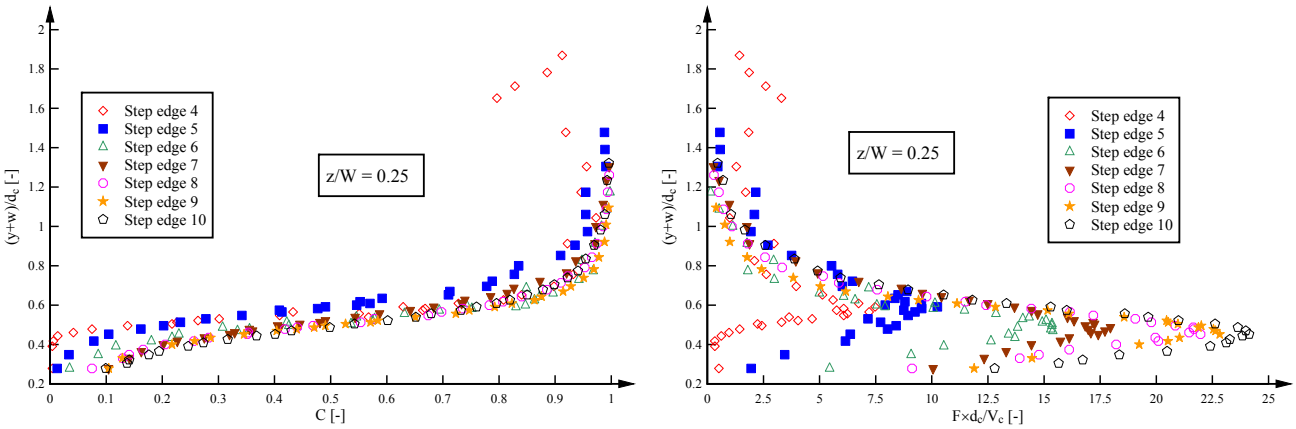

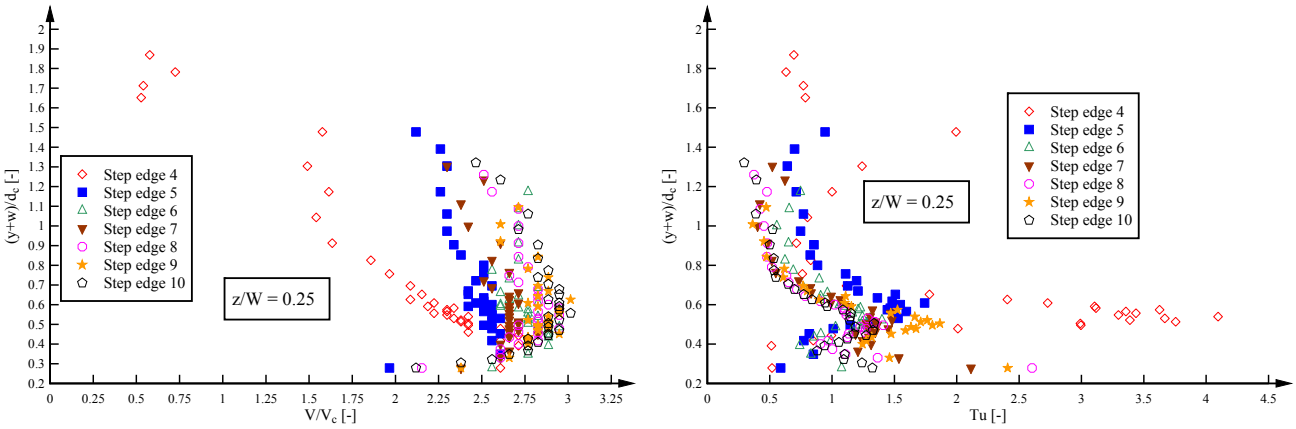

Fig. D-9 – Air-water flow properties on the stepped spillway with in-line configuration of flat and pooled steps (θ = 26.6°) as functions of $(y+w)/d_c$ – Skimming flows: $d_c/h = 1.15$, $Q = 0.063$ m^3/s, $Re = 4.85\times10^5$; Step edges 4-10; Transverse position z/W = 0.5 (channel centreline)

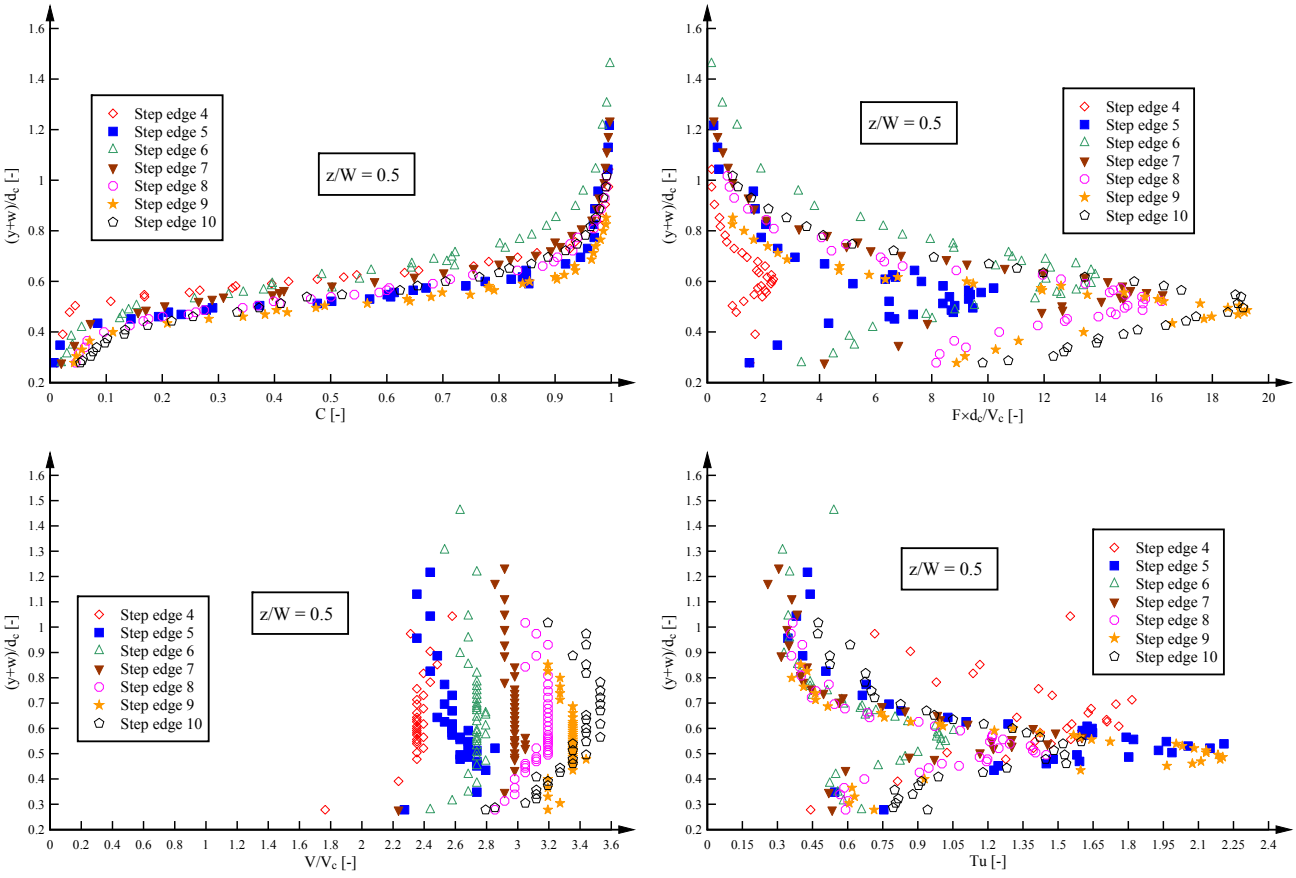

Fig. D-10 – Air-water flow properties on the stepped spillway with in-line configuration of flat and pooled steps (θ = 26.6°) as functions of $(y+w)/d_c$ – Skimming flows: $d_c/h = 1.15$, $Q = 0.063$ m^3/s, $Re = 4.85\times10^5$; Step edges 4-10; Transverse position z/W = 0.75 (flat steps side)

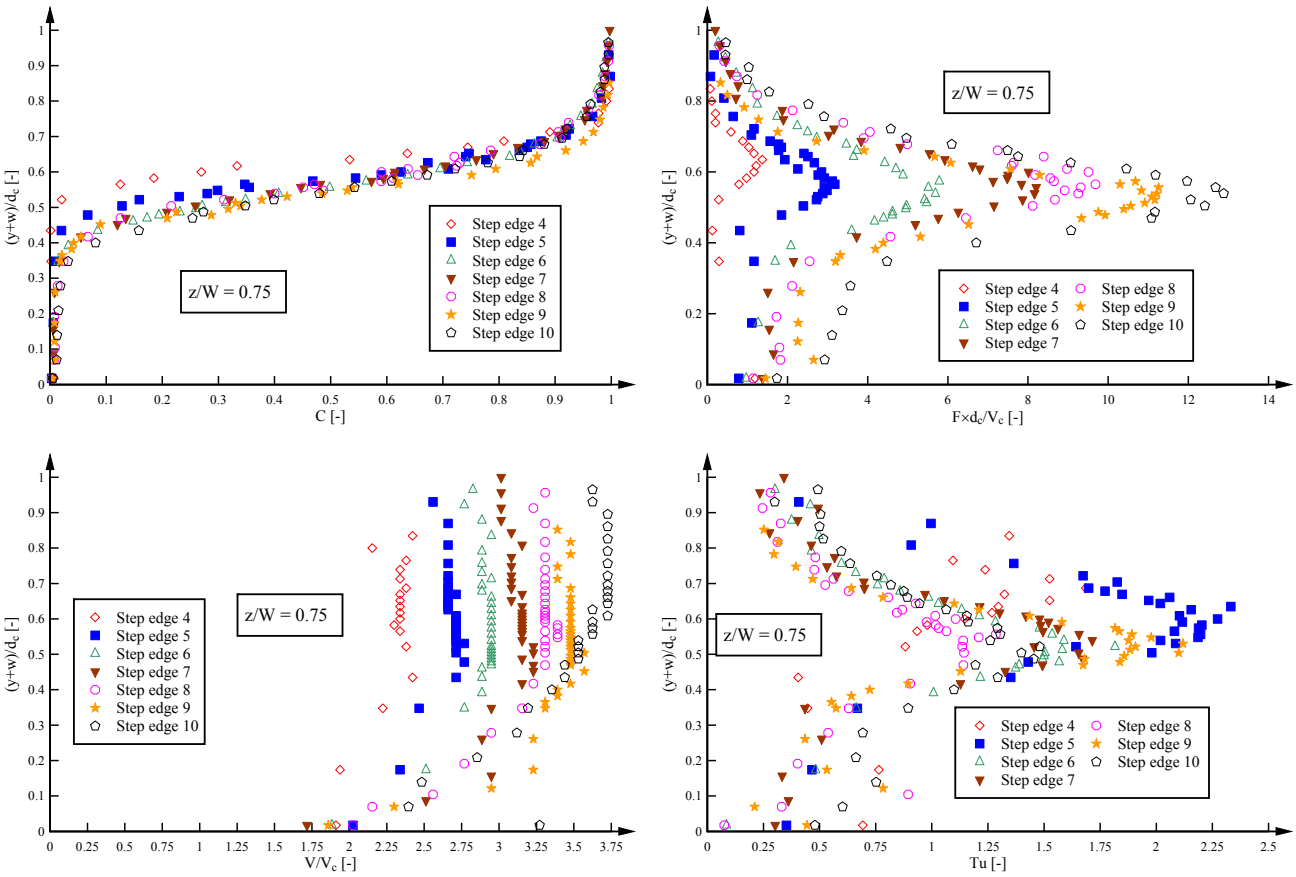

Fig. D-11 – Air-water flow properties on the stepped spillway with in-line configuration of flat and pooled steps (θ = 26.6°) as functions of $(y+w)/d_c$ – Skimming flows: $d_c/h = 1.45$, $Q = 0.090$ m^3/s, $Re = 6.87\times10^5$; Step edges 5-10; Transverse position z/W = 0.25 (pooled steps side)

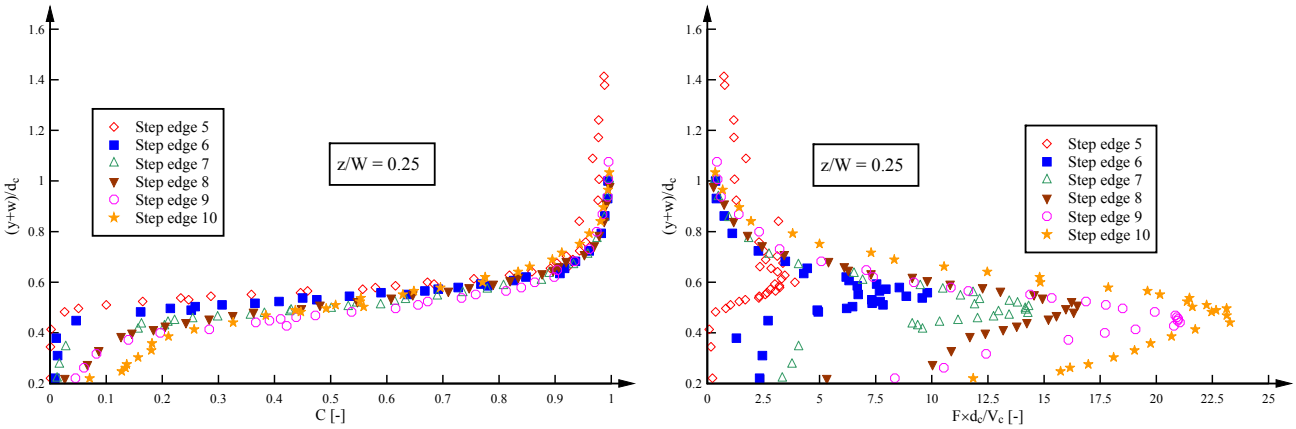

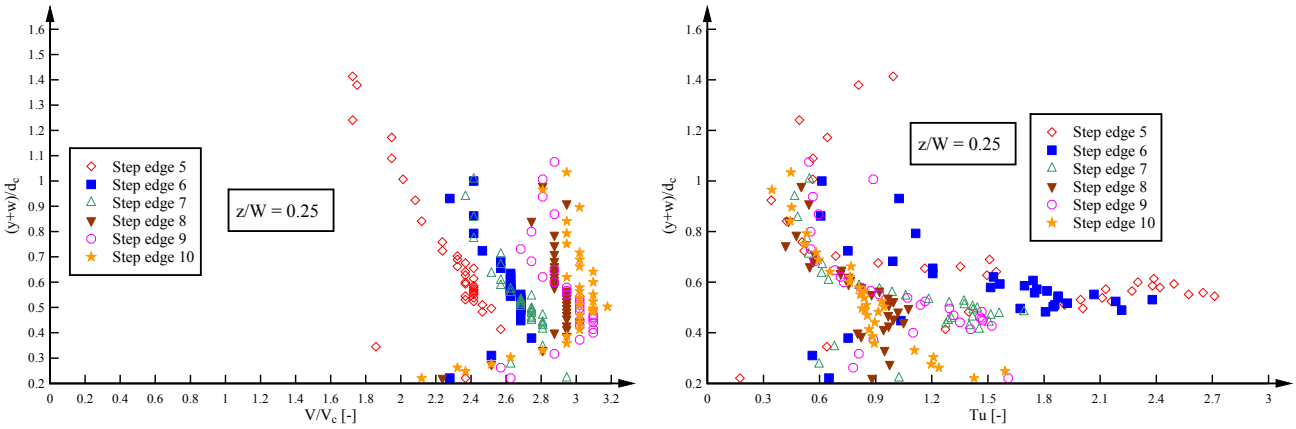

Fig. D-12 – Air-water flow properties on the stepped spillway with in-line configuration of flat and pooled steps (θ = 26.6°) as functions of $(y+w)/d_c$ – Skimming flows: $d_c/h = 1.45$, $Q = 0.090$ m^3/s, $Re = 6.87\times10^5$; Step edges 5-10; Transverse position z/W = 0.5 (channel centreline)

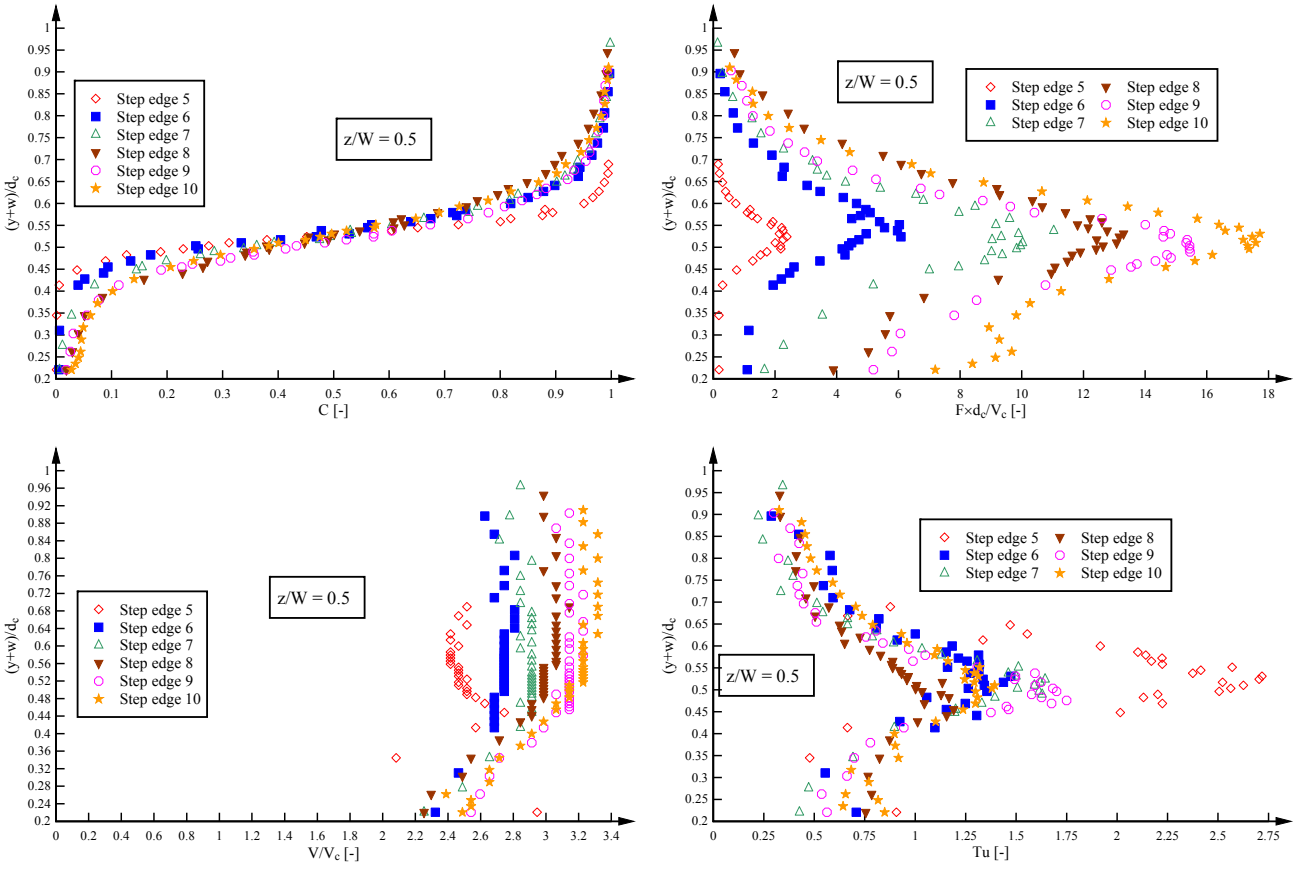

Fig. D-13 – Air-water flow properties on the stepped spillway with in-line configuration of flat and pooled steps (θ = 26.6°) as functions of $(y+w)/d_c$ – Skimming flows: $d_c/h = 1.45$, $Q = 0.090$ m^3/s, $Re = 6.87\times10^5$; Step edges 5-10; Transverse position z/W = 0.75 (flat steps side)

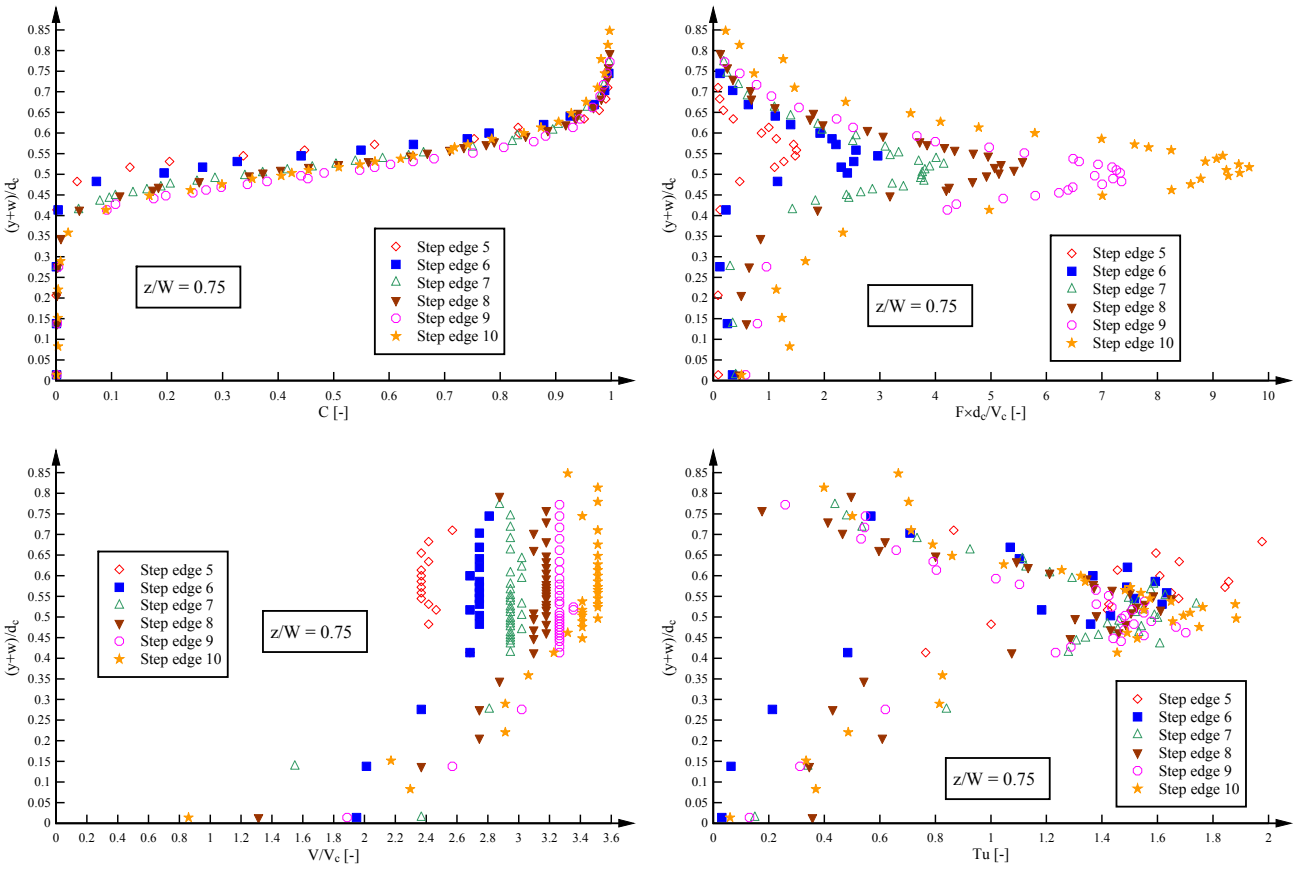

Fig. D-14 – Air-water flow properties on the stepped spillway with in-line configuration of flat and pooled steps (θ = 26.6°) as functions of $(y+w)/d_c$ – Skimming flows: $d_c/h = 1.70$, $Q = 0.113$ m^3/s, $Re = 8.72\times10^5$; Step edges 7-10; Transverse position z/W = 0.25 (pooled steps side)

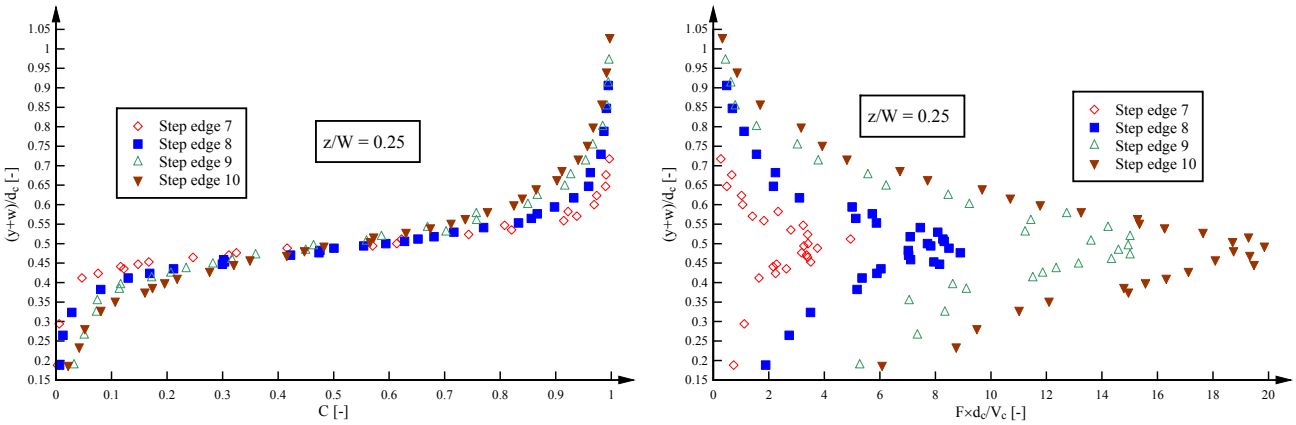

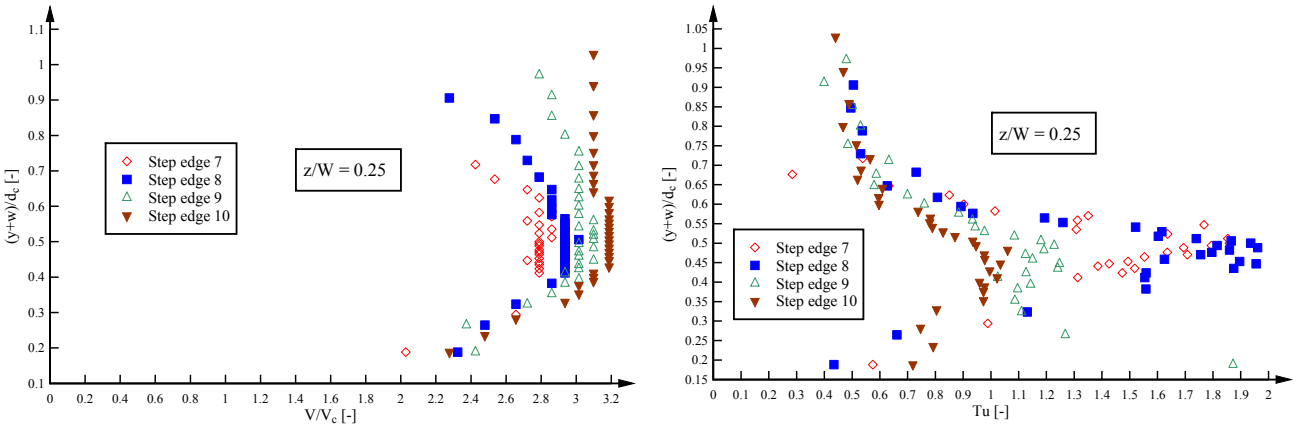

Fig. D-15 – Air-water flow properties on the stepped spillway with in-line configuration of flat and pooled steps (θ = 26.6°) as functions of $(y+w)/d_c$ – Skimming flows: $d_c/h = 1.70$, $Q = 0.113$ m^3/s, $Re = 8.72\times10^5$; Step edges 7-10; Transverse position z/W = 0.5 (channel centreline)

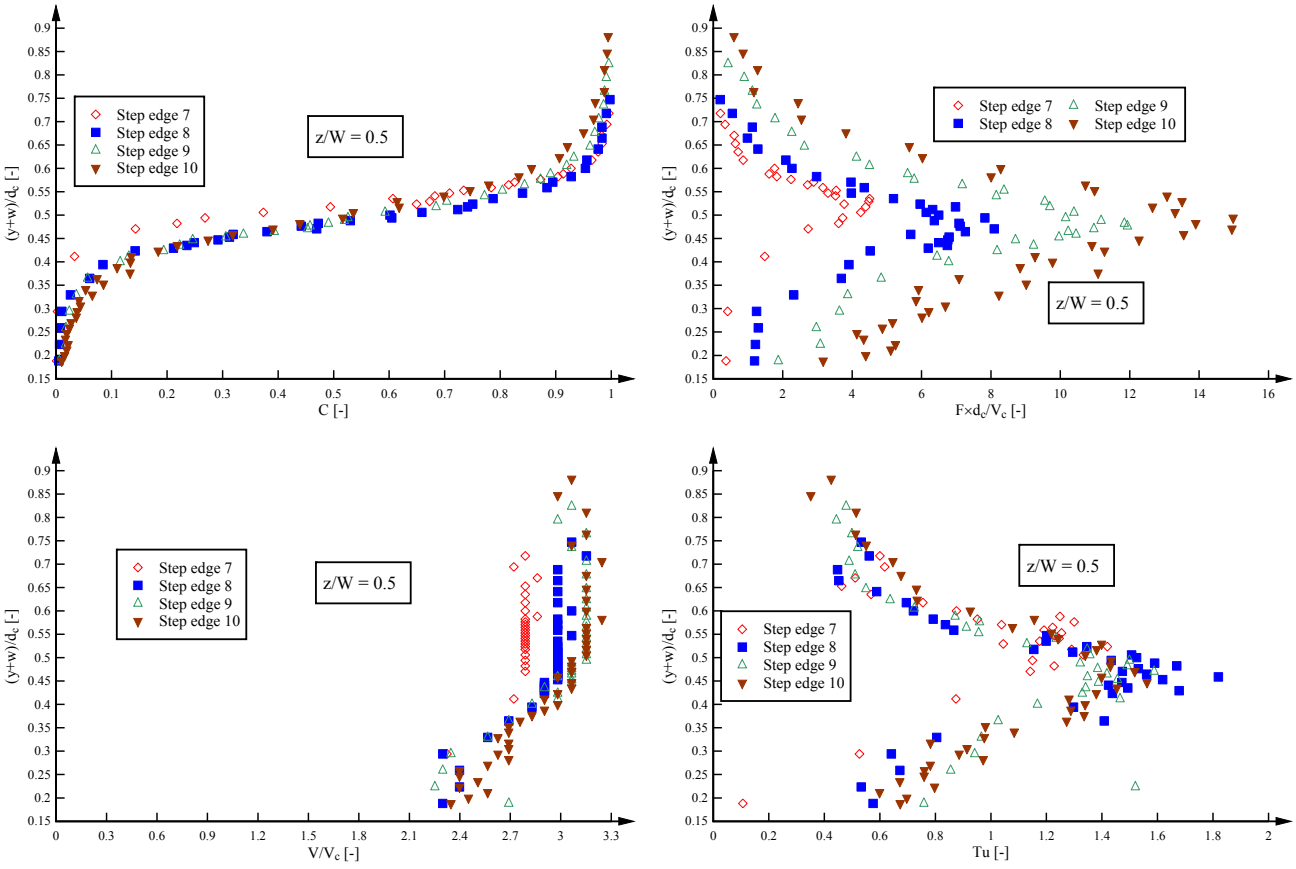

Fig. D-16 – Air-water flow properties on the stepped spillway with in-line configuration of flat and pooled steps (θ = 26.6°) as functions of $(y+w)/d_c$ – Skimming flows: $d_c/h = 1.70$, $Q = 0.113$ m^3/s, $Re = 8.72 \times 10^5$; Step edges 7-10; Transverse position z/W = 0.75 (flat steps side)

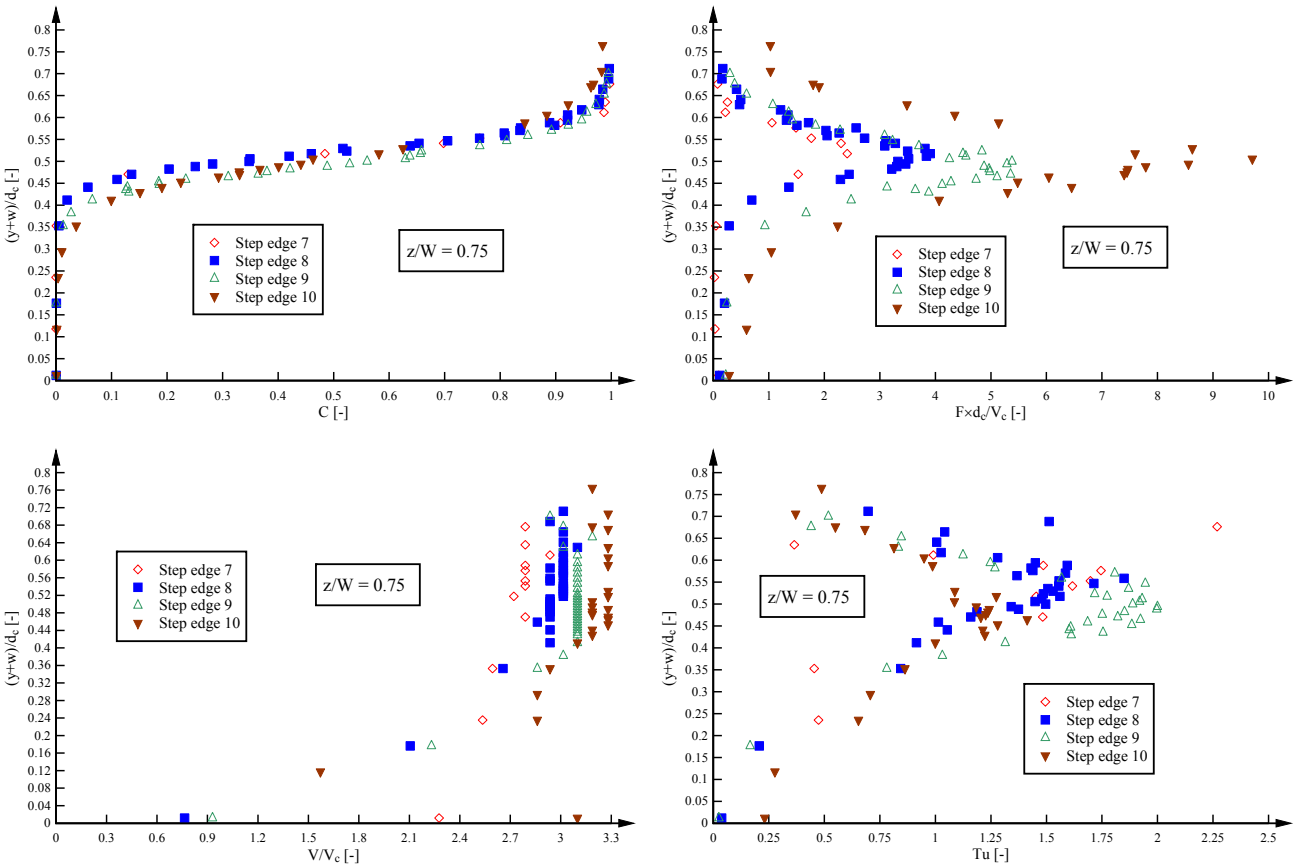

D.3 AIR-WATER FLOW PROPERTIES ON STEPPED SPILLWAY WITH STAGGERED CONFIGURATION OF FLAT AND POOLED STEPS

This section presents the air-water flow properties for the experiments with a double-tip conductivity probe on the stepped spillway with staggered configuration of flat and pooled steps. Table D-10 lists the experimental flow condition for the experiments including the flow regimes.

In section D.3.1, some characteristic air-water flow parameters are presented for all discharges. The parameters are shown for three transverse positions at each step edge and the transverse averaged values are also included (see Appendix F for definition and discussion). Section D.3.2 presents the air-water flow properties for all experiments on the stepped spillway with staggered configuration of flat and pooled steps including the void fraction C, the dimensionless bubble count rate $F \times d_c/V_c$, dimensionless interfacial velocity V/V_c and turbulence intensity Tu. All air-water flow distributions are presented in terms of the dimensionless distance perpendicular to the pseudo bottom formed by the flat step edges $(y+w)/d_c$. The pseudo bottom was defined as the zero position, i.e. $y = 0$.

Table D-10 – Air-water flow measurements with a double-tip conductivity probe (Ø = 0.25 mm) for the stepped spillway with staggered configuration of flat and pooled steps (θ = 26.6°)

Configuration (1)	d_c/h [-] (2)	Q [m^3/s] (3)	Re [-] (4)	Measurement at step edge (5)	Flow regime (6)
Stepped spillway with staggered configuration of flat and pooled steps	0.7	0.030	2.30×10^5	3-10	TRA
	1.15	0.063	4.85×10^5	5-10	SK
	1.45	0.090	6.87×10^5	6-10	SK
	1.7	0.113	8.72×10^5	7-10	SK

Notes: d_c: critical flow depth; h: vertical step height; Q: water discharge; Re: Reynolds number defined in terms of the hydraulic diameter; SK: skimming flow regime; TRA: transition flow regime.

D.2.1 Longitudinal distributions of characteristic air-water flow parameters on the stepped spillway with staggered configuration of flat and pooled steps

Table D-11 – Mean air concentration C_{mean} measured at three transverse positions and transverse averaged calculation on the stepped spillway with staggered configuration of flat and pooled steps ($\theta = 26.6°$); Measurements with a double-tip conductivity probe ($Ø = 0.25$ mm)

d_c/h [-] (1)	Q [m^3/s] (2)	Re [-] (3)	Step edge (4)	C_{mean} at z/W = 0.25 [-] (5)	C_{mean} at z/W = 0.5 [-] (6)	C_{mean} at z/W = 0.75 [-] (7)	C_{mean} (Transverse averaged) [-] (8)
0.7	0.030	2.30×10^5	3	0.572	0.712	0.301	0.505
			4	0.573	0.761	0.636	0.644
			5	0.590	0.702	0.549	0.603
			6	0.509	0.590	0.535	0.539
			7	0.514	0.544	0.528	0.527
			8	0.496	0.712	0.667	0.614
			9	0.670	0.693	0.604	0.651
			10	0.521	0.611	0.562	0.559
1.15	0.063	4.85×10^5	5	0.356	0.505	0.254	0.355
			6	0.319	0.572	0.447	0.430
			7	0.538	0.500	0.340	0.454
			8	0.365	0.477	0.457	0.428
			9	0.494	0.486	0.314	0.425
			10	0.357	0.532	0.508	0.457
1.45	0.090	6.87×10^5	6	0.203	0.433	0.230	0.271
			7	0.401	0.486	0.252	0.366
			8	0.345	0.453	0.355	0.376
			9	0.453	0.414	0.284	0.380
			10	0.341	0.413	0.424	0.390
1.70	0.113	8.72×10^5	7	0.223	0.359	0.175	0.239
			8	0.268	0.367	0.248	0.285
			9	0.368	0.368	0.238	0.319
			10	0.355	0.371	0.363	0.362

Notes: d_c: critical flow depth; h: vertical step height; Q: water discharge; Re: Reynolds number defined in terms of the hydraulic diameter; C_{mean}: mean air concentration; Transverse averaging method defined in Appendix F.

Table D-12 – Maximum bubble count rate F_{max} measured at three transverse positions and transverse averaged calculation on the stepped spillway with staggered configuration of flat and pooled steps ($\theta = 26.6°$); Measurements with a double-tip conductivity probe ($Ø = 0.25$ mm)

d_c/h [-] (1)	Q [m^3/s] (2)	Re [-] (3)	Step edge (4)	F_{max} at z/W = 0.25 [Hz] (5)	F_{max} at z/W = 0.5 [Hz] (6)	F_{max} at z/W = 0.75 [Hz] (7)	F_{max} (Transverse averaged) [Hz] (8)
0.7	0.030	2.30×10^5	3	44.4	49.3	28.4	39.6
			4	78.9	81.4	69.4	76.0
			5	97.9	118.4	118.6	110.8
			6	122.9	134.2	148.1	135.2
			7	123.0	147.9	146.8	138.2
			8	199.1	153.9	242.4	204.0
			9	158.9	156.0	268.5	199.3
			10	157.8	159.8	153.6	156.7
1.15	0.063	4.85×10^5	5	84.8	114.9	46.1	77.8
			6	119.8	169.8	98.6	124.4
			7	131.2	179.8	138.0	145.9
			8	220.0	199.2	220.0	214.8
			9	213.1	218.7	315.0	252.7
			10	299.5	231.2	249.6	263.7
1.45	0.090	6.87×10^5	6	41.5	92.1	40.2	53.7
			7	99.9	133.8	76.4	99.6
			8	153.1	157.8	163.5	158.2
			9	203.5	184.7	233.7	210.1
			10	258.8	196.8	208.1	224.3
1.70	0.113	8.72×10^5	7	62.9	71.9	32.4	53.7
			8	109.9	111.1	88.2	102.1
			9	184.7	138.6	187.8	174.3
			10	217.0	160.2	189.4	192.5

Notes: d_c: critical flow depth; h: vertical step height; Q: water discharge; Re: Reynolds number defined in terms of the hydraulic diameter; F_{max}: maximum bubble count rate; Transverse averaging method defined in Appendix F.

Table D-13 – Characteristic interfacial velocity V_{90} measured at three transverse positions and transverse averaged calculation on the stepped spillway with staggered configuration of flat and pooled steps ($\theta = 26.6°$); Measurements with a double-tip conductivity probe ($Ø = 0.25$ mm)

d_c/h [-] (1)	Q [m^3/s] (2)	Re [-] (3)	Step edge (4)	V_{90} at z/W = 0.25 [m/s] (5)	V_{90} at z/W = 0.5 [m/s] (6)	V_{90} at z/W = 0.75 [m/s] (7)	V_{90} (Transverse averaged) [m/s] (8)
0.7	0.030	2.30×10^5	3	1.90	1.91	3.13	2.36
			4	2.86	2.68	2.29	2.60
			5	2.16	2.05	2.48	2.25
			6	2.48	2.39	2.62	2.51
			7	2.21	2.21	4.49	3.07
			8	2.48	2.38	2.33	2.40
			9	2.03	2.28	2.89	2.42
			10	2.41	2.70	2.53	2.53
1.15	0.063	4.85×10^5	5	2.88	2.87	3.28	3.03
			6	3.10	3.13	2.95	3.05
			7	3.02	3.09	3.28	3.14
			8	3.17	3.20	3.13	3.16
			9	2.77	3.30	3.31	3.11
			10	3.24	3.56	3.07	3.26
1.45	0.090	6.87×10^5	6	3.16	3.51	3.42	3.35
			7	2.99	3.55	3.53	3.33
			8	3.35	3.58	3.69	3.54
			9	3.17	3.69	3.69	3.50
			10	3.43	3.89	3.51	3.58
1.70	0.113	8.72×10^5	7	3.47	3.69	3.79	3.65
			8	3.51	3.89	3.89	3.75
			9	3.64	3.98	3.89	3.82
			10	3.69	4.18	3.79	3.85

Notes: d_c: critical flow depth; h: vertical step height; Q: water discharge; Re: Reynolds number defined in terms of the hydraulic diameter; V_{90}: characteristic interfacial velocity where C = 90%; Transverse averaging method defined in Appendix F.

Table D-14 – Local discharge per unit width q_{local} for measurement at three transverse positions and transverse averaged calculation on the stepped spillway with staggered configuration of flat and pooled steps ($\theta = 26.6°$); Measurements with a double-tip conductivity probe ($Ø = 0.25$ mm)

d_c/h [-] (1)	Q [m^3/s] (2)	Re [-] (3)	Step edge (4)	q_{local} at z/W = 0.25 [m^2/s] (5)	q_{local} at z/W = 0.5 [m^2/s] (6)	q_{local} at z/W = 0.75 [m^2/s] (7)	q_{local} (Transverse averaged) [m^2/s] (8)
0.7	0.030	2.30×10^5	3	0.0705	0.0387	0.0686	0.0618
			4	0.0541	0.0724	0.1155	0.0817
			5	0.0742	0.0478	0.1066	0.0798
			6	0.0683	0.0514	0.0947	0.0740
			7	0.0731	0.0634	0.1373	0.0948
			8	0.0937	0.0432	0.1060	0.0857
			9	0.0881	0.0503	0.0928	0.0804
			10	0.0961	0.0596	0.0776	0.0800
1.15	0.063	4.85×10^5	5	0.1718	0.0905	0.1407	0.1398
			6	0.1405	0.1273	0.1693	0.1480
			7	0.1570	0.1339	0.1487	0.1481
			8	0.1424	0.1417	0.1648	0.1506
			9	0.1432	0.1375	0.1419	0.1413
			10	0.1301	0.1353	0.1514	0.1394
1.45	0.090	6.87×10^5	6	0.1283	0.1384	0.2270	0.1678
			7	0.2248	0.1749	0.2092	0.2065
			8	0.1875	0.1986	0.2156	0.2008
			9	0.2126	0.2252	0.1909	0.2076
			10	0.1835	0.2163	0.1894	0.1939
1.70	0.113	8.72×10^5	7	0.2548	0.2039	0.2556	0.2424
			8	0.2350	0.2298	0.2643	0.2447
			9	0.2756	0.2693	0.2495	0.2642
			10	0.2330	0.2786	0.2678	0.2575

Notes: d_c: critical flow depth; h: vertical step height; Q: water discharge; Re: Reynolds number defined in terms of the hydraulic diameter; q_{local}: local discharge per unit width; Transverse averaging method defined in Appendix F.

Table D-15 – Local mean flow velocity U_{local} for measurement at three transverse positions and transverse averaged calculation on the stepped spillway with staggered configuration of flat and pooled steps (θ = 26.6°); Measurements with a double-tip conductivity probe (Ø = 0.25 mm)

d_c/h [-] (1)	Q [m^3/s] (2)	Re [-] (3)	Step edge (4)	U_{local} at z/W = 0.25 [m/s] (5)	U_{local} at z/W = 0.5 [m/s] (6)	U_{local} at z/W = 0.75 [m/s] (7)	U_{local} (Transverse averaged) [m/s] (8)
0.7	0.030	2.30×10^5	3	1.52	2.10	2.25	1.94
			4	2.31	2.75	1.92	2.27
			5	2.20	2.16	2.37	2.25
			6	2.13	1.97	2.61	2.27
			7	2.05	2.30	3.19	2.54
			8	2.26	2.22	1.99	2.15
			9	2.05	2.25	2.46	2.25
			10	2.48	2.41	2.31	2.40
1.15	0.063	4.85×10^5	5	2.49	3.04	2.93	2.79
			6	3.04	2.85	2.48	2.78
			7	2.70	3.11	3.06	2.94
			8	2.92	3.18	2.61	2.87
			9	2.37	3.42	2.41	2.65
			10	2.76	3.53	2.57	2.88
1.45	0.090	6.87×10^5	6	2.28	3.09	2.53	2.58
			7	2.71	3.33	3.35	3.11
			8	3.21	3.39	2.84	3.12
			9	2.90	3.64	2.88	3.08
			10	3.29	3.68	2.52	3.10
1.70	0.113	8.72×10^5	7	2.68	3.61	3.48	3.21
			8	3.29	3.62	2.97	3.25
			9	3.21	3.81	3.42	3.44
			10	3.61	3.87	3.07	3.47

Notes: d_c: critical flow depth; h: vertical step height; Q: water discharge; Re: Reynolds number defined in terms of the hydraulic diameter; q_{local}: local discharge per unit width; Transverse averaging method defined in Appendix F.

Table D-16 – Characteristic flow depth Y_{90} for measurement at three transverse positions and transverse averaged calculation on the stepped spillway with staggered configuration of flat and pooled steps (θ = 26.6°); Measurements with a double-tip conductivity probe (Ø = 0.25 mm)

d_c/h [-] (1)	Q [m^3/s] (2)	Re [-] (3)	Step edge (4)	Y_{90} at z/W = 0.25 [m] (5)	Y_{90} at z/W = 0.5 [m] (6)	Y_{90} at z/W = 0.75 [m] (7)	Y_{90} (Transverse averaged) [m] (8)
0.7	0.030	2.30×10^5	3	0.1083	0.0640	0.0437	0.0730
			4	0.0548	0.1099	0.1650	0.1099
			5	0.0823	0.0745	0.0998	0.0869
			6	0.0654	0.0636	0.0780	0.0697
			7	0.0732	0.0604	0.0910	0.0767
			8	0.0823	0.0675	0.1693	0.1112
			9	0.1300	0.0728	0.0952	0.1027
			10	0.0809	0.0635	0.0767	0.0750
1.15	0.063	4.85×10^5	5	0.1072	0.0603	0.0645	0.0795
			6	0.0678	0.1046	0.1234	0.0979
			7	0.1258	0.0861	0.0736	0.0963
			8	0.0768	0.0851	0.1162	0.0937
			9	0.1192	0.0783	0.0860	0.0965
			10	0.0733	0.0821	0.1198	0.0929
1.45	0.090	6.87×10^5	6	0.0707	0.0792	0.1167	0.0901
			7	0.1386	0.1021	0.0834	0.1088
			8	0.0892	0.1072	0.1176	0.1044
			9	0.1340	0.1057	0.0926	0.1114
			10	0.0846	0.1002	0.1303	0.1056
1.70	0.113	8.72×10^5	7	0.1223	0.0885	0.0891	0.1014
			8	0.0977	0.1012	0.1199	0.1069
			9	0.1360	0.1120	0.0961	0.1150
			10	0.1002	0.1155	0.1372	0.1179

Notes: d_c: critical flow depth; h: vertical step height; Q: water discharge; Re: Reynolds number defined in terms of the hydraulic diameter; Y_{90}: characteristic flow depth where C = 90%; Transverse averaging method defined in Appendix F.

Table D-17 – Maximum turbulence intensity Tu_{max} for measurement at three transverse positions and transverse averaged calculation on the stepped spillway with staggered configuration of flat and pooled steps ($\theta = 26.6°$); Measurements with a double-tip conductivity probe ($Ø = 0.25$ mm)

d_c/h [-] (1)	Q [m^3/s] (2)	Re [-] (3)	Step edge (4)	Tu_{max} at z/W = 0.25 [-] (5)	Tu_{max} at z/W = 0.5 [-] (6)	Tu_{max} at z/W = 0.75 [-] (7)	Tu_{max} (Transverse averaged) [-] (8)
0.7	0.030	2.30×10^5	3	3.54	8.73	9.90	7.22
			4	7.04	5.89	2.96	5.22
			5	2.72	2.98	5.00	3.64
			6	3.61	2.28	1.99	2.67
			7	1.96	3.41	6.93	4.19
			8	6.54	1.58	3.09	4.01
			9	2.69	2.40	3.04	2.75
			10	4.56	2.37	1.89	3.01
1.15	0.063	4.85×10^5	5	1.26	1.81	4.85	2.74
			6	2.36	0.95	1.70	1.76
			7	1.40	1.28	2.37	1.73
			8	2.55	1.37	1.37	1.81
			9	1.58	1.69	2.39	1.91
			10	2.21	1.31	1.25	1.63
1.45	0.090	6.87×10^5	6	4.19	1.76	1.40	2.54
			7	1.60	1.10	2.84	1.94
			8	2.72	1.18	1.44	1.86
			9	1.27	1.13	2.69	1.77
			10	2.23	1.05	1.41	1.63
1.70	0.113	8.72×10^5	7	1.65	1.88	3.86	2.54
			8	3.33	1.58	1.46	2.19
			9	1.31	1.49	2.87	1.94
			10	2.55	1.10	1.43	1.77

Notes: d_c: critical flow depth; h: vertical step height; Q: water discharge; Re: Reynolds number defined in terms of the hydraulic diameter; Y Tu_{max}: maximum turbulence intensity in a cross-section; Transverse averaging method defined in Appendix F.

D.3.2 Air-water flow properties on the stepped spillway with staggered configuration of flat and pooled steps

Table D-18 summarises the presented data in this section and it indicates the respective position of the graphs in Figures D-17 to D-28. All air-water flow distributions are presented in terms of the dimensionless distance perpendicular to the pseudo-bottom formed by the step edges $(y+w)/d_c$. The pseudo bottom formed by the flat step edges was defined as the zero position, i.e. y = 0.

Table D-18 - Summary of the air-water flow properties on the stepped spillway with staggered configuration of flat and pooled steps and positioning in the following figures (Fig. D-17 to D-28); Illustration as functions of $(y+w)/d_c$

Void fraction C	Dimensionless bubble count rate $F \times d_c/V_c$
Dimensionless interfacial velocity V/V_c	Turbulence intensity Tu

Notes: y: distance normal to the pseudo bottom; C: void fraction; F: bubble count rate; d_c: critical flow depth; V_c: critical flow velocity; V: interfacial velocity; Tu: turbulence intensity.

Fig. D-17 – Air-water flow properties on the stepped spillway with staggered configuration of flat and pooled steps (θ = 26.6°) as functions of $(y+w)/d_c$ – Transition flows: $d_c/h = 0.70$, Q = 0.030 m^3/s, Re = 2.30×10^5; Step edges 3-10; Transverse position z/W = 0.25

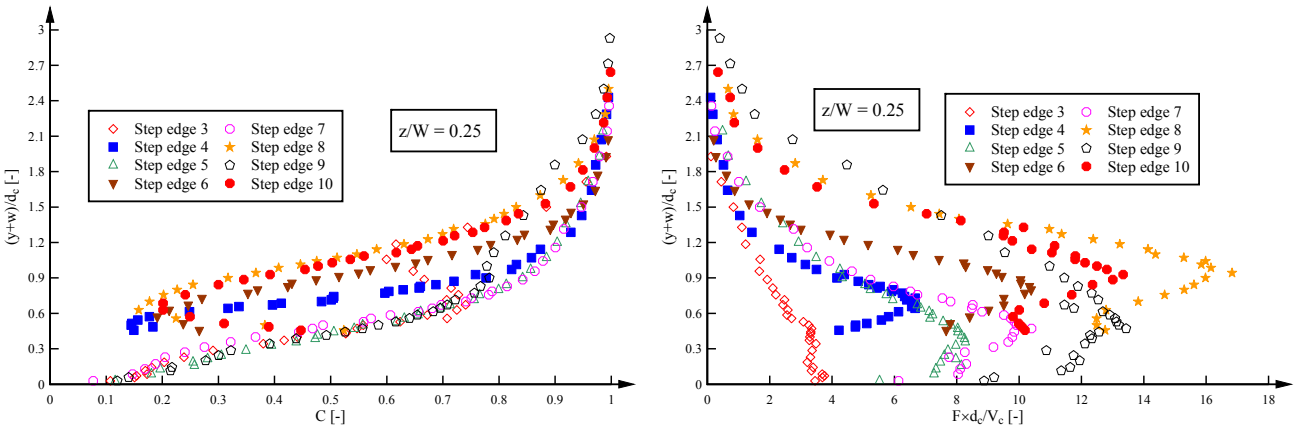

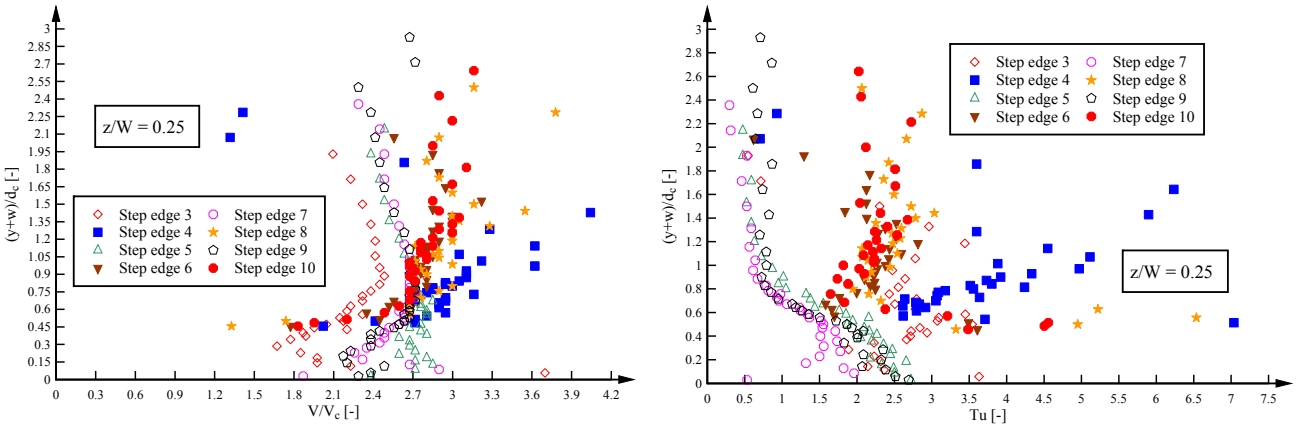

Fig. D-18 – Air-water flow properties on the stepped spillway with staggered configuration of flat and pooled steps (θ = 26.6°) as functions of (y+w)/d_c – Transition flows: d_c/h = 0.70, Q = 0.030 m^3/s, Re = 2.30×10^5; Step edges 3-10; Transverse position z/W = 0.5 (channel centreline)

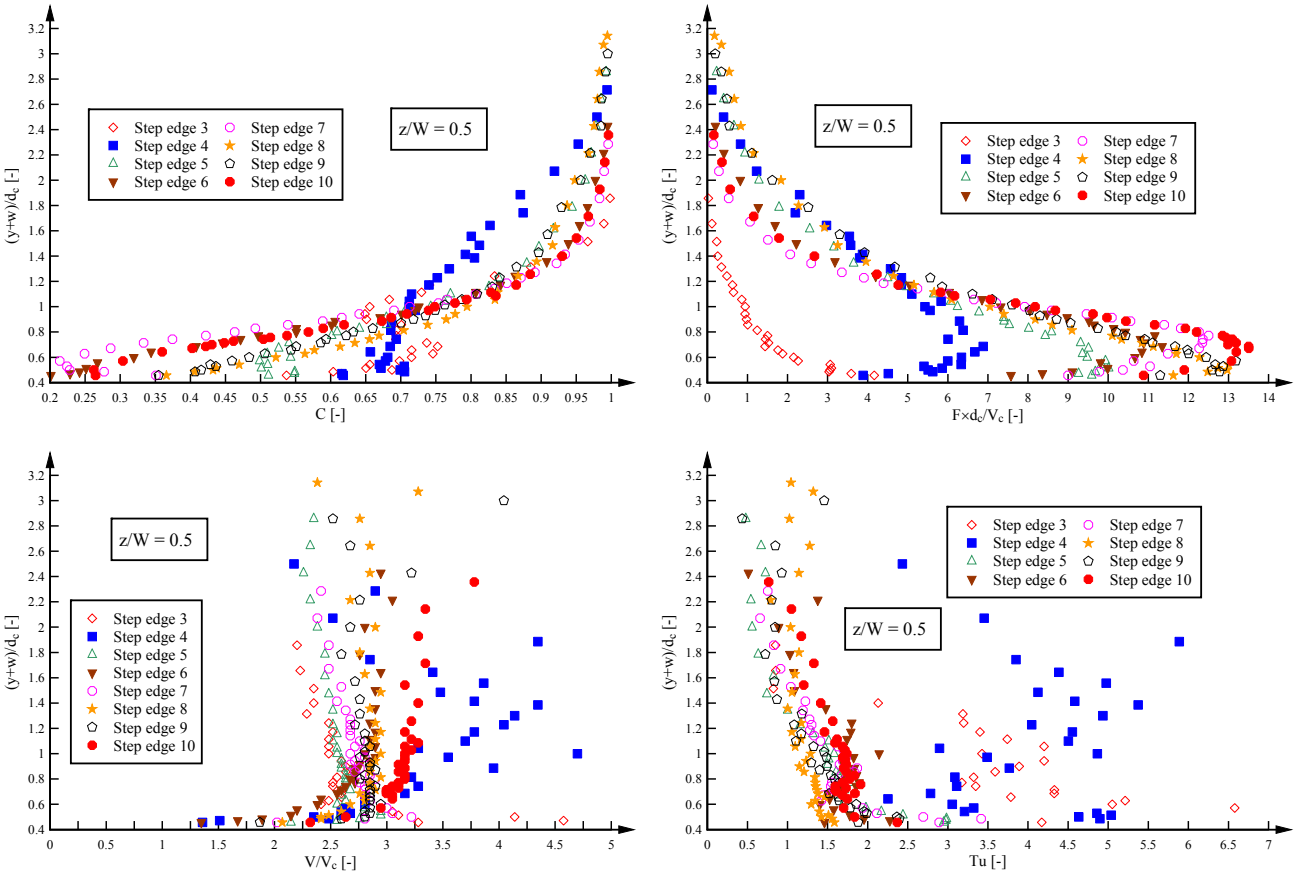

Fig. D-19 – Air-water flow properties on the stepped spillway with staggered configuration of flat and pooled steps (θ = 26.6°) as functions of $(y+w)/d_c$ – Transition flows: $d_c/h = 0.70$, $Q = 0.030$ m^3/s, $Re = 2.30\times10^5$; Step edges 3-10; Transverse position z/W = 0.75

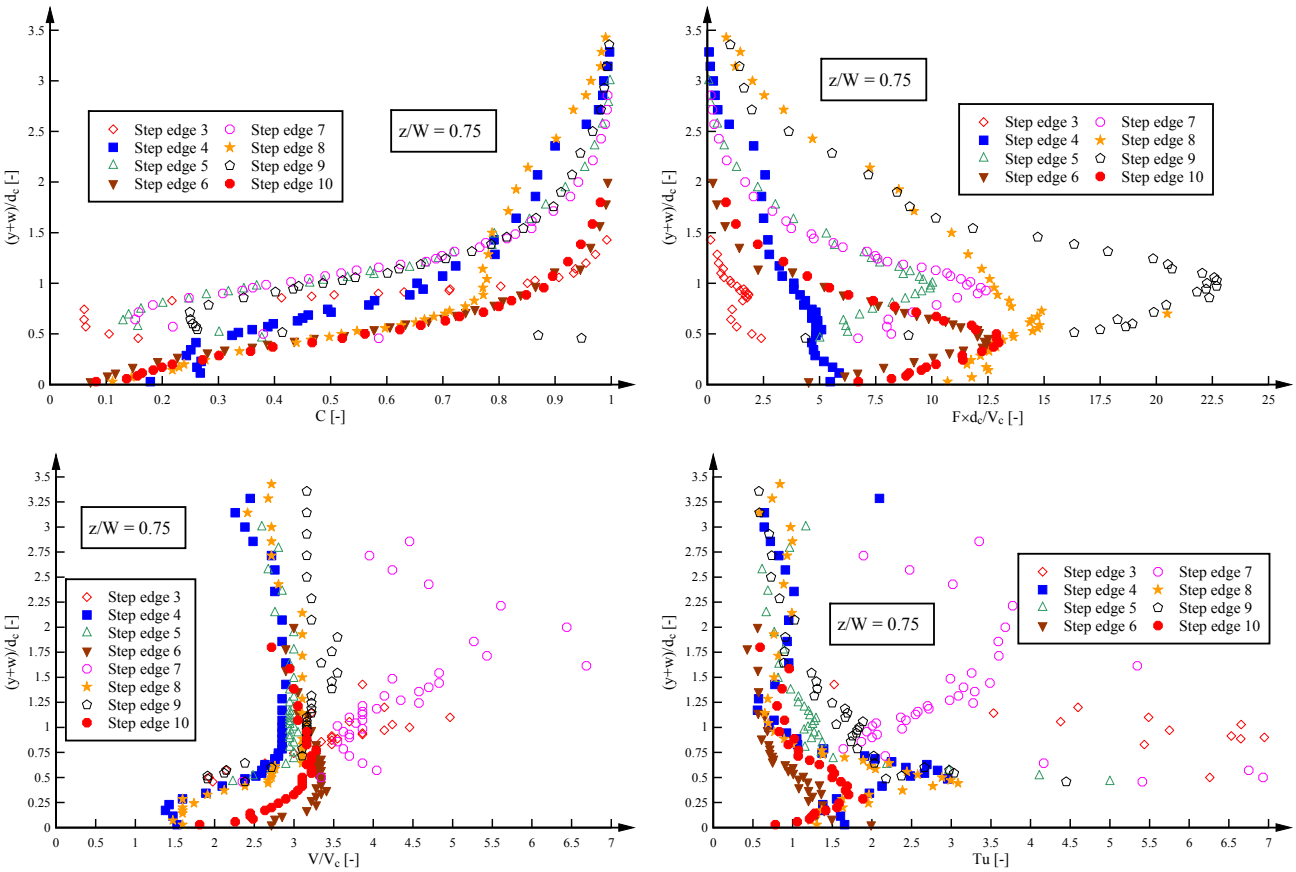

Fig. D-20 – Air-water flow properties on the stepped spillway with staggered configuration of flat and pooled steps (θ = 26.6°) as functions of $(y+w)/d_c$ – Skimming flows: $d_c/h = 1.15$, $Q = 0.063$ m^3/s, $Re = 4.85\times10^5$; Step edges 5-10; Transverse position z/W = 0.25

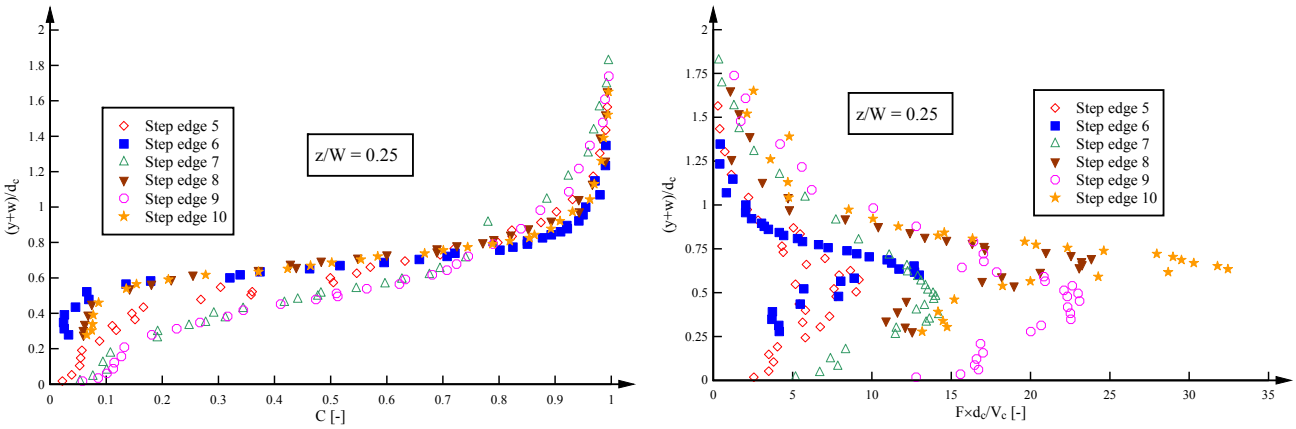

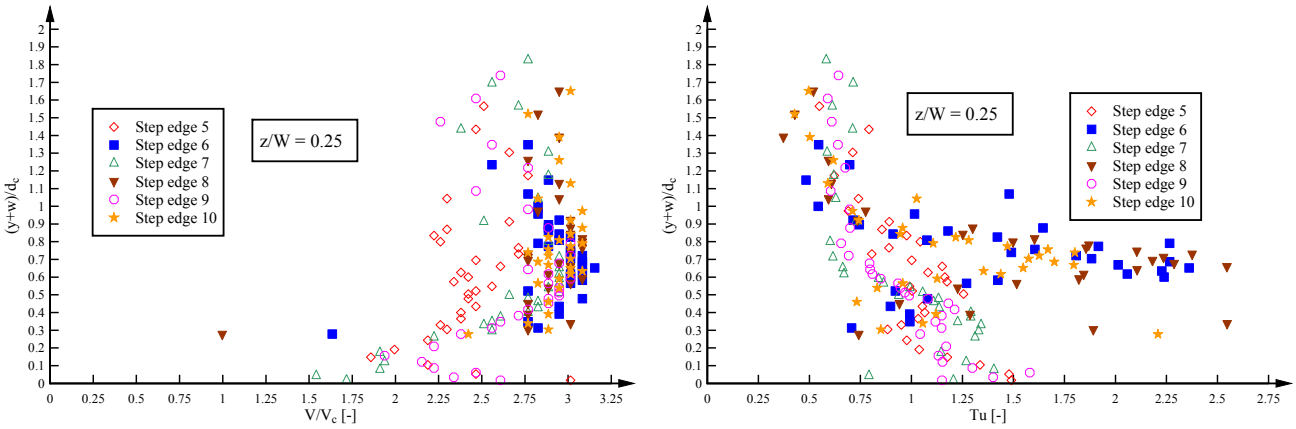

Fig. D-21 – Air-water flow properties on the stepped spillway with staggered configuration of flat and pooled steps (θ = 26.6°) as functions of $(y+w)/d_c$ – Skimming flows: $d_c/h = 1.15$, Q = 0.063 m^3/s, Re = 4.85×10^5; Step edges 5-10; Transverse position z/W = 0.5 (channel centreline)

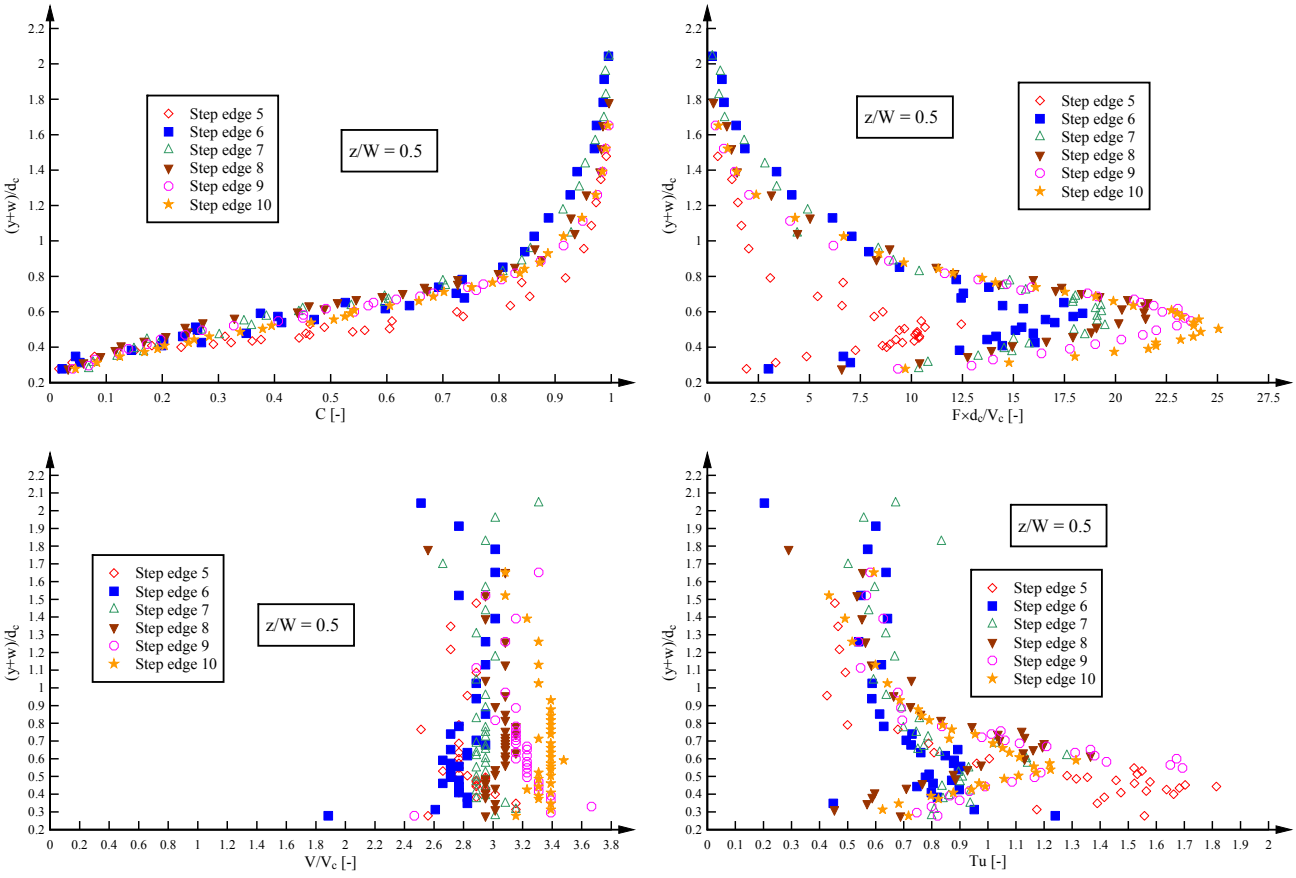

Fig. D-22 – Air-water flow properties on the stepped spillway with staggered configuration of flat and pooled steps (θ = 26.6°) as functions of $(y+w)/d_c$ – Skimming flows: d_c/h = 1.15, Q = 0.063 m^3/s, Re = 4.85×10^5; Step edges 5-10; Transverse position z/W = 0.75

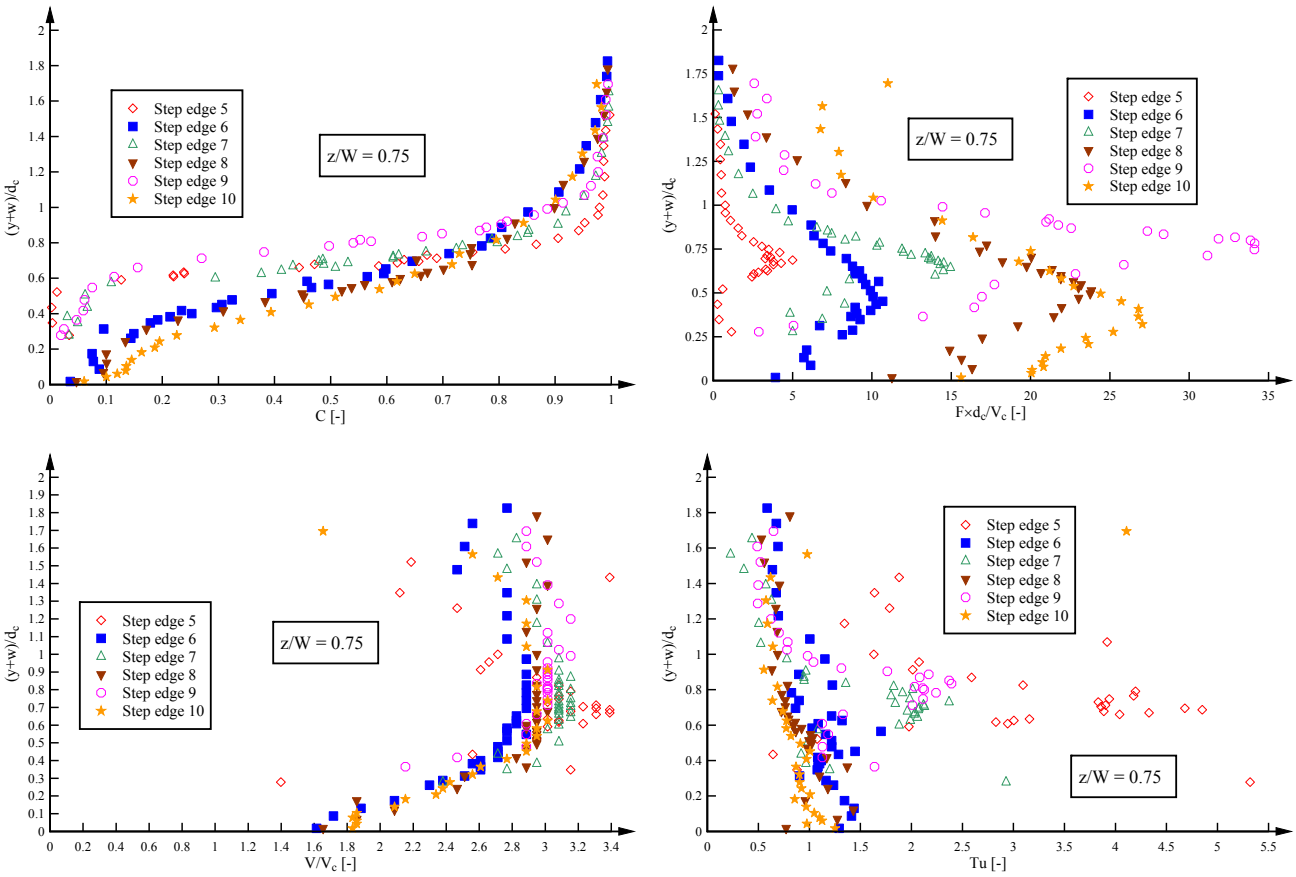

Fig. D-23 – Air-water flow properties on the stepped spillway with staggered configuration of flat and pooled steps (θ = 26.6°) as functions of $(y+w)/d_c$ – Skimming flows: d_c/h = 1.45, Q = 0.090 m^3/s, Re = 6.87×10^5; Step edges 6-10; Transverse position z/W = 0.25

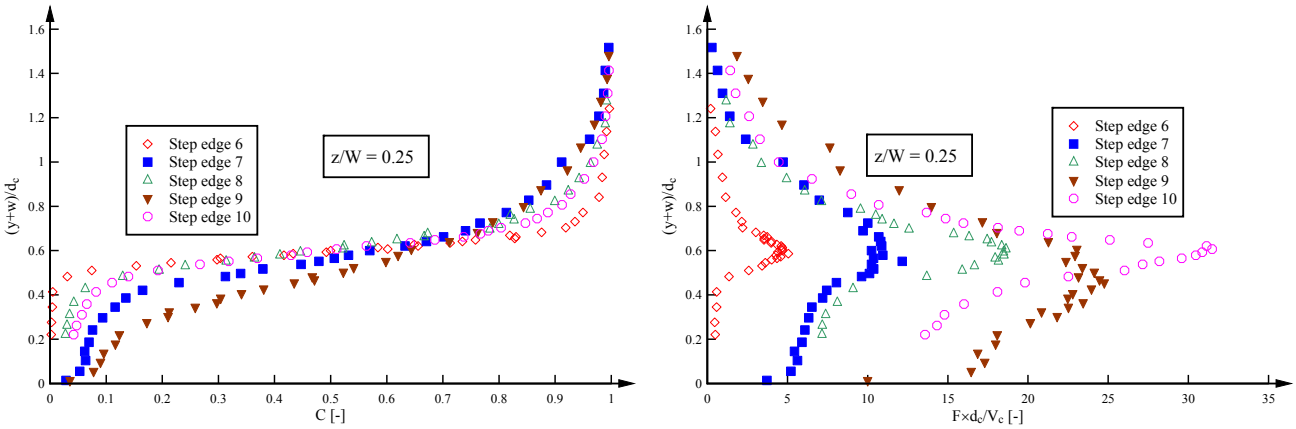

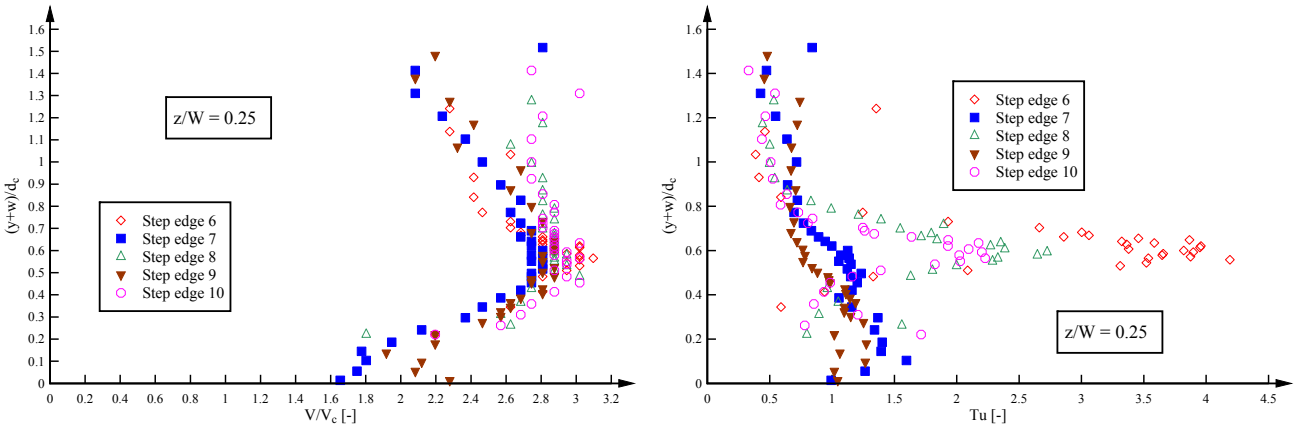

Fig. D-24 – Air-water flow properties on the stepped spillway with staggered configuration of flat and pooled steps (θ = 26.6°) as functions of $(y+w)/d_c$ – Skimming flows: $d_c/h = 1.45$, $Q = 0.090$ m^3/s, $Re = 6.87 \times 10^5$; Step edges 6-10; Transverse position z/W = 0.5 (channel centreline)

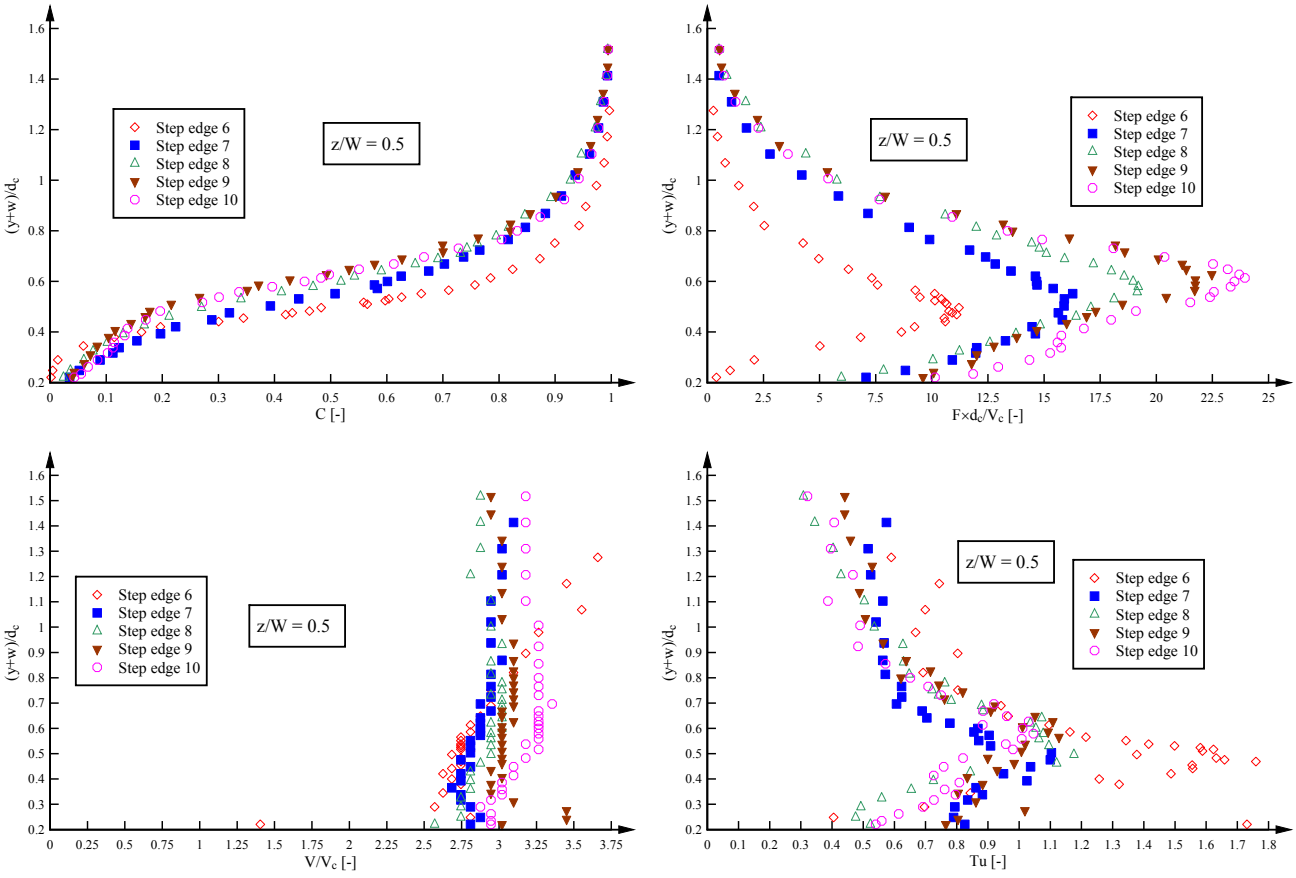

Fig. D-25 – Air-water flow properties on the stepped spillway with staggered configuration of flat and pooled steps (θ = 26.6°) as functions of $(y+w)/d_c$ – Skimming flows: d_c/h = 1.45, Q = 0.090 m^3/s, Re = 6.87×10^5; Step edges 6-10; Transverse position z/W = 0.75

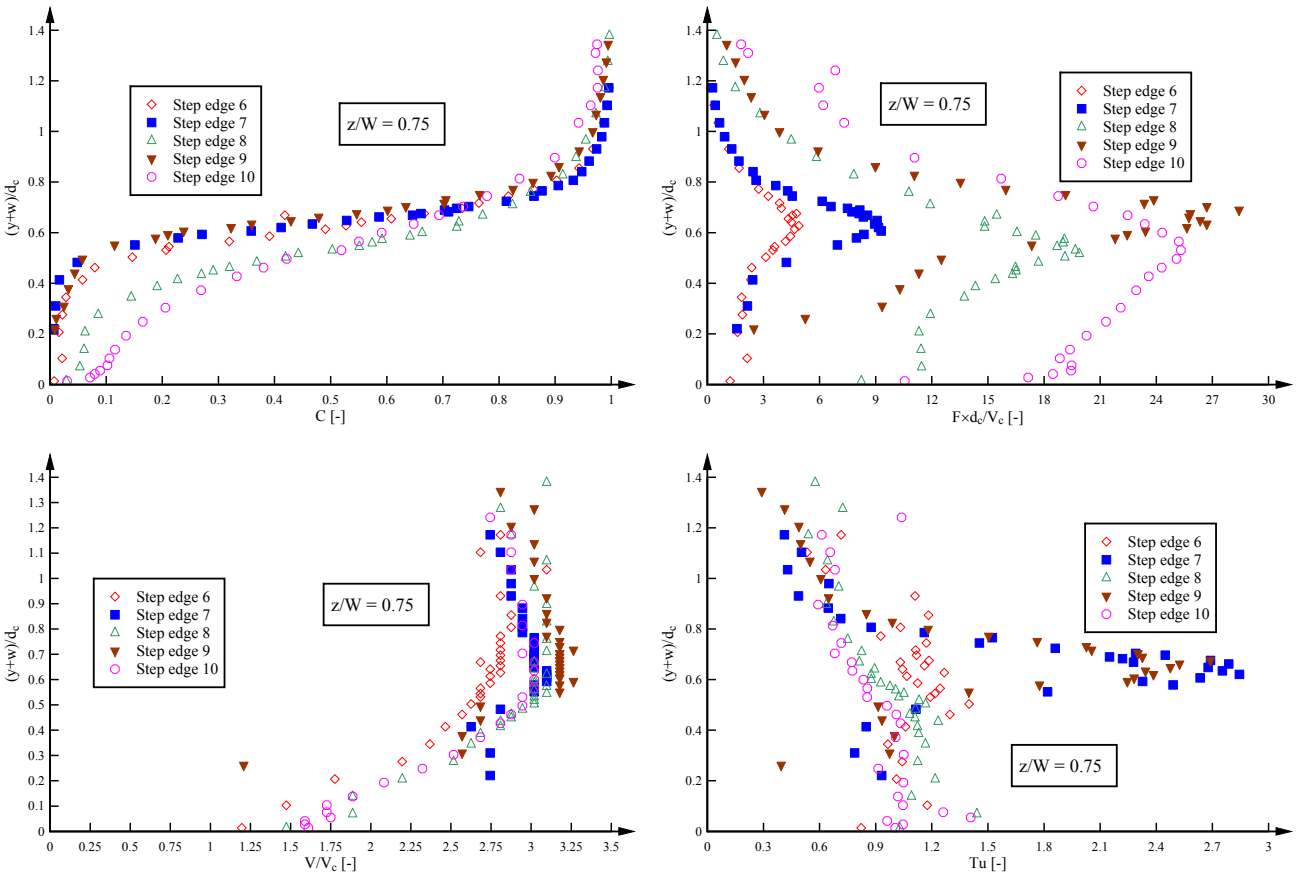

Fig. D-26 – Air-water flow properties on the stepped spillway with staggered configuration of flat and pooled steps (θ = 26.6°) as functions of $(y+w)/d_c$ – Skimming flows: d_c/h = 1.70, Q = 0.113 m^3/s, Re = 8.72×10^5; Step edges 7-10; Transverse position z/W = 0.25

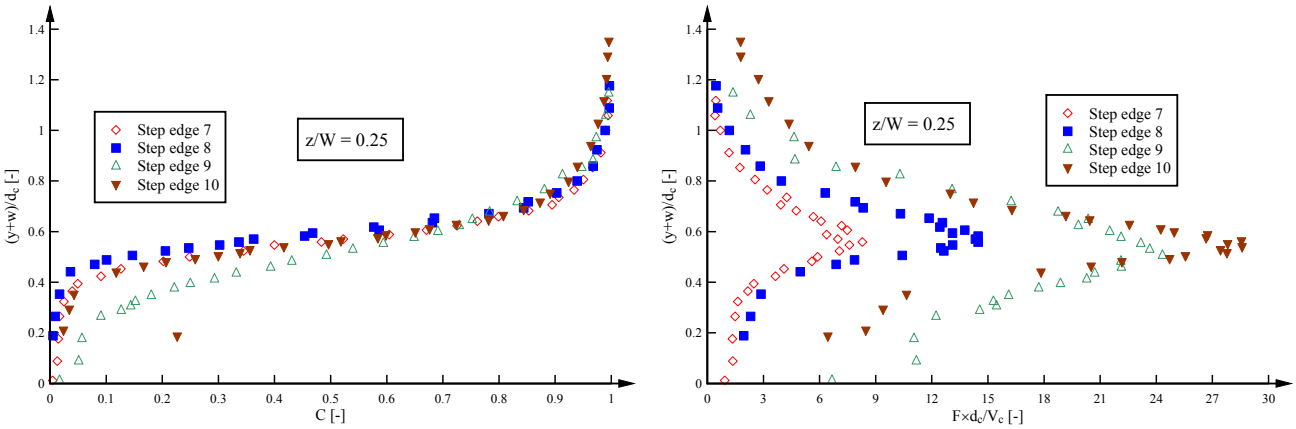

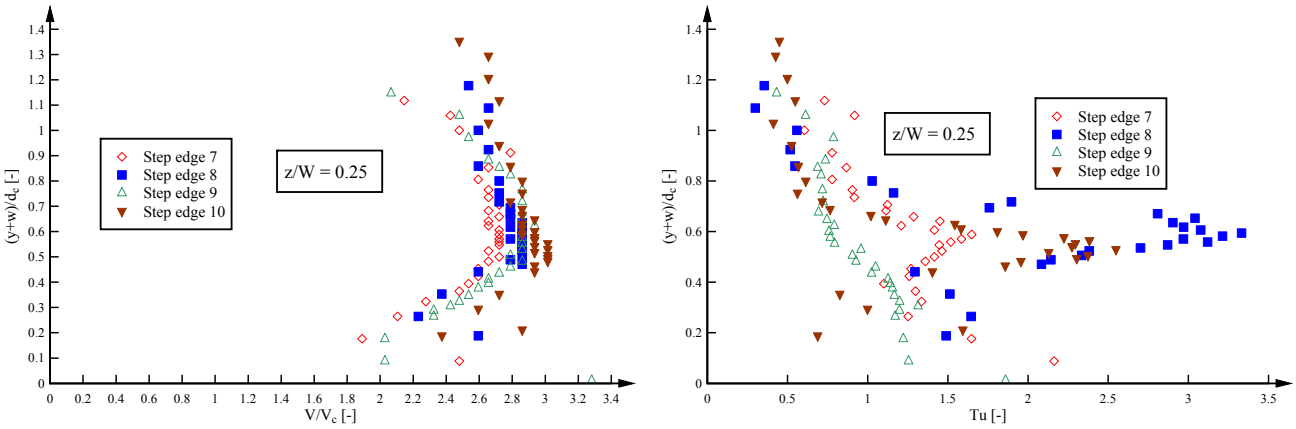

Fig. D-27 – Air-water flow properties on the stepped spillway with staggered configuration of flat and pooled steps (θ = 26.6°) as functions of $(y+w)/d_c$ – Skimming flows: $d_c/h = 1.70$, $Q = 0.113$ m^3/s, $Re = 8.72 \times 10^5$; Step edges 7-10; Transverse position z/W = 0.50 (channel centreline)

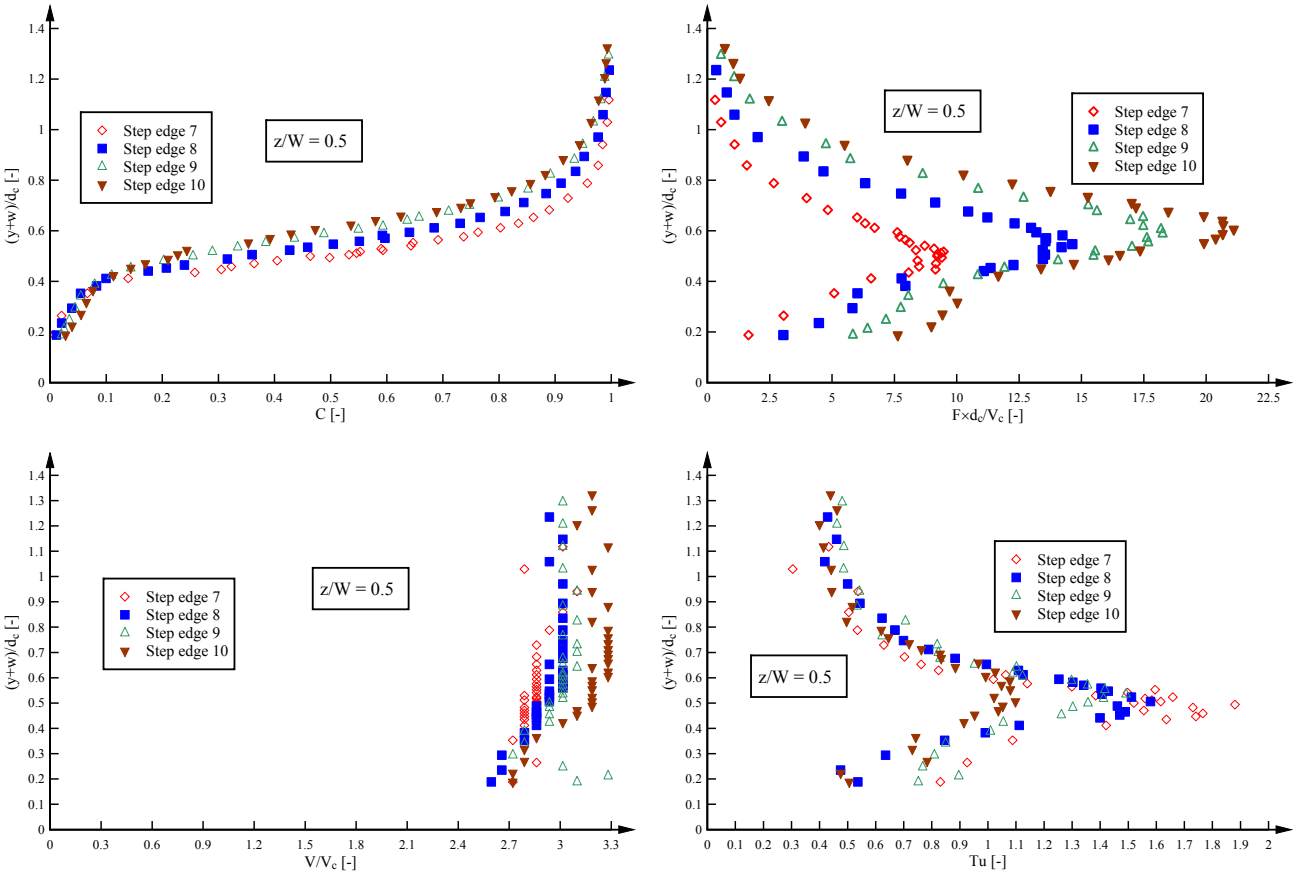

Fig. D-28 – Air-water flow properties on the stepped spillway with staggered configuration of flat and pooled steps (θ = 26.6°) as functions of $(y+w)/d_c$ – Skimming flows: $d_c/h = 1.70$, $Q = 0.113$ m^3/s, $Re = 8.72 \times 10^5$; Step edges 7-10; Transverse position z/W = 0.75

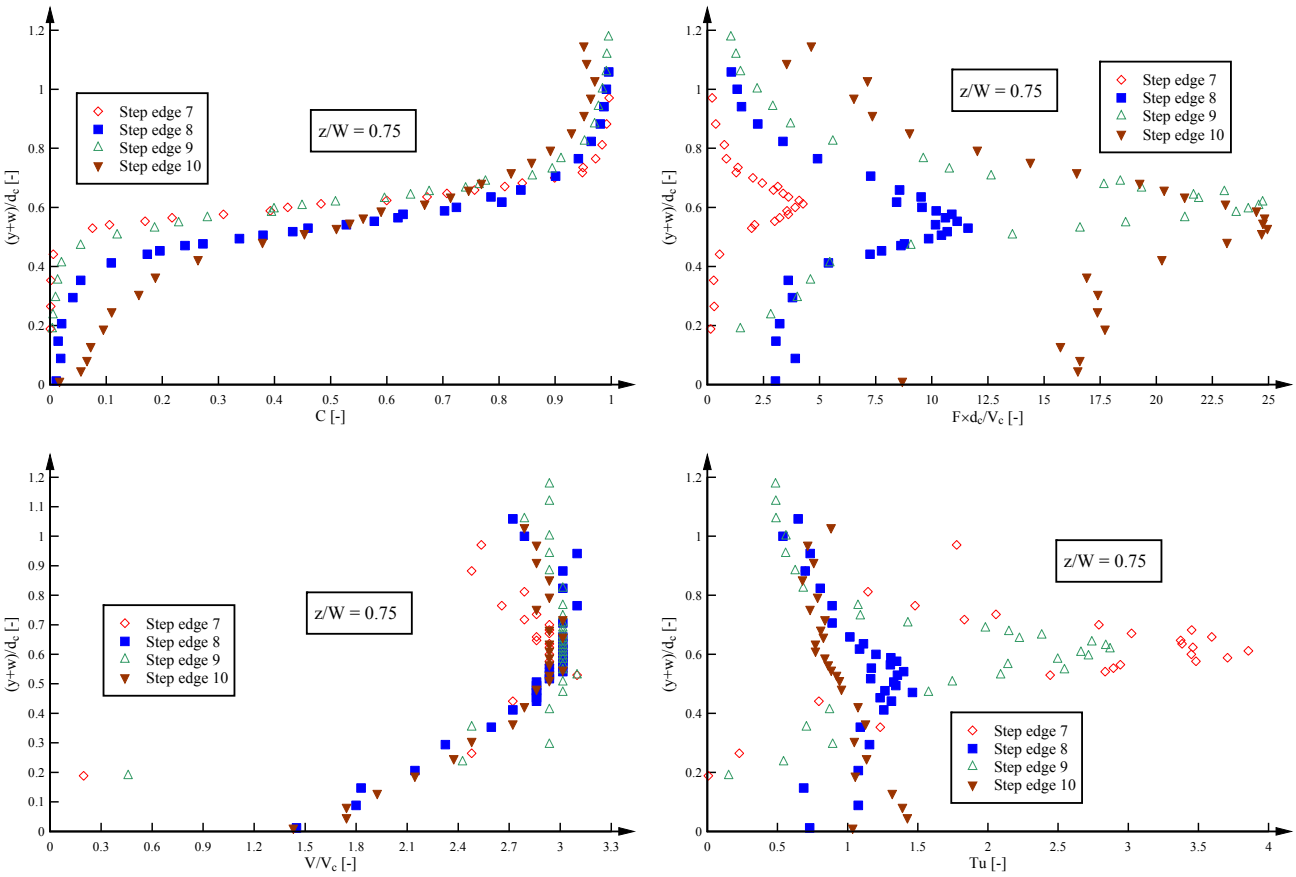

APPENDIX E – AIR-WATER FLOW PROPERTIES IN A PULSATING FLOW ON A POOLED STEPPED SPILLWAY

E.1 PRESENTATION

In the present study, experiments were conducted on a pooled stepped spillway (h = 10 cm, w = 3.1 cm) for a range of flow rates $0.002 \leq Q \leq 0.139$ m^3/s ($0.11 \leq d_c/h \leq 1.94$). For the smallest flow rates $d_c/h < 0.45$, a nappe flow regime existed and the water discharged in a succession of free-falling nappes from one step pool to the following. However, for a flow rate $0.30 \leq d_c/h \leq 0.45$, a pulsating flow was observed in the first step cavity which led to some small instabilities of the free-falling nappes. The pulsations in the first step cavity were periodic with a frequency of about 1 Hz for $d_c/h = 0.3$ while they were observed about every 5 seconds for $d_c/h = 0.45$. The pulsating mechanism was somehow comparable to the self-induced instabilities on a pooled stepped spillway with a slope of 8.9° observed by THORWARTH (2008) and FELDER & CHANSON (2012a). On the 8.9° pooled stepped spillway, the instabilities occurred in the transition flow regime for $1.08 \leq d_c/h \leq 1.76$ and caused some significant flow disturbances including jump waves and instable cavity ejections. The instabilities on the pooled stepped spillway in the present study were much smaller and did not cause significant disturbances of the flow. The flow pattern and the air-water flow properties for a typical flow rate in the pulsating flow Q = 0.013 m^3/s ($d_c/h = 0.4$) are presented in this Appendix.

Notation

C	void fraction defined as the volume of air per unit volume of air and water;
C_{mean}	depth-average void fraction defined in terms of Y_{90}: $C_{mean} = 1 - d/Y_{90}$;
D_H	hydraulic diameter (m);
D_o	dimensionless constant;
d	equivalent clear water flow depth (m);
d_c	critical flow depth (m);
F	air bubble count rate (Hz) defined as the number of detected air bubbles per unit time;
F_{max}	maximum bubble count rate in a cross-section (Hz);
h	vertical step height (m);
K'	dimensionless integration constant;
l	horizontal step length (m);
N	power law exponent;
Q	water discharge (m^3/s);
q_w	water discharge per unit width (m^2/s);
Re	Reynolds number defined in terms of the hydraulic diameter: $Re = \rho_w \times U_w \times D_H/\mu_w$;
Tu	turbulence intensity;

Tu_{max} maximum turbulence intensity in a cross-section;
U_w mean flow velocity (m/s): $U_w = q_w/d$;
V interfacial velocity (m/s);
V_c critical flow velocity (m/s);
V_{90} characteristic interfacial velocity (m/s) where the void fraction is 90%;
w weir height in pooled stepped spillway configuration (m), also called pool height;
Y_{90} characteristic depth (m) where the void fraction is 90%;
y distance (m) measured normal to the invert (or channel bed);
θ angle between pseudo-bottom formed by the step edges and the horizontal;
Ø probe sensor diameter (m).

E.2 AIR-WATER FLOW PATTERNS

Some typical air-water flow patterns of the pulsating flow on the stepped spillway are illustrated in Figures E-1 to E-3 for the dimensionless flow rate $d_c/h = 0.4$. Figure E-1 shows a series of photos of the pulsations in the first step cavity in a side view highlighting the changes in free-surface within the step cavity. During the pulsations, some small waves were ejected from the first step cavity and caused some deviations to the lengths of the free-falling nappes impacting on the next step edges. Figure E-2 shows the pulsations in the first step cavity in a view in flow direction. In Figure E-2, the free-falling nappes are also visible downstream of the first step cavity. With every pulsation, the nappe impact cavity was shifted from the successive step cavity to one step cavity further downstream (Fig. E-3). In Figure E-3, the changes of the nappe flow are illustrated in a view of the whole spillway showing the impact of the pulsations upon the downstream air-water flow patterns. Some deviations of the shapes of the nappes and of the impact area of the free-falling nappes are visible.

Fig. E-1 – Side view of pulsating flow in first step cavity on the pooled stepped spillway ($d_c/h = 0.4$, $Q = 0.013$ m^3/s, $Re = 1.0\times10^5$) - Chronological order from top left corner to bottom right corner

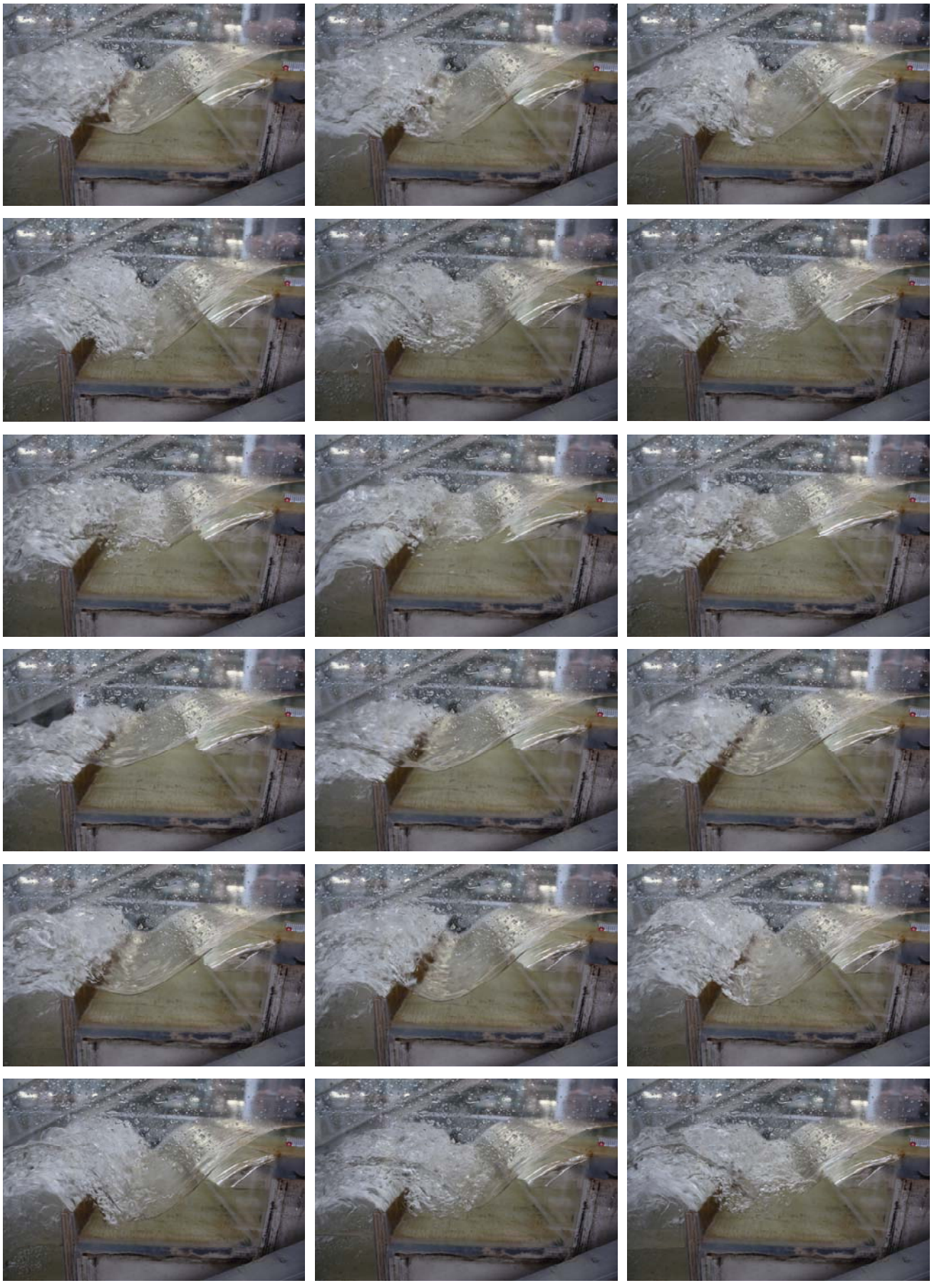

Fig. E-2 – View of pulsating flow in first step cavity in downstream direction on the pooled stepped spillway ($d_c/h = 0.4$, $Q = 0.013$ m^3/s, $Re = 1.0\times10^5$) - Chronological order from top left corner to bottom right corner

Fig. E-3 – Pulsating flow on the pooled stepped spillway ($d_c/h = 0.4$, $Q = 0.013$ m^3/s, $Re = 1.0\times10^5$) - Chronological order from left to right

E.3 CHARACTERISTIC FREQUENCIES

Some detailed analyses of the pulsation frequencies were conducted for $0.30 \leq d_c/h \leq 0.45$. Using some video analysis, the frequencies of the pulsations in the first step edge were visually observed. For the lower boundary of the pulsating flow rates ($d_c/h = 0.3$), the pulsations appeared about every second while, at the upper boundary ($d_c/h = 0.45$), the pulsations were seen about every 5 seconds. The pulsating flow was quasi-periodic for all flow rates.

This section presents the characteristic frequencies for $d_c/h = 0.4$. In a video analysis, the pulsation frequency was identified as about 0.33 Hz (i.e. 3 seconds period). For this flow rate, some detailed air-water flow experiments were conducted with a double-tip conductivity probe for a sampling duration of 180 s with a sampling frequency of 20 kHz per sensor. Some detailed analyses of the raw signals of the double-tip conductivity probe confirmed the visual observations for this flow rate. In Figure E-4, some raw signals of the leading tip conductivity probe are illustrated for two vertical measured positions at step 2, i.e. at the first pooled weir edge downstream of the step cavity with the pulsating flow. The raw signals (Fig. E-4) highlighted the changes in air-water interphases within the pulsating flow. A simple manual count of the phase changes indicated a frequency of the pulsating pattern of about 0.29 to 0.31 Hz which was very close to the characteristic frequencies observed visually.

Please note that it was not possible to observe the interphase changes in any raw signal at any other step edge. From step 3 downstream, the raw signals of the conductivity probe showed a larger number of air-water interface changes linked with a strong aeration of the flow. However, it was possible to notice some characteristic frequencies in a spectral analysis (FFT) of the probe raw signals (Fig. E-5). Figure E-5 shows some typical power spectrum density functions of raw signals of the leading tip of the conductivity probe at several vertical positions and at different step edges. The power spectrum density functions highlighted some characteristic troughs and peaks in a range of about 0.3 to 0.34 Hz (Fig. E-5). These findings confirmed the characteristic pulsation frequencies found during the visual observations and the raw signal analysis at step edge 2.

At the downstream end of the pooled stepped spillway, the pulsating nature of the flow was less pronounced (e.g. Fig. E-3). The FFT spectral analyses at step edges 9 and 10 did not show any characteristic frequencies.

Fig. E-4 – Raw signals of leading tip of double-tip conductivity probe in the pulsating flow on the pooled stepped spillway ($d_c/h = 0.4$, $Q = 0.013$ m^3/s, $Re = 1.0\times10^5$):

(A) Step edge 2, y = 10 mm, C = 0.881, F = 9.89 Hz

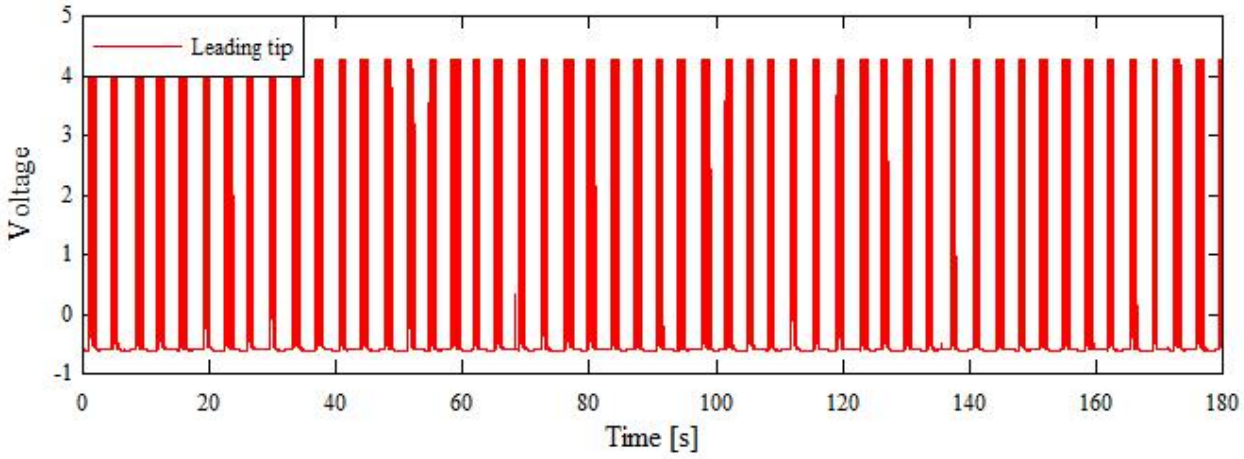

(B) Step edge 2, y = 26 mm, C = 0.548, F = 15.4 Hz

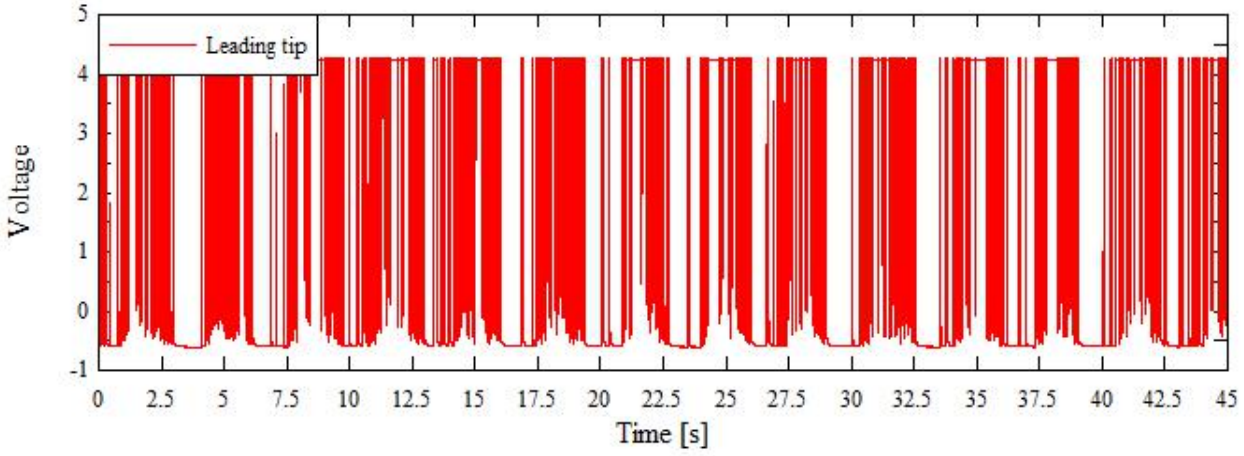

Fig. E-5 – Spectral analysis of the pulsations of the raw phase detection probe signal of the leading tip of a double-tip conductivity probe in the pulsating flow on a pooled stepped spillway ($d_c/h = 0.4$, $Q = 0.013$ m^3/s, Re = 1.0×10^5):

Step edge 3, y = 25 mm, C = 0.670, F = 38.6 Hz

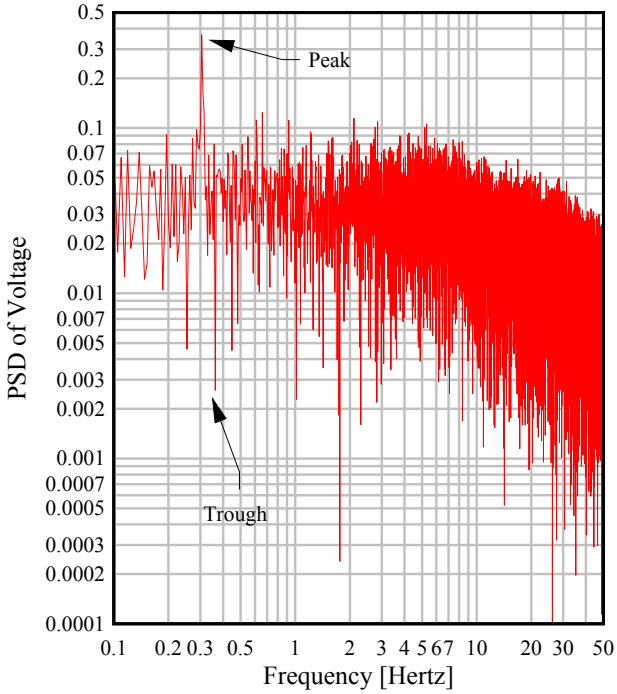

Step edge 5, y = 22 mm, C = 0.490, F = 65.9 Hz

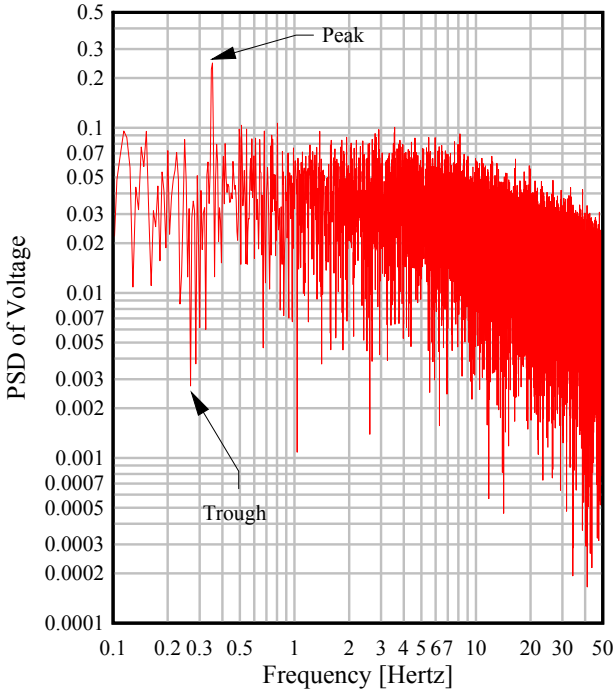

Step edge 6, y = 34 mm, C = 0.493, F = 49.9 Hz

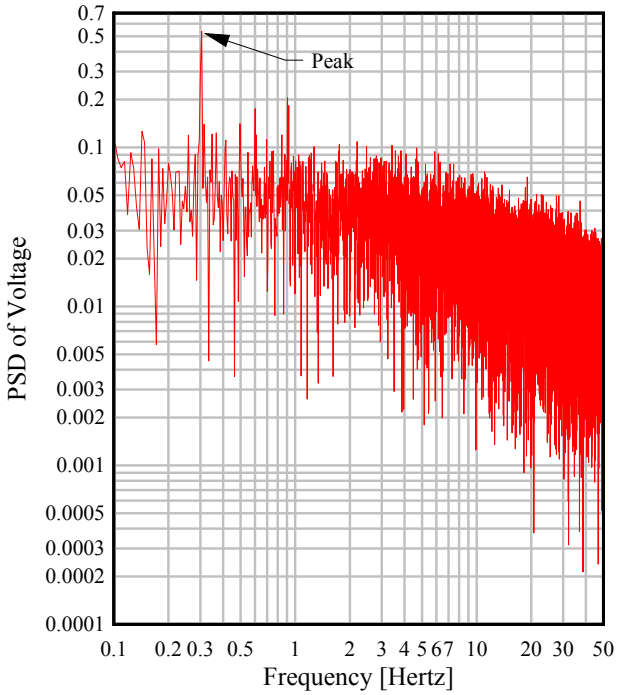

Step edge 8, y = 6 mm, C = 0.374, F = 64.2 Hz

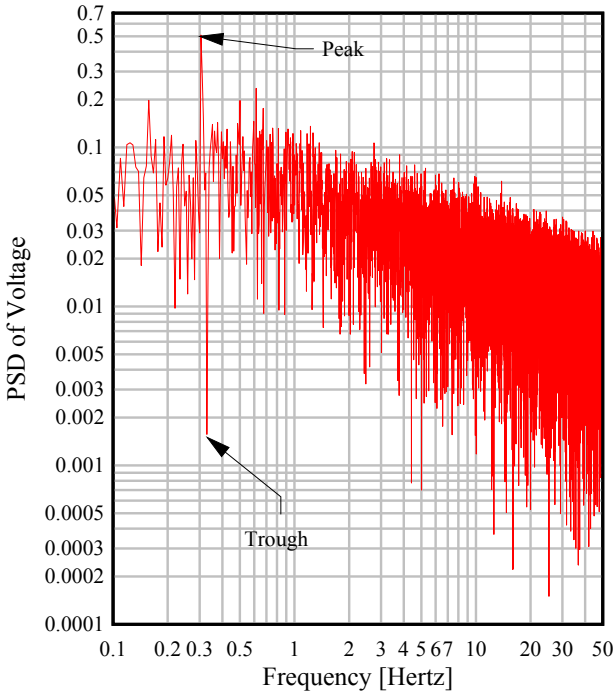

E.4 AIR-WATER FLOW PROPERTIES

For a typical pulsating flow $d_c/h = 0.4$, some detailed analyses of the air-water flow properties was conducted including the void fraction, the bubble count rate, the interfacial velocity and the turbulence intensity. In the section, the characteristic results are presented. Furthermore, some characteristic air-water flow parameters are shown for all step edges.

E.4.1 Void fraction

The void fraction distributions are shown in Figure E-6 as functions of the dimensionless distance perpendicular to the pseudo-bottom formed by the step edges y/Y_{90} (Fig. E-6A) and $(y+w)/d_c$ (Fig. E-6B). Herein Y_{90} is the vertical position where C = 90% and d_c is the critical flow depth. The void fraction distributions showed two different shapes with alternations at every second step edge (Fig. E-6). For step edges 2, 4, 6, 8 and 10, the shapes of the void fraction distributions were qualitatively similar to the observations of TOOMBES & CHANSON (2008) in a free-falling jet. At the other step edges, the void fraction distributions showed some typical S-shapes which were observed in skimming flows in many previous studies on stepped spillways (e.g. CHANSON & TOOMBES 2002; GONZALEZ 2005; BUNG 2011). In Figure E-6A, the S-shaped distributions of void fraction matched very well the advective diffusion equation developed by CHANSON & TOOMBES (2002):

$$C = 1 - \tanh^2\left(K' - \frac{y/Y_{90}}{2 \times D_o} + \frac{(y/Y_{90} - 1/3)^3}{3 \times D_o}\right) \quad \text{(E-1)}$$

where K' is an integration constant and D_o is a function of the depth-averaged void fraction C_{mean} only:

$$K' = 0.32745015 + \frac{1}{2 \times D_o} - \frac{8}{81 \times D_o} \quad \text{(E-2)}$$

$$C_{mean} = 0.7622 \times (1.0434 - \exp(-3.614 \times D_o)) \quad \text{(E-3)}$$

Fig. E-6 – Void fraction distributions in the pulsating flow on the pooled stepped spillway (d_c/h = 0.4, Q = 0.013 m^3/s, Re = 1.0×10^5):

(A) C as function of y/Y_{90} (B) C as function of $(y+w)/d_c$

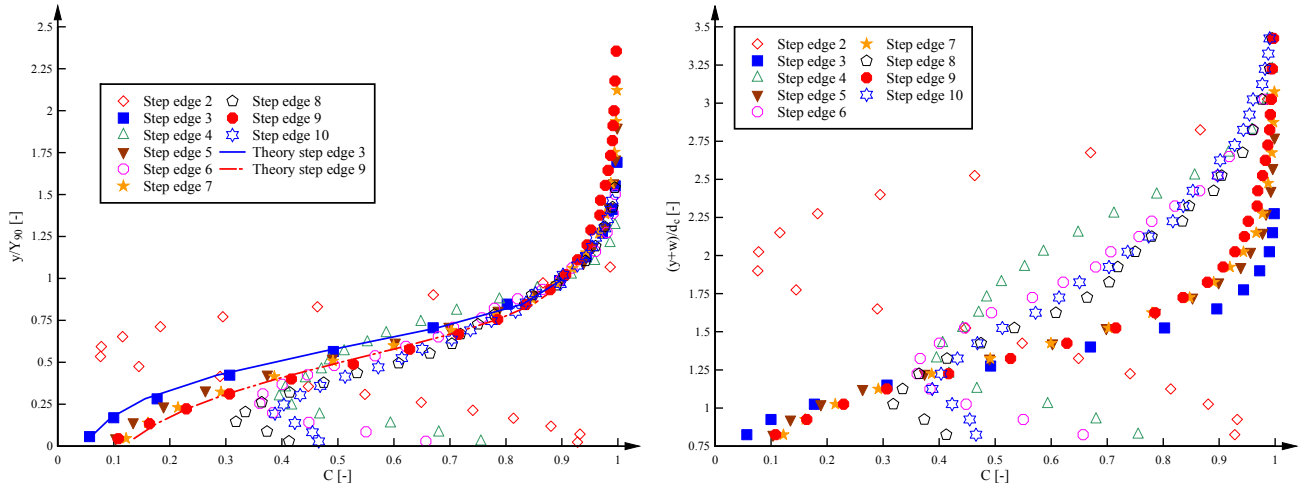

E.4.2 Bubble count rate

The dimensionless bubble count rate $F\times d_c/V_c$ distributions are illustrated in FigureE-7 for all step edges as functions of y/Y_{90} and $(y+w)/d_c$. V_c is the critical flow velocity corresponding to d_c. The distribution of bubble count rates showed typical shapes with maxima for void fractions of about C = 0.3-0.45. A different shape was observed for step edge 2 with a much smaller number of detected bubble and a second smaller peak in the bubble count rate distribution. With increasing distance downstream from the inception point of air entrainment, the bubble frequency increased and no uniform equilibrium flow was observed (Fig. E-7).

Fig. E-7 – Dimensionless bubble count rate distributions in the pulsating flow on the pooled stepped spillway (d_c/h = 0.4, Q = 0.013 m^3/s, Re = 1.0×10^5):

(A) $F\times d_c/V_c$ as function of y/Y_{90} (B) $F\times d_c/V_c$ as function of $(y+w)/d_c$

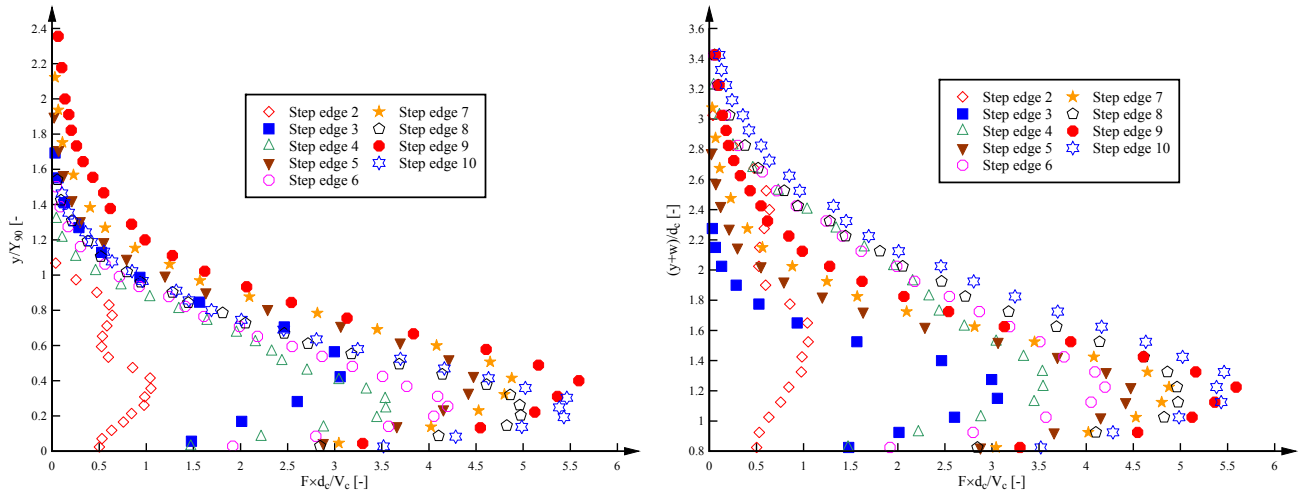

E.4.3 Interfacial velocity

A further air-water flow property is the interfacial time averaged local velocity V which was calculated based upon a cross-correlation analysis of the raw signals of the two tips of the double-tip conductivity probe. The dimensionless interfacial velocity distributions are illustrated in Figure E-8. In Figure E-8A, some distributions of the dimensionless interfacial velocity V/V_{90} are illustrated as a function of y/Y_{90}. Two different shapes of the velocity distributions are visible (Fig. E-8). For the step edges 2, 4, 6, 8 and 10, the interfacial velocity distributions had some shapes similar to those observed at the impact of nappe flow jets (TOOMBES & CHANSON 2008). At the other step edges where some S-shaped void fraction distributions were observed (Fig. E-6), the air-water velocity profiles exhibited a typical power law shape observed in skimming flows. The data there compared well with a power law with exponent of N = 10 (Fig. E-8A):

$$\frac{V}{V_{90}} = \left(\frac{y}{Y_{90}}\right)^{1/N} \qquad 0 \leq y/Y_{90} \leq 1 \text{ (E-4)}$$

For $y/Y_{90} > 1$, the velocity distributions had a uniform profile and were best correlated by:

$$\frac{V}{V_{90}} = 1 \qquad 1 > y/Y_{90} \text{ (E-5)}$$

The distributions of dimensionless interfacial velocity V/V_c (Fig. E-8B) showed similar shapes of V/V_c in the region close to the pool weir edge and some large variations of V/V_c in the flow regions closer to the free-surface.

Fig. E-8 – Dimensionless interfacial velocity distributions in the pulsating flow on the pooled stepped spillway ($d_c/h = 0.4$, $Q = 0.013$ m^3/s, $Re = 1.0\times10^5$):

(A) V/V_{90} as function as y/Y_{90} (B) V/V_c as function of $(y+w)/d_c$

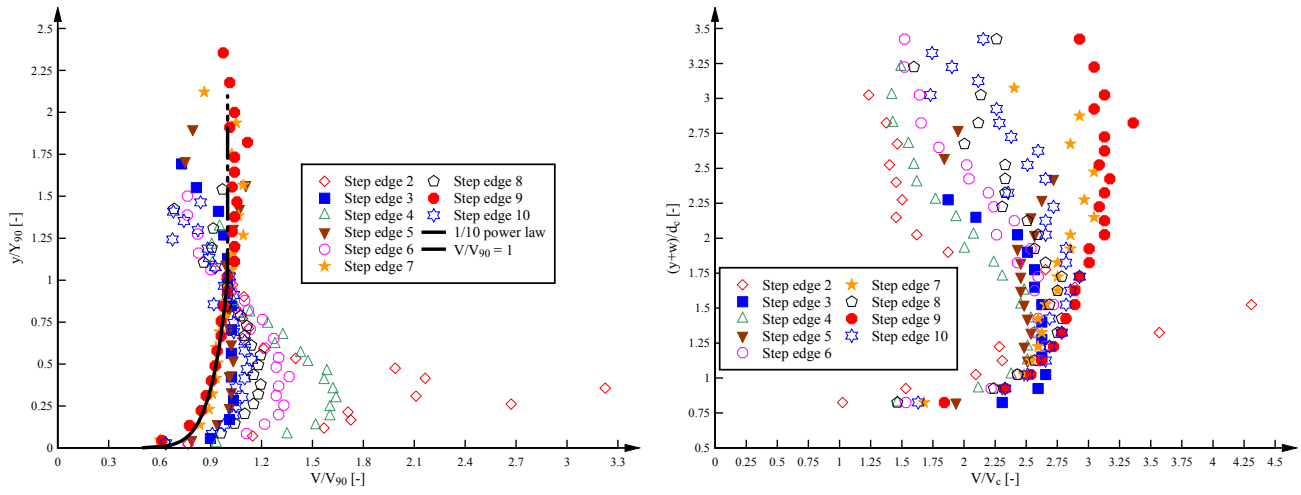

E.4.4 Turbulence intensity

The distributions of the turbulence intensity Tu are illustrated in Figure E-9 as functions of y/Y_{90}

and $(y+w)/d_c$. Similarly to the observations of void fraction and interfacial velocities, two different shapes of the turbulence levels are visible (Fig. E-9). For the step edges with S-shaped void fraction profile, the turbulence intensity distributions showed characteristic shapes similar to skimming flow data with turbulence intensity maxima in the intermediate flow region. For the step edges with void fraction and interfacial velocity distributions similar to impacting nappe flow jets, the turbulence intensities were much larger. The maxima of Tu were about twice as large as on the other step edges and observed also in the intermediate flow region.

Very large turbulence intensities were also observed by FELDER & CHANSON (2012a) and by FELDER et al. (2012) on a pooled stepped spillway with 8.9°. FELDER & CHANSON (2012a) linked the large turbulence levels to some instabilities in the flow on the pooled stepped spillway. They showed that the instationary flow processes contributed significantly to the turbulent kinetic energy of the flow. The large turbulence levels in the present study seem to be linked with the instabilities of the air-water flows caused by the pulsations in the first step cavity. The application of the triple decomposition approach to air-water flows by FELDER & CHANSON (2012a) might identify the contribution of the flow pulsations to the overall turbulence velocity fluctuations.

Fig. E-8 – Turbulence intensity distributions in the pulsating flow on the pooled stepped spillway ($d_c/h = 0.4$, $Q = 0.013$ m^3/s, $Re = 1.0\times10^5$):

(A) Tu as function of y/Y_{90} (B) Tu as function of $(y+w)/d_c$

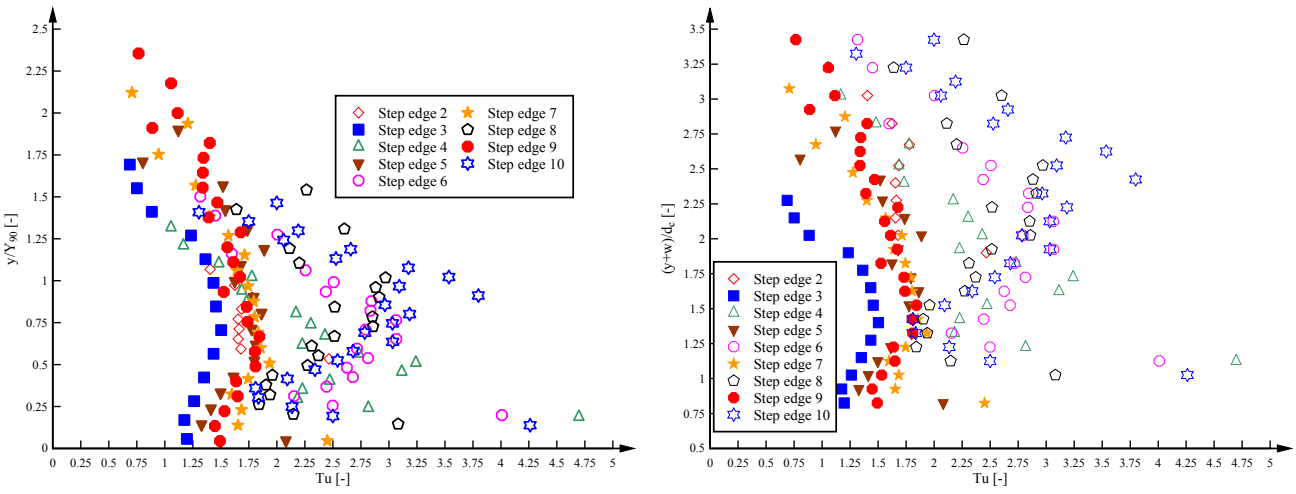

E.4.5 Longitudinal distributions of characteristic air-water flow parameters

Some characteristic air-water flow parameters were calculated for all step edges for the pulsating flow rate $d_c/h = 0.4$. The results are listed in Table E-1 including the mean air concentration C_{mean}, the maximum bubble count rate F_{max}, the characteristic interfacial velocity V_{90}, the mean flow velocity U_w, the equivalent clear-water flow depth d, the characteristic flow depth Y_{90} and the maximum turbulence intensity Tu_{max}. The values in Table E-1 tended to confirm the alternating

pattern of air-water flow properties every second step edge for all investigated parameters.

Some seesaw pattern was observed in several previous studies in skimming flows (BOES 2000; CHANSON & TOOMBES 2002; YASUDA & CHANSON 2003; FELDER & CHANSON 2009b). It was believed to be a characteristic feature of skimming flows on flat stepped spillway (FELDER & CHANSON 2009b). Herein the results were further emphasised by the pulsating nature of the flow. The present findings for the present flow rate on pooled steps highlighted the existence of a strong seesaw pattern of all air-water flow parameters and properties on the pooled stepped spillway.

Table E-1 – Summary of characteristic longitudinal air-water flow parameters in the pulsating flow on the pooled stepped spillway ($Q = 0.013$ m^3/s, $d_c/h = 0.40$, $Re = 1\times10^5$)

Step edge	C_{mean} [-]	F_{max} [Hz]	V_{90} [m/s]	U_w [m/s]	d [m]	Y_{90} [m]	Tu_{max} [-]
(1)	(2)	(3)	(4)	(5)	(6)	(7)	(8)
2	0.487	16.4	0.84	0.58	0.0432	0.0843	2.47
3	0.435	47.9	1.61	1.25	0.0200	0.0354	1.50
4	0.592	55.4	0.98	0.83	0.0303	0.0743	3.24
5	0.472	70.0	1.54	1.13	0.0222	0.0421	1.89
6	0.594	65.7	1.25	0.87	0.0287	0.0706	3.07
7	0.493	76.4	1.74	1.14	0.0220	0.0434	1.94
8	0.593	77.9	1.46	0.89	0.0280	0.0688	2.97
9	0.518	87.5	1.88	1.15	0.0217	0.0450	1.84
10	0.613	85.5	1.60	0.89	0.0280	0.0724	3.80

Notes: C_{mean}: mean void fraction; F_{max}: maximum bubble count rate; V_{90}: characteristic interfacial velocity; U_w: mean flow velocity; d: equivalent clear water flow depth; Y_{90}: characteristic flow depth; Tu_{max}: maximum turbulence intensity.

APPENDIX F – TRANSVERSE AVERAGING OF AIR-WATER FLOW PROPERTIES

F.1 PRESENTATION

Experiments were conducted on a $\theta = 26.6°$ stepped spillway with in-line and staggered configurations of flat and pooled steps. The air-water flow was characterised by some air entrainment by free-surface aeration and some singular aeration processes. Three-dimensional flow motion across the channel width necessitated some air-water flow measurements by double-tip probes at three transverse locations, $z/W = 0.25$, 0.5 and 0.75, where z is the transverse distance measured from the right sidewall and W is the channel width. The measurements delivered a comprehensive data set of the air-water flow properties including distributions of void fraction, bubble count rate, interfacial velocity and turbulence intensity across the channel width W.

Some examples of the unstable and chaotic flow behaviour across the channel width are given in Figure F-1. Note the instabilities in the form of shockwaves and interactions in channel centreline which led to distinct droplet ejection and splashing.

Fig. F-1 - Three-dimensional flow motions on the stepped spillways with non-uniform step shape across the channel width

(A) Stepped spillway with in-line configuration of flat and pooled steps

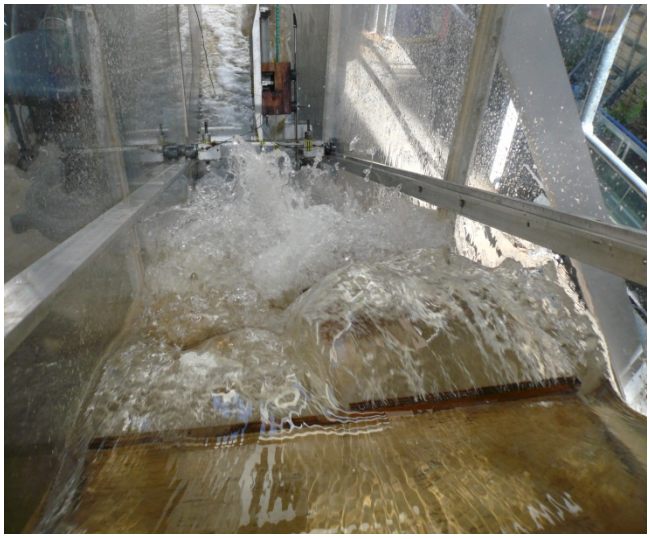

(B) Stepped spillway with staggered configuration of flat and pooled steps

The air-water flow measurements with a double-tip probe showed some significant differences between the three transverse measurement positions. The results for the stepped spillway model with in-line configuration were significantly different between the two sections of the channel.

The measurement positions for the two configurations are shown in Fig. F-2. The double-tip probe

was set at the step or pool edge respectively as the reference position. Some significant differences in terms of the air-water flow properties were presented in chapter 5 and the complete data set was summarised in Appendix D.

Fig. F-2 - Three-dimensional flow motion of the stepped spillway with non-uniform step shape across the channel width

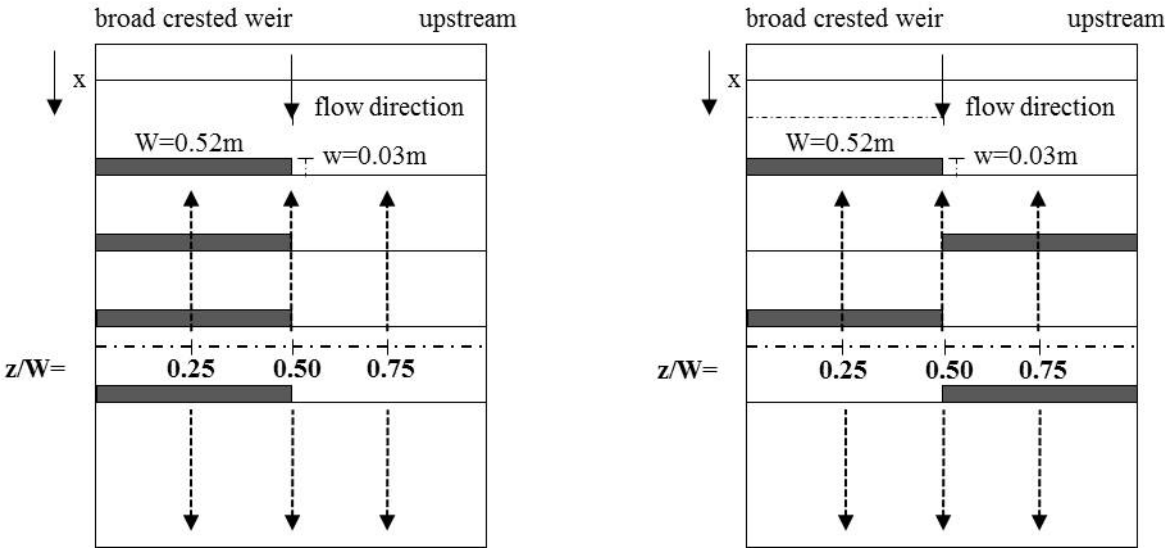

F.2 SENSITIVITY ANALYSIS OF TRANSVERSE AVERAGING APPROACHES

The air-water flow parameters on the stepped spillways with in-line and staggered configuration of flat and pooled steps showed some significant differences in transverse direction at the same step edge for the same low rate. These differences were seen in terms of the air concentration, the velocity and the flow depth and consequently the residual head and the energy dissipation along the stepped spillway. A transverse averaging approach was used to quantify an average air-water flow parameters and the energy dissipation across the channel width. Several transverse averaging approaches were tested using a factored approach for the air-water flow parameters. Herein the mean air concentration C_{mean} could be averaged in transverse direction:

$$C_{mean} = a \times (C_{mean})_{0.25} + b \times (C_{mean})_{0.5} + a \times (C_{mean})_{0.75} \quad (F\text{-}1)$$

with $2 \times a + b = 1$. Equation (F-1) represents the transverse averaged value C_{mean} with $(C_{mean})_{0.25}$ the mean air concentration measured at the transverse position z/W=0.25, $(C_{mean})_{0.5}$ measured at z/W=0.50 and $(C_{mean})_{0.75}$ measured at z/W=0.75. The effects of the factors a and b were tested with a sensitivity analysis (Table F-1). Table F-1 lists the values of the coefficients a and b which were investigated in terms of the mean air concentration C_{mean} and characteristic interfacial velocity V_{90}.

The results for the sensitivity analysis are shown in Figure F-3 for V_{90} and C_{mean} for two characteristic flow rates in transition and skimming flows at all step edges downstream of the

inception point. Figure F-3 illustrates the values of C_{mean} and V_{90} at the three transverse positions as well as the different transverse averaging results for experiments on the stepped spillway with in-line configuration of flat and pooled steps.

Figure F-3 highlights the clear differences between the air-water flow parameters in transverse direction. Furthermore, it shows that several transverse averaging approaches lead to similar results close to the air-water flow measurements in channel centre line. In the present study, the transverse averaging approach 4 with values of a = 0.375 and b = 0.25 was identified as providing a meaningful transverse averaging results.

Table F-1 – Summary of investigated factors a and b for the sensitivity analysis for the transverse averaging approach

Approach No. 1		Approach No. 2		Approach No. 3		Approach No. 4		Approach No. 5		Approach No. 6	
a (1)	b (2)	a (3)	b (4)	a (5)	b (6)	a (7)	b (8)	a (9)	b (10)	a (11)	b (12)
0	1	0.25	0.5	0.33	0.33	0.375	0.25	0.4375	0.125	0.5	0

Fig. E-3 – Effect of the transverse averaging factors a and b on the air-water flow parameters on the stepped spillway with in-line configuration of flat and pooled steps (θ = 26.6°)

(A) Mean air concentration C_{mean}: d_c/h = 0.70, Q = 0.030 m^3/s, Re = 2.30×10^5

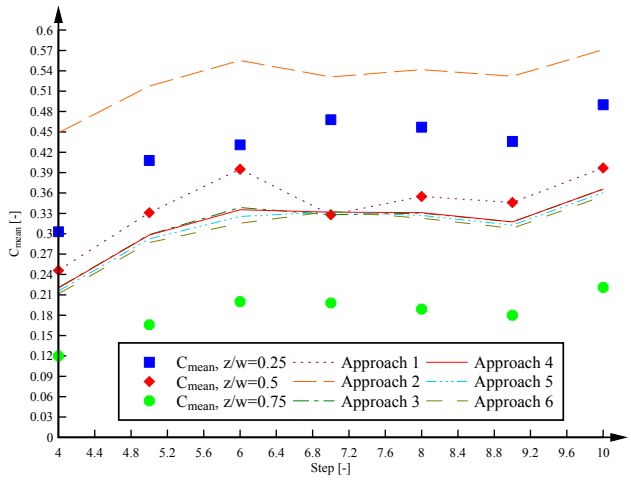

(B) Characteristic interfacial velocity V_{90}: d_c/h = 1.15, Q = 0.063 m^3/s, Re = 4.9×10^5

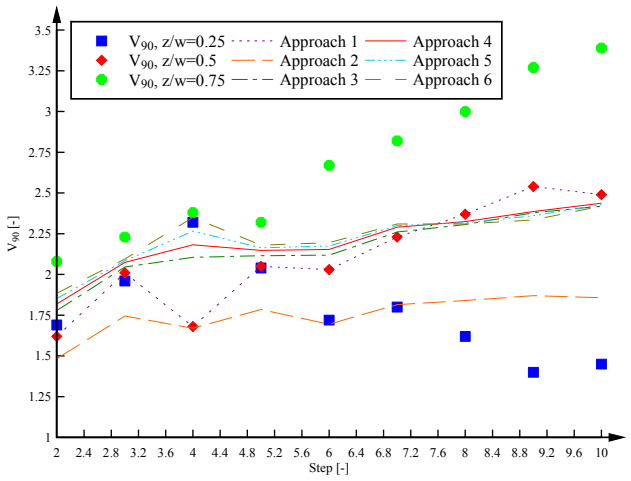

F.3 TRANSVERSE AVERAGING OF LOCAL FLOW RATE, RESIDUAL HEAD AND FRICTION FACTORS

The transverse averaging approach was applied to all air-water flow parameters in the present study. It was used for the calculation of the residual energy and the Darcy friction factors for the stepped spillways with in-line and staggered configurations of flat and pooled steps. The transverse-

averaged residual head for these configurations was calculated as:

$$H_{res} = 0.375 \times \left(d_{local} \times \cos\theta + \frac{U_{local}^{2}}{2 \times g} + w \right)_{0.25} + 0.25 \times \left(d_{local} \times \cos\theta + \frac{U_{local}^{2}}{2 \times g} + w \right)_{0.5} + 0.375 \times \left(d_{local} \times \cos\theta + \frac{U_{local}^{2}}{2 \times g} + w \right)_{0.75} \quad \text{(F-2)}$$

where the numbers in subscript indicated the residual energy at the three transverse measurement locations z/W on the in-line and staggered stepped spillway configurations, d_{local} is the local flow depth for each measurement location and U_{local} is the local flow velocity. The calculation of U_{local} was based upon the calculation of local flow rates:

$$q_{local} = \int_{0}^{Y_{90}} V \times (1 - C) \times dy = U_{local} \times d_{local} \quad \text{(F-3)}$$

Similarly the Darcy-Weisbach friction factors for the stepped spillways with in-line and staggered configurations of flat and pooled stepped steps were calculated using the transverse averaging approach of the air-water flow properties:

$$f_e = 0.375 \times \left(\frac{8 \times g \times S_f \times d_{local}}{U_{local}^{2}} \right)_{0.25} + 0.25 \times \left(\frac{8 \times g \times S_f \times d_{local}}{U_{local}^{2}} \right)_{0.5} + 0.375 \times \left(\frac{8 \times g \times S_f \times d_{local}}{U_{local}^{2}} \right)_{0.75} \quad \text{(6-3)}$$

where the friction slope equals $S_f = - \partial H / \partial x$, H is the transverse-averaged total head, x is the distance in flow direction, C is the void fraction, Y_{90} is the flow depth where C = 90%, d is the equivalent clear water flow depth and U_w is the flow velocity (HENDERSON 1966; CHANSON 2001).

REFERENCES

ANDRÉ, S. (2004). "High velocity aerated flows on stepped chutes with macro-roughness elements." Ph.D. thesis, Laboratoire de Constructions Hydraulics (LCH), EPFL, Lausanne, Switzerland, 272 pages.

AMADOR, A.; SANCHEZ-JUNY, M. and DOLZ, J. (2006). "Characterization of the Nonaerated Flow Region in a Stepped Spillway by PIV." Jl of Fluids Eng., ASME, Vol. 128, No. 6, pp. 1266-1273.

BOES, R.M. (2000). "Zweiphasenströmung und Energieumsetzung an Grosskaskaden." ("Two-Phase Flow and Energy Dissipation on Cascades.") Ph.D. thesis, VAW-ETH, Zürich, Switzerland (in German). (also Mitteilungen der Versuchsanstalt für Wasserbau, Hydrologie and Glaziologie, ETH-Zürich, Switzerland, No. 166).

BUNG, D.B. (2011). "Developing flow in skimming flow regime on embankment stepped spillways. " Journal of Hydraulic Research, IAHR, Vol. 49, No 5, pp. 639-648.

CAROSI, G. and CHANSON, H. (2006). "Air-water time and length scales in skimming flow on a stepped spillway. Application to the spray characterisation." Report no. CH59/06, Division of Civil Engineering, The University of Queensland, Brisbane, Australia, July, 142 pages (ISBN 1864998601).

CAROSI, G., and CHANSON, H. (2008). "Turbulence Characteristics in Skimming Flows on Stepped Spillways." Canadian Journal of Civil Engineering, Vol. 35, No. 9, pp. 865-880 (DOI:10.1139/L08-030).

CHAMANI, M.R. (2000). "Air Inception in Skimming Flow Regime over Stepped Spillways." Proc. International Workshop on Hydraulics of Stepped Spillways, Zürich, Switzerland, H.E. MINOR & W.H. HAGER Editors, Balkema Publ., pp. 61-67.

CHANSON, H. (1994). "Hydraulics of Nappe Flow Regime above Stepped Chutes and Spillways." Australian Civil Engineering Transactions, Iinstitution of Engineers, Australia, Vol. CE36, No. 1, Jan., pp. 69-76.

CHANSON, H. (1995). "Hydraulic Design of Stepped Cascades, Channels, Weirs and Spillways." Pergamon, Oxford, UK, Jan., 292 pages (ISBN 0-08-041918-6).

CHANSON, H. (2001). "The Hydraulics of Stepped Chutes and Spillways." Balkema, Lisse, The Netherlands (ISBN 90 5809 352 2).

CHANSON, H. (2002). "Air-Water Flow Measurements with Intrusive Phase-Detection Probes. Can we Improve their Interpretation ?." *Jl of Hyd. Engrg.*, ASCE, Vol. 128, No. 3, pp. 252-255.

CHANSON, H. (2009). "Turbulent Air-water Flows in Hydraulic Structures: Dynamic Similarity and Scale Effects." Environmental Fluid Mechanics, Vol. 9, No. 2, pp. 125-142 (DOI: 10.1007/s10652-008-9078-3).

CHANSON, H., and CAROSI, G. (2006). "Advanced Post-Processing and Correlation Analyses in High-Velocity Air-Water Flows. 2- Microscopic Properties." Proceedings of the International Junior Researcher and Engineer Workshop on Hydraulic Structures (IJREWHS'06), Montemor-o-Novo, Jorge MATOS and Hubert CHANSON Eds., Report CH61/06, Div. of Civil

Engineering, The University of Queensland, Brisbane, Australia, Dec., pp 149-158 (ISBN 1864998687).

CHANSON, H. and CAROSI, G. (2007). "Turbulent time and length scale measurements in high velocity open channel flows." Experiments in Fluids Vol. 42, No. 3, pp. 385-401.

CHANSON, H. and FELDER, S. (2010). "Turbulence Measurements in Air-Water Self-Aerated Flows: Basic Analysis and Results." in: J.S. CURTIS and S. BALACHANDAR, 7th International Conference on Multiphase Flow ICMF 2010, Tampa FL, USA.

CHANSON, H., and TOOMBES, L. (2001). "Experimental Investigations of Air Entrainment in Transition and Skimming Flows down a Stepped Chute. Application to Embankment Overflow Stepped Spillways." Research Report No. CE158, Dept. of Civil Engineering, The University of Queensland, Brisbane, Australia, July, 74 pages (ISBN 1 864995297).

CHANSON, H. and TOOMBES, L. (2002). "Air-Water Flows down Stepped chutes: Turbulence and Flow Structure Observations." International Journal of Multiphase Flow, Vol. 28, No. 11, pp. 1737-1761.

CHANSON, H., and TOOMBES, L. (2002b). "Experimental Investigations of Air Entrainment in Transition and Skimming Flows down a Stepped Chute." Canadian Journal of Civil Engineering, Vol. 29, No. 1, pp. 145-156.

CHANSON, H. and TOOMBES, L. (2004). "Hydraulics of stepped chutes: The transition flow." Journal of Hydraulic Research, Vol. 42, No. 1, pp. 43-54.

CHANSON, H., YASUDA, Y. and OHTSU, I. (2002). "Flow Resistance in Skimming Flows and its Modelling." Canadian Journal of Civil Engineering, Vol. 29, No. 6, pp. 809-819.

DJENIDI, L., ELAVARASAN, R. and ANOTONIA, R.A. (1999). “The Turbulent Boundary Layer over Transverse Square Cavities.” Journal of Fluid Mechanics, Vol. 395, pp. 271-294.

ELAVARASAN, R., PEARSON, B.R. and ANTONIA, R.A. (1995). ”Visualization of Near Wall Region in a Turbulent Boundary Layer over Transverse Square Cavities with Different Spacing.” Proc. 12th Australian Fluid Mechanics Conf. AFMC, Sydney, Australia, Vol. 1, pp. 485-488.

FELDER, S., and CHANSON, H. (2008). "Turbulence and Turbulent Length and Time Scales in Skimming Flows on a Stepped Spillway. Dynamic Similarity, Physical Modelling and Scale Effects." Hydraulic Model Report No. CH64/07, School of Civil Engineering, The University of Queensland, Brisbane, 217 pages.

FELDER, S., and CHANSON, H. (2009a). "Energy dissipation, flow resistance and gas-liquid interfacial area in skimming flows on moderate-slope stepped spillways." Environmental Fluid Mechanics, Vol. 9, No. 4, pp. 427-441.

FELDER, S., and CHANSON, H. (2009b). "Turbulence, Dynamic Similarity and Scale Effects in High-Velocity Free-Surface Flows above a Stepped Chute." Experiments in Fluids, Vol. 47, No. 1, pp. 1-18.

FELDER, S., and CHANSON, H. (2011a). "Air-Water Flow Properties in Step Cavity down a Stepped Chute." International Journal of Multiphase Flow, Vol. 37, No. 7, pp. 732–745.

FELDER, S., and CHANSON, H. (2011b). "Energy Dissipation down a Stepped Spillway with Non-Uniform Step Heights." Journal of Hydraulic Engineering, ASCE, Vol. 137, No. 11, pp. 1543-1548.

FELDER, S., and CHANSON, H. (2012a). "Air-Water Flow Measurements in Instationary Free-Surface Flows: a Triple Decomposition Technique." Hydraulic Model Report No. CH85/12, School of Civil Engineering, The University of Queensland, Brisbane, Australia (ISBN 9781742720494).

FELDER, S., and CHANSON, H. (2012b). "Free-surface Profiles, Velocity and Pressure Distributions on a Broad-Crested Weir: a Physical study." Journal of Irrigation and Drainage Engineering., ASCE, Vol. 138, No. 12, pp. XXXX (DOI: 10.1061/(ASCE)IR.1943-4774.0000515) (accepted for publication)

FELDER, S., FROMM, C. and CHANSON, H. (2012). "Air Entrainment and Energy Dissipation on a 8.9° Slope Stepped Spillway with Flat and Pooled Steps." Hydraulic Model Report No. CH86/12, School of Civil Engineering, The University of Queensland, Brisbane, Australia (ISBN 9781742720531).

GONZALEZ, C.A. (2005). "An Experimental Study of Free-Surface Aeration on Embankment Stepped Chutes." Ph.D. thesis, Department of Civil Engineering, The University of Queensland, Brisbane, Australia, 240 pages

GONZALEZ, C.A. and CHANSON, H. (2004). "Interactions between Cavity Flow and Main Stream Skimming Flows: an Experimental Study" Canadian Journal of Civil Engineering, Vol. 31, No. 1, pp. 33-44.

GONZALEZ, C.A., and CHANSON, H. (2008). "Turbulence Manipulation in Embankment Stepped Chute Flows: an Experimental Study." European Journal of Mechanics B/Fluids, Vol. 27, No. 4, pp. 388-408.

HAGER, W.H. and MAZUMDER, S.K. (1992). "Supercritical Flow at Abrupt Expansions." Proc. Institution Civil Engineers Water, Maritime. & Energy, UK, Vol. 96, Sept., pp. 153-166.

HENDERSON, F.M. (1966). "Open Channel Flow." MacMillan Company, New York, USA, 522 pages (ISBN 0-02-353510-5).

HORNER, M.W. (1969). "An Analysis of Flow on Cascades of Steps." Ph.D. thesis, University of Birmingham, UK, 357 pages.

KÖKPINAR, M.A. (2004). "Flow over a Stepped Chute with and without Macro-Roughness Elements." Can. Jl of Civil Engineering, Vol. 31, No. 5, pp. 880-891.

MATOS, J., YASUDA, Y., and CHANSON, H. (2001). "Interaction between Free-surface Aeration and Cavity Recirculation in Skimming Flows down Stepped Chutes." Proc. 29th IAHR Congress, Beijing, China, Theme D, Vol. 2, Tsinghua University Press, Beijing, G. LI Ed., pp. 611-617. (CD-ROM, Tsinghua University Press, ISBN 7-900637-10-9.)

MEIRELES, I. and MATOS, J. (2009). "Skimming Flow in the Nonaerated Region of Stepped Spillways over Embankment Dams." Journal of Hydraulic Engineering- ASCE, Vol. 135, No. 8, pp. 685-689.

OHTSU, I. and YASUDA, Y. (1997). "Characteristics of Flow Conditions on Stepped Channels." Proc. 27th IAHR Biennial Congress, San Francisco, USA, Theme D, pp. 583-588.

PEYRAS, L.; ROYET, P. and DEGOUTTE, G. (1992). "Flow and Energy Dissipation over Stepped Gabion Weirs." Jl of Hydraulic Engineering, ASCE, Vol. 118, No. 5, pp. 707-717.

RAJARATNAM, N. (1990). “Skimming Flow in Stepped Spillways.” Jl of Hydraulic Engineering, ASCE, Vol. 116, No. 4, pp. 587-591.

RELVAS, T.R. and PINHEIRO, A.N. (2008). "Inception Point and Air Concentration in Flows on Stepped Chutes lined with Wedge-shaped Concrete Blocks." Jl. of Hydraulic Engineering, ASCE, Vol. 134, No.8, pp. 1042-1051.

RELVAS, T.R. and PINHEIRO, A.N. (2011). "Velocity distribution and energy dissipation along stepped chutes lined with wedge-shaped concrete blocks." Jl. of Hydraulic Engineering, ASCE, Vol. 137, No.4, pp. 423-431.

SCHWALT, M. and HAGER, W.H. (1993). "Supercritical Flow Deflection." Proc. of 25th IAHR Congress, Tokyo, Japan, Volume I, Paper A-10-4, pp 345-352.

SORENSEN, R.M. (1985). "Stepped Spillway Hydraulic Model Investigation." Jl. of Hydraulic Engineering, ASCE, Vol. 111, No.12, pp. 1461-1472.

TAKAHASHI, M., YASUDA, Y., and OHTSU, I. (2008). "Flow Patterns and Energy Dissipation over Various Stepped Chutes. Discussion." Journal of Irrigation and Drainage Engineering, ASCE, Vol. 134, No. 1, pp. 114-116.

THORWARTH, J. (2008). "Hydraulisches Verhalten der Treppengerinne mit eingetieften Stufen – Selbstinduzierte Abflussinstationaritäten und Energiedissipation." ("Hydraulics of Pooled Stepped Spillways – Self-induced Unsteady Flow and Energy Dissipation.") Ph.D. thesis, University of Aachen, Germany (in German).

THORWARTH, J. and KÖNGETER, J. (2006). "Physical Model Test on a Stepped Chute with Pooled Steps – Investigation of Flow Resistance and Flow Instabilities." In: Recent Developments on Hydraulic Structures: From Hybrid Modelling to Operation and Repairs; Cuidad Guayana, Venezuela, October 2006 [International symposium on Hydraulic Structures] / Ed. by Arturo MARCANO et al., Caracas, Venezuela: Venezuelan Society of Hydraulic Engineering, pp. 477 - 486 (ISBN 980-12-2177-1).

TOOMBES, L. (2002). "Experimental Study of Air-Water Flow Properties on Low-Gradient Stepped Cascades." Ph.D. thesis, Dept. of Civil Engineering, University of Queensland, Australia.

TOOMBES, L., and CHANSON, H. (2007). "Surface Waves and Roughness in Self-Aerated Supercritical Flow." Environmental Fluid Mechanics, Vol. 7, No. 3, pp. 259-270

TOOMBES, L. and CHANSON, H. (2008a). "Flow Patterns in Nappe Flow Regime down Low Gradient Stepped Chutes." Journal of Hydraulic Research, IAHR, Vol. 46, No. 1, pp. 4-14.

TOOMBES, L. and CHANSON, H. (2008b). "Interfacial Aeration and Bubble Count Rate Distributions in a Supercritical Flow past a Backward-Facing Step." International Journal of Multiphase Flow, Vol. 34, No. 5, pp. 427-436.

WOOD, I.R. (1991). "Air Entrainment in Free-Surface Flows." IAHR Hydraulic Structures Design Manual No. 4, Hydraulic Design Considerations, Balkema Publ., Rotterdam, The Netherlands, 149 pages.

YASUDA, Y. and CHANSON, H. (2003). "Micro- and Macro-scopic Study of Two-Phase Flow on a Stepped Chute." Proc. 30th IAHR Biennial Congress, Thessaloniki, Greece, J. GANOULIS and P. PRINOS Ed., Vol. D, pp. 695-702

Bibliography

CAROSI, G. and CHANSON, H. (2006). "Air-Water Time and Length Scales in Skimming Flows on a Stepped Spillway. Application to the Spray Characterisation." Report No. CH59/06, Div. of Civil Engineering, The University of Queensland, Brisbane, Australia, July, 142 pages (ISBN 1864998601).

CHANSON, H. (2009). "Embankment Overtopping Protections System and Earth Dam Spillways." in "Dams: Impact, Stability and Design", Nova Science Publishers, Hauppauge NY, USA, Ed. W.P. HAYES and M.C. BARNES, Chapter 4, pp. 101-132 (ISBN 978-1-60692-618-5).

CHANSON, H., and TOOMBES, L. (1997). "Flow Aeration at Stepped cascades." Research Report No. CE155, Dept. of Civil Engineering, University of Queensland, Australia, June, 110 pages (ISBN 0 86776 730 8).

TOOMBES, L., and CHANSON, H. (2007). "Free-Surface Aeration and Momentum Exchange at a Bottom Outlet." *Journal of Hydraulic Research*, IAHR, Vol. 45, No. 1, pp. 100-110

Internet bibliography

Research papers in hydraulic engineering (open access)	{http://espace.library.uq.edu.au/list/author_id/193/}
Air entrainment on chute and stepped spillways	{http://www.uq.edu.au/~e2hchans/self_aer.html}
Embankment overflow stepped spillways: earth dam spillways with precast concrete blocks	{http://www.uq.edu.au/~e2hchans/over_st.html}

Bibliographic reference of the Report CH87/12

The Hydraulic Model research report series CH is a refereed publication published by the School of Civil Engineering at the University of Queensland, Brisbane, Australia.

The bibliographic reference of the present report is:

FELDER, S., GUENTHER, P., and CHANSON, H. (2012). "Air-Water Flow Properties and Energy Dissipation on Stepped Spillways: a Physical Study of Several Pooled Stepped Configurations." *Hydraulic Model Report No. CH87/12*, School of Civil Engineering, The University of Queensland, Brisbane, Australia, 228 pages (ISBN 9781742720555).

The Report CH87/12 is available, in the present form, as a PDF file on the Internet at UQeSpace:

http://espace.library.uq.edu.au/

It is listed at:

http://espace.library.uq.edu.au/list/author_id/193/

HYDRAULIC MODEL RESEARCH REPORT CH

The Hydraulic Model Report CH series is published by the School of Civil Engineering at the University of Queensland. Orders of any reprint(s) of the Hydraulic Model Reports should be addressed to the School Secretary.

School Secretary, School of Civil Engineering, The University of Queensland
Brisbane 4072, Australia - Tel.: (61 7) 3365 3619 - Fax : (61 7) 3365 4599
Url: http://www.eng.uq.edu.au/civil/ Email: hodciveng@uq.edu.au

Report CH	**Unit price**	Quantity	**Total price**
REUNGOAT, D., CHANSON, H., and CAPLAIN, B. (2012). "Field Measurements in the Tidal Bore of the Garonne River at Arcins (June 2012)." Hydraulic Model Report No. CH89/12, School of Civil Engineering, The University of Queensland, Brisbane, Australia, 121 pages (ISBN 9781742720616).	AUD$60.00		
CHANSON, H., and WANG, H. (2012). "Unsteady Discharge Calibration of a Large V-Notch Weir." *Hydraulic Model Report No. CH88/12*, School of Civil Engineering, The University of Queensland, Brisbane, Australia, 50 pages & 4 movies (ISBN 9781742720579).	AUD$60.00		
FELDER, S., GUENTHER, P., and CHANSON, H. (2012). "Air-Water Flow Properties and Energy Dissipation on Stepped Spillways: a Physical Study of Several Pooled Stepped Configurations." *Hydraulic Model Report No. CH87/12*, School of Civil Engineering, The University of Queensland, Brisbane, Australia, 228 pages (ISBN 9781742720555).	AUD$60.00		
FELDER, S., FROMM, C., and CHANSON, H. (2012). "Air Entrainment and Energy Dissipation on a 8.9° Slope Stepped Spillway with Flat and Pooled Steps." *Hydraulic Model Report No. CH86/12*, School of Civil Engineering, The University of Queensland, Brisbane, Australia, 80 pages (ISBN 9781742720531).	AUD$60.00		
FELDER, S., and CHANSON, H. (2012). "Air-Water Flow Measurements in Instationary Free-Surface Flows: a Triple Decomposition Technique." *Hydraulic Model Report No. CH85/12*, School of Civil Engineering, The University of Queensland, Brisbane, Australia, 161 pages (ISBN 9781742720494).	AUD$60.00		
REICHSTETTER, M., and CHANSON, H. (2011). "Physical and Numerical Modelling of Negative Surges in Open Channels." *Hydraulic Model Report No. CH84/11*, School of Civil Engineering, The University of Queensland, Brisbane, Australia, 82 pages (ISBN 9781742720388).	AUD$60.00		
BROWN, R., CHANSON, H., McINTOSH, D., and MADHANI, J. (2011). "Turbulent Velocity and Suspended Sediment Concentration Measurements in an Urban Environment of the Brisbane River Flood Plain at Gardens Point on 12-13 January 2011." *Hydraulic Model Report No. CH83/11*, School of Civil Engineering, The University of Queensland, Brisbane, Australia, 120 pages (ISBN 9781742720272).	AUD$60.00		
CHANSON, H. "The 2010-2011 Floods in Queensland (Australia): Photographic Observations, Comments and Personal Experience." *Hydraulic Model Report No. CH82/11*, School of Civil Engineering, The University of Queensland, Brisbane, Australia, 127 pages (ISBN 9781742720234).	AUD$60.00		

MOUAZE, D., CHANSON, H., and SIMON, B. (2010). "Field Measurements in the Tidal Bore of the Sélune River in the Bay of Mont Saint Michel (September 2010)." *Hydraulic Model Report No. CH81/10*, School of Civil Engineering, The University of Queensland, Brisbane, Australia, 72 pages (ISBN 9781742720210).	AUD$60.00		
JANSSEN, R., and CHANSON, H. (2010). "Hydraulic Structures: Useful Water Harvesting Systems or Relics." *Proceedings of the Third International Junior Researcher and Engineer Workshop on Hydraulic Structures (IJREWHS'10)*, 2-3 May 2010, Edinburgh, Scotland, R. JANSSEN and H. CHANSON (Eds), Hydraulic Model Report CH80/10, School of Civil Engineering, The University of Queensland, Brisbane, Australia, 211 pages (ISBN 9781742720159).	AUD$60.00		
CHANSON, H., LUBIN, P., SIMON, B., and REUNGOAT, D. (2010). "Turbulence and Sediment Processes in the Tidal Bore of the Garonne River: First Observations." *Hydraulic Model Report No. CH79/10*, School of Civil Engineering, The University of Queensland, Brisbane, Australia, 97 pages (ISBN 9781742720104).	AUD$60.00		
CHACHEREAU, Y., and CHANSON, H., (2010). "Free-Surface Turbulent Fluctuations and Air-Water Flow Measurements in Hydraulics Jumps with Small Inflow Froude Numbers." *Hydraulic Model Report No. CH78/10*, School of Civil Engineering, The University of Queensland, Brisbane, Australia, 133 pages (ISBN 9781742720036).	AUD$60.00		
CHANSON, H., BROWN, R., and TREVETHAN, M. (2010). " Turbulence Measurements in a Small Subtropical Estuary under King Tide Conditions." *Hydraulic Model Report No. CH77/10*, School of Civil Engineering, The University of Queensland, Brisbane, Australia, 82 pages (ISBN 9781864999969).	AUD$60.00		
DOCHERTY, N.J., and CHANSON, H. (2010). "Characterisation of Unsteady Turbulence in Breaking Tidal Bores including the Effects of Bed Roughness." *Hydraulic Model Report No. CH76/10*, School of Civil Engineering, The University of Queensland, Brisbane, Australia, 112 pages (ISBN 9781864999884).	AUD$60.00		
CHANSON, H. (2009). "Advective Diffusion of Air Bubbles in Hydraulic Jumps with Large Froude Numbers: an Experimental Study." *Hydraulic Model Report No. CH75/09*, School of Civil Engineering, The University of Queensland, Brisbane, Australia, 89 pages & 3 videos (ISBN 9781864999730).	AUD$60.00		
CHANSON, H. (2009). "An Experimental Study of Tidal Bore Propagation: the Impact of Bridge Piers and Channel Constriction." *Hydraulic Model Report No. CH74/09*, School of Civil Engineering, The University of Queensland, Brisbane, Australia, 110 pages and 5 movies (ISBN 9781864999600).	AUD$60.00		
CHANSON, H. (2008). "Jean-Baptiste Charles Joseph BÉLANGER (1790-1874), the Backwater Equation and the Bélanger Equation." *Hydraulic Model Report No. CH69/08*, Div. of Civil Engineering, The University of Queensland, Brisbane, Australia, 40 pages (ISBN 9781864999211).	AUD$60.00		
GOURLAY, M.R., and HACKER, J. (2008). "Reef-Top Currents in Vicinity of Heron Island Boat Harbour, Great Barrier Reef, Australia: 2. Specific Influences of Tides Meteorological Events and Waves." *Hydraulic Model Report No. CH73/08*, Div. of Civil Engineering, The University of Queensland, Brisbane, Australia, 331 pages (ISBN 9781864999365).	AUD$60.00		
GOURLAY, M.R., and HACKER, J. (2008). "Reef Top Currents in Vicinity of Heron Island Boat Harbour Great Barrier Reef, Australia: 1. Overall influence of Tides, Winds, and Waves." *Hydraulic Model Report CH72/08*, Div. of Civil Engineering, The University of Queensland, Brisbane, Australia, 201 pages (ISBN 9781864999358).	AUD$60.00		

LARRARTE, F., and CHANSON, H. (2008). "Experiences and Challenges in Sewers: Measurements and Hydrodynamics." *Proceedings of the International Meeting on Measurements and Hydraulics of Sewers*, Summer School GEMCEA/LCPC, 19-21 Aug. 2008, Bouguenais, Hydraulic Model Report No. CH70/08, Div. of Civil Engineering, The University of Queensland, Brisbane, Australia (ISBN 9781864999280).	AUD$60.00		
CHANSON, H. (2008). "Photographic Observations of Tidal Bores (Mascarets) in France." *Hydraulic Model Report No. CH71/08*, Div. of Civil Engineering, The University of Queensland, Brisbane, Australia, 104 pages, 1 movie and 2 audio files (ISBN 9781864999303).	AUD$60.00		
CHANSON, H. (2008). "Turbulence in Positive Surges and Tidal Bores. Effects of Bed Roughness and Adverse Bed Slopes." *Hydraulic Model Report No. CH68/08*, Div. of Civil Engineering, The University of Queensland, Brisbane, Australia, 121 pages & 5 movie files (ISBN 9781864999198)	AUD$70.00		
FURUYAMA, S., and CHANSON, H. (2008). "A Numerical Study of Open Channel Flow Hydrodynamics and Turbulence of the Tidal Bore and Dam-Break Flows." *Report No. CH66/08*, Div. of Civil Engineering, The University of Queensland, Brisbane, Australia, May, 88 pages (ISBN 9781864999068).	AUD$60.00		
GUARD, P., MACPHERSON, K., and MOHOUPT, J. (2008). "A Field Investigation into the Groundwater Dynamics of Raine Island." *Report No. CH67/08*, Div. of Civil Engineering, The University of Queensland, Brisbane, Australia, February, 21 pages (ISBN 9781864999075).	AUD$40.00		
FELDER, S., and CHANSON, H. (2008). "Turbulence and Turbulent Length and Time Scales in Skimming Flows on a Stepped Spillway. Dynamic Similarity, Physical Modelling and Scale Effects." *Report No. CH64/07*, Div. of Civil Engineering, The University of Queensland, Brisbane, Australia, March, 217 pages (ISBN 9781864998870).	AUD$60.00		
TREVETHAN, M., CHANSON, H., and BROWN, R.J. (2007). "Turbulence and Turbulent Flux Events in a Small Subtropical Estuary." Report No. CH65/07, Div. of Civil Engineering, The University of Queensland, Brisbane, Australia, November, 67 pages (ISBN 9781864998993)	AUD$60.00		
MURZYN, F., and CHANSON, H. (2007). "Free Surface, Bubbly flow and Turbulence Measurements in Hydraulic Jumps." *Report CH63/07*, Div. of Civil Engineering, The University of Queensland, Brisbane, Australia, August, 116 pages (ISBN 9781864998917).	AUD$60.00		
KUCUKALI, S., and CHANSON, H. (2007). "Turbulence in Hydraulic Jumps: Experimental Measurements." *Report No. CH62/07*, Div. of Civil Engineering, The University of Queensland, Brisbane, Australia, July, 96 pages (ISBN 9781864998825).	AUD$60.00		
CHANSON, H., TAKEUCHI, M, and TREVETHAN, M. (2006). "Using Turbidity and Acoustic Backscatter Intensity as Surrogate Measures of Suspended Sediment Concentration. Application to a Sub-Tropical Estuary (Eprapah Creek)." *Report No. CH60/06*, Div. of Civil Engineering, The University of Queensland, Brisbane, Australia, July, 142 pages (ISBN 1864998628).	AUD$60.00		
CAROSI, G., and CHANSON, H. (2006). "Air-Water Time and Length Scales in Skimming Flows on a Stepped Spillway. Application to the Spray Characterisation." *Report No. CH59/06*, Div. of Civil Engineering, The University of Queensland, Brisbane, Australia, July (ISBN 1864998601).	AUD$60.00		
TREVETHAN, M., CHANSON, H., and BROWN, R. (2006). "Two Series of Detailed Turbulence Measurements in a Small Sub-Tropical Estuarine System." *Report No. CH58/06*, Div. of Civil Engineering, The University of Queensland, Brisbane, Australia, Mar. (ISBN 1864998520).	AUD$60.00		

KOCH, C., and CHANSON, H. (2005). "An Experimental Study of Tidal Bores and Positive Surges: Hydrodynamics and Turbulence of the Bore Front." *Report No. CH56/05*, Dept. of Civil Engineering, The University of Queensland, Brisbane, Australia, July (ISBN 1864998245).	AUD$60.00		
CHANSON, H. (2005). "Applications of the Saint-Venant Equations and Method of Characteristics to the Dam Break Wave Problem." *Report No. CH55/05*, Dept. of Civil Engineering, The University of Queensland, Brisbane, Australia, May (ISBN 1864997966).	AUD$60.00		
CHANSON, H., COUSSOT, P., JARNY, S., and TOQUER, L. (2004). "A Study of Dam Break Wave of Thixotropic Fluid: Bentonite Surges down an Inclined plane." *Report No. CH54/04*, Dept. of Civil Engineering, The University of Queensland, Brisbane, Australia, June, 90 pages (ISBN 1864997710).	AUD$60.00		
CHANSON, H. (2003). "A Hydraulic, Environmental and Ecological Assessment of a Sub-tropical Stream in Eastern Australia: Eprapah Creek, Victoria Point QLD on 4 April 2003." *Report No. CH52/03*, Dept. of Civil Engineering, The University of Queensland, Brisbane, Australia, June, 189 pages (ISBN 1864997044).	AUD$90.00		
CHANSON, H. (2003). "Sudden Flood Release down a Stepped Cascade. Unsteady Air-Water Flow Measurements. Applications to Wave Run-up, Flash Flood and Dam Break Wave." *Report CH51/03*, Dept of Civil Eng., Univ. of Queensland, Brisbane, Australia, 142 pages (ISBN 1864996552).	AUD$60.00		
CHANSON, H,. (2002). "An Experimental Study of Roman Dropshaft Operation : Hydraulics, Two-Phase Flow, Acoustics." *Report CH50/02*, Dept of Civil Eng., Univ. of Queensland, Brisbane, Australia, 99 pages (ISBN 1864996544).	AUD$60.00		
CHANSON, H., and BRATTBERG, T. (1997). "Experimental Investigations of Air Bubble Entrainment in Developing Shear Layers." *Report CH48/97*, Dept. of Civil Engineering, University of Queensland, Australia, Oct., 309 pages (ISBN 0 86776 748 0).	AUD$90.00		
CHANSON, H. (1996). "Some Hydraulic Aspects during Overflow above Inflatable Flexible Membrane Dam." *Report CH47/96*, Dept. of Civil Engineering, University of Queensland, Australia, May, 60 pages (ISBN 0 86776 644 1).	AUD$60.00		
CHANSON, H. (1995). "Flow Characteristics of Undular Hydraulic Jumps. Comparison with Near-Critical Flows." *Report CH45/95*, Dept. of Civil Engineering, University of Queensland, Australia, June, 202 pages (ISBN 0 86776 612 3).	AUD$60.00		
CHANSON, H. (1995). "Air Bubble Entrainment in Free-surface Turbulent Flows. Experimental Investigations." *Report CH46/95*, Dept. of Civil Engineering, University of Queensland, Australia, June, 368 pages (ISBN 0 86776 611 5).	AUD$80.00		
CHANSON, H. (1994). "Hydraulic Design of Stepped Channels and Spillways." *Report CH43/94*, Dept. of Civil Engineering, University of Queensland, Australia, Feb., 169 pages (ISBN 0 86776 560 7).	AUD$60.00		
POSTAGE & HANDLING (per report)	AUD$10.00		
GRAND TOTAL			

OTHER HYDRAULIC RESEARCH REPORTS

Reports/Theses	Unit price	Quantity	Total price

TREVETHAN, M. (2008). "A Fundamental Study of Turbulence and Turbulent Mixing in a Small Subtropical Estuary." Ph.D. thesis, Div. of Civil Engineering, The University of Queensland, 342 pages.	AUD$100.00		
GONZALEZ, C.A. (2005). "An Experimental Study of Free-Surface Aeration on Embankment Stepped Chutes." *Ph.D. thesis*, Dept of Civil Engineering, The University of Queensland, Brisbane, Australia, 240 pages.	AUD$80.00		
TOOMBES, L. (2002). "Experimental Study of Air-Water Flow Properties on Low-Gradient Stepped Cascades." *Ph.D. thesis*, Dept of Civil Engineering, The University of Queensland, Brisbane, Australia.	AUD$100.00		
CHANSON, H. (1988). "A Study of Air Entrainment and Aeration Devices on a Spillway Model." *Ph.D. thesis*, University of Canterbury, New Zealand.	AUD$60.00		
POSTAGE & HANDLING (per report)	AUD$10.00		
GRAND TOTAL			

CIVIL ENGINEERING RESEARCH REPORT CE

The Civil Engineering Research Report CE series is published by the School of Civil Engineering at the University of Queensland. Orders of any of the Civil Engineering Research Report CE should be addressed to the School Secretary.

School Secretary, School of Civil Engineering, The University of Queensland

Brisbane 4072, Australia

Tel.: (61 7) 3365 3619 Fax : (61 7) 3365 4599

Url: http://www.eng.uq.edu.au/civil/ Email: hodciveng@uq.edu.au

Recent Research Report CE	Unit price	Quantity	Total price
CALLAGHAN, D.P., NIELSEN, P., and CARTWRIGHT, N. (2006). "Data and Analysis Report: Manihiki and Rakahanga, Northern Cook Islands - For February and October/November 2004 Research Trips." *Research Report CE161*, Division of Civil Engineering, The University of Queensland (ISBN No. 1864998318).	AUD$10.00		
GONZALEZ, C.A., TAKAHASHI, M., and CHANSON, H. (2005). "Effects of Step Roughness in Skimming Flows: an Experimental Study." *Research Report No. CE160*, Dept. of Civil Engineering, The University of Queensland, Brisbane, Australia, July (ISBN 1864998105).	AUD$10.00		
CHANSON, H., and TOOMBES, L. (2001). "Experimental Investigations of Air Entrainment in Transition and Skimming Flows down a Stepped Chute. Application to Embankment Overflow Stepped Spillways." *Research Report No. CE158*, Dept. of Civil Engineering, The University of Queensland, Brisbane, Australia, July, 74 pages (ISBN 1 864995297).	AUD$10.00		
HANDLING (per order)	AUD$10.00		

GRAND TOTAL			

Note: Prices include postages and processing.

PAYMENT INFORMATION

1- VISA Card

Name on the card :	
Visa card number :	
Expiry date :	
Amount :	AUD$ .....

2- Cheque/remittance payable to: THE UNIVERSITY OF QUEENSLAND and crossed "Not Negotiable".

N.B. For overseas buyers, cheque payable in Australian Dollars drawn on an office in Australia of a bank operating in Australia, payable to: THE UNIVERSITY OF QUEENSLAND and crossed "Not Negotiable".

Orders of any Research Report should be addressed to the School Secretary.

School Secretary, School of Civil Engineering, The University of Queensland
Brisbane 4072, Australia - Tel.: (61 7) 3365 3619 - Fax : (61 7) 3365 4599
Url: http://www.eng.uq.edu.au/civil/ Email: hodciveng@uq.edu.au